

SPECTROSCOPIC AND COMPUTATIONAL INVESTIGATION OF ADENOSYLCOBALAMIN-DEPENDENT ENZYMES AND A MEMBRANE-BOUND FATTY ACID DESATURASE

By

Christopher D. Jordan

A dissertation submitted in partial fulfillment of
the requirements for the degree of

Doctor of Philosophy

(Chemistry)

at the

UNIVERSITY OF WISCONSIN-MADISON

2015

Date of final oral examination: July 21, 2015

This dissertation is approved by the following members of the Final Oral Committee:

Thomas C. Brunold, Professor of Chemistry - Inorganic
Qiang Cui, Professor of Chemistry - Physical
Martin T. Zanni, Professor of Chemistry - Physical
Silvia Cavagnero, Professor of Chemistry - Physical
Brian G. Fox, Professor of Biochemistry

Spectroscopic and Computational Investigation of Adenosylcobalamin-Dependent Enzymes and a Membrane-Bound Fatty Acid Desaturase

Christopher D. Jordan

Under the supervision of Professor Thomas C. Brunold
at the University of Wisconsin-Madison

Coenzyme B₁₂ (5'-deoxyadenosylcobalamin, AdoCbl) is a remarkable cofactor derived from Vitamin B₁₂ and a rare example of a natural, biologically-relevant organometallic compound. All mechanisms employed by AdoCbl-dependent enzymes are initiated by homolysis of the cofactor's Co–C bond to form cob(II)alamin and a highly reactive adenosyl radical. To investigate the interactions between cofactor, enzyme, and substrate that lead to activation of the Co–C bond, spectroscopic and computational techniques were applied to free and enzyme-bound AdoCbl, cob(II)alamin, and related species. This research highlighted the mechanistic implications of differences between AdoCbl-dependent isomerases and eliminases, in which the former bind AdoCbl by substituting its lower axial ligand with a histidine residue.

Spectroscopic changes caused by reducing the electron-donating character of the lower axial ligand of cofactor analogues were found to be similar to those observed when cob(II)alamin binds to isomerases. This observation was used to suggest that the basicity of the coordinating histidine is modulated during turnover by proton uptake into a conserved hydrogen bonding network, thus preferentially stabilizing the cob(II)alamin state. In contrast, an experimentally-validated computational model of AdoCbl bound to the eliminase ethanolamine ammonia lyase (EAL) revealed that destabilization of AdoCbl upon the binding of substrate triggers Co–C bond

homolysis. A subsequent computational study confirmed the importance of two active-site residues, N193 α and Y241 β , and proposed future AdoCbl analogues and EAL variants for spectroscopic characterization.

Stearoyl-CoA desaturase (SCD) is a membrane-bound, non-heme diiron enzyme (NHFe₂) that converts stearoyl-CoA to oleyl-CoA alongside the reduction of O₂ to two water molecules. The active-site architecture of SCD is novel among NHFe₂ enzymes and includes an Fe–Fe separation that precludes the possibility of activating O₂ by binding it as a bridging ligand. A computational investigation of SCD allowed for proposal of a likely O₂ binding site and a putative reaction mechanism.

Lastly, an interactive program that facilitates the implementation of computational analyses of whole-protein systems was written. This program, which has been used by several graduate and postdoctoral researchers and will soon be used by undergraduate researchers, helps lower barriers to the theoretical study of biomolecules.

Acknowledgments

I am keenly aware of all the people who have supported me throughout the process of writing this dissertation. I regret that I do not have the space to thank all of the family, friends, and mentors who have left an indelible mark on me as a scientist and as a person, and that I lack the eloquence to properly thank them for their role in this work. Despite those limitations, I would like to (briefly) mention my sincere gratitude.

Thomas, thank you for being a wonderful advisor, and for surpassing all of my pre-existing expectations. I'm especially grateful for the patience you showed me as I struggled to be productive and contribute to the group during my first two years, and for the support you continued to provide even during my year away from campus. You have shown me what it means to be a creative researcher, a precise writer, a tireless editor, a supportive colleague, and a caring teacher.

To the members of the Brunold group, thank you so much for cultivating a positive atmosphere where collaboration is valued far more than competition. You are all wonderful scientists and people, and I will tremendously miss each of you. To those whom I overlapped with briefly – Kiyong, Karen, Jessica, Olivia – thank you for the examples you set for me as a young graduate student, both through your actions and the writing you left behind. Craig, thank you for being a friendly, welcoming presence at a time when I needed all the encouragement I could get. Beth, thank you for your honest, forthright nature, your prolific sarcasm, and your immeasurably kind heart. Ivan, thank you for your inquisitive spirit, your willingness to start a good conversation at any time, and the incredible patience you demonstrated each and every time I came to you with a silly question about spectroscopy or B₁₂. Kristine, thank you for the energy you brought to the

group from the very first day you joined, for drawing me out of my shell, and for providing me some much-needed remedial education on lab techniques. Mickie, thank you for all of the times you've selflessly done my share of lab chores, especially helium transfers, and for all of the kind words of encouragement you've given me during our last two years as desk neighbors. Nuru, thank you for being my teaching buddy, for the sweet Post-It note messages, and for always listening to me when I need to complain. Stephanie, thank you for being such a steady presence in the lab, for sparking meaningful conversations in the office, and for the invitations to trivia night.

I am very grateful for the skilled hands and sharp minds of my collaborators. Without the efforts of Tilak Chandra, Karen Conrad, Kathy Krasny, and Ted Moore, this thesis would be devoid of any experimental data, and as a result my computations would be meaningless. Excellent conversations with Prof. Jorge Escalante-Semerena, Prof. Kenneth Brown, and Prof. Brian Fox greatly influenced my analyses as well.

I have spent 22 of the last 23 years of my life as a student of some sort, and as I consider the journey I realize how much I need to thank the many teachers who have encouraged me. I owe a special "thank you" to two high school teachers: Grover Price for showing me the joy of chemistry, and Marilyn Mortimer, for teaching me how to write. I owe thanks to my many wonderful professors at Hope College as well, especially Will Polik, Jason Gillmore, Brian Coyle, and Jack Mulder, who all taught me how to think and, incidentally, how to teach.

I'm also thankful for the many people at UW-Madison and Houghton College who have helped me develop as a teacher and made it possible for me to leave grad school with the security of a

teaching job lined up. I want to especially thank my former Houghton colleagues Karen Torraca, John Rowley, and Irmgard Howard, who took a chance on me and gave me a tremendous opportunity. Many of the academic staff at UW-Madison, including Jeanne Hamers, Stephen Block, Oana Martin, and Chad Wilkinson, have gone out of their way to help me and give me new opportunities to develop teaching and mentoring skills as well.

Thank you to the good people at Geneva Campus Church, for taking such good care of me and my family during our time in Madison. You gave us help, love, comfort, and purpose at a time in our lives when we often had very little to offer in return. Your generosity means so much to us.

Last, and most importantly, I need to thank my ever-supportive family. My parents have never ceased to encourage me during the past six years, even as I've found myself incapable of explaining to them what it is that I do. Chapter 8 of this thesis, which is written for a general audience, is dedicated to them. My children, Caroline and Benjamin, have been at once the greatest motivation for finishing my research and the greatest temptation to spend time away from it. It's unlikely they will ever read this dissertation, but the joy they brought me with every smile and every hug were essential for its completion. And finally, Kristie – thank you for staying by my side these last six years, for making the sacrifices you did so that I could pursue this dream, and for never wavering in your faith in me. You are the reason for any remaining sanity that I have.

Contents

Abstract	i
Acknowledgments	iii
Table of Contents	vi
List of Figures	viii
List of Schemes	xii
List of Tables	xiii

CHAPTER 1: <i>Co–C BOND ACTIVATION MECHANISMS EMPLOYED BY ADENOSYLCOBALAMIN-DEPENDENT ENZYMES</i>	1
1.1 Overview	2
1.2 Free Cobalamins and Model Complexes	4
1.3 AdoCbl-Dependent Enzymes	13
1.4 Summary and Organization of this Thesis	21
1.5 References	24

CHAPTER 2: <i>SPECTROSCOPIC AND COMPUTATIONAL STUDIES OF COBALAMIN SPECIES WITH VARIABLE LOWER AXIAL LIGATION: IMPLICATIONS FOR THE MECHANISM OF Co–C BOND ACTIVATION BY CLASS I COBALAMIN-DEPENDENT ISOMERASES</i>	29
2.1 Introduction	30
2.2 Experimental and Computational Methods	35
2.3 Results	38
2.4 Discussion	51
2.5 Conclusion	56
2.6 References	56

CHAPTER 3: <i>SPECTROSCOPIC AND COMPUTATIONAL INVESTIGATION OF THE ADENOSYLCOBALAMIN-DEPENDENT ETHANOLAMINE AMMONIA LYASE: INSIGHT INTO THE MECHANISM OF ENZYMATIC Co–C BOND ACTIVATION</i>	61
3.1 Introduction	62
3.2 Methods	65
3.3 Results	68
3.4 Discussion	81
3.5 Conclusion	90
3.6 References	92

CHAPTER 4: COMPUTATIONAL INVESTIGATION OF THE ADENOSYLCOBALAMIN-DEPENDENT ETHANOLAMINE AMMONIA LYASE: ROLE OF SPECIFIC ENZYME-COFACTOR INTERACTIONS	95
4.1 Introduction	96
4.2 Computational Methods	102
4.3 Results	105
4.4 Discussion	111
4.5 Conclusion	116
4.6 References	117
 CHAPTER 5: COMPUTATIONAL INVESTIGATION OF THE DIOXYGEN BINDING SITE AND A PUTATIVE REACTION MECHANISM OF STEAROYL-COA DESATURASE	 119
5.1 Introduction	120
5.2 Computational Methods	124
5.3 Results	127
5.4 Discussion	133
5.5 Conclusion	139
5.6 References	139
 CHAPTER 6: DEVELOPMENT AND IMPLEMENTATION OF AN INTERACTIVE PROGRAM FOR SETUP AND ANALYSIS OF COMPUTATIONS ON LARGE BIOMOLECULES	 142
6.1 Introduction	143
6.2 Program Architecture	146
6.3 Chemical Considerations	153
6.4 Summary	158
6.5 References	159
 CHAPTER 7: CONCLUSIONS AND FUTURE DIRECTIONS	 161
7.1 Adenosylcobalamin-Dependent Enzymes	162
7.2 Stearoyl-CoA Desaturase	165
7.3 Bulb	166
7.4 Concluding Remarks	167
7.5 References	168
 CHAPTER 8: HOW TO BREAK A BOND: A BRIEF, NON-TECHNICAL ACCOUNT OF COENZYME B12, ONE ENZYME THAT USES IT, AND THE LAST SIX YEARS OF MY LIFE	 169
8.1 Introduction and Motivation	170
8.2 From Atoms to Enzymes: Bonding, Biochemistry, and Catalysis	171
8.3 Matter, Light, and Energy	182
8.4 Results	191
8.5 Conclusion	195
 APPENDIX	 198

List of Figures

Figure 1.1. Adenosylcobalamin.	3
Figure 1.2. General structure of cobinamides and cobaloximes.	6
Figure 1.3. Representative Abs, CD, and MCD spectra of non-alkyl Co(III)Cbls and alkylCbls.	9
Figure 1.4. Abs and MCD spectra of Co(II)Cbl and Co(II)Cbi ⁺ .	12
Figure 1.5. Line drawing of AdePeCbl and structure of AdePeCbl in the active site of diol dehydratase	19
Figure 2.1. Structure of AdoCbl and α -axial ligands used in this study.	31
Figure 2.2. Abs and 7 T MCD spectra obtained at 4.5 K of AdoCbl and Ado(F-Im)Cbl.	39
Figure 2.3. DFT-computed MO diagrams for AdoCbl and Ado(F-Im)Cbl.	41
Figure 2.4. TD-DFT computed Abs spectra for AdoCbl and Ado(F-Im)Cbl.	43
Figure 2.5. Abs and 7 T MCD spectra obtained at 4.5 K of Co(II)Cbl and Co(II)(F-Im)Cbl.	45
Figure 2.6. MCD spectra obtained at 7 T and 4.5 K of Co(II)pyCbi ⁺ , Co(II)(CN-py)Cbi ⁺ , and Co(II)(Me ₂ N-py)Cbi ⁺ .	47
Figure 2.7. TD-DFT computed Abs spectra for Co(II)Cbl, Co(II)(F-Im)Cbl, Co(II)ImCbl, Co(II)(Me-Im)Cbl, and Co(II)(CN-Im)Cbl.	49
Figure 2.8. EDDMs for transitions 1-5 in the TD-DFT computed Abs spectra of Co(II)Cbl and Co(II)(F-Im)Cbl.	50
Figure 2.9. TD-DFT computed Abs spectra for three Co(II)-bound Cbi derivatives: Co(II)pyCbi ⁺ , Co(II)(Me ₂ N-py)Cbi ⁺ , and Co(II)(CN-py)Cbi ⁺ .	51
Figure 2.10. MCD spectra of Co(II)F-Im)Cbl, MMCM-bound Co(II)Cbl, and GM-bound Co(II)Cbl, obtained at 4.5 K and 7 T.	54
Figure 3.1. Adenosylcobalamin.	62
Figure 3.2. Abs spectra at 4.5 K of AdoCbl in solution, the EAL holoenzyme, and the ternary complex.	69

Figure 3.3. MCD spectra at 4.5 K of free AdoCbl, EAL holoenzyme, and EAL ternary complex.	70
Figure 3.4. A comparison of the QM/MM-optimized geometries of the EAL holoenzyme and EAL ternary complex.	72
Figure 3.5. Computed Abs spectra for free AdoCbl and AdoCbl bound to the EAL holoenzyme and ternary complex.	75
Figure 3.6. TD-DFT spectra for models of AdoCbl with variable Co–N _{DMB} distance, ranging from 1.9 Å to 2.6 Å in 0.1 Å intervals.	76
Figure 3.7. TD-DFT spectra for models of AdoCbl bound to the holoenzyme with variable Co–N _{DMB} distance, ranging from 1.9 Å to 2.6 Å in 0.1 Å intervals.	76
Figure 3.8. Computed Abs spectra for AdoCbl-bound WT EAL and three E287 α variants: E287 α D, E287 α Q, and E287 α A.	80
Figure 3.9. Side view and top view of the EDDM for the HOMO \rightarrow LUMO transition of AdoCbl in the EAL holoenzyme.	83
Figure 3.10. EDDMs for three transitions referred to in the text.	84
Figure 3.11. LEFT: Computed transition energies and Abs intensities of the Co 3d _{xz} \rightarrow LUMO transition of AdoCbl models in series 2.	88
Figure 4.1. Adenosylcobalamin.	97
Figure 4.2. Optimized geometries of EAL holoenzyme and ternary complex, including three residues implicated in Co–C bond activation.	100
Figure 4.3. AdoCbl analogues used in this study.	103
Figure 4.4. TD-DFT-computed Abs spectra for AdoCbl bound to the WT, Y241 β A, Y241 β F, Y241 β W, and N193 α A EAL holoenzymes.	110
Figure 4.5. TD-DFT-computed Abs spectra for AdoCbl bound to the WT, Y241 β A, Y241 β F, Y241 β W, and N193 α A EAL ternary complexes.	110
Figure 4.6. Two perspectives of an overlay of optimized geometries of WT-bound and Y241 β W-bound AdoCbl. Hydrogen atoms are omitted for clarity.	112
Figure 5.1. Active-site regions of cytosolic and membrane-bound Δ 9Ds.	121

Figure 5.2. Sequence logo representation of conserved residues in the three His boxes of fatty acid desaturases.	123
Figure 5.3. QM region used for all QM/MM optimizations in this study.	126
Figure 5.4. QM regions of QM/MM-optimized models of Zn ^{II} ₂ -bound SCD obtained with B3LYP and M-06L.	127
Figure 5.5. QM regions of QM/MM-optimized geometries of Fe ^{II} ₂ -bound SCD obtained with B3LYP and M-06L.	128
Figure 5.6. QM/MM-optimized geometries of four putative O ₂ -bound reaction intermediates of SCD.	129
Figure 5.7. Computed QM energies (kJ/mol) of putative reaction intermediates in the proposed SCD mechanism.	133
Figure 5.8. Cartoon of QM/MM-optimized SCD active site in state A.	138
Figure 6.1. Screenshot of interactive bulb session demonstrating the use of alternative coordinates.	147
Figure 6.2. Screenshot of bulb showing the communication of unusually charged amino acids to the user and the option to adjust protonation state.	149
Figure 6.3. Screenshot of bulb depicting the removal of a proton from N _ε of residue H317α of ethanolamine ammonia lyase.	150
Figure 6.4. Screenshot of the first 15 lines of a QM/MM Gaussian09 input file generated by bulb.	152
Figure 6.5. Screenshot of TD-DFT-computed transition compositions and DFT-computed MO compositions, as extracted from an Orca 2.9/3.0 log file by bulb.	157
Figure 8.1. General organization of a protein.	176
Figure 8.2. Coenzyme B ₁₂ and the first step of reactions it helps catalyze; coordination of coenzyme B ₁₂ to an enzyme through a histidine side chain.	178
Figure 8.3. A dilute solution of coenzyme B ₁₂ .	183

- Figure 8.4.** Sketch and picture of a typical absorption spectrophotometer; absorption spectrum of coenzyme B₁₂. **185**
- Figure 8.5.** Setup and results of a magnetic circular dichroism experiment. **188**
- Figure 8.6.** Absorption and MCD spectra of coenzyme B₁₂ and MCD spectrum of Co(II)Cbl as free species and bound to EAL in the presence and absence of ethanolamine. **192**
- Figure 8.7.** Results from computational models of EAL. **194**

List of Schemes

Scheme 1.1. General reaction mechanism employed by AdoCbl-dependent enzymes.	4
Scheme 3.1. General mechanism employed by AdoCbl-dependent enzymes.	63
Scheme 4.1. General reaction mechanism employed by AdoCbl-dependent enzymes.	97
Scheme 5.1. Desaturation of stearoyl-CoA to form oleyl-CoA.	120
Scheme 5.2. Proposed mechanism for the activation of P and subsequent desaturation of substrate in cytosolic $\Delta 9$ Ds.	122
Scheme 5.3. Proposed SCD mechanism.	131
Scheme 8.1. The rearrangement of ethanolamine.	175

List of Tables

Table 2.1. TD-DFT Computed Energies, Oscillator Strengths, and Percent Contributions from Dominant One-Electron Excitations for the Major Electronic Transitions of AdoCbl	43
Table 2.2. TD-DFT Computed Energies, Shifts from Corresponding AdoCbl Transitions, Oscillator Strengths, and Percent Contributions from Dominant One-Electron Excitations for the Major Electronic Transitions of Ado(F-Im)Cbl	44
Table 2.3. Selected Spectral Features of Co(II)(F-Im)Cbl and Shifts Relative to Co(II)Cbl Counterparts	46
Table 2.4. TD-DFT Computed Energies, Percent Contributions from Dominant One-Electron Excitations, and Oscillator Strengths for the Major Electronic Transitions of Co(II)Cbl	49
Table 2.5. TD-DFT Computed Energies, Shifts From Corresponding Co(II)Cbl Transitions, Oscillator Strengths, and Percent Contributions from Dominant One-Electron Excitations for the Major Electronic Transitions of Co(II)(F-Im)Cbl	50
Table 3.1. Relevant structural parameters of AdoCbl in the QM/MM-optimized models of free AdoCbl, the EAL holoenzyme, and the EAL ternary complex.	71
Table 3.2. Key geometric parameters for AdoCbl-bound WT EAL and five variants.	78
Table 3.3. Geometric parameters for AdoCbl-bound WT EAL and three variants in the presence of substrate.	78
Table 3.4. Energies of the α/β bands of AdoCbl models in series 1 and 2 .	87
Table 4.1. Key geometric parameters of AdoCbl-bound WT EAL and four variant holoenzymes.	106
Table 4.2. Key geometric parameters of AdoCbl-bound WT EAL and four variant ternary complexes.	106
Table 4.3. Key geometric parameters of AdoCbl, Ado(BIm)Cbl, and Ado(Im)Cbl as free species and bound to WT and Y241 β W EAL.	107

Table 4.4. Key geometric parameters of AdoCbl, 2'-dAdoCbl, 3'-dAdoCbl, and 2',3'-ddAdoCbl as free species and bound to the WT EAL holoenzyme and ternary complex.	108
Table 5.1. Key geometric parameters of the QM/MM-optimized geometries of Zn^{II} - and Fe^{II} -bound SCD.	128
Table 5.2. Key geometric parameters of the B3LYP-optimized O_2 -bound models of SCD.	130

CHAPTER 1

Co–C Bond Activation Mechanisms Employed by Adenosylcobalamin-Dependent Enzymes

1.1 Overview

Shortly after their nearly simultaneous isolation of vitamin B₁₂ (cyanocobalamin, CNCbl) in 1948,^{1, 2} two independent groups determined that this essential nutrient was a Co-containing coordination compound.^{3, 4} The subsequent discovery that the Co ion in one of the biologically active forms of the vitamin contained an organic 5'-deoxyadenosyl^{5, 6} (Ado) ligand launched an era of sustained research in a wide range of fields that remains active today. Until recently, this adenosylated form of B₁₂ (5'-deoxyadenosylcobalamin, AdoCbl, Figure 1.1) and the related methylated form (methylcobalamin, MeCbl) were the only known natural, biologically relevant organometallic compounds. AdoCbl, MeCbl, and CNCbl belong to a class of compounds known as cob(III)alamins (Co(III)Cbls), which feature a low-spin Co(III) ion ligated equatorially by a tetradentate corrin macrocycle and axially by an intramolecular dimethylbenzimidazole (DMB) base tethered covalently to the corrin ring via a nucleotide loop. A sixth ligand, which defines the compound's name (e.g., *adenosylcobalamin*) and to a large degree determines its reactivity and structural and electronic properties, is coordinated *trans* to the DMB. All Co(III)Cbls can be reduced to Co(II)Cbl, a penta-coordinate species that retains the corrin and DMB ligands but lacks an "upper" axial ligand. This species is an extremely important intermediate in the mechanisms of AdoCbl-dependent enzymes, and its paramagnetic ($S = 1/2$) ground state makes it accessible to a variety of spectroscopic techniques. Although humans cannot synthesize AdoCbl *de novo*, human adenosyltransferase is used to transfer the adenosyl moiety of ATP to Co(II)Cbl.⁷

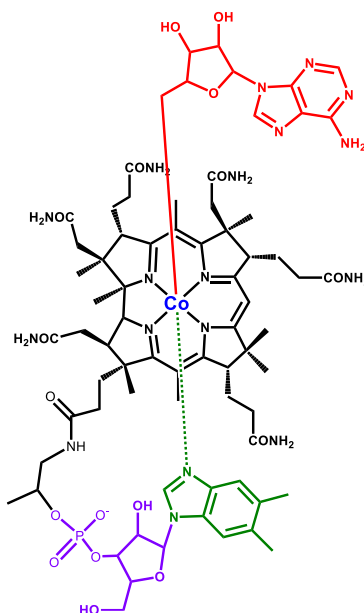
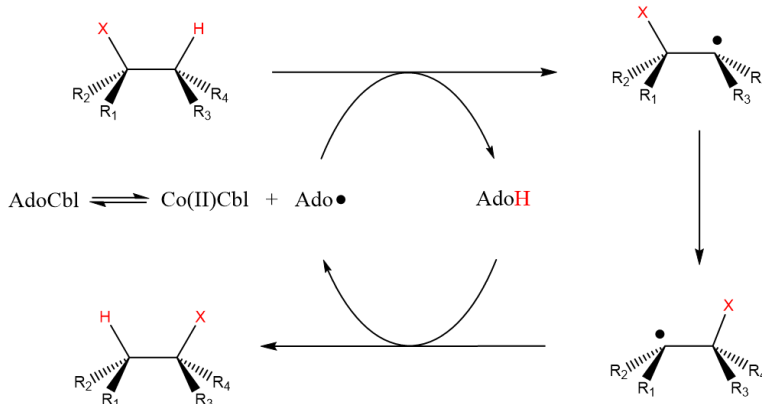


Figure 1.1. Adenosylcobalamin. The structure is color-coded to identify the Co(III) ion (blue), corrin ring (black), Ado (red) and DMB (green) ligands, and nucleotide loop (purple).

AdoCbl is a required cofactor for a number of enzymes that catalyze the 1,2-rearrangements of various organic substrates (Scheme 1.1). The binding of substrate to an AdoCbl-dependent holoenzyme induces homolytic cleavage of the cofactor's Co–C bond, producing Co(II)Cbl and a highly reactive adenosyl radical (Ado[•]). The Ado[•] species abstracts a hydrogen atom from the substrate, producing 5'-deoxyadenosine (AdoH) and a substrate-like radical that undergoes the desired 1,2-rearrangement to form a product-like radical. This latter radical then abstracts a hydrogen from AdoH to form the final product and regenerate Ado[•], which recombines with Co(II)Cbl to close the catalytic cycle. This general mechanism has been widely accepted for several decades now, and recent research on AdoCbl-dependent enzymes has focused on discerning the specific interactions between these enzymes, their substrates, and AdoCbl that lead to efficient catalysis.⁸⁻¹³

Scheme 1.1. General reaction mechanism employed by AdoCbl-dependent enzymes.



Of particular interest are the means by which AdoCbl-dependent enzymes activate the cofactor's Co–C bond. The rate of Co–C bond homolysis of AdoCbl (bond dissociation energy [BDE] of 30 ± 2 kcal/mol,¹⁴ with a corresponding first-order rate constant of $\sim 10^{-9}$ s⁻¹ for bond homolysis¹⁵) is enhanced dramatically by all AdoCbl-dependent enzymes¹⁶⁻²⁰ despite their differences in substrate size and specificity, the requirement for additional cofactors, and, most intriguingly, the mode of binding AdoCbl itself. In principle, this bond activation in enzyme active sites could be achieved through two general means: the imposition of a strained geometry on AdoCbl and its consequent destabilization, or the stabilization of the transition state for Co–C bond homolysis. To evaluate the relative importance of these two modes of bond activation in AdoCbl-dependent enzymes, free and enzyme-bound forms of AdoCbl and related species have been extensively characterized by spectroscopic and computational techniques.

1.2 Free Cobalamins and Model Complexes

AdoCbl, Co(II)Cbl, and other Cbls have been characterized structurally by X-ray crystallography and nuclear magnetic resonance (NMR) spectroscopy, and their properties have also been probed by a variety of spectroscopic methods, including electronic absorption (Abs), circular dichroism (CD), magnetic circular dichroism (MCD), resonance Raman (rR), and electron

paramagnetic resonance (EPR) spectroscopies. Although these techniques provide insight into the electronic, vibrational, and magnetic properties of Cbls, the large size and complicated electronic structure of these species can preclude a detailed analysis of the results they provide. As a consequence, the use of advanced computational methods to assist in spectral interpretation has itself become a vibrant field of B₁₂ research.²¹

Two families of natural and synthetic compounds (Figure 1.2) have been used extensively as Cbl models in order to investigate how the corrin and DMB ligands affect the strength and reactivity of the Co–C bond. The first are the cobinamides (Cbis), intermediates in the *de novo* biosynthesis of Cbls accomplished by various bacteria.²² Cbis contain a complete corrin ring, including all side chains, yet lack the nucleotide loop of Cbls. As such, Cbis readily undergo substitution of the lower axial ligand, and can be used to investigate the steric and electronic effect that this ligand has on the homolysis of the Co–C bond *trans* to it. Even simpler models for Cbls are the cobaloximes (Cbxs), a class of compounds in which two dimethylglyoxime monoanionic ligands (DH) are used to mimic the corrin ring.²³ Since the discovery that, as in AdoCbl and MeCbl, the octahedral ligand field in Co(DH)₂ complexes could be completed by an organic ligand and an N-coordinating base,^{24, 25} an incredible number of these compounds have been synthesized and characterized. Thanks to the prolific work of crystallographers, over 100 structures of Cbxs^{23, 26, 27} have been published since the first reported syntheses in 1964.

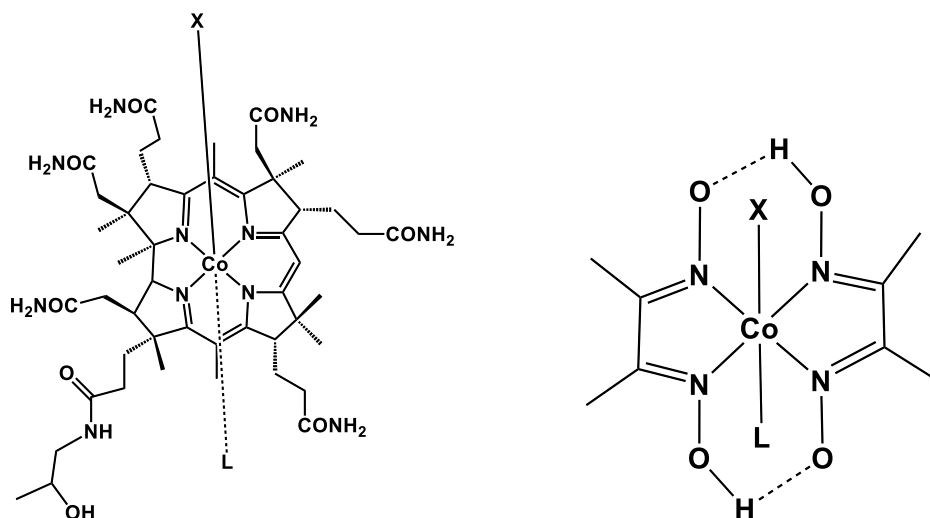


Figure 1.2. General structure of cobinamides (left) and cobaloximes (right).

1.2.1 Structural and Thermodynamic Properties. The first crystal structure of AdoCbl⁶ was published over 50 years ago and was instrumental in proving the cofactor's organometallic nature. Since this breakthrough, the structures of a large number of Cbls, Cbis, and Cbxs have been determined.^{28, 29} These structures have demonstrated how the σ -donor and π -donor/acceptor properties of one axial ligand influence the bond *trans* to it.^{28, 29} In alkylCbls and alkylCbxs, an inverse *trans* influence has been noted, in which a positive correlation exists between the Co–C and Co–N_{ax} bond lengths. Similarly, strong bonds to the lower axial ligand in Cbxs are correlated with higher Co–C BDEs and smaller bond homolysis rate constants. The causes of these correlations are not readily apparent, making it difficult to use trends observed in a series of model compounds to make even qualitative predictions about Co–C bond activation mechanisms employed by AdoCbl-dependent enzymes. One sobering example involves the earliest crystal structures of enzyme-bound AdoCbl species, which revealed both a ligand switch from the native DMB to a protein-derived histidine (His) and unusually long Co–N_{His} and Co–C bonds.³⁰ This led to the erroneous conclusion that AdoCbl-dependent enzymes accomplish homolysis by lengthening the Co–N_{ax} bond to induce a corresponding elongation of the Co–C bond, thus

weakening it. However, in the following years it was shown that (i) the long Co–N_{His} bonds were artifacts of X-ray induced photolysis;³¹ (ii) the DMB ligand is not displaced by a His residue in all AdoCbl-dependent enzymes;³² and (iii) that the Co–C bond strength is in fact unperturbed by lower axial ligand switches.^{33, 34} Thus, it is difficult to propose a mechanism of Co–C bond activation from structural information alone, as the mutual influence of the two axial ligands on each other is clearly quite nuanced.

1.2.2. Electronic Structure. The noticeable differences between the Abs spectra of AdoCbl, Co(II)Cbl, and various other Cbl species have been recognized for over half a century^{35, 36} and have been the subject of studies involving increasingly sophisticated theoretical techniques³⁷⁻³⁹ as new methods were developed and computational power increased. In spite of these efforts, the complex geometric structures of Cbls have made assignment of the various electronic transitions and an explanation of the perturbations observed upon ligand substitution or change in oxidation state quite difficult. It was not until the development of density functional theory (DFT) in the 1980s and 1990s that an adequate computational analysis of Cbls became tractable.⁴⁰ The subsequent development of time-dependent DFT (TD-DFT), used to predict Abs spectra and other excited-state properties, ushered in a new wave of purely theoretical and combined experimental/theoretical studies of Cbls that attempted to extract the maximum amount of information from spectroscopic data.

Beginning in the early 2000s and continuing through the present, the Brunold lab has performed detailed analyses of the electronic spectra of many Cbl and Cbi species.^{21, 41-47} A summary of this work for the species relevant to this thesis is presented here. The most notable spectral differences observed among Co(III)Cbls can be correlated with the presence or absence of an alkyl ligand in the upper axial position (Figure 1.3).⁴¹ Co(III)Cbl species such as H₂OCbl⁺

and CNCbl exhibit two distinct Abs features, including a moderately intense pair of features termed the α/β bands that appear around 18 000 – 20 000 cm^{-1} and a sharp, very intense feature at $\sim 28\,000\text{ cm}^{-1}$ referred to as the γ band (Figure 1.3A). Additionally, several poorly resolved features with lower intensity (the “D/E bands”) are observed at intermediate energies. In contrast, the Abs spectra of alkylCbls such as MeCbl and AdoCbl (Figure 1.3B) do not exhibit a distinct γ band in their Abs spectra. Rather, several overlapping features of intermediate intensity are observed in this region. Additional perturbations, such as changes in the relative intensities of the α/β bands, are also observed.

To better resolve the many Abs features of Co(III)Cbls and assist in their assignments, Brunold and coworkers collected low temperature CD and MCD spectra of several Cbl species and AdoCbi⁺, and computed Abs spectra for these species with TD-DFT.⁴¹ An iterative Gaussian deconvolution of the Abs, CD, and MCD spectra of each species allowed for the identification of at least 13 overlapping features, which were then assigned on the basis of their relative intensities, rR excitation profiles, and a TD-DFT computational analysis. Many of the observed spectral differences between non-alkyl- and alkylCo(III)Cbls (e.g., H₂OCbl⁺ and MeCbl) were explained in terms of increased mixing of occupied Co 3d and corrin π orbitals in alkylCbls due to the presence of the strongly σ -donating alkyl ligand, which causes the filled Co 3d orbitals to shift closer in energy to the corrin frontier orbitals.

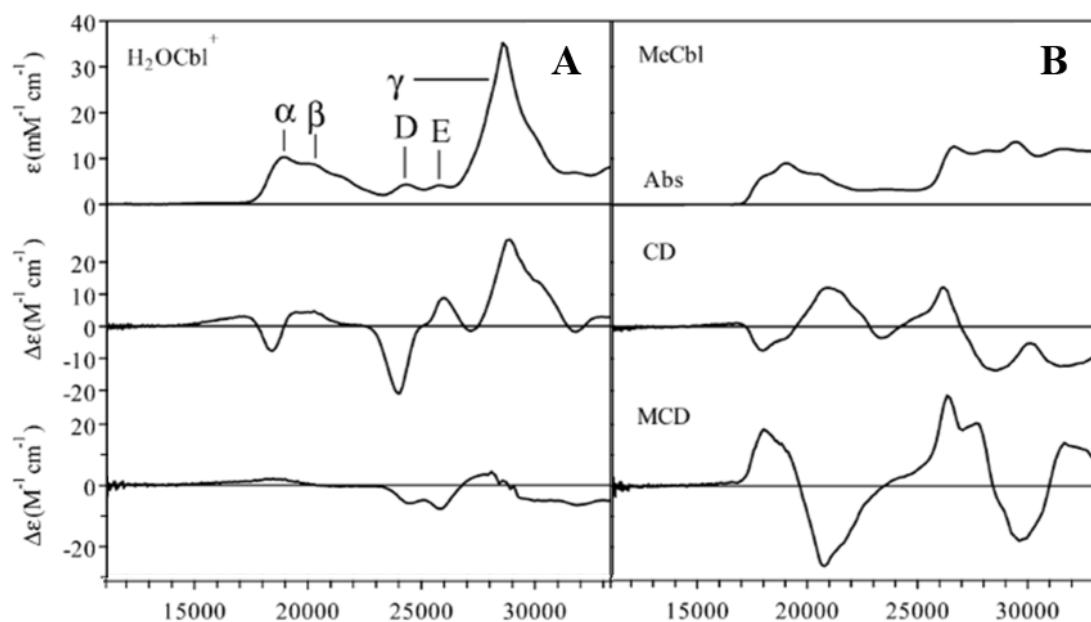


Figure 1.3. Representative Abs, CD, and MCD spectra of non-alkyl Co(III)Cbls (H₂OCbl⁺, left) and alkylCbls (MeCbl, right).⁴¹

This increased orbital mixing has several profound effects on the electronic structures of alkylCbls. Firstly, it causes the HOMO, formally a corrin π orbital, to acquire some Co–C σ^b and Co–N_{DMB} σ^* character, which introduces metal-to-ligand charge transfer (MLCT) character into HOMO \rightarrow corrin π^* transitions, including the one responsible for the α/β bands (assigned to the HOMO \rightarrow LUMO transition). Secondly, it leads to an increase in the number of occupied MOs in close energetic proximity to the HOMO, which in turn leads to the appearance of numerous Abs features with increased MLCT character in the γ region. In contrast, the sharp γ band in non-alkylCo(III)Cbls arises from a relatively pure corrin $\pi \rightarrow \pi^*$ transition. More recently, the Kozlowski lab has published a substantial amount of theoretical work utilizing TD-DFT and more advanced methods to investigate the electronic spectra and excited states of CNCbl,⁴⁸⁻⁵⁰ MeCbl,^{49, 51} and AdoCbl.^{52, 53} While the analyses of the Kozlowski and Brunold groups have led to somewhat different spectral assignments, they mostly agree with one another qualitatively (e.g., both analyses indicate that the transition associated with the α/β bands contains some MLCT character).⁵⁴

Moreover, Kozłowski's work has revealed the types of functionals most appropriate for the study of ground- and excited-state properties of Cbl species,^{55, 56} thus greatly aiding future studies of hitherto poorly characterized B₁₂ derivatives.

The electronic structure of Co(II)Cbl is equally relevant to the elucidation of enzymatic contributions to Co–C bond activation, as a stabilization of this state implies a similar stabilization of the homolysis transition state (see Section 1.3 below). With this in mind, the Brunold group also performed a combined spectroscopic/computational analysis of the reduced cofactor and its derivative Co(II)Cbi⁺ and assigned the main features of their electronic spectra (Figure 1.4).⁴² While the Abs spectrum of Co(II)Cbl lacks the distinct features present in the Co(III)Cbl Abs spectra, its features can be loosely grouped into three categories. The lowest energy features, which possess weak Abs intensity but are readily observable in the MCD spectrum, are assigned as ligand field (LF) transitions within the Co 3d manifold. At intermediate energies, features of more moderate intensity due to transitions with predominantly MLCT character are found, while the intense features in the near UV have been attributed to corrin $\pi \rightarrow \pi^*$ transitions. However, it is important to note that just as in the case of the alkylCo(III)Cbls, the Co 3d and corrin π orbitals are significantly mixed in Co(II)Cbl. As a result, all transitions at intermediate and high energies contain a mixture of both MLCT and corrin $\pi \rightarrow \pi^*$ character. As such, they are all sensitive to some degree to the basicity of the lower axial ligand, as the extent of charge donation from this ligand modulates the relative energies of the Co 3d-based MOs.^{42, 57}

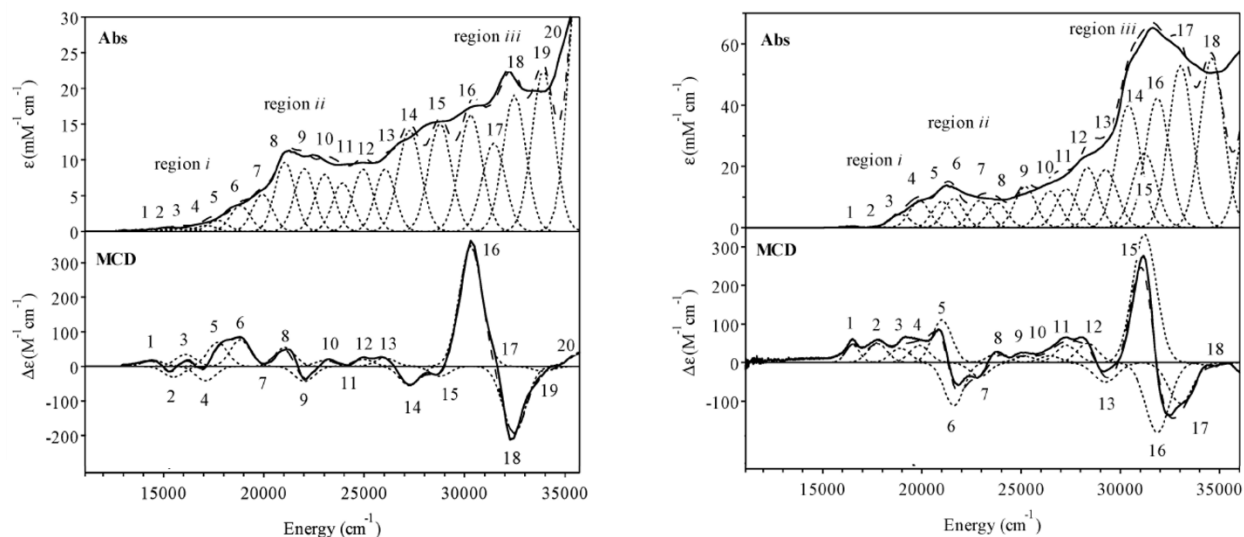


Figure 1.4. Abs and MCD spectra (solid lines) of Co(II)Cbl (left) and Co(II)Cbi⁺ (right). Dashed lines are sums of individual Gaussian bands (dotted lines) produced through an iterative Gaussian deconvolution of the spectra.⁴²

1.2.3. Vibrational Properties. In the early 1970s, several groups reported the first rR spectra of numerous Cbl and Cbi species, including AdoCbl, MeCbl, CNCbl, OHCbl, H₂OCbl⁺, MeCbi⁺, (CN)₂Cbi, and Co(II)Cbl.⁵⁸⁻⁶¹ However, laser-induced photolysis of the Co–C bond of alkylCbIs limited the scope of early rR studies to the analysis of corrin stretching modes. The Co–C stretch of MeCbl was not detected until 1990,⁶² when Marzilli and Yu used Fourier-transform (FT) Raman spectroscopy with non-resonant, near-IR laser excitation to prevent photolysis.⁶³ This technique was later applied to a series of Cbxs with variable axial coordination, and it was demonstrated that the lower axial ligand has no electronic influence and only a minimal steric influence on the force constant of the Co–C bond *trans* to it.⁶⁴ Several years later, Spiro developed a cryogenic rR technique⁶⁵ that prevented photolysis and allowed for the detection of the Co–C stretching mode of AdoCbl. As predicted by the FT-Raman spectra of Cbxs, the Co–C stretching frequency of alkylCbIs is relatively insensitive to the protonation and subsequent replacement of the DMB by a water molecule at low pH.⁶⁶ This observation, which agrees with

previous NMR studies of AdoCbl with⁶⁷ and without⁶⁸ DMB bound, may seem surprising given the fact that displacement of the DMB does affect the Co–C BDE and bond homolysis rate constant of AdoCbl.⁶⁹ However, it is feasible that the change in BDE is due entirely to differences in the relative stability of the Co(II)Cbl state, thus leaving the potential energy curve associated with the Co–C stretch unperturbed near its minimum.

Brunold and coworkers further investigated the vibrational properties of Co(III)Cbls and Co(III)Cbis by collecting rR spectra and excitation profiles for key vibrational features.^{41, 42} The rR spectrum of H₂OCbl⁺ was found to be quite similar to that of MeCbl, indicating that the identity of the upper axial ligand has a minimal effect on the frequencies and compositions of the corrin-centered stretching modes that dominate the rR spectra of these species. The rR excitation profiles were used to determine the polarizations of electronic transitions, which greatly aided in the assignment of the dominant features in the corresponding Abs, CD, and MCD spectra. Importantly, the observed resonance enhancement of the Co–C stretch upon excitation into the α/β bands provided direct evidence that the corresponding electronic transition contains considerable MLCT character. Quite recently, rR excitation profiles for CNCbl, Co(II)Cbl, and the “super-reduced” Co(I)Cbl[–] were used in conjunction with TD-DFT to establish the most comprehensive assignment of the corrin-based vibrational features to date.⁷⁰

1.2.4 EPR Spectroscopy. While Co(III)Cbls and Co(III)Cbis are diamagnetic, a wealth of information can be obtained from EPR studies of their one-electron reduced forms, Co(II)Cbl⁷¹ and Co(II)Cbi⁺.⁷² As the singly occupied MO of Co(II)Cbl is primarily Co 3d_{z²}-based,⁴² EPR spectroscopy serves as an excellent probe of the interaction between the Co(II) ion and its axial DMB ligand, particularly through the hyperfine coupling between the unpaired electron and the nuclear spins of the Co(II) ion ($I = 7/2$ for ⁵⁹Co) and the axial N ($I = 1$ for ¹⁴N). In general, an

increase in covalency or decrease in length of the Co–N_{ax} bond will decrease the superhyperfine coupling to the Co(II) nucleus while increasing the “superhyperfine” coupling to the N_{ax} nucleus. Thus, changes to the Co–N_{ax} bond length in AdoCbl-dependent enzymes can be detected through measurement of hyperfine couplings, and the creative use of isotopic labeling permits identification of the axial base in the absence of structural data.⁷³

1.3 AdoCbl-Dependent Enzymes

Although all known AdoCbl-dependent enzymes share the same general mechanism (*vide supra*), they can be categorized into two distinct classes on the basis of the reactions they catalyze and the mode of cofactor binding. Class I isomerases⁷⁴ catalyze the rearrangement of carbon skeletons and the migration of amino groups. Isomerases that catalyze the latter type of reaction, also known as the aminomutases, are further distinguished by the requirement for a second cofactor, pyridoxal 5'-phosphate (PLP, vitamin B₆). All isomerases bind AdoCbl by displacing the DMB ligand and replacing it with a protein-derived His residue. The coordinating His participates in a hydrogen bonding network with conserved aspartate and lysine/asparagine residues that are part of a conserved DXHXGXX motif^{18, 75, 76} (or DXHXGXN, in one isomerase). The Class II eliminases^{13, 77} differ from the isomerases with respect to the types of substrates and the AdoCbl binding mode utilized. The eliminases all catalyze the rearrangement of 1,2-diols or 1,2-aminoalcohols to place both functional groups on a terminal carbon, which leads to the spontaneous elimination of either water or ammonia to form an aldehyde. Unlike the isomerases, the eliminases bind the cofactor in the “DMB-on” state. Crystal structures of eliminases have revealed the presence of a salt bridge between an arginine side chain and the negatively charged phosphate of AdoCbl, a feature that is missing from the isomerases.

To date, the implications of these different binding modes for the mechanisms by which enzymes accomplish Co–C bond homolysis have not been conclusively determined. Recent research addressing these questions is reviewed in the subsections below, with an emphasis on kinetic, spectroscopic, and computational studies of AdoCbl-dependent enzymes that have provided insight into the mechanism of Co–C bond activation employed by isomerases and eliminases.

1.3.1 AdoCbl-Dependent Isomerases. The first AdoCbl-dependent isomerase to be identified was glutamate mutase (GM), which is responsible for the conversion of glutamate to 3-methylaspartate in the first step of the bacterial fermentation of glutamate.⁷⁸ GM and methylmalonyl-CoA mutase (MMCM),⁷⁹ which converts methylmalonyl-CoA to succinyl-CoA and is the only known human AdoCbl-dependent enzyme, are by far the best-studied isomerases. Other carbon-skeleton mutases include 2-methyleneglutarate mutase (MGM)⁷⁶ and isobutyryl-CoA mutase.⁸⁰ The remaining class I enzymes are aminomutases,⁸¹ such as ornithine-4,5-aminomutase (OAM)⁸² and lysine 5,6-aminomutase (LAM).⁸³ In these latter enzymes, the substrate reacts with the PLP cofactor to form an aldimine (i.e., R–CH=NH–R') intermediate, the species from which the adenosyl radical generated by Co–C bond homolysis abstracts a hydrogen atom. The inclusion of PLP necessitates differences in some mechanistic steps for the carbon-skeleton mutases and aminomutases.⁸⁴ However, as the role of PLP appears to be related to activation of the substrate, and since the interaction between the PLP and AdoCbl cofactors appears to be minimal, it is likely that both of these sub-classes of isomerases function in a similar manner with regards to Co–C bond activation.

Crystal structures have been solved for GM,⁸⁵⁻⁸⁷ MMCM,^{30, 88, 89} OAM,⁹⁰ and LAM,⁹¹ many in the presence of AdoCbl, substrate, and/or analogues thereof. The earliest structures

provided the first conclusive evidence of the cofactor's DMB-off, His-on binding mode, although they revealed erroneously long Co—N_{ax} bond lengths. The wealth of structural data for isomerases also provides information about changes in protein conformation induced by substrate binding. All AdoCbl-dependent enzymes undergo substantial geometric changes when the substrate binds,⁹² but these are particularly notable in the isomerases because of the cofactor's position at the interface of two distinct secondary structure motifs. The inherent flexibility that comes from having the cofactor and substrate bind at this interface allows for a significant rearrangement of the active site upon substrate binding, as observed in multiple crystal structures of isomerases and predicted computationally.^{93, 94}

The isomerase crystal structures also allowed for the identification of potentially important active site residues, prompting a number of site-directed mutagenesis studies to assess the importance of individual amino acids. Most studies have focused on residues implicated in the binding of substrate, such as E171⁹⁵ and R100⁹⁶ in GM and H225 in OAM.⁹⁷ Vlasie et al. investigated a tyrosine residue (Y89) in MMCM that undergoes the largest movement upon substrate binding to that enzyme.⁹⁸ Crystal structures of MMCM in the absence and presence of substrate⁸⁸ had suggested that movement of Y89 induced by substrate binding repositions the adenine moiety of the Ado ligand. Thus, Y89 was proposed to act as a “molecular wedge,” destabilizing the AdoCbl ground state. While the authors did find that the Y89A and Y89F variants were less active than WT MMCM by about a factor of 10³, destabilization of the Co—C bond by this means seems relatively unimportant based on the lack of spectroscopic evidence of perturbations to AdoCbl in the presence of substrate.⁹⁹ Moreover, aristeromycylcobalamin, in which the upper axial ligand is a carbocyclic analogue of Ado, is not a competent cofactor in MMCM.¹⁰⁰ That such a sterically conservative modification can cause a complete loss of activity

suggests that the role of Y89 has less to do with its bulkiness than its electrostatic interaction with the Ado ligand. A similar role has been proposed for a conserved glutamate residue (E338 in OAM,¹⁰¹ E392 in MMCM,¹⁰¹ E330 in GM¹⁰²) that appears to form hydrogen bonds to each of the –OH groups of the Ado ligand, thus imposing a specific orientation of that ligand in the active site.

While amino acids that interact with the Ado ligand and substrate are clearly essential for Co–C bond activation, several studies have addressed the importance of the observed His-on coordination of AdoCbl. Replacement of the coordinating His (H16 in GM,¹⁰³ H610 in MMCM,¹⁰⁴ H485 in MGM¹⁰⁵) with Gln or Asn results in near-complete loss of activity, despite the fact that base-off AdoCbl analogues can bind strongly to these enzymes (*vide infra*). Similarly, even a conservative Asp to Glu substitution affecting the DXHXGXX motif was found to reduce activity more than 100-fold,^{103, 105} suggesting that the electron-donating ability of the His ligand is modulated by the conserved hydrogen-bonding network, which in turn affects the Co–C bond *trans* to it.^{57, 106}

While site-directed mutagenesis studies have provided clues regarding the importance of individual amino acid residues, cofactor analogues have been used to identify the structural features of AdoCbl that are critical for catalytic activity. This line of research has focused primarily on investigating the effects of changes to the cofactor's Ado ligand, nucleotide loop, and DMB ligand. It was shown that Cbi species lacking the nucleotide loop present in AdoCbl (AdoCbi⁺ and AdoCbi⁺ methyl phosphate, which differ by the absence and presence of the phosphate group, respectively) do not undergo His coordination upon binding to MMCM, nor are they capable of supporting enzyme activity.¹⁰⁷ Interestingly, a third Cbi derivative (AdoCbi⁺-GDP) was found to be a competent cofactor of MMCM despite remaining His-off, a finding that demonstrates the importance of the nucleotide loop for enzyme activity.¹⁰⁸ Similarly, an AdoCbl analogue in which

the DMB was replaced with a tolyl group without any modification of the nucleotide loop was shown to support catalytic activity in both GM and MMCM.¹⁷

An additional method of studying the interactions between cofactor, enzyme, and substrate is the spectroscopic characterization of enzyme-bound AdoCbl and Co(II)Cbl. Since these compounds have been thoroughly characterized, perturbations (or lack thereof) to their electronic or vibrational spectra that accompany their binding to the enzyme or the addition of substrate to the holoenzyme can be interpreted in the context of previously-made assignments. For example, Dong et al. used cryogenic rR spectroscopy to show that the binding of AdoCbl to GM and MMCM minimally affects the Co–C stretching frequency and, thus, the Co–C bond strength.^{33, 34} Subsequently, researchers in the Brunold lab used computational methods to interpret the Abs, CD, MCD, rR, and EPR spectra of AdoCbl and Co(II)Cbl bound to GM¹⁰⁹ and MMCM^{99, 106} in the absence and presence of substrate analogues. Their analysis revealed no significant electronic structural difference between free AdoCbl and AdoCbl bound to GM or MMCM in the absence or presence of substrate analogues. However, the binding of Co(II)Cbl to GM and MMCM induced moderate blue-shifts of electronic transitions known to have MLCT character (*vide supra*), an observation consistent with stabilization of the manifold of Co 3d orbitals. The addition of substrate to either of these holoenzymes resulted in further blue-shifts of these transitions. These results were interpreted to indicate that isomerases accelerate the rate of Co–C bond homolysis at least in part via stabilization of the Co(II)Cbl post-homolysis product.

Computational investigations of AdoCbl-dependent isomerases have been instrumental in complementing these experimental studies. However, the empirical nature of DFT and the necessary approximations built into methods like quantum mechanical/molecular mechanical (QM/MM) geometry optimizations make conclusions based on theoretical premises alone

tentative, as the distinction between technical artifact and physically significant observation is rarely clear in the absence of corroborating experimental evidence. QM/MM studies of MMCM¹¹⁰⁻¹¹² and GM¹¹³ have generally attempted to determine whether or not the enzyme active sites place any strain on the AdoCbl or Co(II)Cbl structures, as well as to evaluate if this strain can be offset to some degree by favorable electrostatic interactions between the cofactor and the enzyme or substrate. These computations have allowed for the identification of important amino acid residues that might not be readily obvious from X-ray structural data alone. Despite this apparent success, the fact that the theoretical results have rarely been validated on the basis of experimental data, as well as the lack of agreement among these studies regarding the relative importance of AdoCbl destabilization and transition state stabilization, has limited their impact. Note that several detailed computational investigations of the aminomutases have also been published in recent years,^{93, 114, 115} but these have mainly focused on the role of the substrate, PLP cofactor, and large-scale protein motions rather than the AdoCbl cofactor.

1.3.2 AdoCbl-dependent Eliminases. Three eliminases have been extensively studied in recent decades: diol dehydratase (DD), glycerol dehydratase (GD), and ethanolamine ammonia lyase (EAL). The former two share many structural similarities^{19, 32, 116-118} and can utilize the same substrates (glycerol, 1,2-propanediol, and 1,2-ethanediol), but differ with respect to their affinities for those substrates. EAL is used to convert ethanolamine to acetaldehyde and ammonia, compounds that serve as a metabolic intermediate and a nitrogen source, respectively.^{119, 120} Crystal structures of DD,^{32, 116, 117} GD,^{19, 118} and EAL¹²¹ show significant similarities in the AdoCbl- and substrate-binding sites, although DD and GD require the presence of a Ca²⁺ ion to bind the cofactor.¹²² In the case of EAL¹²¹ and DD,¹¹⁶ the use of adeninylpentylcobalamin (AdePeCbl, Figure 1.5), an inactive cofactor analogue in which the ribosyl moiety of the Ado

ligand is replaced with a pentamethylene $-(CH_2)_5-$ group, revealed that the two enzymes have nearly identical adenine-binding sites. Of particular importance is the presence of five hydrogen bonds between the Ado ligand's adenine ring and the protein, which help lock that portion of the cofactor into a specific conformation. The simultaneous imposition of geometric constraints on the lower half of the cofactor (e.g., through the formation of a salt bridge with the AdoCbl phosphate group) could cause the Co–C bond to lengthen in order to accommodate this strain.

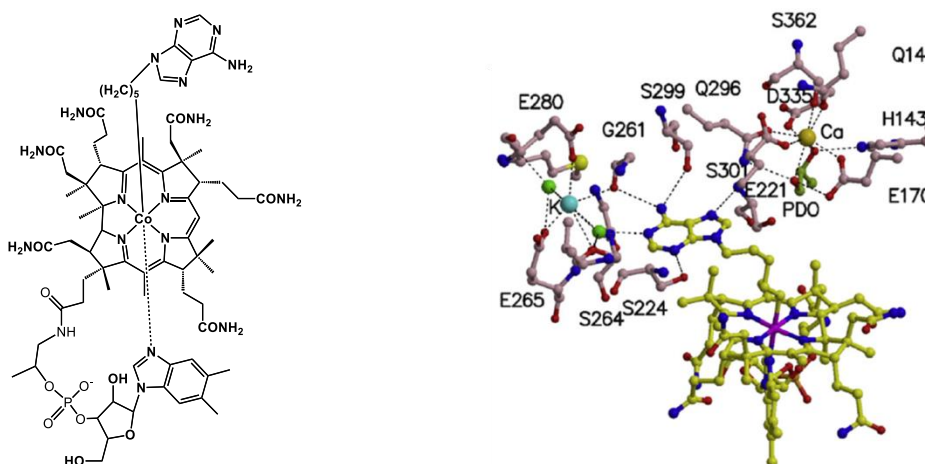


Figure 1.5. Line drawing of AdePeCbl (left), and structure of AdePeCbl in the active site of DD (right).¹¹⁶ Residues in the substrate- (1,2-propanediol, PDO) and adenine-binding sites are labeled.

This hypothesis is supported by the many kinetics studies of cofactor analogues with modifications to the Ado ligand. AdoCbl analogues in which the Ado ribosyl moiety is replaced by an alkyl spacer have no coenzymic activity, although partial coenzyme activity (up to ~30%) is shown by those that feature a five-membered ring, even if the ring lacks one of the hydrogen-bonding sites that the native ribosyl moiety has.^{123, 124} Introduction of methylene or dimethylene spacers between the Co and the adenosyl ligand also inhibit enzyme-induced Co–C bond homolysis,¹²⁵ possibly because increases in the cofactor's flexibility will allow these analogues to satisfy the geometric constraints described above without elongating the Co–C bond. Meanwhile, changes anywhere in the adenine ring cause a substantial loss of activity and weaker

binding.^{126, 127} The importance of the hydrogen bonding between protein and this part of the cofactor has also been demonstrated by site-directed mutagenesis.¹²⁸

Cofactor analogue studies have also demonstrated the importance of AdoCbl's lower axial ligand for enzymatic function in the eliminases. Replacement of the DMB ligand with pyridine results in tighter cofactor binding but a decrease in k_{cat} by about a factor of 4;¹²⁹ later studies using benzimidazole and imidazole ligands¹³⁰ provided further evidence that the incorporation of altered bases can cause activity to drop significantly. Also, substitution of the nucleotide loop with a $-(\text{CH}_2)_n-$ spacer leads to a complete loss of activity unless $n = 3$ or $n = 4$, in which case a moderate decrease in k_{cat} and either a minimal ($n = 3$) or substantial ($n = 4$) increase in K_M are observed.¹³¹ The implication of these results is that the size of the nucleotide loop and identity of the lower axial ligand affect the ability of the enzyme to bind the cofactor and promote Co–C bond homolysis. This conclusion is entirely consistent with the imposition of rigid constraints on the native cofactor in the eliminase holoenzymes suggested by the crystallographic and kinetic studies described above.

The changes to eliminase active sites induced by the binding of substrate have been studied primarily through site-directed mutagenesis. Like the cofactor's Ado ligand, the substrates of these enzymes engage in multiple strong hydrogen bonding and electrostatic interactions with the protein and, in the case of DD and GD, the Ca^{2+} ion found in the active site. Crystal structures of EAL have revealed five residues directly involved in binding substrate, and alanine substitution at any of these sites results in the loss of at least 97% of EAL's activity. Similarly, three DD amino acids (for H143,¹³⁴ E170,¹³⁵ and D335¹³⁵) involved in binding substrate are essential for that enzyme's function. The loss of activity may be explained by the inability of the altered active site to adopt the appropriate conformation for Co–C bond activation. This hypothesis is supported by

the crystal structures of DD and EAL, which revealed that the WT enzymes undergo large-scale conformational changes in response to substrate binding,⁹² although there is some spectroscopic evidence suggesting that AdoCbl itself is not strongly perturbed by the binding of substrate.¹³⁶ Computational studies of DD have also been essential for predicting the effect of substitutions of residues that bind substrate^{137, 138} and for the identification of the Ca^{2+} ion present in that enzyme's active site (previously thought to be a K^+ ion).¹³⁹

1.4 Summary and Organization of this Thesis

A vast number of spectroscopic, crystallographic, kinetic, and computational studies have been undertaken to improve our knowledge of how the Co–C bond is affected by AdoCbl-dependent enzymes. At the time of this writing, it appears that AdoCbl-dependent isomerases and eliminases may achieve this activation by different means. Class I isomerases likely achieve Co–C bond activation primarily through stabilization of the Co(II)Cbl and Ado^\bullet post-homolysis products, while destabilization of AdoCbl is the currently favored mechanism for Class II eliminases. Even as consensus regarding these general mechanisms develops, the precise roles of active-site amino acid residues and the specific interactions between enzyme, cofactor, and substrate that lead to the remarkable acceleration of Co–C bond homolysis remain incompletely understood. In the research summarized in the following three chapters, a combined spectroscopic/computational methodology is used to evaluate possible roles for the conserved DXHXGXX motif in isomerases and specific active-site residues in EAL.

- Chapter 2 presents a combined spectroscopic/computational investigation of Cbl and Cbi species with variable axial coordination. This study correlates the electron-donating capability of the lower axial ligand with the energies of MLCT transitions of Co(II)Cbl and its analogues. The MCD spectrum of a Co(II)Cbl analogue in which the

much weaker base 5-fluoroimidazole replaces the DMB ligand closely mimics the spectra of GM- and MMCM-bound Co(II)Cbl. This observation is used to suggest that Co–C bond homolysis in isomerases involves stabilization of Co(II)Cbl through a reduction in charge donation from the coordinating His residue.

- Chapter 3 describes a combined spectroscopic/computational investigation of AdoCbl bound to EAL in the presence and absence of substrate. This investigation reveals that unlike the AdoCbl-dependent isomerases, EAL perturbs the cofactor's electronic structure when it binds. An experimentally-validated computational model of the EAL holoenzyme was used to propose a mechanism for Co–C bond activation via AdoCbl destabilization.
- Chapter 4 extends the analysis of EAL by describing a computational study of EAL variants and cofactor analogues selected on the basis of the Co–C bond activation mechanism proposed in Chapter 3. The geometric and electronic effects of binding (i) AdoCbl to EAL variants and (ii) AdoCbl analogues to WT EAL were studied. Variants and analogues predicted to have features distinct from those of AdoCbl bound to WT EAL were recommended for future study.
- Chapter 5 describes a preliminary investigation of membrane-bound stearyl-CoA desaturase (SCD), a non-heme diiron enzyme that utilizes O₂ to desaturate long-chain fatty acids with a high degree of regio- and stereoselectivity. The first SCD crystal structure was recently solved, revealing a novel active site with an unusually long Fe–Fe distance, unprecedented among non-heme diiron enzymes. Computational techniques similar to those used in Chapters 2–4 were applied to SCD to determine a likely O₂ binding site and to propose a putative reaction mechanism.

- Chapter 6 addresses the practical matter of performing these computational analyses by describing bulb, a program that facilitates QM/MM geometry optimizations and TD-DFT excited state calculations on large, enzymatic systems. Bulb was written concurrently with the completion of the research presented in this thesis, and was used in the setup and analysis of the majority of the computations discussed in the other chapters. Bulb's program architecture and implicit assumptions are described in this chapter.
- Chapter 7 concludes this work by placing the research described in Chapters 2-6 in their proper context, including a brief analysis of promising avenues for future research in these fields.

1.5 References

1. Rickes, E. L.; Brink, N. G.; Koniuszy, F. R.; Wood, T. R.; Folkers, K., *Science* **1948**, *107*, 396-397.
2. Smith, E. L.; Parker, L. F. J., *The Biochemical journal* **1948**, *43*, viii.
3. Smith, E. L., *Nature [London]* **1948**, *162*, 144-145.
4. Rickes, E. L.; Brink, N. G.; Koniuszy, F. R.; Wood, T. R.; Folkers, K., *Science* **1948**, *108*, 134-134.
5. Barker, H. A.; Weissbach, H.; Smyth, R. D., *Proc Natl Acad Sci* **1958**, *44*, 1093-1097.
6. Lenhert, P. G.; Hodgkin, D. C., *Nature* **1961**, *192*, 937-938.
7. Mera, P. E.; Escalante-Semerena, J. C., *Applied Microbiology and Biotechnology* **2010**, *88*, 41-48.
8. Marsh, E. N. G.; Melendez, G. D. R., *Biochimica Et Biophysica Acta-Proteins and Proteomics* **2012**, *1824*, 1154-1164.
9. Marsh, E. N. G., *Biochemical Society Transactions* **2009**, *37*, 336-342.
10. Banerjee, R.; Ragsdale, S. W., *Annual Review of Biochemistry* **2003**, *72*, 209-247.
11. Brown, K. L., *Chemical Reviews* **2005**, *105*, 2075-2149.
12. Sandala, G. M.; Smith, D. M.; Radow, L., *Accounts of Chemical Research* **2010**, *43*, 642-651.
13. Toraya, T., *Archives of Biochemistry and Biophysics* **2014**, *544*, 40-57.
14. Hay, B. P.; Finke, R. G., *Journal of the American Chemical Society* **1986**, *108*, 4820-4829.
15. Brown, K. L.; Zou, X., *Inorganic Chemistry* **1991**, *30*, 4185-4191.
16. Miyamoto, E.; Watanabe, F.; Yamaji, R.; Inui, H.; Sato, K.; Nakano, Y., *Journal of Nutritional Science and Vitaminology* **2002**, *48*, 242-246.
17. Poppe, L.; Bothe, H.; Broker, G.; Buckel, W.; Stupperich, E.; Retey, J., *Journal of Molecular Catalysis B-Enzymatic* **2000**, *10*, 345-350.
18. Ratnatilleke, A.; Vrijbloed, J. W.; Robinson, J. A., *Journal of Biological Chemistry* **1999**, *274*, 31679-31685.
19. Yamanishi, M.; Yunoki, M.; Tobimatsu, T.; Sato, H.; Matsui, J.; Dokiya, A.; Iuchi, Y.; Oe, K.; Suto, K.; Shibata, N.; Morimoto, Y.; Yasuoka, N.; Toraya, T., *European Journal of Biochemistry* **2002**, *269*, 4484-4494.
20. Bachovchin, W. W.; Eagar, R. G.; Moore, K. W.; Richards, J. H., *Biochemistry* **1977**, *16*, 1082-1092.
21. Brunold, T. C.; Conrad, K. S.; Liptak, M. D.; Park, K., *Coordination Chemistry Reviews* **2009**, *253*, 779-794.
22. Warren, M. J.; Raux, E.; Schubert, H. L.; Escalante-Semerena, J. C., *Natural Product Reports* **2002**, *19*, 390-412.
23. Brescianipahor, N.; Forcolin, M.; Marzilli, L. G.; Randaccio, L.; Summers, M. F.; Toscano, P. J., *Coordination Chemistry Reviews* **1985**, *63*, 1-125.
24. Schrauze, G. N., *Accounts of Chemical Research* **1968**, *1*, 97-&.
25. Schrauzer, G. N.; Kohnle, J., *Chemische Berichte* **1964**, *97*, 3056-3064.
26. Randaccio, L.; Pahor, N. B.; Zangrando, E.; Marzilli, L. G., *Chemical Society Reviews* **1989**, *18*, 225-250.
27. DeRidder, D. J. A.; Zangrando, E.; Burgi, H. B., *Journal of Molecular Structure* **1996**, *374*, 63-83.
28. Randaccio, L.; Geremia, S.; Nardin, G.; Wuerger, J., *Coordination Chemistry Reviews* **2006**, *250*, 1332-1350.
29. De March, M.; Demitri, N.; Geremia, S.; Hickey, N.; Randaccio, L., *Journal of Inorganic Biochemistry* **2012**, *116*, 215-227.
30. Mancina, F.; Keep, N. H.; Nakagawa, A.; Leadlay, P. F.; McSweeney, S.; Rasmussen, B.; Bosecke, P.; Diat, O.; Evans, P. R., *Structure* **1996**, *4*, 339-350.

31. Trommel, J. S.; Warncke, K.; Marzilli, L. G., *Journal of the American Chemical Society* **2001**, *123*, 3358-3366.
32. Shibata, N.; Masuda, J.; Tobimatsu, T.; Toraya, T.; Suto, K.; Morimoto, Y.; Yasuoka, N., *Structure with Folding & Design* **1999**, *7*, 997-1008.
33. Dong, S. L.; Padmakumar, R.; Maiti, N.; Banerjee, R.; Spiro, T. G., *Journal of the American Chemical Society* **1998**, *120*, 9947-9948.
34. Dong, S. L.; Padmakumar, R.; Banerjee, R.; Spiro, T. G., *Journal of the American Chemical Society* **1999**, *121*, 7063-7070.
35. Bonnett, R., *Chemical Reviews* **1963**, *63*, 573-605.
36. Hill, J. A.; Pratt, J. M.; Williams, R. J. P., *Jour Theoret Biol* **1962**, *3*, 423-445.
37. Day, P., *Theoretica Chimica Acta* **1967**, *7*, 328-&.
38. Offenhar.Po; Offenhar.Bh; Fung, M. M., *Journal of the American Chemical Society* **1970**, *92*, 2966-&.
39. Schrauze.Gn; Lee, L. P.; Sibert, J. W., *Journal of the American Chemical Society* **1970**, *92*, 2997-&.
40. Jensen, K. P.; Ryde, U., *Coordination Chemistry Reviews* **2009**, *253*, 769-778.
41. Stich, T. A.; Brooks, A. J.; Buan, N. R.; Brunold, T. C., *Journal of the American Chemical Society* **2003**, *125*, 5897-5914.
42. Stich, T. A.; Buan, N. R.; Brunold, T. C., *Journal of the American Chemical Society* **2004**, *126*, 9735-9749.
43. Liptak, M. D.; Brunold, T. C., *Journal of the American Chemical Society* **2006**, *128*, 9144-9156.
44. Liptak, M. D.; Fleischhacker, A. S.; Matthews, R. G.; Telser, J.; Brunold, T. C., *Journal of Physical Chemistry B* **2009**, *113*, 5245-5254.
45. Conrad, K. S.; Brunold, T. C., *Inorganic Chemistry* **2011**, *50*, 8755-8766.
46. Reig, A. J.; Conrad, K. S.; Brunold, T. C., *Inorganic Chemistry* **2012**, *51*, 2867-2879.
47. Pallares, I. G.; Brunold, T. C., *Inorganic Chemistry* **2014**, *53*, 7676-7691.
48. Lodowski, P.; Jaworska, M.; Kornobis, K.; Andruniow, T.; Kozlowski, P. M., *Journal of Physical Chemistry B* **2011**, *115*, 13304-13319.
49. Solheim, H.; Kornobis, K.; Ruud, K.; Kozlowski, P. M., *Journal of Physical Chemistry B* **2011**, *115*, 737-748.
50. Kornobis, K.; Kumar, N.; Wong, B. M.; Lodowski, P.; Jaworska, M.; Andruniow, T.; Ruud, K.; Kozlowski, P. M., *Journal of Physical Chemistry A* **2011**, *115*, 1280-1292.
51. Kornobis, K.; Kumar, N.; Lodowski, P.; Jaworska, M.; Piecuch, P.; Lutz, J. J.; Wong, B. M.; Kozlowski, P. M., *Journal of Computational Chemistry* **2013**, *34*, 987-1004.
52. Andruniow, T.; Jaworska, M.; Lodowski, P.; Zgierski, M. Z.; Dreos, R.; Randaccio, L.; Kozlowski, P. M., *Journal of Chemical Physics* **2009**, *131*.
53. Liu, H.; Kornobis, K.; Lodowski, P.; Jaworska, M.; Kozlowski, P. M., *Frontiers in chemistry* **2013**, *1*, 41.
54. Harris, D. A.; Stickrath, A. B.; Carroll, E. C.; Sension, R. J., *Journal of the American Chemical Society* **2007**, *129*, 7578-7585.
55. Kuta, J.; Patchkovskii, S.; Zgierski, M. Z.; Kozlowski, P. M., *Journal of Computational Chemistry* **2006**, *27*, 1429-1437.
56. Kuta, J.; Wuerge, J.; Randaccio, L.; Kozlowski, P. M., *Journal of Physical Chemistry A* **2009**, *113*, 11604-11612.
57. Conrad, K. S.; Jordan, C. D.; Brown, K. L.; Brunold, T. C., *Inorganic Chemistry* **2015**, *54*, 3736-3747.
58. Mayer, E.; Gardiner, D. J.; Hester, R. E., *Journal of the Chemical Society-Faraday Transactions II* **1973**, *69*, 1350-1358.
59. Mayer, E.; Gardiner, D. J.; Hester, R. E., *Biochimica Et Biophysica Acta* **1973**, *297*, 568-570.
60. Wozniak, W. T.; Spiro, T. G., *Journal of the American Chemical Society* **1973**, *95*, 3402-3404.
61. Salama, S.; Spiro, T. G., *Journal of Raman Spectroscopy* **1977**, *6*, 57-60.

62. Nie, S. M.; Marzilli, P. A.; Marzilli, L. G.; Yu, N. T., *Journal of the Chemical Society-Chemical Communications* **1990**, 770-771.
63. Nie, S. M.; Marzilli, L. G.; Yu, N. T., *Journal of the American Chemical Society* **1989**, *111*, 9256-9258.
64. Nie, S. M.; Marzilli, P. A.; Marzilli, L. G.; Yu, N. T., *Journal of the American Chemical Society* **1990**, *112*, 6084-6091.
65. Dong, S. L.; Padmakumar, R.; Banerjee, R.; Spiro, T. G., *Journal of the American Chemical Society* **1996**, *118*, 9182-9183.
66. Dong, S. L.; Padmakumar, R.; Banerjee, R.; Spiro, T. G., *Inorganica Chimica Acta* **1998**, *270*, 392-398.
67. Summers, M. F.; Marzilli, L. G.; Bax, A., *Journal of the American Chemical Society* **1986**, *108*, 4285-4294.
68. Bax, A.; Marzilli, L. G.; Summers, M. F., *Journal of the American Chemical Society* **1987**, *109*, 566-574.
69. Hay, B. P.; Finke, R. G., *Journal of the American Chemical Society* **1987**, *109*, 8012-8018.
70. Park, K.; Brunold, T. C., *Journal of Physical Chemistry B* **2013**, *117*, 5397-5410.
71. Harmer, J.; Van Doorslaer, S.; Gromov, I.; Schweiger, A., *Chemical Physics Letters* **2002**, *358*, 8-16.
72. Van Doorslaer, S.; Jeschke, G.; Epel, B.; Goldfarb, D.; Eichel, R. A.; Krautler, B.; Schweiger, A., *Journal of the American Chemical Society* **2003**, *125*, 5915-5927.
73. Abend, A.; Bandarian, V.; Nitsche, R.; Stupperich, E.; Retey, J.; Reed, G. H., *Archives of Biochemistry and Biophysics* **1999**, *370*, 138-141.
74. Banerjee, R., *Chemical Reviews* **2003**, *103*, 2083-2094.
75. Marsh, E. N. G.; Holloway, D. E., *Febs Letters* **1992**, *310*, 167-170.
76. Beatrix, B.; Zelder, O.; Linder, D.; Buckel, W., *European Journal of Biochemistry* **1994**, *221*, 101-109.
77. Toraya, T., *Chemical Reviews* **2003**, *103*, 2095-2127.
78. Barker, H. A.; Rooze, V.; Suzuki, F.; Iodice, A. A., *Journal of Biological Chemistry* **1964**, *239*, 3260-3266.
79. Babior, B. M.; Woodams, A. D.; Brodie, J. D., *Journal of Biological Chemistry* **1973**, *248*, 1445-1450.
80. Brendelberger, G.; Retey, J.; Ashworth, D. M.; Reynolds, K.; Willenbrock, F.; Robinson, J. A., *Angewandte Chemie-International Edition in English* **1988**, *27*, 1089-1091.
81. Wu, B.; Szymanski, W.; Heberling, M. M.; Feringa, B. L.; Janssen, D. B., *Trends in Biotechnology* **2011**, *29*, 352-362.
82. Somack, R.; Costilow, R. N., *Biochemistry* **1973**, *12*, 2597-2604.
83. Baker, J. J.; Vanderdr.C; Stadtman, T. C., *Biochemistry* **1973**, *12*, 1054-1063.
84. Frey, P. A.; Reed, G. H., *Biochimica Et Biophysica Acta-Proteins and Proteomics* **2011**, *1814*, 1548-1557.
85. Tollinger, M.; Konrat, R.; Hilbert, B. H.; Marsh, E. N. G.; Krautler, B., *Structure* **1998**, *6*, 1021-1033.
86. Reitzer, R.; Gruber, K.; Jogl, G.; Wagner, U. G.; Bothe, H.; Buckel, W.; Kratky, C., *Structure with Folding & Design* **1999**, *7*, 891-902.
87. Hoffmann, B.; Konrat, R.; Bothe, H.; Buckel, W.; Krautler, B., *European Journal of Biochemistry* **1999**, *263*, 178-188.
88. Mancia, F.; Evans, P. R., *Structure with Folding & Design* **1998**, *6*, 711-720.
89. Mancia, F.; Smith, G. A.; Evans, P. R., *Biochemistry* **1999**, *38*, 7999-8005.
90. Wolthers, K. R.; Levy, C.; Scrutton, N. S.; Leys, D., *Journal of Biological Chemistry* **2010**, *285*, 13942-13950.
91. Lepore, B. W.; Ruzicka, F. J.; Frey, P. A.; Ringe, D., *Proceedings of the National Academy of Sciences of the United States of America* **2005**, *102*, 13819-13824.

92. Dowling, D. P.; Croft, A. K.; Drennan, C. L., Radical Use of Rossmann and TIM Barrel Architectures for Controlling Coenzyme B-12 Chemistry. In *Annual Review of Biophysics, Vol 41*, Rees, D. C., Ed. Annual Reviews: Palo Alto, 2012; Vol. 41, pp 403-427.
93. Menon, B. R. K.; Fisher, K.; Rigby, S. E. J.; Scrutton, N. S.; Leys, D., *Journal of Biological Chemistry* **2014**, 289, 34161-34174.
94. Brunk, E.; Kellett, W. F.; Richards, N. G. J.; Rothlisberger, U., *Biochemistry* **2014**, 53, 3830-3838.
95. Madhavapeddi, P.; Marsh, E. N. G., *Chemistry & Biology* **2001**, 8, 1143-1149.
96. Patwardhan, A.; Marsh, E. N. G., *Archives of Biochemistry and Biophysics* **2007**, 461, 194-199.
97. Makins, C.; Miros, F. N.; Scrutton, N. S.; Wolthers, K. R., *Bioorganic Chemistry* **2012**, 40, 39-47.
98. Vlasie, M. D.; Banerjee, R., *Journal of the American Chemical Society* **2003**, 125, 5431-5435.
99. Brooks, A. J.; Vlasie, M.; Banerjee, R.; Brunold, T. C., *Journal of the American Chemical Society* **2004**, 126, 8167-8180.
100. Weigl, U.; Heimberger, M.; Pierik, A. L.; Retez, J., *Chemistry-a European Journal* **2003**, 9, 652-660.
101. Makins, C.; Pickering, A. V.; Mariani, C.; Wolthers, K. R., *Biochemistry* **2013**, 52, 878-888.
102. Roman-Melendez, G. D.; von Glehn, P.; Harvey, J. N.; Mulholland, A. J.; Marsh, E. N. G., *Biochemistry* **2014**, 53, 169-177.
103. Chen, H. P.; Marsh, E. N. G., *Biochemistry* **1997**, 36, 7884-7889.
104. Vlasie, M.; Chowdhury, S.; Banerjee, R., *Journal of Biological Chemistry* **2002**, 277, 18523-18527.
105. Pierik, A. J.; Ciceri, D.; Lopez, R. F.; Kroll, F.; Broker, G.; Beatrix, B.; Buckel, W.; Golding, B. T., *Biochemistry* **2005**, 44, 10541-10551.
106. Brooks, A. J.; Vlasie, M.; Banerjee, R.; Brunold, T. C., *Journal of the American Chemical Society* **2005**, 127, 16522-16528.
107. Chowdhury, S.; Banerjee, R., *Biochemistry* **1999**, 38, 15287-15294.
108. Chowdhury, S.; Thomas, M. G.; Escalante-Semerena, J. C.; Banerjee, R., *Journal of Biological Chemistry* **2001**, 276, 1015-1019.
109. Brooks, A. J.; Fox, C. C.; Marsh, E. N. G.; Vlasie, M.; Banerjee, R.; Brunold, T. C., *Biochemistry* **2005**, 44, 15167-15181.
110. Freindorf, M.; Kozlowski, P. M., *Journal of the American Chemical Society* **2004**, 126, 1928-1929.
111. Kwiecien, R. A.; Khavrutskii, I. V.; Musaev, D. G.; Morokuma, K.; Banerjee, R.; Paneth, P., *Journal of the American Chemical Society* **2006**, 128, 1287-1292.
112. Li, X.; Chung, L. W.; Paneth, P.; Morokuma, K., *Journal of the American Chemical Society* **2009**, 131, 5115-5125.
113. Jensen, K. P.; Ryde, U., *Journal of the American Chemical Society* **2005**, 127, 9117-9128.
114. Pang, J. Y.; Scrutton, N. S.; Sutcliffe, M. J., *Chemistry-a European Journal* **2014**, 20, 11390-11401.
115. Maity, A. N.; Ke, S. C., *Computational and Theoretical Chemistry* **2013**, 1022, 1-5.
116. Masuda, J.; Shibata, N.; Morimoto, Y.; Toraya, T.; Yasuoka, N., *Structure with Folding & Design* **2000**, 8, 775-788.
117. Shibata, N.; Masuda, J.; Morimoto, Y.; Yasuoka, N.; Toraya, T., *Biochemistry* **2002**, 41, 12607-12617.
118. Liao, D. I.; Dotson, G.; Turner, I.; Reiss, L.; Emptage, M., *Journal of Inorganic Biochemistry* **2003**, 93, 84-91.
119. Bradbeer, C., *Journal of Biological Chemistry* **1965**, 240, 4675-&.
120. Chang, G. W.; Chang, J. T., *Nature* **1975**, 254, 150-151.
121. Shibata, N.; Tamagaki, H.; Hieda, N.; Akita, K.; Komori, H.; Shomura, Y.; Terawaki, S.; Mori, K.; Yasuoka, N.; Higuchi, Y.; Toraya, T., *Journal of Biological Chemistry* **2010**, 285, 26484-26493.

122. Toraya, T.; Honda, S.; Mori, K., *Biochemistry* **2010**, *49*, 7210-7217.
123. Toraya, T.; Ushio, K.; Fukui, S.; Hogenkamp, H. P. C., *Journal of Biological Chemistry* **1977**, *252*, 963-970.
124. Ichikawa, M.; Toraya, T., *Biochimica Et Biophysica Acta* **1988**, *952*, 191-200.
125. Fukuoka, M.; Nakanishi, Y.; Hannak, R. B.; Krautler, B.; Toraya, T., *Febs Journal* **2005**, *272*, 4787-4796.
126. Ushio, K.; Fukui, S.; Toraya, T., *Biochimica Et Biophysica Acta* **1984**, *788*, 318-326.
127. Toraya, T.; Matsumoto, T.; Ichikawa, M.; Itoh, T.; Sugawara, T.; Mizuno, Y., *Journal of Biological Chemistry* **1986**, *261*, 9289-9293.
128. Ogura, K.; Kunita, S.; Mori, K.; Tobimatsu, T.; Toraya, T., *Febs Journal* **2008**, *275*, 6204-6216.
129. Toraya, T.; Miyoshi, S.; Mori, M.; Wada, K., *Biochimica Et Biophysica Acta-Protein Structure and Molecular Enzymology* **1994**, *1204*, 169-174.
130. Fukuoka, M.; Yamada, S.; Miyoshi, S.; Yamashita, K.; Yamanishi, M.; Zou, X.; Brown, K. L.; Toraya, T., *Journal of Biochemistry* **2002**, *132*, 935-943.
131. Toraya, T.; Ishida, A., *Journal of Biological Chemistry* **1991**, *266*, 5430-5437.
132. Mori, K.; Oiwa, T.; Kawaguchi, S.; Kondo, K.; Takahashi, Y.; Toraya, T., *Biochemistry* **2014**, *53*, 2661-2671.
133. Chen, Z. G.; Zietek, M. A.; Russell, H. J.; Tait, S.; Hay, S.; Jones, A. R.; Scrutton, N. S., *Chembiochem* **2013**, *14*, 1529-1533.
134. Kinoshita, K.; Kawata, M.; Ogura, K.-i.; Yamasaki, A.; Watanabe, T.; Komoto, N.; Hieda, N.; Yamanishi, M.; Tobimatsu, T.; Toraya, T., *Biochemistry* **2008**, *47*, 3162-3173.
135. Kawata, M.; Kinoshita, K.; Takahashi, S.; Ogura, K.; Komoto, N.; Yamanishi, M.; Tobimatsu, T.; Toraya, T., *Journal of Biological Chemistry* **2006**, *281*, 18327-18334.
136. Robertson, W. D.; Wang, M.; Warncke, K., *Journal of the American Chemical Society* **2011**, *133*, 6968-6977.
137. Kamachi, T.; Toraya, T.; Yoshizawa, K., *Journal of the American Chemical Society* **2004**, *126*, 16207-16216.
138. Kamachi, T.; Toraya, T.; Yoshizawa, K., *Chemistry-a European Journal* **2007**, *13*, 7864-7873.
139. Kamachi, T.; Takahata, M.; Toraya, T.; Yoshizawa, K., *Journal of Physical Chemistry B* **2009**, *113*, 8435-8438.

CHAPTER 2

***Spectroscopic and Computational Studies of Cobalamin
Species with Variable Lower Axial Ligation:
Implications for the Mechanism of Co–C Bond
Activation by Class I Cobalamin-Dependent Isomerases***

Reprinted with permission from: Conrad, K.S.; Jordan, C.D.; Brown, K.L.; Brunold, T.C. *Inorganic Chemistry*, **2015**, 54, 3736-3747. Copyright 2015, American Chemical Society.

MCD spectra were collected by K. Conrad; adenosyl(5-fluoroimidazole)cobalamin was provided by T. Chandra.

2.1 Introduction

Coenzyme B₁₂ (5'-deoxyadenosylcobalamin, AdoCbl) has attracted extensive scientific interest due to its complex structure and biological role in initiating rearrangement reactions that proceed via a radical mechanism.¹⁻³ AdoCbl-dependent enzymes play important roles in fermentation and catabolism,^{4,5} and are found mostly in bacteria. In humans, the only enzyme requiring AdoCbl for activity is methylmalonyl-CoA mutase (MMCM).⁶ AdoCbl consists of a six-coordinate, low-spin Co(III) ion ligated equatorially by four nitrogens of a tetrapyrrolic corrin macrocycle and coordinated axially by a 5'-deoxyadenosyl group in the upper (β) position and a dimethylbenzimidazole base (DMB) in the lower (α) position (Figure 2.1). The DMB base is also covalently bound to a side chain of the corrin ring through a nucleotide loop. In biological systems, the radical reactions involving AdoCbl are initiated by enzyme-induced homolytic cleavage of the cofactor's Co-C bond. The rate by which AdoCbl-dependent enzymes accelerate Co-C bond homolysis is remarkable (~12 orders of magnitude, corresponding to a lowering of the bond dissociation energy by about 17 kcal/mol).^{7,8} The products of this homolysis reaction are a 5-coordinate Co(II)Cbl species and an adenosyl radical (Ado•). The Ado• radical abstracts a hydrogen atom from the substrate molecule to form 5'-deoxyadenosine and a substrate-based radical. Rearrangement of this radical species, followed by re-abstraction of the hydrogen from adenosine, leads to the formation of product. Once the product is released, Ado• and Co(II)Cbl combine to regenerate AdoCbl and close the catalytic cycle.

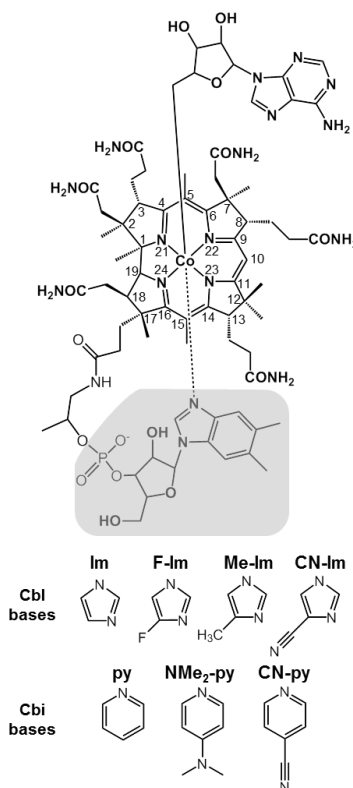


Figure 2.1. Structure of AdoCbl and α -axial ligands used in this study. Note that in cobinamides, the shaded region including the nucleotide loop and native DMB ligand are missing. The coordinating nitrogen in the imidazole bases is proximate to the substituent.

Two classes of AdoCbl-dependent isomerases exist that differ with respect to the mode by which the cofactor binds to the enzyme active site. Class I isomerases,¹ which include MMCM, replace the lower axial DMB ligand with a protein-derived histidine (His) residue, so as to bind the cofactor in a “His-on” manner. This coordinating histidine always participates in a hydrogen bonding network as part of a nearly completely-conserved DXHXGXX sequence.^{9,10} (In one class I enzyme, 2-methyleneglutarate mutase, the AdoCbl-binding sequence is DXHXGXN.)¹¹ Alternatively, Class II eliminases^{2,12} retain the axial DMB coordination upon incorporation of the cofactor into the enzyme active site, thus binding it in a “DMB-on” fashion.

While cofactor analogues with modified lower axial ligands can retain most of their activity in Class I enzymes,^{13,14} even when they do not exhibit His coordination,¹⁵ mutation of the

coordinating His¹⁶⁻¹⁸ or its hydrogen bonding partners^{16,17} causes a dramatic loss in activity. Despite this evidence for the importance of the lower axial ligand environment, most experimental investigations¹⁹⁻²⁴ of B₁₂-dependent isomerases have focused on the interaction between the protein, its substrate, and the cofactor's upper axial ligand. Thus, the means by which the His and its conserved hydrogen bonding partners contribute to catalysis have not yet been determined.

In principle, enzymatic activation of the cofactor's Co–C bond may be achieved via a combination of two fundamentally different mechanisms. In one mechanism,^{25,26} the protein activates this bond by destabilizing the six-coordinate AdoCbl reactant state by imposing geometric and/or electronic constraints within the active site. Alternatively, in the other mechanism,²⁷ the enzyme stabilizes the 5-coordinate Co(II)Cbl and Ado[•] post-homolysis products through favorable hydrogen bonding and/or electrostatic interactions within the active site. While both mechanisms may contribute to a lowering of the Co–C bond homolysis barrier, the importance of the latter mechanism is supported by previous spectroscopic and computational investigations from our laboratory^{28,29} and several other studies,^{20,23,30-32} including recent computational work on MMCM.³³

Spectroscopic studies of the glutamate mutase (GM)²⁹ and MMCM^{28,34} Class I enzymes have led to the proposal that the post-homolysis product stabilization is achieved, in part, by a relatively uniform stabilization of the Co 3d-based molecular orbitals (MOs) of Co(II)Cbl bound to these proteins. This stabilization was particularly apparent in the corresponding magnetic circular dichroism (MCD) spectra, which showed that binding of Co(II)Cbl to GM and MMCM induced noticeable blue-shifts of features in a region of the spectrum that is dominated by metal-to-ligand charge transfer (MLCT) transitions, while the ligand field (LF) and corrin-based p→p* transitions displayed negligible shifts. Alternatively, the MCD spectra of free and GM- or

MMCM-bound AdoCbl were found to be nearly identical, indicating that enzyme-induced perturbations to the electronic structure of AdoCbl are relatively minor.^{29,34}

The means by which the Co 3d-based MOs of enzyme-bound Co(II)Cbl are tuned by Class I isomerases, and to what extent the α -axial ligand contributes to this tuning, remains an open question. One possibility is the coupling of the Co–C bond homolysis step to proton uptake by the His, Asp, Lys triad in the conserved DXHXGXX motif that provides the α -axial His ligand in both MMCM and GM.³⁵ Coupling of Co–C bond homolysis to proton uptake would reduce charge donation from the axial His ligand to the cobalt ion in enzyme-bound Co(II)Cbl, thus stabilizing this state. Such a mechanism is reminiscent of Pratt’s “molecular switch” postulate, which theorized that changes in protein conformation – or, in this case, protonation – could thermodynamically favor certain states.^{36,37} To evaluate the effect of reducing the donor strength of the α -axial ligand on the rate of Co–C bond homolysis, Brown and coworkers prepared a unique analogue of AdoCbl, adenosyl(5-fluoroimidazole)cobalamin [Ado(F-Im)Cbl], that possesses a 5-fluoroimidazole in the α -axial position. They found that when the Ado(F-Im)Cbl analogue was used as a cofactor in ribonucleoside triphosphate reductase (RNTR), which binds AdoCbl in the “DMB-on” form, k_{obs} dropped ~65-fold from the value obtained with adenosyl(imidazole)cobalamin (AdoImCbl) and over 300-fold from that of the native (i.e., AdoCbl-bound) enzyme.³⁸ This reduction in catalytic efficiency led to the suggestion that the low basicity of F-Im³⁹ ($\text{pK}_{\text{b}} = 11.6$) relative to that of Im⁴⁰ ($\text{pK}_{\text{b}} = 7.2$) is responsible for the enhanced stability of the Co–C bond in RNTR-bound Ado(F-Im)Cbl.⁴¹

Previous computational studies have established a weak dependence of the Co–C bond dissociation energy on the basicity of the trans α -axial base.⁴² The question of whether the Co–N_{ax} bond length correlates with the energy required for the homolytic cleavage of the Co–C bond was

initially raised when hyper-long Co-N_{ax} bonds were observed in the X-ray crystal structures of MMCM-bound AdoCbl⁴³ and subsequent EXAFS spectroscopic studies.⁴⁴ However, computations have revealed that the length of the Co-N_{ax} bond has only minor effects on the energy required for Co-C bond homolysis; thus, elongation of the Co-N_{ax} bond alone cannot account for the extent of enzymatic activation.⁴⁵ Nevertheless, the unique nature of the C-Co-N_{ax} axial bonding scheme, with its competing σ and π effects has continued to be the subject of a variety of computational,⁴⁶⁻⁴⁹ kinetic,⁵⁰ and spectroscopic^{51,52} studies.

In the present study, we have characterized Ado(F-Im)Cbl and its one-electron reduced form, Co(II)(F-Im)Cbl, by using electronic absorption (Abs) and magnetic circular dichroism (MCD) spectroscopies. To complement our experimental data, we carried out computations on these species, as well as the reduced forms of three other cobalamin analogues: Co(II)(imidazole)cobalamin [Co(II)ImCbl], Co(II)(5-cyanoimidazole)cobalamin [Co(II)(CN-Im)Cbl] and Co(II)(5-methylimidazole)cobalamin [Co(II)(Me-Im)Cbl]. Additional spectroscopic and computational studies were performed on a series of Co(II) cobinamide [Co(II)Cbi⁺] species, which lack the native cofactor's nucleotide loop and DMB (Figure 2.1). Cobinamides with axial ligation from pyridine (py), 4-cyanopyridine (CN-py), and 4-(dimethylamino)-pyridine (Me₂N-py) were investigated. The geometries of all Cbl and Cbi species were optimized using a quantum mechanics/molecular mechanics (QM/MM) method, and the optimized geometries were used to compute Abs spectra with time-dependent density functional theory (TD-DFT). Collectively, our spectroscopic and computational results indicate that a reduction in the basicity of the lower axial ligand induces changes to the cofactor's electronic structure in the reduced state similar to those observed upon binding of Co(II)Cbl to Class I isomerases.

2.2 Experimental and Computational Methods

2.2.1 Cofactor Analogue Syntheses. Ado(5-F-Im)Cbl was synthesized using a “guided biosynthesis” in which the fermentation of *Propionibacterium shermanii* on media supplemented with 4(5)-fluoroimidazole produced CN(5-F-Im)Cbl and CN(4-F-Im)Cbl. Subsequent separation and adenosylation of the CN(5-F-Im)Cbl derivative to form Ado(5-F-Im)Cbl was completed according to previously published procedures, and the product was characterized as described in the literature.^{38,53-56}

All pyridine bases, (py, CN-py, and Me₂N-py), dicyanocobinamide [(CN)₂Cbi], methanol, and sodium borohydride (NaBH₄) were purchased from Sigma-Aldrich and used as obtained. Diaquocobinamide [(H₂O)₂Cbi²⁺] was prepared as described previously, by reducing (CN)₂Cbi with NaBH₄ and loading the reaction mixture on a C18 SepPack column, washing with doubly distilled H₂O, and eluting the product with methanol.^{57,58} Co(II)Cbi⁺ was prepared by the addition of NaBH₄ to a degassed solution of (H₂O)₂Cbi²⁺ containing 60% (v/v) glycerol. The pyridine solutions also contained 60% (v/v) glycerol, and were degassed before adding an ~3-fold molar excess to the Co(II)Cbi⁺ solution. The conversion of Co(II)Cbi⁺ to pyridylcobinamide [Co(II)pyCbi⁺] was monitored spectrophotometrically. The syntheses of 4-cyanopyridylcobinamide [Co(II)(CN-py)Cbi⁺] and 4-dimethylaminopyridylcobinamide [Co(II)(Me₂N-py)Cbi⁺] were accomplished by the same procedure using the appropriate pyridine derivative. The identities of these compounds were confirmed by EPR spectroscopy (Figure A.2.1 and Table A.2.1).⁵⁹

2.2.2 Spectroscopy. Low-temperature Abs and MCD spectra were obtained using a Jasco J-715 spectropolarimeter in conjunction with an Oxford Instruments SM-4000 8 T magnetocryostat. All MCD spectra reported herein were obtained by taking the difference

between spectra collected with the magnetic field aligned parallel and antiparallel to the light propagation axis to eliminate contributions from the natural CD and glass strain. X-Band EPR spectra were obtained using a Bruker ESP 300E spectrometer equipped with an Oxford ESR 900 continuous-flow liquid helium cryostat and an Oxford ITC4 temperature controller, and a Varian EIP model 625A frequency counter. In each case a modulation frequency of 100 kHz was used, along with a modulation amplitude of 10.456 G, and a time constant of 40.96 ms. EPR spectral fits to obtain g and A values were completed using the WEPR program developed by Dr. Frank Neese.⁶⁰

2.2.3 Computational Methods. All computational models were generated from the highest resolution X-ray crystal structure of AdoCbl (CCDC file: DADCBL).⁶¹ Initial geometries for Co(II)Cbl and all cofactor analogues included in this study were constructed from this structure by adding or removing the necessary atoms *in silico*. A geometry optimization of each model was performed with the ONIOM QM/MM method⁶² as implemented in Gaussian 09.⁶³ The QM region for all models consisted of the Co ion, the corrin macrocycle, the complete lower axial ligand, and, in the adenosylated models, the ribose moiety of the upper axial ligand. The MM region consisted of the remainder of the upper axial ligand (when present) and all corrin side chains. All covalent bonds spanning the QM/MM boundary were capped with hydrogen atoms (i.e., link atoms) during the QM steps of the optimization. The new X–H bond lengths were set equal to the original bond length scaled by 0.709. The QM region was treated with the BP86 density functional,^{64,65} which is known to be well-suited for obtaining realistic geometries of cobalamins.⁶⁶ The spin-unrestricted formalism was used for all Co(II) models. The triple-zeta basis set with an additional polarization function (TZVP) developed by Ahlrichs⁶⁷ was used for the Co ion and all coordinating N and C atoms, while the split-valence polarized (SVP) basis set from the same group⁶⁸ was used for all

other atoms. The MM region was modeled with the force field specifically developed for cobalamins by Marques et al.⁶⁹ The default ONIOM convergence criteria for SCF cycles and geometry optimizations were used. The optimized coordinates of all models are reported in Tables at the end of Appendix A.2.

TD-DFT was used to compute Abs spectra for the QM regions of all optimized models. The scheme for capping the QM region with hydrogen atoms was the same as in the geometry optimizations described above. All MM atoms aside from those explicitly replaced with H atoms were included in the computations as point charges with values defined by the force field used in the QM/MM optimization. The 60 lowest-energy transitions involving MOs within ± 4 Hartree of the HOMO-LUMO gap were computed by employing the B3LYP density functional^{64,70} and the same basis sets as in the geometry optimizations. While B3LYP is known to poorly predict some cobalamin properties, such as Co–C bond dissociation energies, we have used it successfully in the past to compute Abs spectra of cobalamin species in both the Co(III) and Co(II) oxidation states.^{28,71,72} Additionally, it has been noted the Abs spectra predicted by BP86 and B3LYP display negligible differences.⁷³ Nevertheless, additional DFT and TD-DFT computations were performed using the TPSSh hybrid functional⁷⁴ to ensure that our findings were not biased by the computational method used (Figures A.2.2–A.2.4). All TD-DFT computations were performed with the Orca 2.9.1 program⁷⁵ and used the resolution of the identity⁷⁶ and Tamm-Dancoff approximations⁷⁷ to speed up the calculations. Simulated Abs spectra were generated on the basis of the TD-DFT results by using a constant bandwidth of 1500 cm^{-1} for all transitions. All isosurface plots of MOs and electron density difference maps (EDDMs) were generated with PyMol⁷⁸ using isodensity values of 0.06 and 0.003 a.u., respectively.

2.3 Results

2.3.1. Spectroscopic Data for AdoCbl and Ado(F-Im)Cbl. The Abs and MCD spectra of AdoCbl and Ado(F-Im)Cbl are shown in Figure 2.2. In general, the Abs spectra of alkylcobalamins exhibit many overlapping features that can be loosely grouped into three categories.⁷² The lowest energy features, termed the α/β bands, peak below 21 000 cm^{-1} . They have been assigned as the electronic origin and vibronic sideband of the HOMO \rightarrow LUMO (corrin $\pi \rightarrow \pi^*$) transition. The transitions responsible for the features at slightly higher energies (the D/E bands) also contain corrin $\pi \rightarrow \pi^*$ character, along with some metal-to-ligand charge transfer (MLCT) character. The dominant features above 26 000 cm^{-1} are collectively referred to as the γ bands, which arise from energetically proximate transitions involving primarily corrin $\pi \rightarrow \pi^*$ excitation. The same sets of transitions also produce the major features in the MCD spectrum. However, because the MCD signal is a signed quantity and the intensity is governed by different selection rules than the Abs intensity, MCD spectroscopy provides a much better probe of the number of transitions contributing to a given spectral region. A previous spectroscopic and computational investigation of methylcobalamin, another biologically relevant Co(III)Cbl species whose Abs and MCD spectra are nearly indistinguishable from those of AdoCbl, revealed that the γ bands have contributions from at least seven distinct electronic transitions with varying degrees of corrin- $\pi \rightarrow \pi^*$, MLCT, and ligand-to-metal charge transfer (LMCT) character.⁷² As a result, this spectral region is particularly sensitive to axial ligand substitutions, as demonstrated in a recent spectroscopic and computational investigation of a series of Co(III)Cbl and Co(III)Cbi⁺ species.⁷⁹

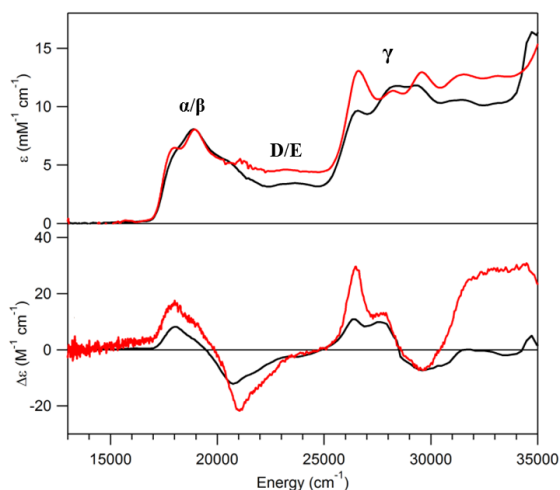


Figure 2.2. Abs and 7 T MCD spectra obtained at 4.5 K of AdoCbl (black) and Ado(F-Im)Cbl (red).

Despite the difference in lower axial ligand basicity, AdoCbl and Ado(F-Im)Cbl exhibit similar electronic Abs spectra. Likewise, the MCD spectra of these species are qualitatively similar, although the negative feature at $20\,700\text{ cm}^{-1}$ in the AdoCbl spectrum is blue-shifted by $\sim 300\text{ cm}^{-1}$ in the Ado(F-Im)Cbl spectrum. Moreover, a significant redistribution of the intensities and small changes in the positions of the γ bands are observed in both the Abs and MCD spectra. Although these changes are small in magnitude, they are more significant than those induced by the binding of AdoCbl to the Class I isomerases MMCM and GM.^{29,34}

2.3.2. Computational Data for AdoCbl and Ado(F-Im)Cbl. The geometry optimizations of complete AdoCbl and Ado(F-Im)Cbl models resulted in cofactor structures with small but noticeable differences (Figure A.2.5). While the sterically bulky DMB ligand of AdoCbl has little conformational flexibility, the smaller F-Im ligand rotates around the Co–N_{ax} bond, as indicated by an opening of the C₁₀(cor)–Co–N_{ax}–C₁(Im/DMB) dihedral angle from 94.4° to 102.8° . This rotation induces geometric changes along the side chain that connects the lower axial ligand to the corrin ring, which causes one of the nitrogen atoms coordinated to the Co to be pushed out

of the equatorial plane (Table A.2.2). Substitution of DMB with F-Im also leads to a decrease in the Co–N_{ax} bond length from 2.382 to 2.328 Å. In contrast, the upper axial Co–C bond length is virtually unperturbed by the lower axial ligand switch, changing by a mere 0.001 Å from AdoCbl to Ado(F-Im)Cbl. The lack of a change in Co–C bond length is consistent with a previous theoretical investigation, which found no correlation between lower axial ligand basicity and Co–C bond length in cobinamides.⁴²

The computed MO diagrams for AdoCbl and Ado(F-Im)Cbl are shown in Figure 2.3. The main differences between the two are the relative energies of the MOs containing contributions from the lower axial ligand. Although the heavily mixed compositions of the MOs make direct comparisons difficult, we note that in Ado(F-Im)Cbl the F-Im-based orbitals (e.g., MO #201) are considerably lower in energy than the non-bonding Co 3d_{xy}-based orbital (MO #204). Thus, the MOs derived from the frontier orbitals of the F-Im ligand contain little contributions from the Co 3d manifold and corrin ring orbitals. On the other hand, the DMB-derived MOs of AdoCbl are higher in energy than the Co 3d_{xy}-based orbital (MOs #221/222 versus MO #216), and thus contain large orbital contributions from the rest of the cofactor.

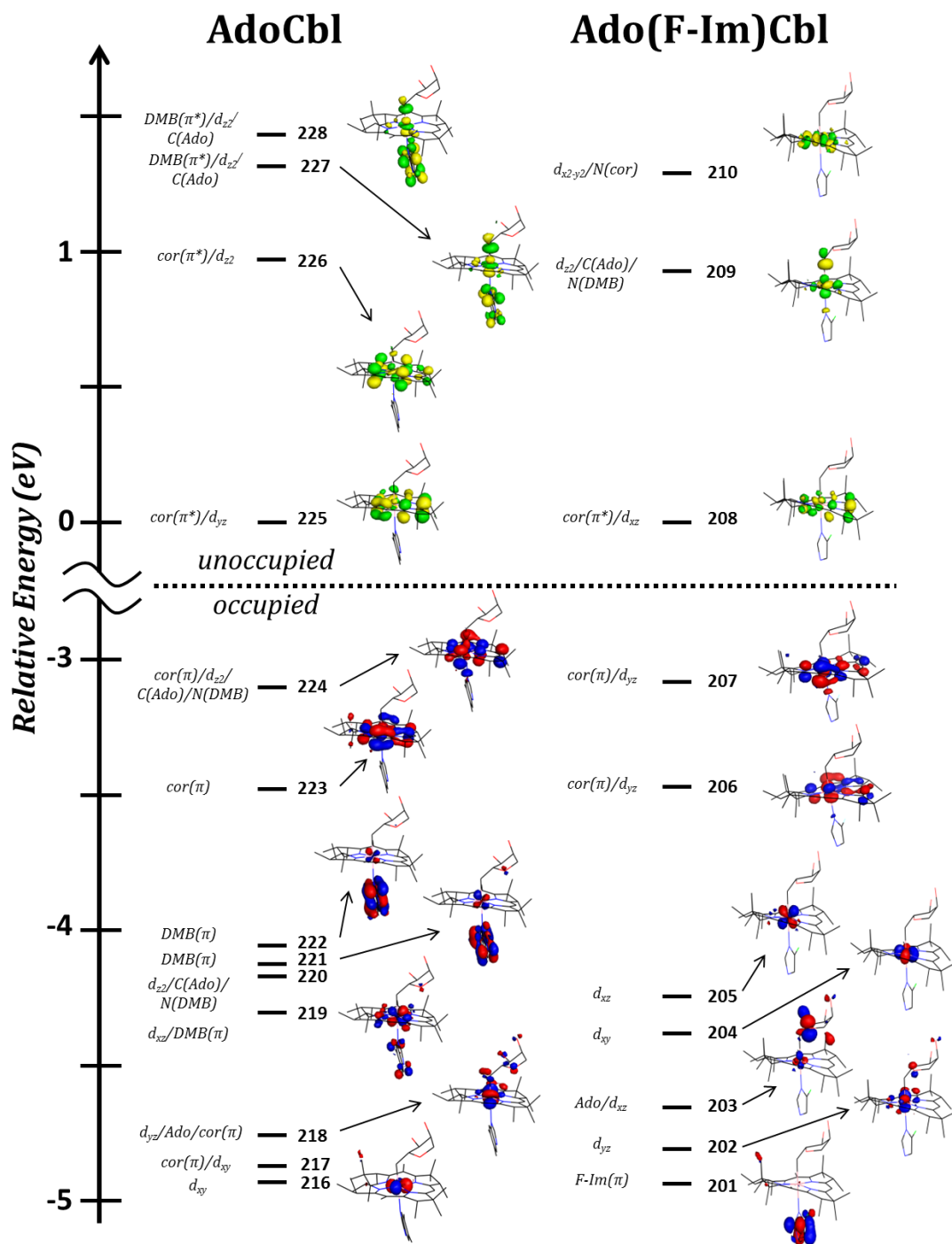


Figure 2.3. DFT-computed MO diagrams for AdoCbl and Ado(F-Im)Cbl. MOs were shifted vertically to align the LUMOs at 0 eV. Occupied orbitals are shown in red and blue; unoccupied orbitals in green and yellow.

The TD-DFT computed Abs spectra for AdoCbl and Ado(F-Im)Cbl are shown in Figure 2.4, and details regarding key transitions are provided in Tables 2.1 and 2.2. The spectra are very similar in the α/β and D/E regions aside from a slightly smaller splitting between the two regions in the Ado(F-Im)Cbl spectrum. The lower ligand substitution does, however, give rise to a major rearrangement of intensity in the γ region. Although the close energetic proximity of numerous transitions with similar character make a qualitative analysis of this region difficult, one important observation is the appearance of a new feature $\sim 1000\text{ cm}^{-1}$ lower in energy than the onset of the γ region in the Ado(F-Im)Cbl spectrum. This feature is due to transition 5, which mainly entails HOMO (corrin π) \rightarrow LUMO+2 (Co $3d_{x^2-y^2}$) excitation. The corresponding transition in the AdoCbl spectrum occurs at much higher energy because of the larger destabilization of the Co $3d_{x^2-y^2}$ -based orbital (MO #230, Figure A.2.6). The relative stabilization of the Co $3d_{x^2-y^2}$ -based orbital (MO #210) in Ado(F-Im)Cbl is unlikely to be a direct consequence of the lower axial ligand switch, but may be a result of the increased folding of the corrin ring in the Ado(F-Im) model, which mitigates the σ^* antibonding interaction between the Co $3d_{x^2-y^2}$ orbital and the “lone pairs” on the four coordinating nitrogens of the corrin ring. While the experimental Abs spectrum of Ado(F-Im)Cbl seemingly lacks the new feature observed in the computed spectrum, shifts of one or more of the transitions contributing to the γ bands could be responsible for the intensity redistribution in this region. As such, the experimental and computed Abs spectra agree on there being small changes in the α/β and D/E regions, and more significant perturbations to the γ bands when the DMB ligand of AdoCbl is replaced with F-Im.

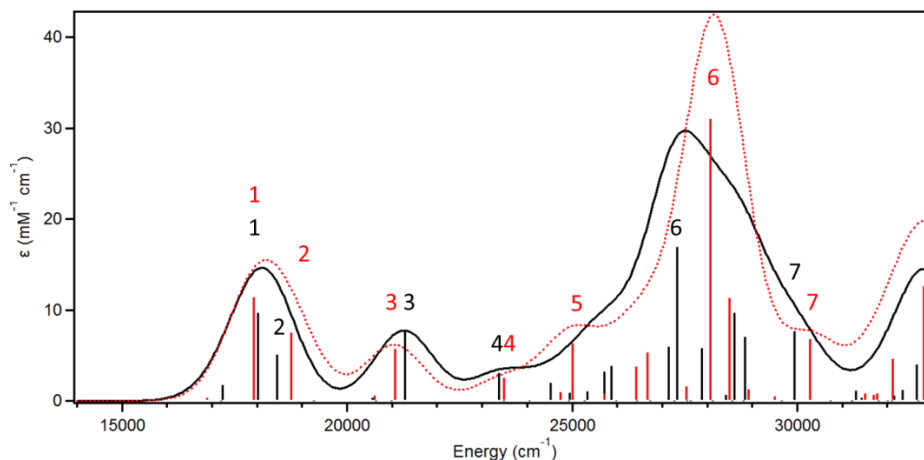


Figure 2.4. TD-DFT computed Abs spectra for AdoCbl (black, solid) and Ado(F-Im)Cbl (red, dashed). A uniform red-shift of 3000 cm^{-1} was applied to facilitate a comparison with the experimental spectra in Figure 2.2. The computed energies and intensities of individual transitions are shown as sticks. Details regarding the labeled transitions are provided in Tables 2.1 and 2.2.

Table 2.1. TD-DFT Computed Energies, Oscillator Strengths, and Percent Contributions from Dominant One-Electron Excitations for the Major Electronic Transitions of AdoCbl

State	E (cm^{-1})	f	Transition	%	Donor MO	Acceptor MO
1	18014	0.06689	224 \rightarrow 225	53	corrin π /Co $3d_{z^2}$ / C(Ado)/N(DMB)	corrin π^* /Co $3d_{yz}$
2	18445	0.0350	224 \rightarrow 225	20	corrin π /Co $3d_{z^2}$ / C(Ado)/N(DMB)	corrin π^* /Co $3d_{yz}$
			219 \rightarrow 227	10	Co $3d_{xz}$ /DMB- π	DMB- π^* /Co $3d_{z^2}$ / C(Ado)
3	21279	0.0524	223 \rightarrow 225	64	corrin π	corrin π^* /Co $3d_{yz}$
			224 \rightarrow 226	22	corrin π /Co $3d_{z^2}$ / C(Ado)/N(DMB)	corrin π^* /Co $3d_{z^2}$
4	23367	0.0208	219 \rightarrow 225	28	Co $3d_{xz}$ /DMB- π	corrin π^* /Co $3d_{yz}$
			222 \rightarrow 225	22	DMB- π	corrin π^* /Co $3d_{yz}$
			221 \rightarrow 225	22	DMB- π	corrin π^* /Co $3d_{yz}$
5	-	-	-	-	-	-
6	27327	0.1170	224 \rightarrow 226	30	corrin π /Co $3d_{z^2}$ / C(Ado)/N(DMB)	corrin π^* /Co $3d_{z^2}$
			223 \rightarrow 226	15	corrin π	corrin π^* /Co $3d_{z^2}$
7	29939	0.0530	218 \rightarrow 225	42	Co $3d_{yz}$ /Ado/corrin π	corrin π^* /Co $3d_{yz}$
			216 \rightarrow 225	18	Co $3d_{xy}$	corrin π^* /Co $3d_{yz}$

Table 2.2. TD-DFT Computed Energies, Shifts from Corresponding AdoCbl Transitions, Oscillator Strengths, and Percent Contributions from Dominant One-Electron Excitations for the Major Electronic Transitions of Ado(F-Im)Cbl

State	E (cm ⁻¹)	Shift (cm ⁻¹)	f	Transition	%	Donor MO	Acceptor MO
1	17927	-87	0.0787	207 → 208	61	corrin π /Co 3d _{yz}	corrin π^* /Co 3d _{xz}
2	18760	315	0.0516	207 → 208	24	corrin π /Co 3d _{yz}	corrin π^* /Co 3d _{xz}
				205 → 210	17	Co 3d _{xz}	Co 3d _{x²-y²} /N(cor)
3	21073	-206	0.0395	206 → 208	61	corrin π /Co 3d _{yz}	corrin π^* /Co 3d _{xz}
				207 → 209	29	corrin π /Co 3d _{yz}	Co 3d _{z²} /C(Ado)/ N(F-Im)
4	23491	124	0.0174	205 → 208	67	Co 3d _{xz}	corrin π^* /Co 3d _{xz}
5	25008	-	0.0437	207 → 210	60	corrin π /Co 3d _{yz}	Co 3d _{x²-y²} /N(cor)
6	28062	735	0.2145	207 → 209	26	corrin π /Co 3d _{yz}	Co 3d _{z²} /C(Ado)/ N(F-Im)
				207 → 210	15	corrin π /Co 3d _{yz}	Co 3d _{x²-y²} /N(cor)
7	30287	348	0.0469	200 → 208	38	Ado	corrin π^* /Co 3d _{xz}
				202 → 208	28	Co 3d _{yz}	corrin π^* /Co 3d _{xz}

2.3.3. Spectroscopic Data for Co(II)Cbl and Co(II)-bound Derivatives. The Abs and MCD spectra of Co(II)Cbl and Co(II)(F-Im)Cbl are presented in Figure 2.5. The Co(II)Cbl Abs and MCD spectra have previously been analyzed by our laboratory,⁷¹ which led to the following general band assignments. The lowest energy features (< 17 000 cm⁻¹) are due to LF transitions. These formally parity-forbidden transitions carry negligible intensity in the Abs spectrum, but gain intensity in the MCD spectrum through spin-orbit coupling. All features above 17 000 cm⁻¹ arise from transitions involving a combination of MLCT and corrin $\pi \rightarrow \pi^*$ one-electron excitations. The former dominate for transitions between 17 000 cm⁻¹ and 20 500 cm⁻¹, while the latter are the main contributors to the intense transitions at higher energies.

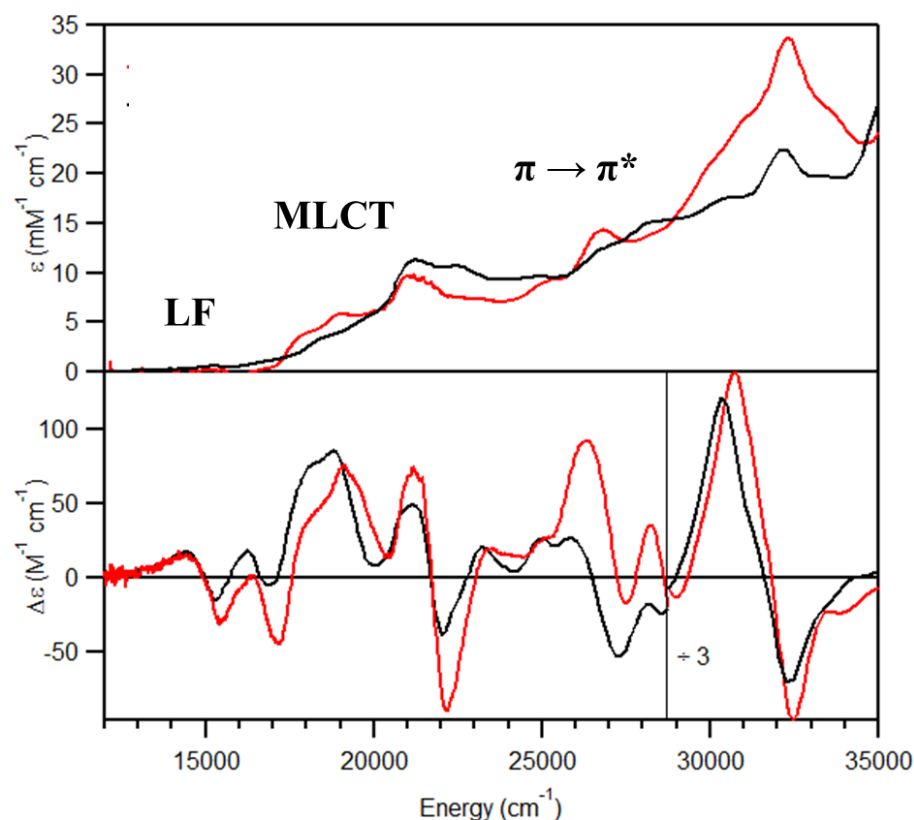


Figure 2.5. Abs and 7 T MCD spectra obtained at 4.5 K of Co(II)Cbl (black) and Co(II)(F-Im)Cbl (red).

Visual inspection of the Co(II)Cbl and Co(II)(F-Im)Cbl Abs and MCD spectra reveals small variations in the intensities and positions of certain features. To quantify these changes, we performed iterative Gaussian deconvolutions of the Abs and MCD spectra using the lowest acceptable number of individual transitions required to fit the experimental data (Figure A.2.7, Tables A.2.3 and A.2.4). Of the 18 transitions in the Co(II)Cbl spectrum below 35 000 cm⁻¹ identified in this analysis, 11 exhibit blue-shifts of 100 cm⁻¹ or more upon switching the lower axial ligand to F-Im (Table 2.3). These 11 transitions are all centered above 16 000 cm⁻¹, indicating they have predominantly MLCT or corrin $\pi \rightarrow \pi^*$ character. The origin of these blue-shifts is explored computationally in section 2.4.

Table 2.3. Selected Spectral Features of Co(II)(F-Im)Cbl and Shifts Relative to Co(II)Cbl Counterparts

Band	Energy (cm ⁻¹)	Shift (cm ⁻¹)	Assignment ^a
4	17 260	150	MLCT/ $\pi \rightarrow \pi^*$
5	17 900	200	MLCT/ $\pi \rightarrow \pi^*$
6	19 170	340	MLCT/ $\pi \rightarrow \pi^*$
8	21 300	250	$\pi \rightarrow \pi^*$ / MLCT
12	25 150	200	$\pi \rightarrow \pi^*$ / MLCT
13	26 390	350	$\pi \rightarrow \pi^*$ / MLCT
14	27 460	200	$\pi \rightarrow \pi^*$ / MLCT
15	28 380	380	$\pi \rightarrow \pi^*$ / MLCT
16	28 900	130	$\pi \rightarrow \pi^*$ / MLCT
17	30 650	350	$\pi \rightarrow \pi^*$ / MLCT
18	31 670	220	$\pi \rightarrow \pi^*$ / MLCT
20	32 510	-140	$\pi \rightarrow \pi^*$ / MLCT
21	34 170	-1600	$\pi \rightarrow \pi^*$ / MLCT

^aSee text for more details.

To further investigate the influence of the α -axial ligand basicity on the electronic spectra of Co(II)Cbl analogues, we also performed spectroscopic studies of Co(II)pyCbi⁺, Co(II)(CN-py)Cbi⁺, and Co(II)(Me₂N-py)Cbi⁺. The MCD spectra of these three species (Figure 2.6) are very similar to those obtained for Co(II)Cbl and Co(II)(F-Im)Cbl (Figure 2.5), also exhibiting low energy LF transitions and higher energy MLCT and corrin $\pi \rightarrow \pi^*$ transitions. Inspection of these spectra reveals that an increased basicity of the lower axial ligand is correlated with a general red-shift of Abs and MCD features. Specifically, the Co(II)(Me₂N-py)Cbi⁺ (pK_b of Me₂N-py = 4.3) spectrum is red-shifted relative to the Co(II)pyCbi⁺ (pK_b of py = 8.7) spectrum, which in turn is red-shifted from that of Co(II)(CN-py)Cbi⁺ (pK_b of CN-py = 12.1). As in the case of the Co(II)Cbl and Co(II)(F-Im)Cbl spectra, the largest shifts involve features at intermediate and high energies (above 17 000 cm⁻¹).

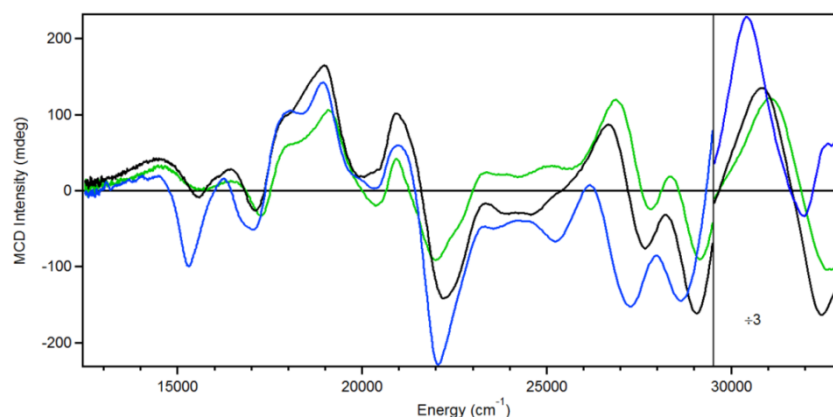


Figure 2.6. MCD spectra obtained at 7 T and 4.5 K of Co(II)pyCbi^+ (black), $\text{Co(II)(CN-py)Cbi}^+$ (green), and $\text{Co(II)(Me}_2\text{N-py)Cbi}^+$ (blue).

2.3.4. Computational Data for Co(II)Cbl and Co(II) -bound Derivatives. To identify the electronic structural origin of the differences in the Abs and MCD spectra of Co(II)Cbl and Co(II)(F-Im)Cbl , and to explore how the basicity of the lower axial ligand is linked to these differences, we computed equilibrium geometries and Abs spectra for Co(II)Cbl and seven Co(II) -bound derivatives. Three of these derivatives are the Cbi species with variable pyridyl bases described in the previous section, and the remaining four are Cbl species with modified bases, including the spectroscopically characterized derivative Co(II)(F-Im)Cbl , as well as Co(II)ImCbl , Co(II)(CN-Im)Cbl , and Co(II)(Me-Im)Cbl .

The TD-DFT computed Abs spectra for Co(II)Cbl and the four Co(II)Cbl derivatives are shown in Figure 2.7 and a summary of the relevant results obtained for Co(II)Cbl and Co(II)(F-Im)Cbl is provided in Tables 2.4 and 2.5. (Isosurface plots of all frontier MOs can be found in Tables A.2.5 and A.2.6.) An initial comparison of the computed spectra for Co(II)Cbl and Co(II)(F-Im)Cbl reveals that many of the major features of the latter are blue-shifted relative to those of the former, as observed in the experimental MCD spectra (Table 2.3). This is especially apparent for the transitions with energies between 20 000 and 31 000 cm^{-1} , a range in which five of the most intense transitions are computed at higher energies in the Co(II)(F-Im) spectrum.

Features in this region of the Abs and MCD spectra of Co(II)Cbl have previously been attributed to transitions with predominant MLCT and corrin $\pi \rightarrow \pi^*$ character (*vide supra*). These assignments are corroborated by the computed electron density difference maps (EDDMs) for transitions 1–5 shown in Figure 2.8.

A direct comparison of the TD-DFT results for Co(II)Cbl and Co(II)(F-Im)Cbl is complicated by the fact that the MOs involved in the transitions at energies $> 31\,000\text{ cm}^{-1}$ have considerable contributions from the lower axial ligand, making it unclear whether the predicted spectral differences are actually due to the decreased basicity of F-Im. To address this issue, we extended our computational analysis to models of Co(II)Cbl derivatives with substituted imidazole bases more closely related to F-Im. As shown in Figure 2.7, all major Abs features below $35\,000\text{ cm}^{-1}$ shift when the lower axial ligand is varied, with the lowest-energy features found in Co(II)(Im)Cbl, followed by Co(II)(Me-Im)Cbl, Co(II)(F-Im)Cbl, and Co(II)CN-Im(Cbl). This trend reflects the electron-withdrawing power of the Im substituents, with $\text{Me} < \text{F} < \text{CN}$. The Co(II)ImCbl model provides an exception to this trend, as it would ordinarily be expected to have transitions between those of Co(II)(Me-Im)Cbl and Co(II)(F-Im)Cbl. This anomaly is likely a result of the much shorter Co–N_{ax} bond distance in Co(II)ImCbl (2.11 \AA) than in the other Co(II)Cbl models possessing substituted Im bases ($2.17 - 2.23\text{ \AA}$) due, at least in part, to steric crowding with the corrin ring in the latter. Thus, even though Im is a weaker base than Me-Im,⁸⁰ the shorter bond distance in Co(II)ImCbl leads to increased charge donation from the α -axial ligand, effectively mimicking the binding of a stronger base.

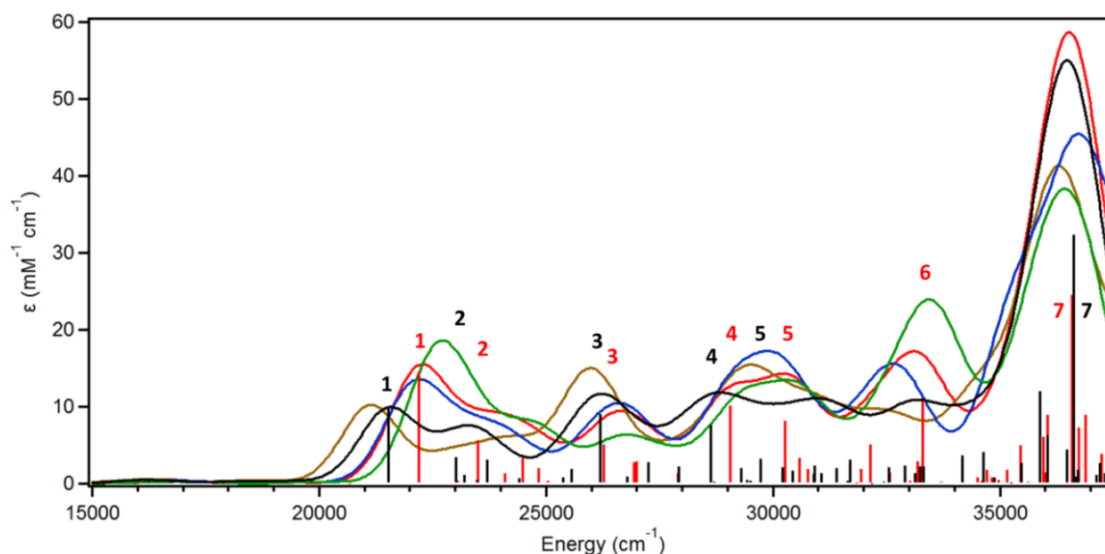


Figure 2.7. TD-DFT computed Abs spectra for Co(II)Cbl (black), Co(II)(F-Im)Cbl (red), Co(II)ImCbl (gold), Co(II)(Me-Im)Cbl (blue), and Co(II)(CN-Im)Cbl (green). The computed energies and intensities of individual transitions of Co(II)Cbl and Co(II)(F-Im)Cbl are shown as sticks. Details regarding the labeled transitions are provided in Tables 2.4 and 2.5.

Table 2.4. TD-DFT Computed Energies, Percent Contributions from Dominant One-Electron Excitations, and Oscillator Strengths for the Major Electronic Transitions of Co(II)Cbl

State	E (cm ⁻¹)	f	Transition	%	Donor MO	Acceptor MO
1	21529	0.0666	191b → 193b	45	corrin π /Co 3d _{z²}	corrin π^* /Co 3d _{yz}
			193a → 194a	19	corrin π /Co 3d _{z²} / N(DMB)	corrin π^* /Co 3d _{yz}
2	23006	0.0235	192a → 194a	14	corrin π /Co 3d _{yz}	corrin π^* /Co 3d _{yz}
			192b → 193b	13	Co 3d _{yz} /corrin π	corrin π^* /Co 3d _{yz}
			191a → 194a	12	Co 3d _{xz} /DMB(π)	corrin π^* /Co 3d _{yz}
			191b → 194b	11	Corrin π /Co 3d _{z²}	corrin π^* /Co 3d _{xz}
3	26202	0.0622	190a → 194a	63	Co 3d _{z²} /N(DMB)/ corrin π	corrin π^* /Co 3d _{yz}
4	28627	0.0527	192b → 194b	15	Co 3d _{yz} /corrin π	corrin π^* /Co 3d _{xz}
			192a → 195a	12	corrin π /Co 3d _{yz}	corrin π^* /Co 3d _{xz}
			191b → 194b	11	corrin π /Co 3d _{z²}	corrin π^* /Co 3d _{xz}
5	29726	0.0217	189b → 193b	32	DMB(π)	corrin π^* /Co 3d _{yz}
			192b → 195b	11	Co 3d _{yz} /corrin π	DMB(π^*)
6	-	-	-	-	-	-
7	36629	0.2237	191b → 197b	17	corrin π / Co 3d _{z²}	corrin π^*
			190a → 198a	8	Co 3d _{z²} /N(DMB)/ corrin π	corrin π^* / Co 3d _{x²-y²}
			183b → 193b	6	corrin π	corrin π^* /Co 3d _{yz}
			185b → 193b	6	corrin π	corrin π^* /Co 3d _{yz}

Table 2.5. TD-DFT Computed Energies, Shifts From Corresponding Co(II)Cbl Transitions, Oscillator Strengths, and Percent Contributions from Dominant One-Electron Excitations for the Major Electronic Transitions of Co(II)(F-Im)Cbl

State	E (cm ⁻¹)	Shift (cm ⁻¹)	f	Transition	%	Donor MO	Acceptor MO
1	22191	662	0.1007	174b → 176b	46	corrin π /Co 3d _{yz}	corrin π^* /Co 3d _{yz}
				176a → 177a	25	corrin π / Co 3d _{z²} /N(F-Im)	corrin π^* /Co 3d _{yz}
2	23498	492	0.0389	175b → 176b	21	corrin π /Co 3d _{yz}	corrin π^* /Co 3d _{yz}
				175a → 177a	18	corrin π /Co 3d _{yz}	corrin π^* /Co 3d _{yz}
				174b → 177b	13	corrin π /Co 3d _{yz}	corrin π^* /Co 3d _{z²}
3	26268	66	0.0352	174a → 177a	47	Co 3 d _{xz} /corrin π	corrin π^* /Co 3d _{yz}
				175a → 178a	24	corrin π /Co 3d _{yz}	corrin π^* /Co 3d _{yz}
4	29056	429	0.0699	175b → 177b	19	corrin π /Co 3d _{yz}	corrin π^* /Co 3d _{z²}
				175a → 178a	12	corrin π /Co 3d _{yz}	corrin π^* /Co 3d _{xz}
				174b → 180b	8	corrin π /Co 3d _{yz}	corrin π^* /F-Im(π^*)
5	30272	546	0.0564	176a → 178a	23	corrin π / Co 3d _{z²} /N(F-Im)	corrin π^* /Co 3d _{yz}
				175b → 180b	13	corrin π /Co 3d _{yz}	corrin π^* /F-Im (π^*)
				172a → 177a	13	Co 3d _{yz} /corrin π	corrin π^* /Co 3d _{yz}
6	33289	-	0.0766	173a → 178a	19	Co 3d _{z²} /N(F-Im)	corrin π^* /Co 3d _{xz}
				169a → 177a	17	Co 3d _{xy} /F-Im- π	corrin π^* /Co 3d _{yz}
				172a → 177a	13	Co 3d _{yz} /corrin π	corrin π^* /Co 3d _{yz}
7	36588	-41	0.1694	174b → 180b	19	corrin π /Co 3d _{yz}	corrin π^* /F-Im(π^*)
				173a → 178a	8	Co 3d _{z²} /N(F-Im)	corrin π^* /Co 3d _{xz}
				167b → 176b	8	Corrin π	corrin π^* /Co 3d _{yz}

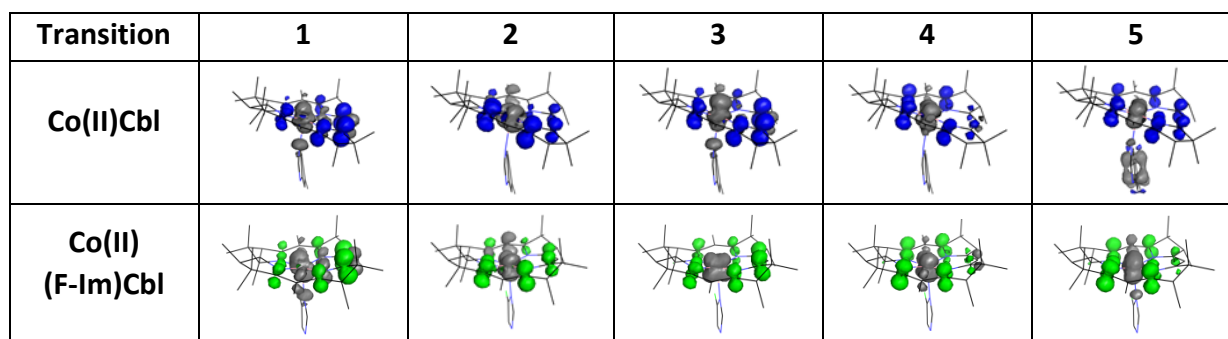


Figure 2.8. EDDMs for transitions 1-5 in the TD-DFT computed Abs spectra of Co(II)Cbl and Co(II)(F-Im)Cbl in Figure 2.7. Regions of electron density loss are shown in gray and regions of electron density gain are shown in blue [Co(II)Cbl] or green [Co(II)(F-Im)Cbl].

The TD-DFT computed Abs spectra for the three Co(II)Cbi⁺ derivatives are presented in Figure 2.9. Consistent with our experimental data (Figure 2.6), transitions at energies < 20 000 cm⁻¹ have predominantly LF character and thus carry little Abs intensity (note that the intense feature at 17 000 cm⁻¹ in the computed Co(II)(CN-py)Cbi⁺ Abs spectrum is due to a transition with significant Co 3d → (CN-py) π* character). As was predicted for the Co(II)-bound Cbl models, all computed transitions for the Co(II)Cbi⁺ derivatives above 20 000 cm⁻¹ contain considerable MLCT character. Most importantly, sizeable blue-shifts of most Abs features are predicted computationally when the basicity of the lower axial ligand is decreased (Me₂N-py < py < CN-py), consistent with our MCD data (Figure 2.6).

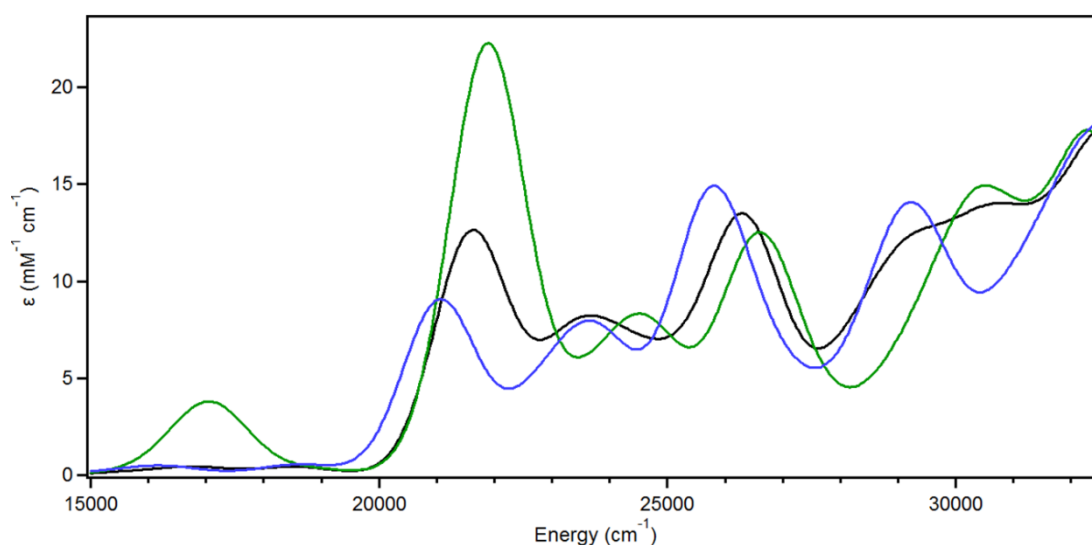


Figure 2.9. TD-DFT computed Abs spectra for three Co(II)-bound Cbi derivatives: Co(II)pyCbi⁺ (black), Co(II)(Me₂N-py)Cbi⁺ (blue), and Co(II)(CN-py)Cbi⁺ (green).

2.4 Discussion

The mechanism by which AdoCbl-dependent isomerases accomplish the impressive rate enhancement of homolytic cleavage of the cofactor's Co–C bond has been the subject of intense investigation. Despite extensive research indicating a relative stabilization of the enzyme-bound

Co(II)Cbl state, the role of the conserved DXHXGXX motif has not yet been conclusively determined. In the following sections, we discuss the implications of our spectroscopic and computational results with regards to the role that this hydrogen bonding network may play in the mechanism of Co–C bond activation employed by Class I isomerases.

2.4.1 Axial Ligand Effects on Electronic Structures of Co(III)Cbls. A comparison of the AdoCbl and Ado(F-Im)Cbl spectroscopic and computational results reveals that altering the basicity of the lower axial ligand has relatively minor effects on the electronic structure of the cofactor. Differences observed in the γ region of the Abs spectra can be attributed to different degrees of mixing between the various corrin $\pi \rightarrow \pi^*$ and CT transitions that contribute to this region. Both our computational analysis and spectroscopic data indicate that the electronic structures of AdoCbl and Ado(F-Im)Cbl are similar but not identical. Most notably, the F-Im frontier orbitals exhibit less mixing with the Co 3d orbitals because of the reduced basicity of the F-Im ligand relative to DMB. The most noticeable impact of this difference on the computed Abs spectra for AdoCbl and Ado(F-Im)Cbl is a redistribution of intensity in the γ region.

2.4.2. Axial Ligand Effects on Co(II)Cbl and its Analogues. The most significant differences between the experimental MCD spectra of Co(II)(F-Im)Cbl and Co(II)Cbl occur in the 17 000 – 20 000 cm^{-1} region, which is dominated by MLCT transitions. In general, the major features in this region of the Co(II)(F-Im)Cbl spectrum are blue-shifted relative to their counterparts in the Co(II)Cbl spectrum. A Gaussian deconvolution of the Abs and MCD spectra reveals that features outside this energy window also undergo blue-shifts in response to lower axial ligand substitution. Similar shifts are predicted for the transitions that dominate the computed Abs spectra. An inspection of the corresponding EDDMs reveals that these transitions have significant MLCT character. A blue-shifting of MLCT transitions can be explained by invoking a stabilization

of all Co 3d-based MOs relative to the ligand MOs, which could be accomplished by a reduction in electron donation from the α -axial ligand to the Co(II) ion. Though other factors may contribute to these blue-shifts, our results are consistent with a stabilization of the Co(II) form of the cofactor via replacement of the lower axial ligand with a weaker base. To confirm that the observed spectral changes are indeed due, primarily, to changes in α -axial ligand basicity, we performed experimental and computational studies of multiple Co(II)Cbl and Co(II)Cbi⁺ species with variable lower axial ligation. The MCD spectra of the Co(II)Cbi⁺ derivatives indicate that a decrease in lower axial ligand basicity causes blue-shifts of features throughout the spectrum, an observation corroborated by our TD-DFT results. Similarly, the computational study of additional Co(II)Cbl derivatives reveals that MLCT transitions of these species are blue-shifted in the presence of weaker α -axial ligands.

The fact that replacement of the DMB ligand with F-Im induces more noticeable changes to the Abs and MCD spectra of Co(II)Cbl than to those of AdoCbl can be explained in terms of the different relative importance of the axial bonding interactions in these species. In Co(II)Cbl, the singly occupied Co 3d_{z²}-based MO is characterized by a strong σ^* -antibonding interaction with the coordinating nitrogen of the lower axial ligand. Replacement of the axial ligand with a weaker base results in a large reduction of this antibonding interaction and thus causes a significant stabilization of the Co 3d_{z²}-based MO. Alternatively, in AdoCbl, the stabilizing effect of a weaker α -axial ligand is limited because the Co 3d_{z²}-based MO also contains a large σ^* -antibonding contribution from the strongly σ -donating Ado ligand. Consequently, reducing the basicity of the α -axial ligand results in more modest changes to the cofactor's electronic structure in the Co(III) state. Consistent with these predictions, it has previously been shown that a correlation exists between the Co–C bond dissociation energy and α -axial ligand basicity in cobaloximes, a class of

synthetic Cbl model complexes.⁴⁸ However, the weakening of the Co–C bond predicted upon replacement of the native DMB ligand with the more weakly donating Im or F-Im bases is far smaller than what is observed in AdoCbl-dependent enzymes, implying that the actual mechanism of Co–C bond activation is more complicated.

2.4.3. Implications for Co–C Bond Activation by Class I Isomerases. The biological relevance of the Co(II)(F-Im)Cbl cofactor analogue is highlighted by the striking resemblance of its MCD spectrum and those of Co(II)Cbl bound to the Class I isomerases GM and MMCM (Figure 2.10). Given this similarity, it is likely that the perturbations to the electronic structure of Co(II)Cbl induced by binding to GM and MMCM are analogous to those induced by replacing the lower axial ligand with a weaker base. However, our results indicate that the same ligand switch that causes these changes in the Co(II) form of the free cofactor also induces small changes to the Co(III) form, and that these changes do not mimic those seen upon AdoCbl binding to GM²⁹ and MMCM.³⁴ Thus, it appears that the reduced basicity of F-Im makes Co(II)(F-Im)Cbl an excellent model for enzyme-bound Co(II)Cbl, while Ado(F-Im)Cbl only partially mimics enzyme-bound AdoCbl.

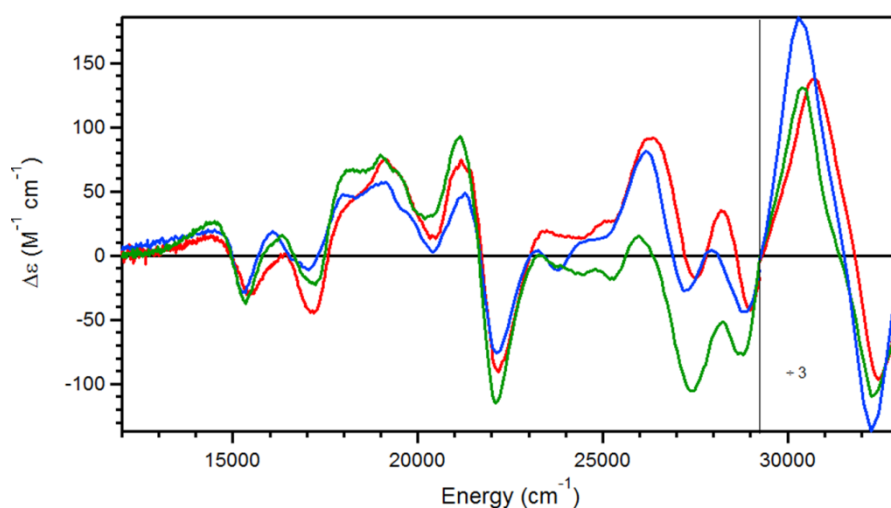


Figure 2.10. MCD spectra of Co(II)F-Im)Cbl (red), MMCM-bound Co(II)Cbl (green), and GM-bound Co(II)Cbl (blue), obtained at 4.5 K and 7 T.

The blue-shifts of the MLCT transitions in the MCD spectra of the enzyme-bound versus free Co(II)Cbl cofactor were interpreted previously^{28,29} as an indication of a uniform stabilization of the Co 3d orbitals. Class I isomerases like GM and MMCM may facilitate this stabilization through a hydrogen-bonding network within the His, Asp, Lys triad of conserved residues. Proton uptake by this triad would reduce the electron donating power of the coordinating His, resulting in reduced charge donation from the His to the Co ion. Since the spectral perturbations associated with the reduced basicity of this ligand are observed only in the Co(II)Cbl form of the enzyme-bound cofactor, we propose that proton uptake is coupled to Co–C bond homolysis. The preferential stabilization of the post-homolysis Co(II)Cbl product over the AdoCbl form by the enzyme active site is expected to provide a significant contribution to the overall reduction in the barrier to Co–C bond homolysis. Interestingly, this mechanism is only possible in Class I isomerases, because of the unique His-on binding mode employed by these enzymes. Class II eliminases, which bind AdoCbl in the DMB-on form, must lower the barrier to homolysis by another mechanism, given that the native DMB ligand is incapable of hydrogen bonding. Therefore, the reduced catalytic efficiency of Ado(F-Im)Cbl in RNTR is likely caused by factors other than the low basicity of the F-Im ligand. Indeed, preliminary MCD spectroscopic data obtained for AdoCbl and Co(II)Cbl bound to the Class II enzyme ethanolamine ammonia lyase (not shown) are more consistent with a mechanism invoking destabilization of the AdoCbl reactant state, as opposed to stabilization of the Co(II)Cbl post-homolysis product.

Finally, we note that the addition of substrate causes further blue-shifts of the MCD features of GM- and MMCM-bound Co(II)Cbl,^{28,29} suggesting that an additional decrease in the α -axial ligand basicity occurs in this process. Since the hydrogen bonding network is unlikely to take up another proton, it may be that binding of substrate affects the relative positioning of

Co(II)Cbl and/or the position of the proton. That is, the presence of substrate may induce changes to the geometry of the cofactor or the DXHXGXX motif such that the extra proton present in the Co(II)Cbl state becomes more closely associated with the His, which therefore becomes an even weaker base. This mechanism would allow the enzyme to control the timing of Co–C bond homolysis, ensuring that the highly reactive Ado[•] radical is formed only when substrate is available to reduce the risk of undesirable side reactions or radical escape into the cell.

2.5 Conclusion

There are many possible ways to account for the 10¹²-fold acceleration of the homolytic Co–C bond cleavage that is achieved by the AdoCbl-dependent Class I isomerases.⁸¹ Increasing evidence exists^{20,23,28,29,32,82} indicating that this rate acceleration is due, at least in part, to a stabilization of the post-homolysis Ado[•] and Co(II)Cbl products within the active site by a combination of favorable electrostatic interactions and electronic effects involving the axial base. We have presented evidence that one factor contributing to the stabilization of the Co(II)Cbl intermediate is a reduction in charge donation from the lower axial ligand to the central Co ion, which results in a fairly uniform stabilization of the Co 3d-based MOs. In the enzyme active site, this stabilization could occur via proton uptake by the catalytic triad, thus explaining the necessity of this conserved motif for the impressive enzymatic acceleration of Co–C bond homolysis by Class I isomerases.

2.6 References

- (1) Banerjee, R. *Chem. Rev.* **2003**, *103*, 2083.
- (2) Toraya, T. *Arch. Biochem. Biophys.* **2014**, *544*, 40.
- (3) Marsh, E. N. G.; Melendez, G. D. R. *Biochim. Biophys. Acta, Proteins Proteomics* **2012**, *1824*, 1154.
- (4) Brown, K. L. *Chem. Rev.* **2005**, *105*, 2075.
- (5) Roth, J. R.; Lawrence, J. G.; Bobik, T. A. *Annu. Rev. Microbiol.* **1996**, *50*, 137.
- (6) Kolhouse, J. F.; Allen, R. H. *Proc. Natl. Acad. Sci. U. S. A.* **1977**, *74*, 921.

- (7) Chowdhury, S.; Banerjee, R. *Biochemistry* **2000**, 39, 7998.
- (8) Marsh, E. N. G.; Ballou, D. P. *Biochemistry* **1998**, 37, 11864.
- (9) Marsh, E. N. G.; Holloway, D. E. *FEBS Lett.* **1992**, 310, 167.
- (10) Ratnatilleke, A.; Vrijbloed, J. W.; Robinson, J. A. *J. Biol. Chem.* **1999**, 274, 31679.
- (11) Beatrix, B.; Zelder, O.; Linder, D.; Buckel, W. *Eur. J. Biochem.* **1994**, 221, 101.
- (12) Toraya, T. *Chem. Rev.* **2003**, 103, 2095.
- (13) Poppe, L.; Stupperich, E.; Hull, W. E.; Buckel, T.; Retey, J. *Eur. J. Biochem.* **1997**, 250, 303.
- (14) Poppe, L.; Bothe, H.; Broker, G.; Buckel, W.; Stupperich, E.; Retey, J. *J. Mol. Catal. B: Enzym.* **2000**, 10, 345.
- (15) Chowdhury, S.; Thomas, M. G.; Escalante-Semerena, J. C.; Banerjee, R. *J. Biol. Chem.* **2001**, 276, 1015.
- (16) Pierik, A. J.; Ciceri, D.; Lopez, R. F.; Kroll, F.; Broker, G.; Beatrix, B.; Buckel, W.; Golding, B. T. *Biochemistry* **2005**, 44, 10541.
- (17) Chen, H. P.; Marsh, E. N. G. *Biochemistry* **1997**, 36, 7884.
- (18) Vlasie, M.; Chowdhury, S.; Banerjee, R. *J. Biol. Chem.* **2002**, 277, 18523.
- (19) Vlasie, M. D.; Banerjee, R. *J. Am. Chem. Soc.* **2003**, 125, 5431.
- (20) Makins, C.; Pickering, A. V.; Mariani, C.; Wolthers, K. R. *Biochemistry* **2013**, 52, 878.
- (21) Madhavapeddi, P.; Marsh, E. N. G. *Chem. Biol. (Oxford, U. K.)* **2001**, 8, 1143.
- (22) Xia, L.; Ballou, D. P.; Marsh, E. N. G. *Biochemistry* **2004**, 43, 3238.
- (23) Roman-Melendez, G. D.; von Glehn, P.; Harvey, J. N.; Mulholland, A. J.; Marsh, E. N. G. *Biochemistry* **2014**, 53, 169.
- (24) Weigl, U.; Heimberger, M.; Pierik, A. L.; Retey, J. *Chem. - Eur. J.* **2003**, 9, 652.
- (25) Ng, F. T. T.; Rempel, G. L.; Halpern, J. *Inorg. Chim. Acta* **1983**, 77, L165.
- (26) Halpern, J. *Science* **1985**, 227, 869.
- (27) Sharma, P. K.; Chu, Z. T.; Olsson, M. H. M.; Warshel, A. *Proc. Natl. Acad. Sci. U. S. A.* **2007**, 104, 9661.
- (28) Brooks, A. J.; Vlasie, M.; Banerjee, R.; Brunold, T. C. *J. Am. Chem. Soc.* **2005**, 127, 16522.
- (29) Brooks, A. J.; Fox, C. C.; Marsh, E. N. G.; Vlasie, M.; Banerjee, R.; Brunold, T. C. *Biochemistry* **2005**, 44, 15167.
- (30) Durbeej, B.; Sandala, G. M.; Bucher, D.; Smith, D. M.; Radom, L. *Chem. - Eur. J.* **2009**, 15, 8578.
- (31) Dolker, N.; Maseras, F.; Siegbahn, P. E. M. *Chem. Phys. Lett.* **2004**, 386, 174.
- (32) Friedrich, P.; Baisch, U.; Harrington, R. W.; Lyatuu, F.; Zhou, K.; Zelder, F.; McFarlane, W.; Buckel, W.; Golding, B. T. *Chem. - Eur. J.* **2012**, 18, 16114.
- (33) Li, X.; Chung, L. W.; Paneth, P.; Morokuma, K. *J. Am. Chem. Soc.* **2009**, 131, 5115.
- (34) Brooks, A. J.; Vlasie, M.; Banerjee, R. V.; Brunold, T. C. *J. Am. Chem. Soc.* **2004**, 126, 8167.
- (35) Ludwig, M. L.; Matthews, R. G. *Annu. Rev. Biochem.* **1997**, 66, 269.

- (36) Pratt, J. M. *J. Inorg. Biochem.* **1986**, 28, 145.
- (37) Pratt, J. M. *Chem. Soc. Rev.* **1985**, 14, 161.
- (38) Brown, K. L. *Dalton Trans.* **2006**, 1123.
- (39) Yeh, H. J. C.; Kirk, K. L.; Cohen, L. A.; Cohen, J. S. *J. Chem. Soc., Perkin Trans. 2* **1975**, 928.
- (40) Marques, H. M.; Egan, T. J.; Marsh, J. H.; Mellor, J. R.; Munro, O. Q. *Inorg. Chim. Acta* **1989**, 166, 249.
- (41) Note that while fluoro substituents have nuanced effects on the reactivity of aromatic compounds because of competing inductive and resonance effects, in this work we used F-Im primarily because of its reduced basicity that results from the substituent's electron withdrawing power
- (42) Kozlowski, P. M.; Zqierski, M. Z. *J. Phys. Chem. B* **2004**, 108, 14163.
- (43) Mancia, F.; Keep, N. H.; Nakagawa, A.; Leadlay, P. F.; McSweeney, S.; Rasmussen, B.; Bosecke, P.; Diat, O.; Evans, P. R. *Structure* **1996**, 4, 339.
- (44) Scheuring, E.; Padmakumar, R.; Banerjee, R.; Chance, M. R. *J. Am. Chem. Soc.* **1997**, 119, 12192.
- (45) Jensen, K. P.; Ryde, U. *J. Mol. Struct.: THEOCHEM* **2002**, 585, 239.
- (46) Andruniow, T.; Kuta, J.; Zgierski, M. Z.; Kozlowski, P. M. *Chem. Phys. Lett.* **2005**, 410, 410.
- (47) Kuta, J.; Wuerges, J.; Randaccio, L.; Kozlowski, P. M. *J. Phys. Chem. A* **2009**, 113, 11604.
- (48) De March, M.; Demitri, N.; Geremia, S.; Hickey, N.; Randaccio, L. *J. Inorg. Biochem.* **2012**, 116, 215.
- (49) Govender, P. P.; Navizet, I.; Perry, C. B.; Marques, H. M. *J. Phys. Chem. A* **2013**, 117, 3057.
- (50) Sirovatka, J. M.; Finke, R. G. *Inorg. Chem.* **1999**, 38, 1697.
- (51) Dong, S.; Padmakumar, R.; Banerjee, R.; Spiro, T. G. *J. Am. Chem. Soc.* **1996**, 118, 9182.
- (52) Puckett, J., J. M.; Mitchell, M. B.; Hirota, S.; Marzilli, L. G. *Inorg. Chem.* **1996**, 35, 4656.
- (53) Horig, J. A.; Renz, P.; Heckmann, G. *J. Biol. Chem.* **1978**, 253, 7410.
- (54) Kraeutler, B.; Konrat, R.; Stupperich, E.; Faerber, G.; Gruber, K.; Kratky, C. *Inorg. Chem.* **1994**, 33, 4128.
- (55) Stupperich, E.; Steiner, I.; Ruhlemann, M. *Anal. Biochem.* **1986**, 155, 365.
- (56) Renz, P.; Donald, B. M.; Lemuel, D. W. *Methods Enzymol.* **1971**, 18, Part C, 82.
- (57) Park, K.; Mera, P. E.; Escalante-Semerena, J. C.; Brunold, T. C. *Biochemistry* **2008**, 47, 9007.
- (58) Stich, T. A.; Buan, N. R.; Escalante-Semerena, J. C.; Brunold, T. C. *J. Am. Chem. Soc.* **2005**, 127, 8710.
- (59) Harmer, J.; Van Doorslaer, S.; Gromov, I.; Schweiger, A. *Chem. Phys. Lett.* **2002**, 358, 8.

- (60) Neese, F. Electronic Structure and Spectroscopy of Novel Copper Chromophores in Biology. Ph.D. Thesis, University of Konstanz, 1997
- (61) Lenhert, P. G. *Proc. R. Soc. London, Ser. A* **1968**, 303, 45.
- (62) Vreven, T.; Byun, K. S.; Komaromi, I.; Dapprich, S.; Montgomery, J. A.; Morokuma, K.; Frisch, M. J. *J. Chem. Theory Comput.* **2006**, 2, 815.
- (63) Gaussian 09; Revision D.01; Frisch, M. J.; Trucks, G. W.; Schlegel, H. B.; Scuseria, G. E.; Robb, M. A.; Cheeseman, J. R.; Scalmani, G.; Barone, V.; Mennucci, B.; Petersson, G. A.; Nakatsuji, H.; Caricato, M.; Li, X.; Hratchian, H. P.; Izmaylov, A. F.; Bloino, J.; Zheng, G.; Sonnenberg, J. L.; Hada, M.; Ehara, M.; Toyota, K.; Fukuda, R.; Hasegawa, J.; Ishida, M.; Nakajima, T.; Honda, Y.; Kitao, O.; Nakai, H.; Vreven, J. A.; Montgomery, J., A.; Peralta, J. E.; Ogliaro, F.; Bearpark, M.; Heyd, J. J.; Brothers, E.; Kudin, K. N.; Staroverov, V. N.; Kobayashi, R.; Normand, J.; Raghavachari, K.; Rendell, A.; Burant, J. C.; Iyengar, S. S.; Tomasi, J.; Cossi, M.; Rega, N.; Millam, J. M.; Klene, M.; Knox, J. E.; Cross, J. B.; Bakken, V.; Adamo, C.; Jaramillo, J.; Gomperts, R.; Stratmann, R. E.; Yazyev, O.; Austin, A. J.; Cammi, R.; Pomelli, C.; Ochterski, J. W.; Martin, R. L.; Morokuma, K.; Zakrzewski, V. G.; Voth, G. A.; Salvador, P.; Danneberg, J. J.; Dapprich, S.; Daniels, A. D.; Farkas, O.; Foresman, J. B.; Ortiz, J. V.; Cioslowski, J.; Fox, D. G.; Gaussian Inc.: Wallingford, CT, 2009.
- (64) Becke, A. D. *J. Chem. Phys.* **1993**, 98, 1372.
- (65) Perdew, J. P. *Phys. Rev. B: Condens. Matter Mater. Phys.* **1986**, 33, 8822.
- (66) Kuta, J.; Patchkovskii, S.; Zgierski, M. Z.; Kozlowski, P. M. *J. Comput. Chem.* **2006**, 27, 1429.
- (67) Schafer, A.; Huber, C.; Ahlrichs, R. *J. Chem. Phys.* **1994**, 100, 5829.
- (68) Schafer, A.; Horn, H.; Ahlrichs, R. *J. Chem. Phys.* **1992**, 97, 2571.
- (69) Marques, H. M.; Ngoma, B.; Egan, T. J.; Brown, K. L. *J. Mol. Struct.* **2001**, 561, 71.
- (70) Lee, C. T.; Yang, W. T.; Parr, R. G. *Phys. Rev. B: Condens. Matter Mater. Phys.* **1988**, 37, 785.
- (71) Stich, T. A.; Buan, N. R.; Brunold, T. C. *J. Am. Chem. Soc.* **2004**, 126, 9735.
- (72) Stich, T. A.; Brooks, A. J.; Buan, N. R.; Brunold, T. C. *J. Am. Chem. Soc.* **2003**, 125, 5897.
- (73) Kornobis, K.; Kumar, N.; Lodowski, P.; Jaworska, M.; Piecuch, P.; Lutz, J. J.; Wong, B. M.; Kozlowski, P. M. *J. Comput. Chem.* **2013**, 34, 987.
- (74) Tao, J. M.; Perdew, J. P.; Staroverov, V. N.; Scuseria, G. E. *Phys. Rev. Lett.* **2003**, 91, 4.
- (75) Neese, F. *Wiley Interdiscip. Rev.: Comput. Mol. Sci.* **2012**, 2, 73.
- (76) Neese, F.; Olbrich, G. *Chem. Phys. Lett.* **2002**, 362, 170.
- (77) Hirata, S.; Head-Gordon, M. *Chem. Phys. Lett.* **1999**, 314, 291.
- (78) The PyMOL Molecular Graphics System, Version 1.5.0.4 Schrodinger, LLC.
- (79) Reig, A. J.; Conrad, K. S.; Brunold, T. C. *Inorg. Chem.* **2012**, 51, 2867.
- (80) Hofmann, K. *Imidazole and its derivatives*; Interscience Publishers: New York, NY, 1953; Vol. 6.

- (81) Jensen, K. P.; Ryde, U. *J. Am. Chem. Soc.* **2005**, *127*, 9117.
- (82) Buckel, W.; Friedrich, P.; Golding, B. T. *Angew. Chem., Int. Ed.* **2012**, *51*, 9974.

CHAPTER 3

*Spectroscopic and Computational Investigation of the
Adenosylcobalamin-Dependent
Ethanolamine Ammonia Lyase:
Insight into the Mechanism of Enzymatic
Co–C Bond Activation*

Ethanolamine ammonia lyase used to prepare samples for this work was expressed and purified by Kathy Krasny and Dr. Theodore Moore in the laboratories of Professor Jorge Escalante-Semerena in the Department of Bacteriology at the University of Wisconsin-Madison and the Department of Microbiology at the University of Georgia.

3.1 Introduction

Coenzyme B₁₂, also known as 5'-deoxyadenosylcobalamin (AdoCbl, Figure 3.1), is a remarkable cofactor utilized by many diverse organisms to assist in the 1,2-isomerization of various substrates.¹⁻³ AdoCbl features several unusual structural features, the roles of which have been extensively studied and debated. At its center is a Co(III) ion in an octahedral ligand environment, consisting of: 1) a tetradentate corrin macrocycle; 2) a dimethylbenzimidazole (DMB) lower axial ligand that is intramolecularly tethered to the corrin ring via a nucleotide loop; and 3) 5'-deoxyadenosyl group that to a large extent determines the properties, reactivity, and name of the cofactor. The presence of this ligand makes AdoCbl an exceedingly rare example of a natural, biologically relevant organometallic compound.

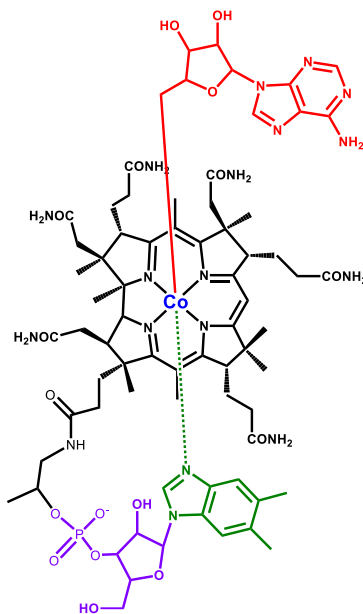
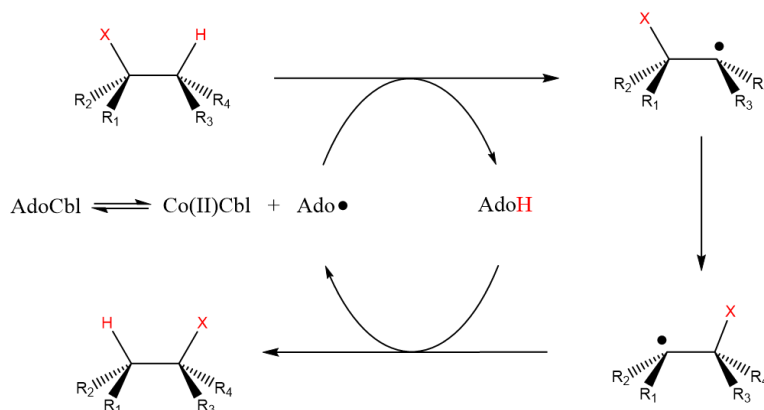


Figure 3.1. Adenosylcobalamin. The structure is color-coded to identify the Co(III) ion (blue), corrin ring (black), Ado (red) and DMB (green) ligands, and nucleotide loop (purple).

Scheme 3.1. General mechanism employed by AdoCbl-dependent enzymes.

All AdoCbl-dependent enzymes are thought to function via the same general mechanism (Scheme 3.1),^{4, 5} whereby homolysis of the cofactor's Co–C bond in AdoCbl is used to generate an organic adenosyl radical, Ado•, and the one-electron reduced cob(II)alamin, or Co(II)Cbl. The Ado• radical abstracts a hydrogen atom from the substrate to produce a substrate-like radical, S•, and 5'-deoxyadenosine (AdoH). The rearrangement of S• to form a product-like radical, P•, is then followed by re-abstraction of a hydrogen from AdoH. This step produces the final product and regenerates Ado•, which combines with the Co(II)Cbl to form AdoCbl and complete the catalytic cycle. Because uncatalyzed Co–C bond homolysis is very slow (rate constant of 10^{-9} s^{-1}),⁶ its activation energy must be substantially lowered for effective catalysis to occur. Kinetic studies of AdoCbl-dependent enzymes have shown that the effective rate constant of Co–C bond homolysis is increased by as many as 12 orders of magnitude in the enzyme active site, which is consistent with a lowering of the activation energy by 17 kcal/mol.^{7, 8} (Kinetic coupling between this step and the subsequent hydrogen abstraction has been observed in some enzymes,⁸⁻¹⁰ and thus stabilization of AdoH and S• may also contribute to the increased rate of homolytic bond cleavage.) The precise nature of the interactions between enzyme, cofactor, and substrate that lead to this rate enhancement remain incompletely understood.

Despite sharing a common mechanism, AdoCbl-dependent enzymes do exhibit some striking differences that allow for their general classification into Class I isomerases and Class II eliminases. The most puzzling distinction between the classes is the different cofactor binding modes they exhibit. Class I isomerases¹¹ bind the cofactor by displacing the DMB ligand with a protein-derived histidine side chain. Previous research by our group¹²⁻¹⁴ has led to the proposal that the electron-donating capabilities of this histidine residue are tuned via hydrogen-bonding interactions involving a network of amino acid side chains conserved in a DXHXGXX motif,¹⁵⁻¹⁷ and that this tuning results in a preferential stabilization of Co(II)Cbl relative to AdoCbl within the enzyme/cofactor complex. Because the Co–C bond homolysis is endergonic, it is likely to have a late transition state. Thus, stabilization of Co(II)Cbl, perhaps by a coupling of Co–C bond homolysis to proton uptake by the DXHXGXX motif,¹³ should give rise to a sizable stabilization of the transition state.

Interestingly, the Class II AdoCbl-dependent eliminases, which catalyze the rearrangement of small 1,2-diols or 1,2-amino-alcohols to place both functional groups on the terminal carbon,³ bind the cofactor with the Co–N_{DMB} bond intact.¹⁸⁻²¹ This poses an interesting dilemma, as the DMB base is incapable of participating in hydrogen bonding networks analogous to that involving the coordinating His residue in the isomerases. Thus, while the eliminases and isomerases similarly reduce the activation energy of the Co–C bond homolysis, they must employ different mechanisms to do so.

The eliminases diol dehydratase (DD) and ethanolamine ammonia lyase (EAL) have been studied extensively through X-ray crystallography²²⁻²⁴ and kinetics studies.²⁵⁻³² Fukuoka et al. synthesized AdoCbl analogues with either benzimidazole (Bzm) or imidazole (Im) bases in place of the native DMB, and tested the activity of these analogues in EAL.³³ The use of Bzm and Im

resulted in catalytic activities of 91% and 9%, respectively, of those observed with AdoCbl, indicating that the steric bulk of the lower axial ligand may play a role in activating the Co–C bond. Subsequent studies of analogues with modified Ado ligands lacking the ribosyl moiety's hydroxyl groups³⁴ or potential hydrogen bonding sites in the adenine ring³⁵ were also shown to exhibit diminished activity. These observations demonstrate that the cumulative effects of numerous protein-cofactor interactions on both the upper and lower faces of AdoCbl are necessary for maximum activity.^{12, 14}

In this study, we have performed a spectroscopic and computational investigation of EAL-bound AdoCbl in the presence and absence of its substrates ethanolamine and 2-aminopropanol to obtain insight into the mechanism of Co–C bond activation employed by EAL. Collectively, our results indicate that EAL imposes geometric constraints on the enzyme-bound cofactor that become more pronounced in the presence of substrate. These constraints may contribute to activation of the Co–C bond for homolysis via substrate-induced destabilization of AdoCbl, a mechanism that may be general to eliminases.

3.2 Methods

3.2.1 Sample Preparation. AdoCbl and (S)-2-amino-1-propanol, a slow substrate of EAL,³⁶ were purchased from Sigma-Aldrich and used as obtained. EAL was prepared in ~8 mM HEPES buffer. Samples used for absorption (Abs) and magnetic circular dichroism (MCD) measurements of free AdoCbl were prepared in a ~50% (v/v) glycerol/MQ H₂O glassing mixture and then frozen in liquid N₂. Samples of the EAL holoenzyme were prepared by addition of AdoCbl to the EAL apoenzyme in slightly less than a 1:1 stoichiometric ratio of AdoCbl:EAL active sites. Glycerol was then added to make a 50-60% (v/v) glycerol/HEPES glassing mixture and the samples were frozen in liquid N₂. To prepare samples of substrate-bound EAL

holoenzyme, the same procedure was used except for the addition of an excess of (S)-2-amino-1-propanol before the addition of glycerol. The final concentration of AdoCbl in all samples was 0.1-0.2 mM.

3.2.2. Spectroscopy. Low temperature Abs and 7 T MCD spectra were collected with a Jasco J-715 spectropolarimeter in conjunction with an Oxford Instruments SM4000-8T magnetocryostat. All reported MCD spectra were obtained by taking the difference of spectra collected with the magnetic field aligned parallel and antiparallel to the light propagation axis in order to remove contributions from the CD background signal and glass strain.

3.2.3 Computational Methods. Geometry Optimizations. A recent crystal structure of EAL²² containing both ethanolamine and the AdoCbl analogue adeninylpentylcobalamin (PDB: 3ABS) was used to generate initial coordinates for all computational models of the holoenzyme and ternary complex. The native cofactor was constructed *in silico* by replacing the pentamethylene moiety of the analogue with a ribosyl moiety. The pdb2pqr program³⁷ was used to add hydrogen atoms to ethanolamine, all crystallographic water molecules, and EAL (assuming a pH of 7), while Reduce³⁸ was used to protonate AdoCbl. PyMol³⁹ was utilized to create all *in silico* EAL variants. The optimized AdoCbl coordinates from the WT ternary complex were employed as initial coordinates for the optimization of the free AdoCbl model.

All geometry optimizations were carried out in two steps with the Gaussian09 computational package.⁴⁰ An initial molecular mechanics (MM) optimization using the AMBER force field⁴¹ was performed to ensure reasonable placement of hydrogen atoms and to relieve any strained conformations. AMBER parameters for portions of serine ($-\text{CH}_2\text{OH}$) and protonated lysine ($-\text{CH}_2\text{NH}_3^+$) were used as MM parameters for ethanolamine. The AdoCbl coordinates were

frozen in these optimizations; however, the force field from Marques et al.⁴² was used for the cofactor to account for non-bonding interactions between AdoCbl and the protein and/or substrate.

The coordinates from the converged MM optimization were used to generate input files for the subsequent QM/MM optimizations. The QM portion of the calculation included the cofactor's Co(III) ion, the ribose moiety of the Ado ligand, the DMB ligand, and the corrin ring core plus the first carbon of each side chain. The MM region contained the remainder of the corrin ring's side chains and the nucleotide loop connecting the ring to the DMB, and the entirety of the protein, all solvent molecules, and the substrate. All covalent bonds spanning the QM/MM boundary were capped with hydrogen atoms (i.e., link atoms) during the QM steps of the optimization. The new X–H bond lengths were set equal to the original bond length scaled by a factor of 0.709. Additionally, all EAL residues and solvent molecules more than 5 Å away from the QM region were frozen. All QM/MM computations were performed at the BP86^{43,44}/AMBER level of theory, as BP86 has previously been shown to be the preferred density functional for the reproduction of geometric parameters of cobalamins.⁴⁵ The LanL2DZ basis set⁴⁶⁻⁴⁸ was used for all QM atoms. The AMBER force field parameters for ethanolamine and AdoCbl were identical to those in the MM optimizations. The default convergence criteria were used in most cases. However, some optimizations reached a point where the models exhibited negligible atomic displacements for many steps while still possessing maximum and/or RMS forces that were slightly above the convergence cutoff. These models were considered converged if the maximum and RMS forces were within a factor of 5 of the corresponding default convergence criteria.

TD-DFT Calculations. Time-dependent density functional theory (TD-DFT) was used in conjunction with the B3LYP hybrid functional^{49,50} to compute the electronic Abs spectrum of the optimized QM region of each model with the ORCA 2.9 computational package.⁵¹ All atoms from

the MM region except for those replaced by link atoms were included in the TD-DFT computation as point charges with magnitudes equal to those used in the MM calculations. All TD-DFT computations were performed with the resolution of the identity⁵² and Tamm-Dancoff approximations⁵³ to speed up the calculations. The 60 lowest energy transitions within ± 4 Hartree of the HOMO-LUMO gap were computed for each model. The triple-zeta basis set with an additional polarization function (TZVP) developed by Ahlrichs⁵⁴ was used for the Co ion and all coordinating N and C atoms, while the same group's split-valence polarized (SVP) basis set⁵⁵ was used for all other QM atoms. The TD-DFT results were used to simulate Abs spectra using a constant bandwidth of 1500 cm^{-1} for each transition. All isosurface plots of MOs and electron density difference maps (EDDMs) were created in PyMol³⁹ with isodensity surfaces of 0.06 and 0.003 a.u., respectively.

3.3 Results

3.3.1 Spectroscopic Data for WT EAL. As was reported previously by Chen et al., the Abs spectrum of AdoCbl undergoes minor changes upon the addition of apoEAL (Figure 3.2).⁵⁶ In particular, two specific changes can be readily noted. First, the binding of AdoCbl to apoEAL induces a blue-shift of about 175 cm^{-1} of the lowest-energy features, generally referred to as the α/β bands. Additionally, increased Abs intensity is observed in the $23\,000 - 25\,000\text{ cm}^{-1}$ region. The features above $25\,000\text{ cm}^{-1}$, collectively called the γ region, also exhibit increases in Abs intensity, as well as blue-shifts of features between $28\,000$ and $30\,000\text{ cm}^{-1}$. The α/β bands have been extensively studied experimentally and theoretically, thus permitting a relatively straightforward interpretation of changes involving these bands (Section 3.4.1). However, the cofactor's complicated electronic structure and the poor resolution of the many overlapping

features contributing to the remainder of the Abs spectrum make immediate identification and interpretation of additional changes difficult.

The subsequent addition of substrate to the holoenzyme (to form what is referred to here as the ternary complex) induces additional changes to the cofactor's Abs spectrum. The α/β bands of AdoCbl in the ternary complex are blue-shifted from their counterparts of the free cofactor but red-shifted from those of AdoCbl in the holoenzyme. These band shifts, along with spectral changes observed at energies greater than $27\,000\text{ cm}^{-1}$, demonstrate that the electronic structure of AdoCbl in the ternary complex is distinct from those of the free and EAL-bound cofactor. There are additional perturbations to the Abs spectrum at intermediate energies, but the poor resolution of the overlapping features again makes assignment difficult.

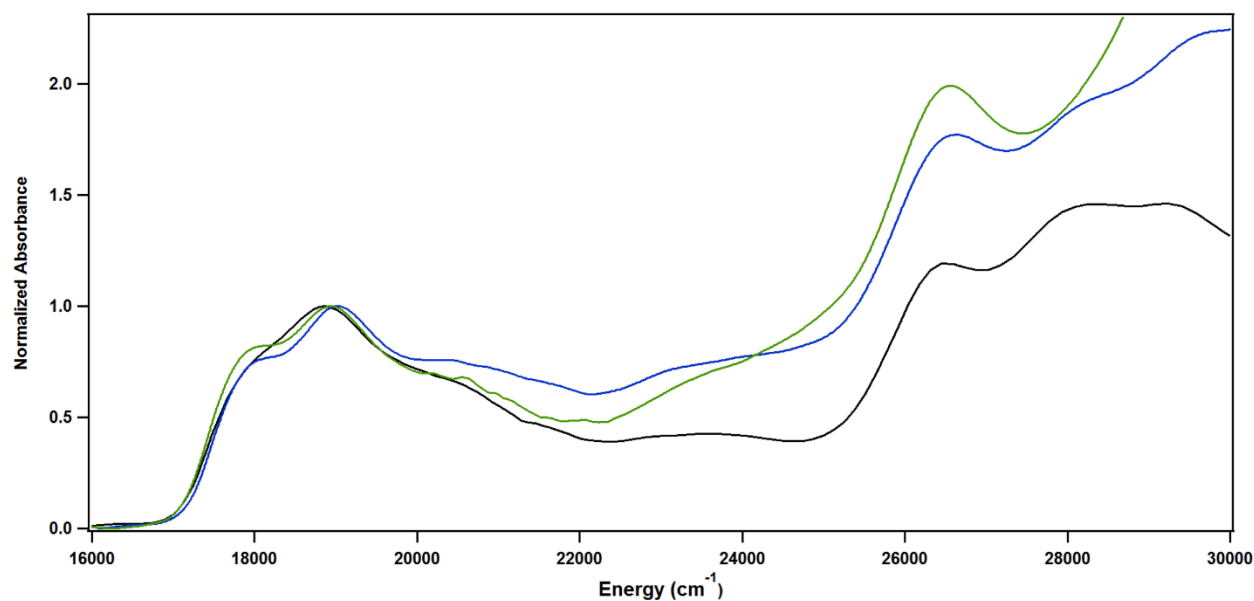


Figure 3.2. Abs spectra at 4.5 K of AdoCbl in solution (black), the EAL holoenzyme (blue), and the ternary complex (green). Spectra are normalized to an absorbance of 1 at the α/β band maxima.

The MCD spectra of free AdoCbl, the EAL holoenzyme, and the EAL ternary complex are shown in Figure 3.3. Because the MCD signal is a signed quantity, these spectra allow for the identification of transitions that might overlap or otherwise be obscured by more intense features

in the corresponding Abs spectrum. Of particular interest is the small derivative-shaped feature with positive and negative peaks at 24 400 and 25 000 cm^{-1} , respectively, in the holoenzyme MCD spectrum (referred to as feature **A** in Figure 3.3). This feature has no obvious counterpart in the free cofactor's MCD spectrum, but previous Gaussian deconvolutions⁵⁷ of the AdoCbl Abs, CD, and MCD spectra of the related species methylcobalamin (Figure A.3.1) revealed the presence of a broad, low-intensity, derivative-shaped feature at 24 000 – 26 000 cm^{-1} . While in the MCD spectrum of free AdoCbl this feature is typically obscured by the sharp positive feature at 26 300 cm^{-1} , it appears to be red-shifted in the holoenzyme, allowing for its direct observation.

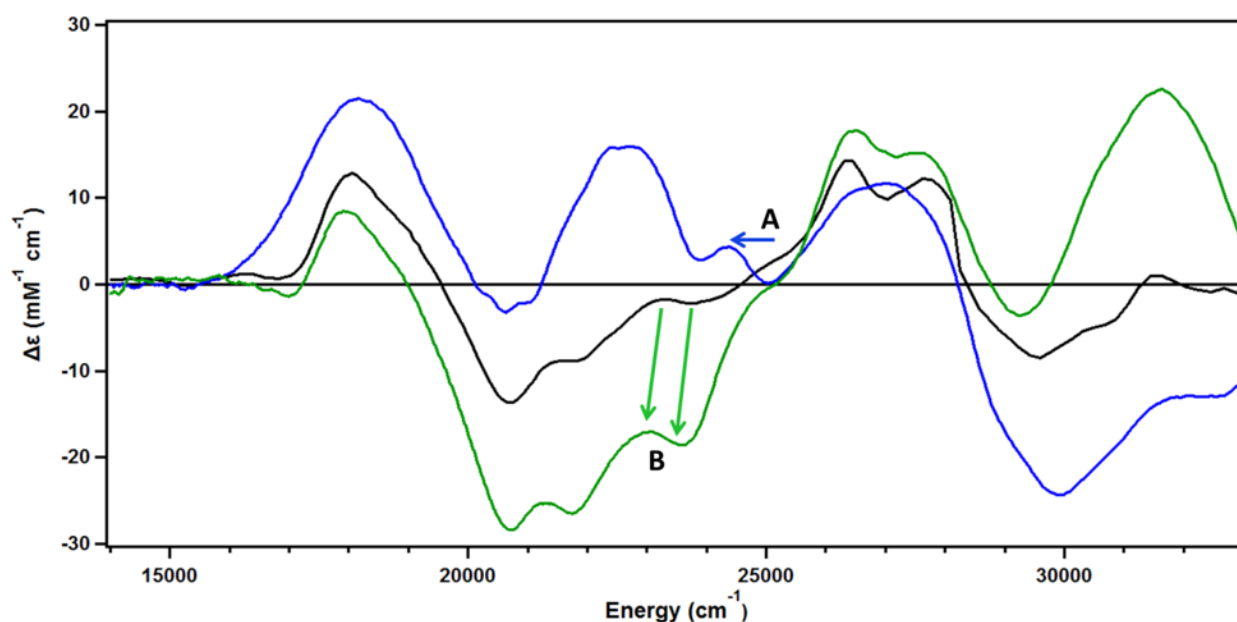


Figure 3.3. MCD spectra at 4.5 K of free AdoCbl (black), EAL holoenzyme (blue), and EAL ternary complex (green). Features **A** and **B** are described in the text.

The MCD spectrum of the ternary complex can be used to better identify changes in the cofactor's electronic structure caused by the addition of substrate. The shift observed for feature **A** upon holoenzyme formation is opposite of that observed upon the addition of substrate; as in the free cofactor's spectrum, feature **A** is only observed as a low-energy shoulder to the intense

positively-signed band at 26 500 cm^{-1} . Another noteworthy change in the ternary complex's spectrum is the red-shifting of a derivative-shaped feature found centered around 23 200 cm^{-1} (feature **B**). Interestingly, this feature was left unperturbed by the initial binding of AdoCbl, suggesting that the binding of AdoCbl to EAL and the addition of substrate induce distinct changes to the cofactor's electronic structure.

3.3.2 Computational Results for WT EAL. Relevant structural parameters of AdoCbl in the QM/MM-optimized models of the free cofactor, holoenzyme, and ternary complex are presented in Table 3.1. The Co–N_{DMB} bond of AdoCbl is predicted to shorten substantially from 2.38 Å to 2.27 Å upon cofactor binding to apoEAL. This change is accompanied by a tilting of the DMB ligand relative to the plane of the corrin ring. Because of the DMB ligand's rigid planarity, its tilt angle can be defined as the Co–N_{DMB}–C _{ϵ ,DMB} bond angle. Deviations of this angle from 180°, in which the Co–N_{DMB} bond vector lies in the DMB plane, can affect the electronic structure of AdoCbl by decreasing the overlap between the Co 3d_{z²} orbital and the N_{DMB} lone pair. Thus, it is interesting to note that upon binding of AdoCbl to EAL, the tilt angle decreases by 6.4° (from 166.7° to 160.3°). The geometry at the upper face of AdoCbl remains largely unchanged in this process, with the Co–C bond length remaining constant at 2.03 Å.

Table 3.1. Relevant structural parameters of AdoCbl in the QM/MM-optimized models of free AdoCbl, the EAL holoenzyme, and the EAL ternary complex. All distances are in Å and all angles are in degrees.

Model	r(Co-C)	r(Co-N _{DMB})	DMB tilt angle	$\theta(\text{Co-C-C})$
Free AdoCbl	2.03	2.38	166.7	128.4
Holoenzyme	2.03	2.27	160.3	125.6
Ternary Complex	2.12	2.45	163.4	137.8

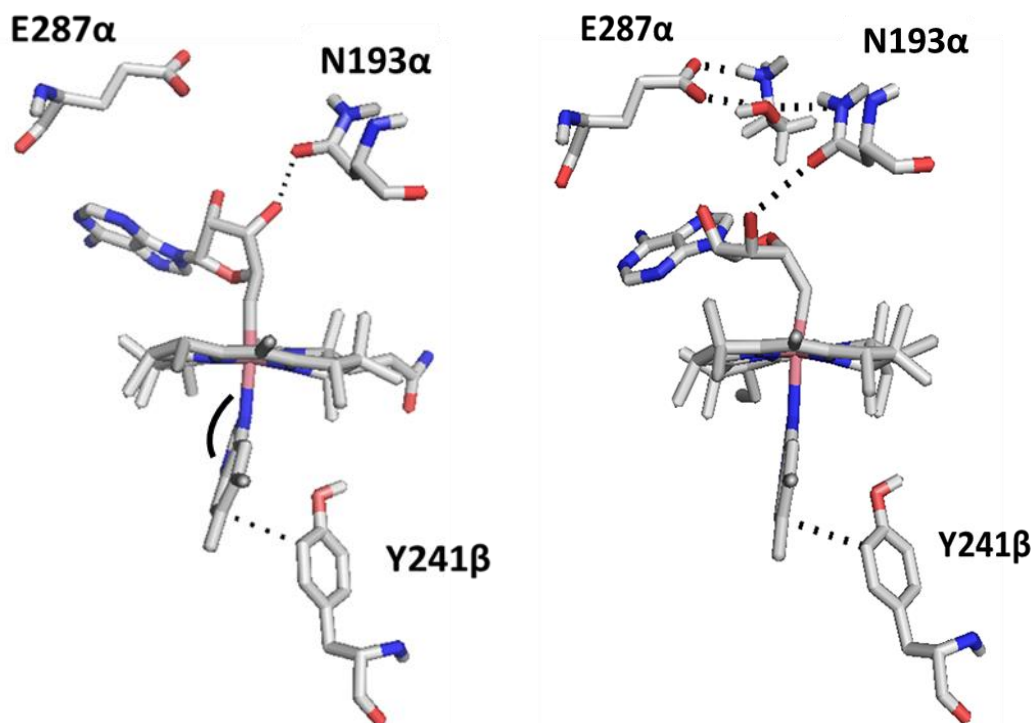


Figure 3.4. A comparison of the QM/MM-optimized geometries of the EAL holoenzyme (left) and EAL ternary complex (right). Closest contacts between the cofactor and N193α and Y241β are shown with dashed lines, as are the H-bonds between the substrate, E287α, and N193α. The DMB tilt angle is shown for the holoenzyme model.

Inspection of the optimized active-site geometry of the EAL holoenzyme reveals multiple amino acids that may share some responsibility for the observed distortions of the AdoCbl cofactor (Figure 3.4, left). The geometric changes at the lower face of AdoCbl appear to be due primarily to Y241β, which encroaches on the DMB from one side. The shortest $C_{\text{DMB}} - C_{\text{Y241}\beta}$ distance is 3.38 Å in the holoenzyme, and this close contact is likely responsible for changes to the tilt angle.

The binding of substrate to the EAL holoenzyme is predicted to induce further geometric changes to AdoCbl. In the optimized model of the ternary complex, both the $\text{Co}-\text{N}_{\text{DMB}}$ and $\text{Co}-\text{C}$ axial bonds of AdoCbl are considerably elongated from their counterparts in free AdoCbl and the holoenzyme. Additionally, a notable opening of the $\text{Co}-\text{C}-\text{C}$ angle occurs in response to substrate binding as a result of the twisting of the adenosyl group to optimize hydrogen-bonding interactions

between the Ado ligand and the newly rearranged active site (*vide infra*). The tilting of the DMB group in the ternary complex is much less severe than in the holoenzyme, as indicated by an increased tilt angle of 163.4° , which is roughly halfway between the values for the free and enzyme-bound cofactor.

The rearrangement of the EAL active site upon substrate binding is substantial (Figure 3.4, right), as no fewer than six amino acid residues reorient to form hydrogen bonds or other interactions with the substrate. Two of these residues appear to be chiefly responsible for the changes in AdoCbl geometry predicted in this state. E287 α fixes the orientation of the substrate through two hydrogen bonds, while N193 α is the only residue to form hydrogen bonds to both AdoCbl and the substrate. Substrate binding to the holoenzyme appears to cause N193 α to move toward the Ado ligand, with the amide oxygen of the N193 α side chain approaching to within 2.95 Å of the 3'-OH group of the Ado ligand's ribosyl moiety. This movement may be responsible, at least in part, for the observed lengthening of the Co–C bond and opening of the Co–C–C bond angle.

TD-DFT was used to calculate the electronic Abs spectrum of free AdoCbl, as well as of AdoCbl in the EAL holoenzyme and ternary complex. While a useful method for calculating excitation energies, we have noted previously that TD-DFT systematically underestimates these energies for cobalamins.⁵⁷ In the past, we have accounted for this discrepancy by applying a uniform blue-shift to computed Abs spectra to align the dominant features with those of experimental Abs spectra. However, in the present study, distinct shifts are required for the computed Abs spectra of the three models. This is due to the difference in their sizes, which range from 209 atoms for the free AdoCbl model to more than 10 000 atoms for those of EAL. To demonstrate that the presence of additional MM atoms (modeled as point charges) in the

holoenzyme and ternary complex models indeed affect the computed transition energies, we performed an additional TD-DFT calculation for the cofactor using its optimized geometry in the holoenzyme and ignoring some or all of the point charges representing EAL (Figure A.3.2). The exclusion of the EAL point charges results in a nearly uniform red-shift of the Abs spectrum by 1440 cm^{-1} , with one notable exception that will be discussed in Section 3.4.2. Therefore, to facilitate a direct comparison between our experimental and computed Abs spectra, we took advantage of the fact that the lowest energy feature of the γ region is observed at $26\,200\text{ cm}^{-1}$ in all three of our experimental Abs spectra and shifted the computed spectra to align that feature. Thus, in our analysis we compare the position of all features relative to the most prominent γ band.

The computed Abs spectra for free AdoCbl and AdoCbl bound to the EAL holoenzyme and ternary complex are presented in Figure 3.5. Most notably, the three models display the experimentally observed trend in the AdoCbl α/β band energies (free AdoCbl < ternary complex < holoenzyme). Furthermore, the models of holoenzyme- and ternary complex-bound AdoCbl each demonstrate the growth of Abs features at $22\,000 - 24\,000\text{ cm}^{-1}$ that are consistent with the red-shifting of features **A** and **B** into this energy window observed in the MCD spectra of these states. The agreement of the experimental and computed spectra demonstrates that the theoretical methods utilized here are well-suited to describe changes to the electronic structure of AdoCbl in the enzymatic environment. As such, the models of AdoCbl bound to the EAL holoenzyme and ternary complex warrant further investigation to determine the specific relationships between changes in key geometric parameters and the observed spectroscopic shifts.

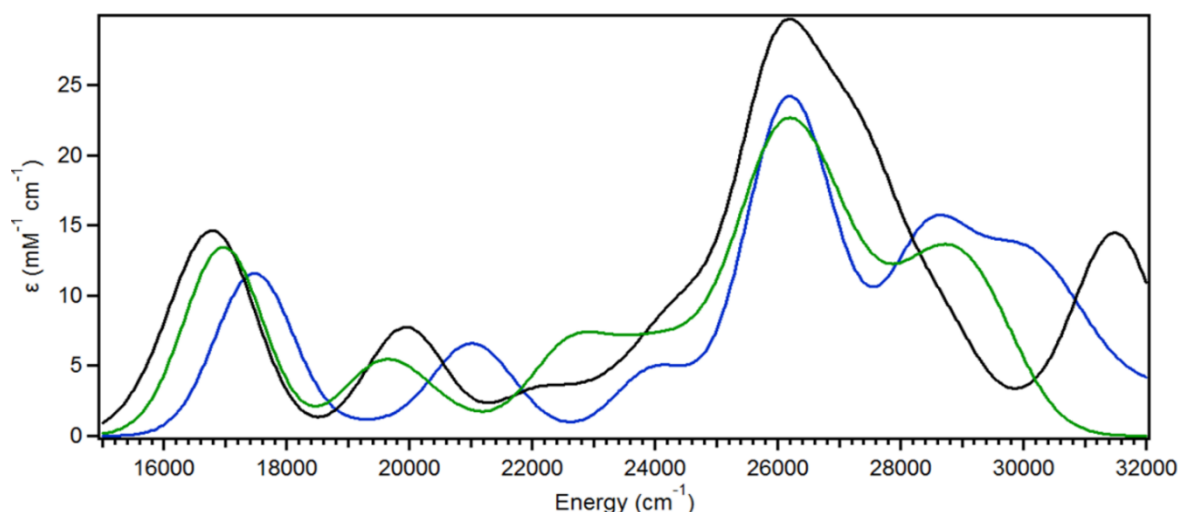


Figure 3.5. Computed Abs spectra for free AdoCbl (black) and AdoCbl bound to the EAL holoenzyme (blue) and ternary complex (green). All models are shifted to align the maximum intensity to $26\,200\text{ cm}^{-1}$.

To determine the effect of changes to the Co–N_{DMB} bond length and DMB tilt angle on the computed Abs spectrum of AdoCbl, we calculated Abs spectra for two series of cofactor geometries. In the first (Figure 3.6, series **1**), the optimized coordinates of free AdoCbl were fixed except for the Co–N_{DMB} bond distance, which was varied from 1.9 Å to 2.6 Å in 0.1 Å increments. The second series (Figure 3.7, series **2**) used the same Co–N_{DMB} bond lengths but otherwise used the optimized coordinates of EAL-bound AdoCbl. One additional geometry was added to each series (with a Co–N_{DMB} bond length of 2.27 Å for series **1** and 2.38 Å for series **2**) so that, when combined with the spectra in Figure 3.5, each series included models with both equilibrium Co–N_{DMB} bond lengths.

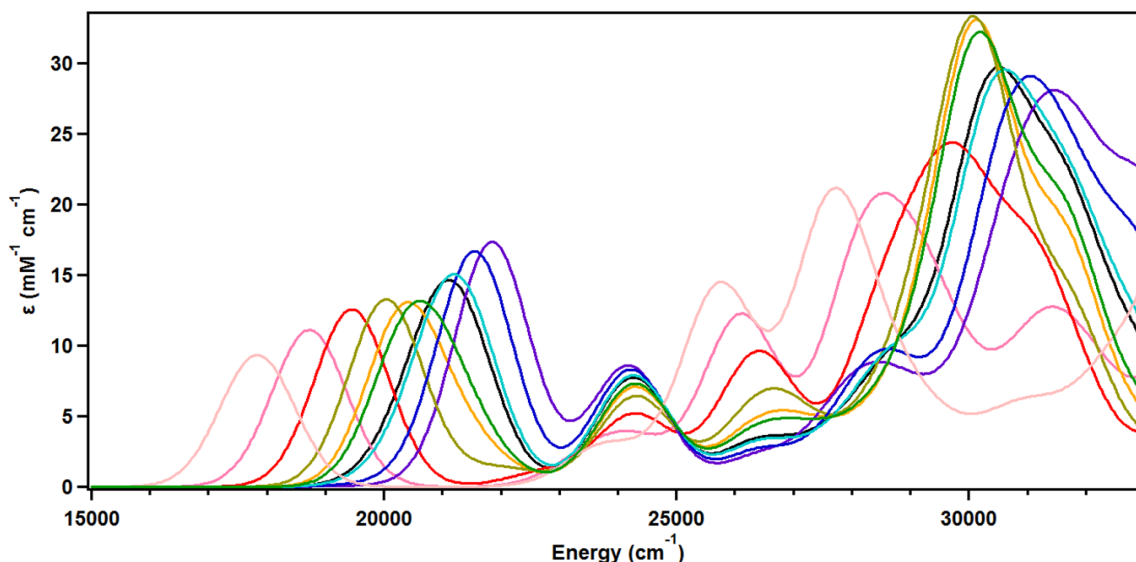


Figure 3.6. TD-DFT spectra for models of AdoCbl with variable Co–N_{DMB} distance, ranging from 1.9 Å (pink) to 2.6 Å (purple) in 0.1 Å intervals. The DMB tilt angle was kept constant at 166.7° as in the optimized structure of free AdoCbl. Also included are computed spectra for AdoCbl with the Co–N_{DMB} distance fixed at 2.27 Å (orange) and 2.38 Å (black). All spectra are unshifted; otherwise, the black spectrum is identical to the red spectrum in Figure 3.5.

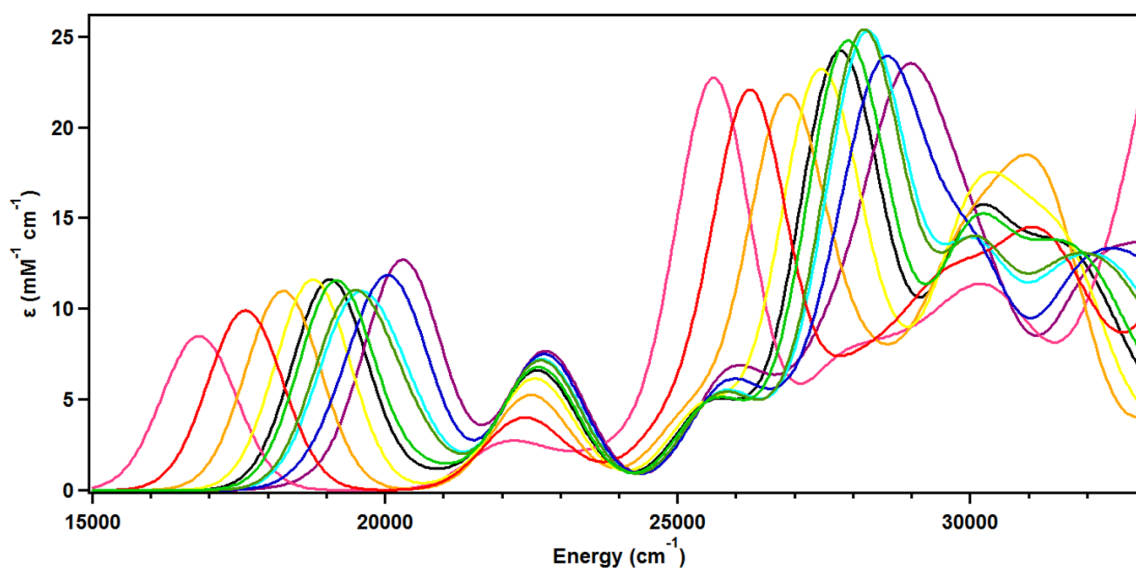


Figure 3.7. TD-DFT spectra for models of AdoCbl bound to the holoenzyme with variable Co–N_{DMB} distance, ranging from 1.9 Å (pink) to 2.6 Å (purple) in 0.1 Å intervals. The DMB tilt angle was kept constant at 160.3° as in the optimized holoenzyme model. Also included are computed spectra with the Co–N_{DMB} distance at 2.27 Å (black) and 2.38 Å (green). All spectra are unshifted; otherwise, the black spectrum is identical to the blue spectrum in Figure 3.5.

The computed Abs spectra for the models in series **1** demonstrate the dramatic effect that axial perturbations have on the positions and intensities of all electronic transitions. The behavior of the α/β bands is straightforward, as they shift to higher energies as the Co–N_{DMB} bond is lengthened. However, the effect of this bond length on features at higher energies is more subtle, as the band-shape of the γ region appears to undergo several qualitative changes as the Co–N_{DMB} bond length is increased. At short Co–N_{DMB} distances (1.9 – 2.2 Å), the γ region consists of two distinct features separated by at least 2000 cm⁻¹. As the Co–N_{DMB} bond grows longer, the higher energy feature blue-shifts and intensifies while the lower energy feature's intensity diminishes greatly. At intermediate Co–N_{DMB} bond lengths (2.2 – 2.3 Å) the γ region appears as a single, intense feature, though that feature is in fact composed of several moderately intense transitions. Further lengthening of the lower axial bond length causes the more intense transitions that contribute to the γ band to blue-shift while other, weaker transitions red-shift. The net effect of these competing trends is the appearance of a shoulder to the most intense feature of the γ band at Co–N_{DMB} bond lengths of ~2.40 Å, which becomes a distinct feature if the DMB is pulled even farther away.

Similar trends can be seen in the computed Abs spectra for the models in series **2**. Again, the α/β bands and the features in the γ region exhibit blue-shifts as the Co–N_{DMB} bond lengthens. While the energies of the features observed at intermediate energies do not appear to follow a clear trend, a low-energy shoulder to the γ band develops at Co–N_{DMB} bond lengths exceeding 2.1 Å. As in the free cofactor, this shoulder becomes a distinct feature as the Co–N_{DMB} bond gets longer. Although this feature actually blue-shifts, the larger blue-shift of the γ band ensures that the energy difference between these two features increases.

3.3.3 Computational Analysis of Select EAL Variants. The roles of E287 α , N193 α , and Y241 β were investigated computationally by generating whole-protein models of five *in silico* variants holoenzymes: E287 α A, E287 α D, E287 α Q, Y241 α A, and N193 α A. Additionally, we have computationally investigated the ternary complexes of the E287 α A, E287 α D, and N193 α A variants. Key geometric parameters for these AdoCbl-bound variants are presented in Tables 3.2 and 3.3.

Table 3.2. Key geometric parameters for AdoCbl-bound WT EAL and five variants. All angles are in degrees and all distances in Å.

Model	r(Co-C)	r(Co-N _{DMB})	DMB tilt	θ (Co-C-C)	r(O _{Ado} -O _{N193})
WT	2.03	2.27	160.3	125.6	3.39
E287 α A	2.03	2.34	161.3	125.5	3.60
E287 α D	2.03	2.32	162.6	126.4	3.59
E287 α Q	2.03	2.31	161.9	125.8	3.56
Y241 α A	2.03	2.40	163.9	125.5	3.82
N193 α A	2.02	2.32	160.6	126.2	N/A

Table 3.3. Geometric parameters for AdoCbl-bound WT EAL and three variants in the presence of substrate. All angles are in degrees and all distances in Å.

Model	r(Co-C)	r(Co-N _{DMB})	DMB tilt	θ (Co-C-C)	r(O _{Ado} -O _{N193})
WT	2.12	2.45	163.4	137.8	2.95
E287 α A	2.02	2.29	161.3	126.9	3.61
E287 α D	2.02	2.26	168.7	127.3	3.37
N193 α A	2.02	2.32	168.6	127.0	N/A

Our computational results suggest that AdoCbl adopts a less distorted geometry in the E287 α variants than in WT EAL. Even the relatively conservative E287 α D and E287 α Q substitutions result in longer Co-N_{DMB} bonds (2.32 Å and 2.31 Å, respectively) than the computationally predicted Co-N_{DMB} bond length of 2.38 Å for WT EAL-bound AdoCbl. The variant-bound AdoCbl species also exhibit more relaxed DMB tilt angles (162.6° and 161.9°), showing that even minor perturbations to the E287 α side chain can mitigate the already weak

constraints placed on the cofactor's geometry in the holoenzyme. Interestingly, the Co–C bond distance is constant among all of these variants. This result suggests that the increase in the Co–N_{DMB} bond length is caused by an “upshift” of both the Co ion and the Ado ligand in the active site while the position of the DMB ligand remains fixed. The E287 α A substitution creates a larger cavity in the active site, allowing for further relaxation of the cofactor geometry. In this variant, the calculated Co–N_{DMB} bond length is 2.34 Å, much closer to the bond length in the free cofactor than in the WT holoenzyme.

It has previously been shown that the E287 α D and E287 α Q substitutions have a small but noticeable effect on the Abs spectrum of EAL-bound AdoCbl.⁵⁶ The most noticeable changes involve the transitions slightly lower in energy than those responsible for the γ band (i.e., in the region of features **A** and **B**). As mentioned previously in this chapter, it is difficult to identify the origin of the most strongly perturbed features in this region on the basis of Abs spectra alone. However, we do note that the features responsible for the increased intensity in the general vicinity of features of **A** and **B** are shifted to lower energy in the computed Abs spectrum for each of the variants. Small red-shifts of the positions of the α/β bands of EAL-bound AdoCbl may also be caused by the E287 α D and E287 α Q substitutions, although the predicted shifts are within the range of experimental uncertainty. Overall, the E287 α A substitution induces more dramatic changes to the computed Abs spectrum, including a sizable blue-shift of the α/β bands.

In the analysis of our TD-DFT results, we acknowledged that just as the inclusion of EAL point charges caused a shift in the computed excitation energies, the removal of point charges associated with E287 α (e.g., via an E287 α A substitution) caused a shift that can mask any meaningful changes we wish to observe. Thus, as in our comparison of the computed Abs spectra for free AdoCbl, the holoenzyme, and the ternary complex, we note that the most prominent feature

in the γ region is unperturbed in the experimental spectra of the EAL variant holoenzymes, and consequently chose to align that feature in our computed spectra (Figure 3.8). Upon doing so, we found that the computations qualitatively reproduce the experimentally observed changes. The E287 α D and E287 α Q substitutions cause a red-shift of EAL-bound AdoCbl features beneath the γ band without substantially affecting the α/β bands. The less conservative E287 α A substitution results in a 134 cm^{-1} blue-shift of the α/β bands, in qualitative agreement with the experimentally observed $\sim 350 \text{ cm}^{-1}$ shift.

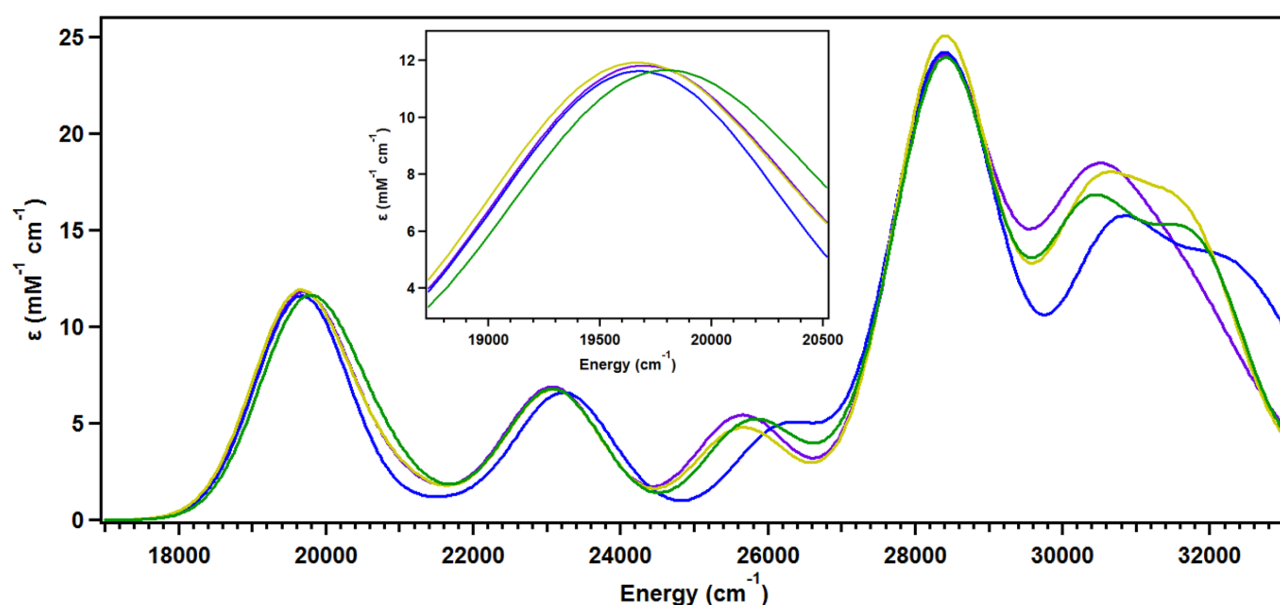


Figure 3.8. Computed Abs spectra for AdoCbl-bound WT EAL (blue) and three E287 α variants: E287 α D (purple), E287 α Q (gold), and E287 α A (green). The spectra were shifted to align the γ bands at 28 400 cm^{-1} . The inset shows the positions of the α/β band maxima.

It was shown by Chen et al. that the E287 α A, E287 α D, and E287 α Q substitutions all had a significant impact on EAL activity. While the E287 α A variant was, perhaps unsurprisingly, unable to achieve turnover, the E287 α D and E287 α Q variants displayed a 1000-fold increase in K_M and 10- and 100-fold decreases in k_{cat} , respectively. That these substitutions affect both K_M and k_{cat} implies that E287 α is required for both strong substrate binding and the correct positioning

of the substrate in the active site. The optimized geometries of our E287 α A and E287 α D variant ternary complex models, which do not show the lengthened Co–C bond, strained Co–C–C bond angle, and short Ado–N193 α distance seen in the WT ternary complex, are consistent with the observed loss of activity.

On the basis of the general agreement between theory and experiment regarding the E287 α variants, we now comment briefly on the computed geometries for the Y241 β A and N193 α A variants. Our results suggest that substitution of these residues with alanine has pronounced effects on the cofactor's geometry. In Section 3.2, we discussed the putative role of Y241 β in both decreasing the Co–N_{DMB} bond length and the DMB tilt angle of EAL-bound AdoCbl. Neither of these changes are observed in the Y241 β A variant, which appears to bind AdoCbl in a conformation more similar to that adopted by the free cofactor than WT-bound AdoCbl. The removal of N193 α has a moderate effect on the geometry of AdoCbl in the holoenzyme, similar to what is predicted for the E287 α variants featuring conservative substitutions. However, unlike in the WT enzyme, addition of substrate to the N193 α A variant has no effect on the cofactor's axial bond lengths. The implication of these computed geometries with respect to the mechanism of Co–C bond activation employed by EAL is discussed further in Section 3.4.4 below.

3.4 Discussion

As described in the Results section, the computed Abs spectra for AdoCbl bound to WT and variant EALs are in reasonable agreement with the available experimental spectra, thus lending credibility to the QM/MM optimized geometries. These geometries provide useful insight into the specific interactions between the protein, cofactor, and substrate that contribute to the enzymatic Co–C bond activation for homolysis. We will now discuss (1) the assignments of the transitions perturbed by the binding of AdoCbl to EAL and the addition of substrate; (2) the effect

of the protein environment on the calculated and observed spectra; (3) the relationship between the perturbed transitions and changes to the cofactor's geometry (i.e., spectro-structural correlations); and (4) the effect of replacing E287 α , N193 α , and Y241 β on the structure and reactivity of AdoCbl in the holoenzyme and ternary complex.

3.4.1 Spectral assignments. The electronic structure of AdoCbl has previously been extensively studied, both experimentally and theoretically. Of the many overlapping features that are present in the Abs and MCD spectra, the α/β bands have perhaps the clearest assignment. Computationally, these have been shown to have primarily HOMO \rightarrow LUMO character. The HOMO of AdoCbl is best described as a corrin π orbital with a small but important contribution from the Co 3d_{z²} orbital and the axial ligands. Specifically, it contains both a Co–C σ^b bonding interaction and a Co–N_{DMB} σ^* antibonding interaction. These contributions to the HOMO's composition make this orbital sensitive to axial perturbations. The LUMO, on the other hand, is a mostly ligand-based, corrin π^* MO. Thus, the transition responsible for the α/β bands contains significant corrin $\pi \rightarrow \pi^*$ character (which contributes to their high intensity), and a small amount of metal-to-ligand charge transfer (MLCT) character, which makes their energies susceptible to the axial bonding environment. This mixed character can be seen in the electron-density difference map (EDDM) in Figure 3.9, which depicts the changes in electron density for this computed transition.

Compared to the α/β bands, much less is known about the transitions at intermediate energies that are also affected by the binding of AdoCbl to EAL. On the basis of the MCD spectra of the holoenzyme and ternary complex, it was concluded in Section 3.1 that different transitions are perturbed by the two binding events. To this end, we computed EDDMs for the transitions in the TD-DFT spectra that appear to corroborate the experimental trends. These are transition 18 in

the holoenzyme spectrum, and transitions 22 and 23 in the ternary complex spectrum (Figure 3.10; see Figure A.3.3 for the contribution of these transitions to the computed Abs spectra).

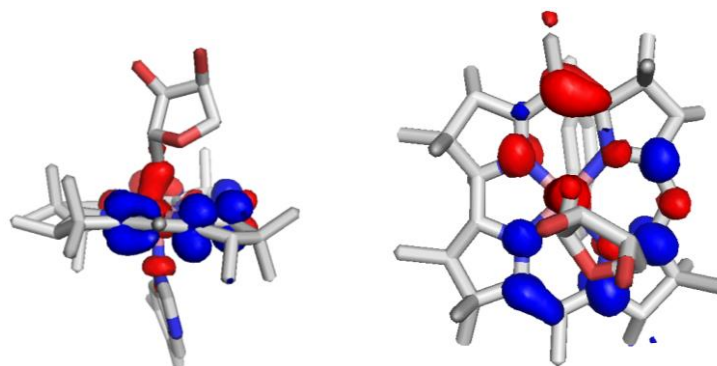


Figure 3.9. Side view (left) and top view (right) of the EDDM for the HOMO \rightarrow LUMO transition of AdoCbl in the EAL holoenzyme. This transition is responsible for the α/β bands in the blue trace of Figure 3.5. Red regions indicate loss of electron density; blue regions indicate gain.

Transition 18 in the computed holoenzyme spectrum is solely responsible for the new feature that appears at a slightly lower energy than the intense γ band. On the basis of its EDDM (Figure 3.10, left) we can assign this feature as the Co $3d_{xz} \rightarrow$ LUMO MLCT transition. Given the high degree of mixing between Co $3d$, corrin σ and π orbitals, DMB σ and π orbitals, and the Ado σ orbital, it is not always straightforward to compare transitions from two AdoCbl models, as even small geometric changes can produce MOs with significantly different compositions. However, there is an analogous feature due to the Co $3d_{xz} \rightarrow$ LUMO transition (Figure A.3.4) in the spectrum of the free cofactor. This feature is at slightly higher energy, and contributes to the low-energy shoulder of the γ band. Thus, these models predict that the newly observed feature in the holoenzyme spectrum is due to the red-shifted counterpart of a transition that is concealed by the γ band in the spectrum of free AdoCbl.

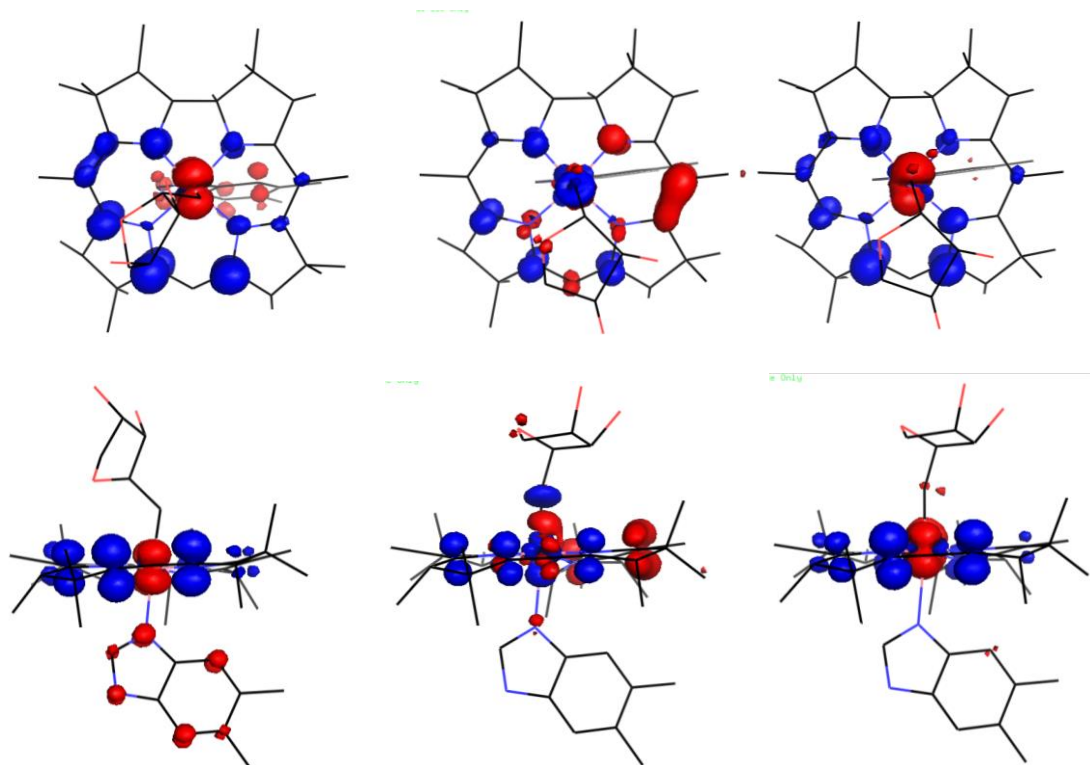


Figure 3.10. EDDMs for three transitions referred to in the text. The top row contains views from the top, and the bottom row shows views from the side. LEFT: Transition 18 in the holoenzyme. MIDDLE: Transition 22 in the ternary complex. RIGHT: Transition 23 in the ternary complex.

The $\text{Co } 3d_{xz} \rightarrow \text{LUMO}$ transition in the ternary complex is transition 23 (Figure 3.10, right), one of the two transitions predicted to provide the intensity observed experimentally in the 23 000 – 24 500 cm^{-1} range. This prediction conflicts with the experimental MCD spectrum, in which the feature that red-shifts upon AdoCbl binding to EAL is observed to shift in the opposite direction upon substrate binding. Since we cannot attribute the new features of AdoCbl in the ternary complex to transition 23, transition 22 in this model (Figure 3.10, middle) takes on extra importance. On its own, the EDDM for this transition does not allow for a straightforward assignment, but inspection of the contributing one-electron excitations (Table A.3.1) allows us to identify it as the $\text{HOMO} \rightarrow \text{Co } 3d_{z^2}$ transition. There is an analogous transition (Figure A.3.5) in free AdoCbl. Like the $\text{Co } 3d_{xz} \rightarrow \text{LUMO}$ transition, the $\text{HOMO} \rightarrow \text{Co } 3d_{z^2}$ transition also

contributes to the low-energy shoulder of the γ band in the free cofactor. This finding indicates that the transition responsible for feature **B** in the ternary spectrum is also a transition that is red-shifted out of the γ band.

3.4.2 Effect of EAL on AdoCbl Abs Spectrum. The erroneous prediction that the Co $3d_{xz} \rightarrow$ LUMO transition of AdoCbl in the EAL holoenzyme will red-shift upon the addition of substrate can be explained by the effect of our choice to include the MM point charges of EAL in the computation of all TD-DFT spectra. As described previously, the primary effect of including these charges is a uniform blue-shift of the computed spectrum. However, several transitions at energies between the α/β bands and the γ band – most notably the Co $3d_{xz} \rightarrow$ LUMO transition in question here – experience less of a blue-shift than the others, and thus the model lacking the point charges compares quite poorly with experiment. Moreover, it is evident from the EDDM of the Co $3d_{xz} \rightarrow$ LUMO transition in the absence of point charges (Figure A.3.6) that the donor MO in that model contains no significant contribution from the DMB, making it qualitatively appear like the corresponding transition in the ternary complex (Figure 3.10, right). Interestingly, it is possible to qualitatively reproduce the predicted holoenzyme spectrum by including only the point charges associated with the Y241 β side chain (Figure A.3.2).

From these observations, we conclude that the Y241 β side chain can influence the Abs spectrum of AdoCbl at intermediate energies, and that the computed electronic structure of our models will be sensitive to the DMB–Y241 β distance, especially the MOs with significant DMB character. Thus, the inordinately low excitation energy predicted for the Co $3d_{xz} \rightarrow$ LUMO transition in the ternary complex model may be due to some combination of the greater DMB–Y241 β distance relative to that in the holoenzyme, as the overestimation of the effects of this geometric change would cause an underestimation of this transition energy.

3.4.3 Spectro-structural Correlations. The two major changes observed in the cofactor's geometry upon binding to the apoenzyme both occur at the lower axial position; i.e., the Co–N_{DMB} bond length and the DMB tilt angle. In principle, these have competing effects on the energy of the HOMO and thus the energy of the α/β bands. That is, shortening the Co–N_{DMB} bond should increase the σ^* character of the HOMO, destabilize it, and red-shift transitions originating from it; on the other hand, decreasing the DMB tilt angle should reduce the Co 3d_{z²}/N(sp²) antibonding interaction, stabilize the HOMO, and blue-shift those transitions.

Both of these effects can be observed in the computed spectra for the models in series **1** and **2** shown in Figures 3.6 and 3.7 and the α/β band maxima presented in Table 3.4. Specifically, decreasing the Co–N_{DMB} bond length at a fixed DMB tilt angle causes the α/β bands to red-shift, while decreasing the tilt angle at a fixed bond length causes these same transitions to blue-shift. The dependence of the computed transition energy on the tilt angle appears to be quite small, with a predicted change of around 50 – 150 cm⁻¹ for the decrease by 6.4° from the tilt angle of AdoCbl in the WT holoenzyme. However, when comparing the positions of these bands to those of the γ bands, as done for the spectral comparisons in Figure 3.5, we see that the tilt angle can have a significant effect on the relative position of these two features. For example, at the Co–N_{DMB} bond distance observed in the WT holoenzyme (2.27 Å), a decrease in the tilt angle from 166.7° to 160.3° should cause the α/β band maximum to move ~600 cm⁻¹ closer to the γ band maximum. While the direction of the observed shift is difficult to predict when these two effects are in competition, as predicted computationally for AdoCbl-binding to EAL, the overall observed blue-shift can be explained solely in terms of these two geometric parameters.

Table 3.4. Energies of the α/β bands of AdoCbl models in series **1** and **2**. The corresponding Abs spectra are those shown in Figures 3.6 and 3.7, respectively.

Co-N _{DMB} distance (Å)	α/β maximum (absolute) (cm ⁻¹)		α/β maximum (relative to γ band) (cm ⁻¹)	
	Tilt angle = 160.3°	Tilt angle = 166.7°	Tilt angle = 160.3°	Tilt angle = 166.7°
1.9	18 069	17 830	– 10 606	– 9649
2.0	18 856	18 719	– 10 812	– 9682
2.1	19 506	19 438	– 9341	– 10 196
2.2	20 054	20 054	– 9272	– 10 058
2.27	20 362	20 430	– 9066	– 9648
2.3	20 738	20 618	– 8656	– 9563
2.38	21 149	21 114	– 7971	– 9374
2.5	21 559	21 559	– 7493	– 9477
2.6	21 867	21 833	– 9032	– 9614

The formation of the ternary complex induces a lengthening of both axial bonds and an increase in the DMB tilt angle of AdoCbl. Again, the changes at the cofactor's lower face are in competition, but this time there is also a reduction in the Co–C σ^b interaction that typically dominates the character of the HOMO. As the Co–C bond becomes significantly longer – by nearly 0.1 Å – the net effect of these geometric changes is a destabilized HOMO and red-shifted α/β bands.

The changes in features **A** and **B** can similarly be explained in terms of the changes in geometry along the C–Co–N_{DMB} axis. In a perfectly octahedral ligand field environment, the Co 3d_{xz}- and 3d_{yz}-based MOs are part of the triply degenerate t_{2g} set of MOs. In the case of AdoCbl, however, these MOs are differentiated by the ability of the 3d_{xz} orbital to have π interactions with the DMB orbitals. While the magnitude of this interaction is tuned by the axial bond length, it is less sensitive to the DMB tilt angle. When the Co–N_{DMB} bond is shortened, as in the holoenzyme, the π^* interaction between the Co 3d_{xz} and DMB π orbitals increases. This causes the donor orbital for the Co 3d_{xz} \rightarrow LUMO transition to become destabilized and the observed transition to shift to lower energy. Figure 3.11 shows the energies of this transition in the computed Abs spectra for the

series **2** models. While the changes are subtle at larger bond lengths, the shortening of the lower axial bond is nearly always accompanied by a decrease in transition energy. Thus, the shortened Co–N_{DMB} bond is a ready explanation for the red-shift of feature **A** observed in the experimental MCD spectra (Figure 3.3) and computed Abs spectra (Figure 3.5).

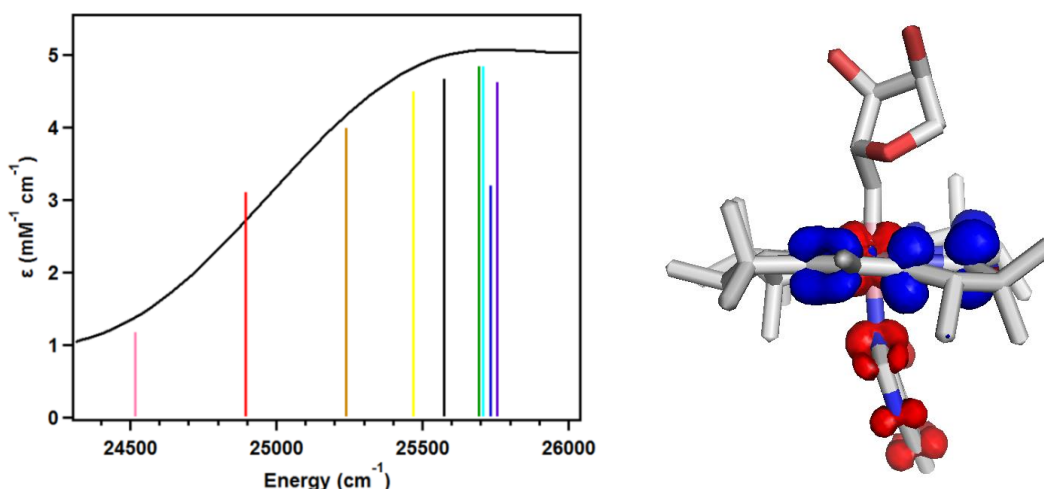


Figure 3.11. LEFT: Computed transition energies and Abs intensities of the Co $3d_{xz} \rightarrow$ LUMO transition of AdoCbl models in series **2**. The colors of the sticks correspond to the color of the traces in Figure 3.7. The black trace is the Abs envelope for fully optimized EAL-bound AdoCbl (Co–N_{DMB} distance of 2.27 Å). RIGHT: Representative EDDM for this transition, from the model with a Co–N_{DMB} bond length of 2.21 Å (dark orange stick).

The red-shift of feature **B** (HOMO \rightarrow Co $3d_{z^2}$ transition) in the ternary complex can also be explained on the basis of geometric perturbations. Like the corrin-based HOMO, the Co $3d_{z^2}$ -based MO contains large contributions from the axial ligands. Unlike the HOMO, however, which has mixed bonding and antibonding character, the Co $3d_{z^2}$ -based MO is σ -antibonding with respect to both axial ligands. Consequently, the lengthening of these axial bonds upon formation of the ternary complex causes a sizable stabilization of the Co $3d_{z^2}$ -based MO. The HOMO, on the other hand, experiences competing stabilizing and destabilizing effects on account of its mixed axial bonding/antibonding character. The net result of this competition is a slight destabilization

of the HOMO. Thus, the HOMO \rightarrow Co 3d_{z²} transition is significantly red-shifted in the ternary complex.

The spectro-structural relationships relevant to our observed WT EAL spectra are summarized as follows: first, binding of AdoCbl to the apoenzyme causes the Co–N_{DMB} bond to shorten and the DMB tilt angle to decrease. These changes cause a blue-shift of the α/β bands via stabilization of the HOMO and a red-shift of an MLCT transition originating from the destabilized Co 3d_{xz}-based MO (feature **A**). The addition of substrate induces a dramatic lengthening of both axial bonds. This leads to a destabilization of the HOMO and stabilization of the Co 3d_{z²} orbital, and thus a red-shift of both the α/β bands and the HOMO \rightarrow Co 3d_{z²} transition (feature **B**). The longer lower axial bond stabilizes the Co 3d_{xz} orbital and moves feature **A** higher in energy, where it contributes to the γ bands.

3.4.4 Role of E287 α , N193 α , and Y241 β in the catalytic mechanism. The experimental validation of our computational models for AdoCbl-bound WT and variant EAL holoenzymes and ternary complexes allows us to propose the following roles for E287 α , N193 α , and Y241 β . First, we note that E287 α has previously been implicated as essential for substrate binding and efficient Co–C bond homolysis, despite the fact it is too far from the cofactor to directly interact with its Ado ligand. However, because of its ability to form two hydrogen bonds with the substrate, E287 α is the amino acid most responsible for the reorganization of the active site when the substrate binds. We propose that it is N193 α that directly disturbs the equilibrium geometry of the adenosyl ligand upon formation of the ternary complex, and that its ability to form simultaneous hydrogen bonds to the substrate and the adenosyl ligand provides the driving force for it to do so. This mechanism is sensitive to the relative positioning of the substrate and adenosyl ligand, and thus even conservative substitutions (e.g., E287 α D) will relieve some geometric constraints and decrease the

strain on the Co–C bond. Evidence to this effect is provided by the geometries of the E287 α D, E287 α A, and N193 α A ternary complexes, all of which exhibit an essentially unperturbed Co–C bond relative to free AdoCbl.

Just as E287 α is essential because of its role in positioning the substrate, Y241 β may be critical because of its role in proper positioning of the cofactor. By comparison of our WT and Y241 β A models, we conclude that the presence of a large, bulky side chain is necessary for the cofactor to demonstrate the shortened Co–N_{DMB} bond and decreased DMB tilt angle that produce the observed changes to the experimental Abs and MCD spectra. We speculate that the removal of Y241 β would result in a more relaxed AdoCbl geometry in which the cofactor sits lower in the EAL active site. Such a change would likely have a deleterious effect on EAL's catalytic activity, as the hydrogen bonds between N193 α , substrate, and Ado ligand in the ternary complex could now be formed without significantly perturbing the Co–C bond.

3.5 Conclusion

Any activation of the Co–C bond requires the lowering of the free energy barrier to homolysis. Provided that the transition state of this step is sufficiently late, this could be achieved by a preferential stabilization of the Co(II)Cbl and Ado• products relative to AdoCbl. In Class I enzymes, which utilize the base-off, His-on binding motif, it is believed that the activation occurs, at least in part, through selective stabilization of the Co(II)Cbl species. As described previously, one mechanism of inducing this stabilization utilizes the hydrogen bonding capabilities of the coordinating histidine and the conserved DXHXGXX motif. The lack of these capabilities in DMB suggests that a different mechanism of Co–C bond activation must be at work in the Class II enzyme EAL.

In principle, the barrier to homolysis could also be lowered through destabilization of AdoCbl, perhaps through the exertion of a geometric strain on the cofactor that is relieved through homolysis. This general mechanism, often termed the “strain hypothesis”, has been proposed many times before. Previously, our group has dismissed this hypothesis for Class I enzymes because of the lack of any observable change to the electronic spectrum of AdoCbl in either the holoenzyme or the ternary complex in the Class I enzymes MMCM and GM. Other experimentalists and theorists have also come to the conclusion that electrostatic stabilization of Ado• and Co(II)Cbl is essential in the isomerases. However, the results presented and discussed above offer evidence that the strain hypothesis is at work in EAL.

Careful consideration of this hypothesis reveals two criteria that must be fulfilled for an enzyme to use this mechanism to break the Co–C bond. First, the formation of the holoenzyme itself must not impose a significant strain on the cofactor. Should binding to EAL cause major distortions to the cofactor’s geometry, the binding affinity of AdoCbl would be expected to drop precipitously. However, the observed affinity of AdoCbl for all classes of enzymes that utilize it is quite high. Thus, the strain on the Co–C bond must be exerted solely in the ternary complex, and not in the holoenzyme. This implicates a major rearrangement of the active site, especially near the Ado ligand, upon substrate binding. Since the rearrangement depends on the presence of substrate, such a mechanism would prevent undesired Co–C homolysis, thereby also allowing these enzymes to control the timing of Ado• formation. Given the many possible hydrogen bonds that could exist between the Ado ligand and nearby amino acids, a substantial rearrangement upon addition of substrate is reasonable, and our models predict that this has a significant impact on the Ado geometry and the Co–C bond length.

The second criterion is more subtle, yet it follows from the first: the apoenzyme must bind AdoCbl in a way that limits the cofactor's conformational flexibility. Should AdoCbl be able to readily adapt to the rearranged active site in the ternary complex, it would do so without paying the energetic costs associated with a longer Co–C bond. However, should the lower half of the cofactor (i.e., the corrin ring, nucleotide loop, and DMB) be held firmly in place, it is possible to envision a rearrangement of the active site that triggers a lengthening of the Co–C bond. Thus, the steric interaction between the DMB and Y241 β may also be essential for EAL's functionality.

According to our experimentally validated computational model, EAL fits these two general criteria. Unlike the Class I enzymes GM and MMCM, there is a clear perturbation to the electronic structure of the cofactor in the EAL holoenzyme, corresponding to a relatively minor geometric disturbance of the lower face of the cofactor. The subsequent binding of substrate causes EAL to put significant strain on the Co–C bond, causing its dramatic elongation. We propose that this mechanism is responsible for the enhanced rate of Co–C bond homolysis in EAL, and possibly in the other Class II eliminases as well. Our analysis has also led to the proposal of well-defined roles for three active site residues, including the first identification of Y241 β as a potential residue of interest. We plan to test the putative roles of Y241 β and N193 α in Co–C bond activation through experimental studies of select EAL variants in the near future.

3.6 References

1. Banerjee, R.; Ragsdale, S. W., *Annual Review of Biochemistry* **2003**, 72, 209-247.
2. Brown, K. L., *Chemical Reviews* **2005**, 105, 2075-2149.
3. Toraya, T., *Archives of Biochemistry and Biophysics* **2014**, 544, 40-57.
4. Babior, B. M., *Journal of Biological Chemistry* **1970**, 245, 6125-&.
5. Babior, B. M.; Woodams, A. D.; Brodie, J. D., *Journal of Biological Chemistry* **1973**, 248, 1445-1450.
6. Brown, K. L.; Zou, X., *Inorganic Chemistry* **1991**, 30, 4185-4191.
7. Chowdhury, S.; Banerjee, R., *Biochemistry* **2000**, 39, 7998-8006.
8. Marsh, E. N. G.; Ballou, D. P., *Biochemistry* **1998**, 37, 11864-11872.
9. Padmakumar, R.; Banerjee, R., *Biochemistry* **1997**, 36, 3713-3718.
10. Licht, S. S.; Booker, S.; Stubbe, J. A., *Biochemistry* **1999**, 38, 1221-1233.

11. Banerjee, R., *Chemical Reviews* **2003**, *103*, 2083-2094.
12. Brooks, A. J.; Vlasie, M.; Banerjee, R.; Brunold, T. C., *Journal of the American Chemical Society* **2004**, *126*, 8167-8180.
13. Brooks, A. J.; Vlasie, M.; Banerjee, R.; Brunold, T. C., *Journal of the American Chemical Society* **2005**, *127*, 16522-16528.
14. Brooks, A. J.; Fox, C. C.; Marsh, E. N. G.; Vlasie, M.; Banerjee, R.; Brunold, T. C., *Biochemistry* **2005**, *44*, 15167-15181.
15. Marsh, E. N. G.; Holloway, D. E., *Febs Letters* **1992**, *310*, 167-170.
16. Ratnatilleke, A.; Vrijbloed, J. W.; Robinson, J. A., *Journal of Biological Chemistry* **1999**, *274*, 31679-31685.
17. Beatrix, B.; Zelder, O.; Linder, D.; Buckel, W., *European Journal of Biochemistry* **1994**, *221*, 101-109.
18. Yamanishi, M.; Yamada, S.; Ishida, A.; Yamauchi, J.; Toraya, T., *Journal of Biochemistry* **1998**, *124*, 598-601.
19. Yamanishi, M.; Yamada, S.; Muguruma, H.; Murakami, Y.; Tobimatsu, T.; Ishida, A.; Yamauchi, J.; Toraya, T., *Biochemistry* **1998**, *37*, 4799-4803.
20. Yamanishi, M.; Yunoki, M.; Tobimatsu, T.; Sato, H.; Matsui, J.; Dokiya, A.; Iuchi, Y.; Oe, K.; Suto, K.; Shibata, N.; Morimoto, Y.; Yasuoka, N.; Toraya, T., *European Journal of Biochemistry* **2002**, *269*, 4484-4494.
21. Akita, K.; Hieda, N.; Baba, N.; Kawaguchi, S.; Sakamoto, H.; Nakanishi, Y.; Yamanishi, M.; Mori, K.; Toraya, T., *Journal of Biochemistry* **2010**, *147*, 83-93.
22. Shibata, N.; Tamagaki, H.; Hieda, N.; Akita, K.; Komori, H.; Shomura, Y.; Terawaki, S.; Mori, K.; Yasuoka, N.; Higuchi, Y.; Toraya, T., *Journal of Biological Chemistry* **2010**, *285*, 26484-26493.
23. Shibata, N.; Masuda, J.; Tobimatsu, T.; Toraya, T.; Suto, K.; Morimoto, Y.; Yasuoka, N., *Structure with Folding & Design* **1999**, *7*, 997-1008.
24. Shibata, N.; Masuda, J.; Morimoto, Y.; Yasuoka, N.; Toraya, T., *Biochemistry* **2002**, *41*, 12607-12617.
25. Ogura, K.; Kunita, S.; Mori, K.; Tobimatsu, T.; Toraya, T., *Febs Journal* **2008**, *275*, 6204-6216.
26. Fukuoka, M.; Nakanishi, Y.; Hannak, R. B.; Krautler, B.; Toraya, T., *Febs Journal* **2005**, *272*, 4787-4796.
27. Toraya, T.; Miyoshi, S.; Mori, M.; Wada, K., *Biochimica Et Biophysica Acta-Protein Structure and Molecular Enzymology* **1994**, *1204*, 169-174.
28. Ishida, A.; Toraya, T., *Biochemistry* **1993**, *32*, 1535-1540.
29. Toraya, T.; Ishida, A., *Journal of Biological Chemistry* **1991**, *266*, 5430-5437.
30. Ichikawa, M.; Toraya, T., *Biochimica Et Biophysica Acta* **1988**, *952*, 191-200.
31. Toraya, T.; Ushio, K.; Fukui, S.; Hogenkamp, H. P. C., *Journal of Biological Chemistry* **1977**, *252*, 963-970.
32. Ushio, K.; Fukui, S.; Toraya, T., *Biochimica Et Biophysica Acta* **1984**, *788*, 318-326.
33. Fukuoka, M.; Yamada, S.; Miyoshi, S.; Yamashita, K.; Yamanishi, M.; Zou, X.; Brown, K. L.; Toraya, T., *Journal of Biochemistry* **2002**, *132*, 935-943.
34. Magnusson, O. T.; Frey, P. A., *Journal of the American Chemical Society* **2000**, *122*, 8807-8813.
35. Toraya, T.; Matsumoto, T.; Ichikawa, M.; Itoh, T.; Sugawara, T.; Mizuno, Y., *Journal of Biological Chemistry* **1986**, *261*, 9289-9293.
36. Bandarian, V.; Reed, G. H., *Biochemistry* **2000**, *39*, 12069-12075.
37. Dolinsky, T. J.; Nielsen, J. E.; McCammon, J. A.; Baker, N. A., *Nucleic Acids Research* **2004**, *32*, W665-W667.
38. Word, J. M.; Lovell, S. C.; Richardson, J. S.; Richardson, D. C., *Journal of Molecular Biology* **1999**, *285*, 1735-1747.
39. The PyMOL Molecular Graphics System, Version 1.5.0.4 Schrodinger, LLC.
40. Gaussian 09; Revision D.01; Frisch, M. J.; Trucks, G. W.; Schlegel, H. B.; Scuseria, G. E.; Robb, M. A.; Cheeseman, J. R.; Scalmani, G.; Barone, V.; Mennucci, B.; Petersson, G. A.; Nakatsuji, H.;

- Caricato, M.; Li, X.; Hratchian, H. P.; Izmaylov, A. F.; Bloino, J.; Zheng, G.; Sonnenberg, J. L.; Hada, M.; Ehara, M.; Toyota, K.; Fukuda, R.; Hasegawa, J.; Ishida, M.; Nakajima, T.; Honda, Y.; Kitao, O.; Nakai, H.; Vreven, J. A.; Montgomery, J. A.; Peralta, J. E.; Ogliaro, F.; Bearpark, M.; Heyd, J. J.; Brothers, E.; Kudin, K. N.; Staroverov, V. N.; Kobayashi, R.; Normand, J.; Raghavachari, K.; Rendell, A.; Burant, J. C.; Iyengar, S. S.; Tomasi, J.; Cossi, M.; Rega, N.; Millam, J. M.; Klene, M.; Knox, J. E.; Cross, J. B.; Bakken, V.; Adamo, C.; Jaramillo, J.; Gomperts, R.; Stratmann, R. E.; Yazyev, O.; Austin, A. J.; Cammi, R.; Pomelli, C.; Ochterski, J. W.; Martin, R. L.; Morokuma, K.; Zakrzewski, V. G.; Voth, G. A.; Salvador, P.; Danneberg, J. J.; Dapprich, S.; Daniels, A. D.; Farkas, O.; Foresman, J. B.; Ortiz, J. V.; Cioslowski, J.; Fox, D. G. Gaussian Inc.: Wallingford, CT, 2009.
41. Cornell, W. D.; Cieplak, P.; Bayly, C. I.; Gould, I. R.; Merz, K. M.; Ferguson, D. M.; Spellmeyer, D. C.; Fox, T.; Caldwell, J. W.; Kollman, P. A., *Journal of the American Chemical Society* **1995**, *117*, 5179-5197.
 42. Marques, H. M.; Ngoma, B.; Egan, T. J.; Brown, K. L., *Journal of Molecular Structure* **2001**, *561*, 71-91.
 43. Perdew, J. P., *Physical Review B* **1986**, *33*, 8822-8824.
 44. Becke, A. D., *Physical Review A* **1988**, *38*, 3098-3100.
 45. Kuta, J.; Patchkovskii, S.; Zgierski, M. Z.; Kozlowski, P. M., *Journal of Computational Chemistry* **2006**, *27*, 1429-1437.
 46. Hay, P. J.; Wadt, W. R., *Journal of Chemical Physics* **1985**, *82*, 299-310.
 47. Hay, P. J.; Wadt, W. R., *Journal of Chemical Physics* **1985**, *82*, 270-283.
 48. Wadt, W. R.; Hay, P. J., *Journal of Chemical Physics* **1985**, *82*, 284-298.
 49. Lee, C. T.; Yang, W. T.; Parr, R. G., *Physical Review B* **1988**, *37*, 785-789.
 50. Becke, A. D., *Journal of Chemical Physics* **1993**, *98*, 1372-1377.
 51. Neese, F., *Wiley Interdisciplinary Reviews-Computational Molecular Science* **2012**, *2*, 73-78.
 52. Neese, F.; Olbrich, G., *Chemical Physics Letters* **2002**, *362*, 170-178.
 53. Hirata, S.; Head-Gordon, M., *Chemical Physics Letters* **1999**, *314*, 291-299.
 54. Schafer, A.; Huber, C.; Ahlrichs, R., *Journal of Chemical Physics* **1994**, *100*, 5829-5835.
 55. Schafer, A.; Horn, H.; Ahlrichs, R., *Journal of Chemical Physics* **1992**, *97*, 2571-2577.
 56. Chen, Z. G.; Zietek, M. A.; Russell, H. J.; Tait, S.; Hay, S.; Jones, A. R.; Scrutton, N. S., *Chembiochem* **2013**, *14*, 1529-1533.
 57. Stich, T. A.; Brooks, A. J.; Buan, N. R.; Brunold, T. C., *Journal of the American Chemical Society* **2003**, *125*, 5897-5914.

CHAPTER 4

Computational Investigation of the Adenosylcobalamin-Dependent Ethanolamine Ammonia Lyase:

Role of Specific Enzyme-Cofactor Interactions

4.1 Introduction

5'-deoxyadenosylcobalamin (AdoCbl, coenzyme B₁₂, Figure 4.1) is an essential bioinorganic cofactor that assists in catalyzing the 1,2-rearrangements of various organic substrates.¹⁻³ AdoCbl contains a low-spin Co(III) ion ligated equatorially by a tetradentate corrin macrocycle and axially by an organic 5'-deoxyadenosyl (Ado) ligand, from which it derives its name, and a dimethylbenzimidazole (DMB) ligand, which is tethered covalently to a corrin side chain via a nucleotide loop. The cofactor's organometallic bond distinguishes it (and the related methylcobalamin) as unique in biology, and has inspired decades of research dedicated to understanding its character and reactivity.⁴ Despite the diverse array of substrates utilized by AdoCbl-dependent enzymes, there is wide agreement that the first step in the catalytic cycle of all such enzymes is Co–C bond homolysis induced by the binding of substrate (Scheme 4.1).^{5, 6} This produces the one-electron reduced cob(II)alamin (Co(II)Cbl) and a highly reactive Ado• radical, which quickly abstracts a hydrogen atom from the substrate to form a substrate-like radical and 5'-deoxyadenosine. The substrate-like radical undergoes 1,2-rearrangement before re-abstracting a hydrogen from 5'-deoxyadenosine to form the final product and regenerate Ado•, which combines with Co(II)Cbl to close the catalytic cycle. In order to accomplish catalysis, AdoCbl-dependent enzymes lower the activation energy of the highly endergonic Co–C bond homolysis by around 17 kcal/mol, consistent with an increase in the effective rate constant by 12 orders of magnitude.^{7, 8}

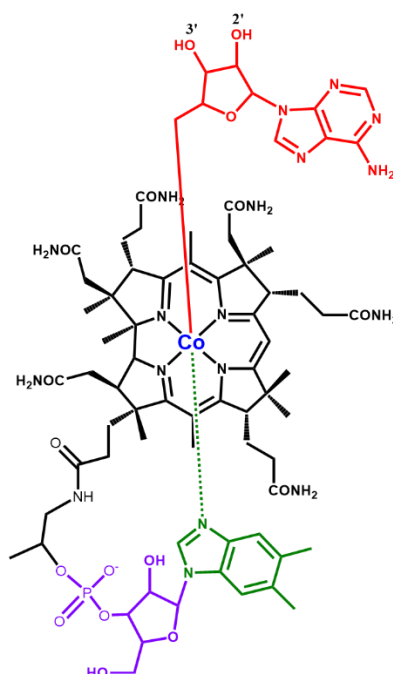
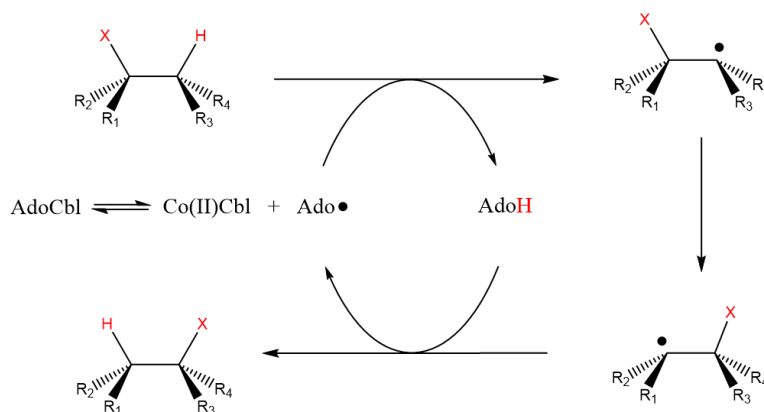


Figure 4.1. Adenosylcobalamin. The structure is color-coded to identify the Co(III) ion (blue), corrin ring (black), Ado (red) and DMB (green) ligands, and nucleotide loop (purple). The 2'- and 3'-OH groups of the Ado ligand are labeled.

Scheme 4.1. General reaction mechanism employed by AdoCbl-dependent enzymes.



The mechanistic similarities of AdoCbl-dependent enzymes belie important distinctions that allow for their classification as either Class I isomerases⁹ or Class II eliminases.³ The former catalyze the migration of carbon skeletons or amino groups, and bind AdoCbl by displacing the native DMB ligand with a protein-derived histidine (His) side chain, part of a conserved

DXHXGXX motif¹⁰⁻¹² (in one case: DXHXGXN). The eliminases rearrange 1,2-diols or 1,2-amino alcohols into geminal 1,1-diols or 1,1-amino alcohols, which spontaneously eliminate either water or ammonia to form an aldehyde. Unlike the isomerases, the eliminases bind AdoCbl without a ligand switch, maintaining the coordination of the DMB ligand.¹³⁻¹⁶ The binding modes exhibited by isomerases and eliminases suggest that they may promote Co–C bond homolysis by different means. However, the exact nature of the interaction between AdoCbl, AdoCbl-dependent enzymes, and substrate molecules that leads to activation of this bond has not yet been determined.

In principle, the barrier to bond homolysis could be lowered through destabilization of the AdoCbl ground state or stabilization of the bond homolysis transition state within the enzyme active site. As the latter would also imply stabilization of the post-homolysis Co(II)Cbl and Ado• products (due to the endergonicity of this reaction step), spectroscopic probes of the cofactor's electronic structure when bound to enzymes in the AdoCbl and Co(II)Cbl states can provide significant insight into which general mechanism is employed by the enzyme. Such an experimental approach has been used to successfully identify transition state stabilization in the isomerases glutamate mutase (GM)¹⁷ and methylmalonyl-CoA mutase (MMCM).¹⁸ The binding of Co(II)Cbl to GM and MMCM induces blue-shifts in a number of its electronic transitions with significant metal-to-ligand charge transfer (MLCT) character,¹⁹ which were shifted further upon addition of substrate analogues (to form the so-called “ternary complex”). These shifts were interpreted as the result of stabilization of the manifold of Co 3d-based MOs in the holoenzyme. Conversely, no perturbations to the AdoCbl absorption (Abs) or magnetic circular dichroism (MCD) spectra were observed in the GM or MMCM holoenzymes,^{17, 20} even in the presence of substrate analogues. It was recently shown (Chapter 2) that the electronic spectra of isomerase-bound Co(II)Cbl are remarkably similar to those of Co(II)(5-fluoroimidazole)Cbl, which possesses

a much weaker electron-donating axial ligand than DMB. However, the adenosylated form of this analogue fails to exhibit spectra that similarly mimic isomerase-bound AdoCbl. These observations were used to suggest that the basicity of the coordinating His in isomerases may be modulated during turnover, perhaps by proton uptake into the conserved DXHXGXX motif's hydrogen bonding network concomitant with Co–C bond homolysis. According to this hypothesis, the coordinating His and its hydrogen bonding partners are essential components of the transition state stabilization mechanism employed by the isomerases.

In that light, the curious lack of His coordination in eliminases invites further exploration. As the native DMB ligand is incapable of forming hydrogen bonds with the side chains of any eliminase residues, the Co–C bond must be activated by a different mechanism than that proposed for the isomerases. To investigate this possibility, we previously carried out an initial spectroscopic and computational characterization of ethanolamine ammonia lyase (EAL), an eliminase that catalyzes the conversion of 1,2-ethanolamine to acetaldehyde (Chapter 3). This analysis showed that the interactions of EAL with AdoCbl are distinct from those observed with GM and MMCM, and result in subtle but significant spectral changes to the AdoCbl Abs and MCD spectra in the EAL holoenzyme and ternary complex. Geometry optimizations performed with an experimentally-validated quantum mechanics/molecular mechanics (QM/MM) method were used to show that EAL imposes important geometric constraints on the cofactor in both the holoenzyme and ternary complex (Figure 4.2). Specifically, Y241 β was found to encroach on the DMB ligand in the holoenzyme, causing decreases in the Co–N_{DMB} bond length and the DMB tilt angle. (The DMB tilt angle, defined as the Co–N_{DMB}–C _{ϵ ,DMB} angle, is a measure of the relative orientation of the DMB and corrin rings.) The addition of substrate to our models caused a reorganization of the active site as six residues adjusted their positions to form hydrogen bonds with the substrate. One

glutamate residue, E287 α , appeared essential for orienting the substrate through two hydrogen bonds, while an asparagine residue, N193 α , maintained hydrogen bonds with both the substrate and the 3'-hydroxyl group of the Ado ligand. It was suggested that the imposition of steric constraints on the lower half of AdoCbl, primarily through Y241 β , constrain the cofactor's geometry so much that accommodation of the ternary complex's rearranged active site can only occur through elongation of the Co–C bond. Such a model proposes that the primary means of Co–C bond activation in EAL, and by extension the other eliminases, is AdoCbl destabilization rather than transition state stabilization.

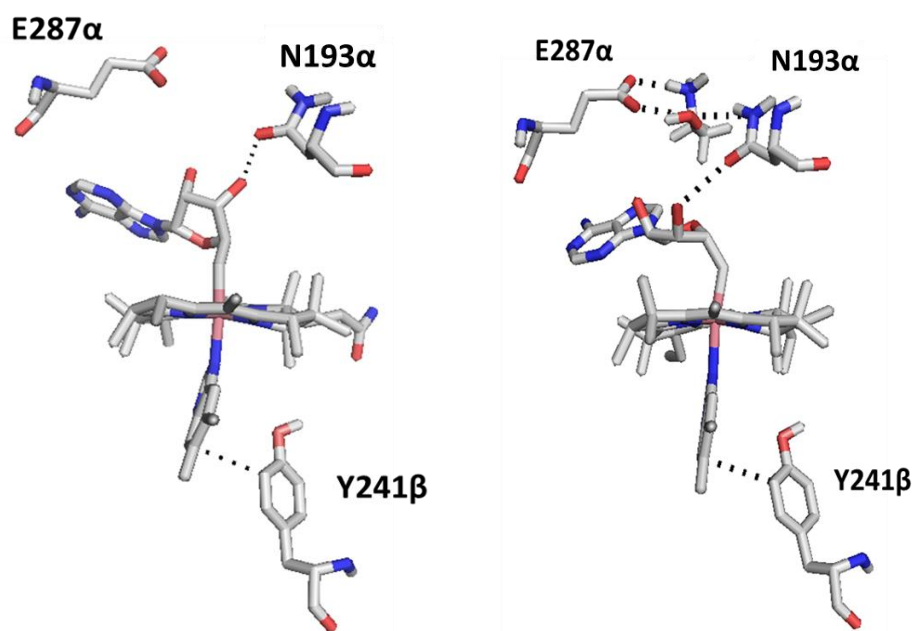


Figure 4.2. Optimized geometries of EAL holoenzyme (left) and ternary complex (right), including three residues implicated in Co–C bond activation. Methods used to generate these structures are described in Chapter 3.

The theoretical methodology used in the previous study was validated on the basis of its successful reproduction of observed spectroscopic features of AdoCbl bound to WT EAL and three E287 α variants.²¹ While this represents the extent of available spectroscopic data for EAL variants, our computational methods can in principle be applied to study the consequences of any desired

substitution. We pursued this in a limited fashion by investigating AdoCbl bound to the Y241 β A and N193 α A variants. Although these models await experimental confirmation, the contrast in geometric features between the variants and WT EAL provides useful insight into the specific interactions between cofactor and enzyme that lead to Co–C bond activation. That is, the changes to the cofactor's axial bond lengths and DMB tilt angle caused by the *in silico* site-directed mutagenesis provide information about how WT EAL affects the AdoCbl structure.

In this chapter, we extend our computational analysis by performing QM/MM geometry optimizations and time-dependent density functional theory (TD-DFT) computations on select EAL variants and AdoCbl analogues. The purpose of this is two-fold. First, we aim to provide further evidence that the specific EAL-AdoCbl interactions identified in Chapter 3 are indeed responsible for the geometric changes ascribed to them. To that end, we studied the N193 α A, Y241 β A, Y241 β F, and Y241 β W variants, as well as cofactor analogues possessing smaller lower axial ligands or Ado ligands lacking the 2'- and/or 3'-OH groups. Second, we acknowledge that the experimental characterization of novel EAL variants or synthetic AdoCbl analogues requires significant investments of time, money, and energy. Given the complexity of AdoCbl and the large number of EAL residues that form non-bonding contacts with it, it is not feasible to make every variant or analogue that may potentially provide insight into eliminase mechanisms. Furthermore, experimental validation of our model requires that the species selected for experimental characterization have spectroscopic features distinct from those of the AdoCbl-bound WT EAL holoenzyme and/or ternary complex. Using our previously-validated approach, we identify which variants and analogues are most promising and recommend their future study.

4.2 Computational Methods

4.2.1 Geometry Optimizations. Initial coordinates for all computational models of variant holoenzymes and ternary complexes were generated from a recent crystal structure of EAL complexed with ethanolamine and the AdoCbl analogue adeninylpentylcobalamin (PDB: 3ABS).²² PyMol²³ was used to create the following *in silico* EAL variants: N193αA, Y241βA, Y241βF, and Y241βW. For each variant, the pdb2pqr program²⁴ was used to add hydrogen atoms to ethanolamine, all crystallographic water molecules, and EAL (with an assumed pH of 7), while Reduce²⁵ was used to protonate AdoCbl after manual replacement of the adeninylpentyl ligand with an Ado ligand. Models of AdoCbl bound to each variant holoenzyme and ternary complex were studied.

Five cofactor analogues (Figure 4.3) were also constructed from the AdoCbl coordinates: 2',5'-dideoxyadenosylcobalamin (2'-dAdoCbl), 3'5'-dideoxyadenosylcobalamin (3'-dAdoCbl), 2',3',5'-trideoxyadenosylcobalamin (2',3'-ddAdoCbl), adenosyl(benzimidazole)cobalamin [Ado(BIm)Cbl], and adenosyl(imidazole)cobalamin [Ado(Im)Cbl]. 2'-dAdoCbl, 3'-dAdoCbl, and 2',3'-ddAdoCbl were optimized *in vacuo* as well as in the WT EAL holoenzyme and ternary complex. Ado(BIm)Cbl and Ado(Im)Cbl were studied *in vacuo* and in the WT and Y241βW holoenzymes.

All geometry optimizations were carried out according to the procedure used in Chapter 3. In brief, the Gaussian09 computational package²⁶ was first used to carry out an initial molecular mechanics (MM) optimization with the AMBER force field.²⁷ AMBER parameters for portions of serine (–CH₂OH) and protonated lysine (–CH₂NH₃⁺) were used as MM parameters for ethanolamine and the force field from Marques et al.²⁸ was used to account for non-bonding

interactions between it and the protein and/or substrate. AdoCbl was frozen during this optimization.

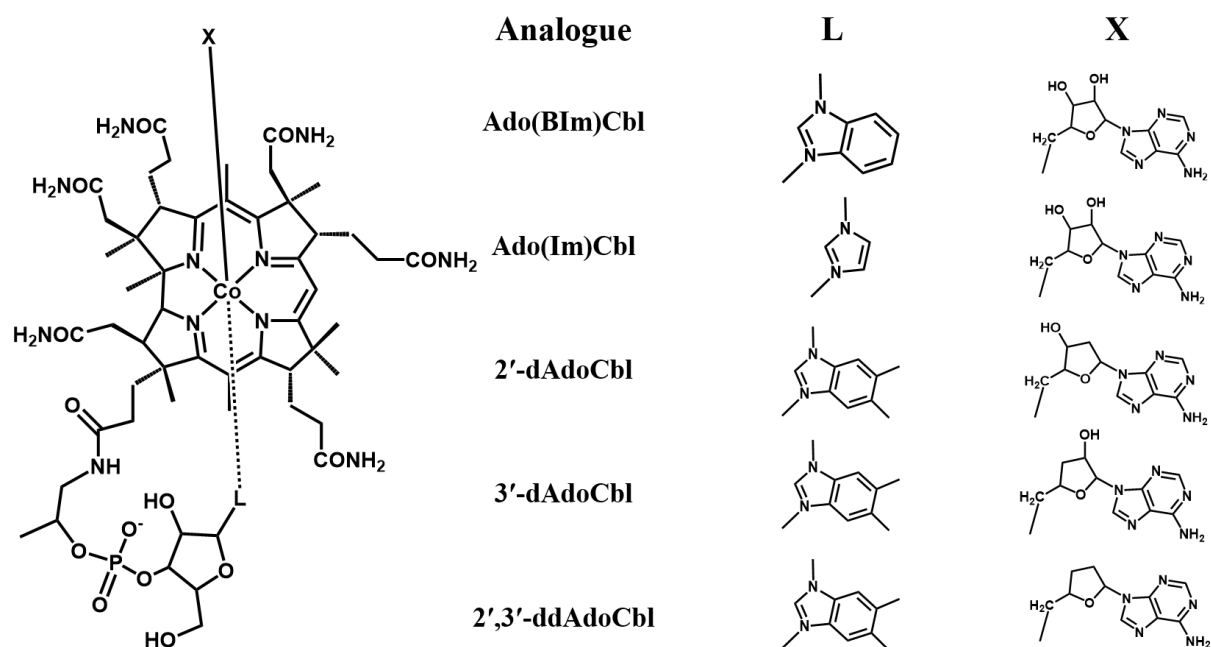


Figure 4.3. AdoCbl analogues used in this study. See text for abbreviations.

The coordinates from the converged MM optimization were used to generate input for all subsequent QM/MM optimizations. The QM region included the cofactor's Co(III) ion, the ribose moiety of the Ado ligand, the DMB ligand, and the corrin ring core, including the first carbon of each side chain, while the MM region consisted of the rest of the cofactor, the entirety of the protein and substrate, and all solvent molecules. All EAL residues and solvent molecules more than 5 Å away from the QM region were frozen. All covalent bonds spanning the QM/MM boundary were capped with hydrogen atoms (i.e., link atoms) during the QM steps of the optimization. The new X–H bond lengths were set equal to the original bond length scaled by a factor of 0.709. All QM/MM computations were performed at the BP86^{29, 30}/AMBER level of theory, as BP86 has been previously shown to be adequate for the reproduction of geometric parameters of cobalamins.³¹ The LanL2DZ basis set³²⁻³⁴ was used for all QM atoms. All force field

parameters were identical to those in the initial MM optimization. The default convergence criteria were used in most cases. However, some optimizations reached a point where the models exhibited negligible atomic displacements for many steps while still possessing maximum and/or RMS forces that were slightly too high for convergence. These models were considered converged if the maximum and RMS forces were within a factor of 5 of the appropriate default convergence criterion.

4.2.2 TD-DFT Calculations. The Orca 2.9 computational package³⁵ was used to compute the electronic Abs spectra of the optimized QM region of each model (including link atoms) with time-dependent density functional theory (TD-DFT). Atoms from the MM region, with the exception of those replaced by link atoms, were included in the TD-DFT computation as point charges with magnitude equal to those used in the MM calculations. All TD-DFT computations were performed with the resolution of the identity³⁶ and Tamm-Dancoff approximations³⁷ to speed up the calculations. The 60 lowest energy transitions within ± 4 Hartree of the HOMO-LUMO gap were computed with the B3LYP density functional.^{38, 39} The triple-zeta basis set with an additional polarization function (TZVP) developed by Ahlrichs⁴⁰ was used for the Co ion and all coordinating N and C atoms, while the same group's split-valence polarized (SVP) basis set⁴¹ was used for all other QM atoms. Abs spectra were plotted from the TD-DFT results by using a constant bandwidth of 1500 cm^{-1} for all transitions. As explained in Chapter 3, a change in the number or magnitude of point charges representing atoms from the MM region can cause significant shifts in the TD-DFT-computed spectrum. These changes in the MM region are unavoidable consequences of studying EAL variants. In order to compare the computed Abs spectra of WT and variant holoenzymes and ternary complexes, the variant energy axes were shifted to align the maximum

intensity feature with that of the corresponding WT spectrum. This is consistent with our analysis of the AdoCbl-bound E287 α variants.

4.3 Results

4.3.1. Optimized Geometries of EAL Variants and Cofactor Analogues. Key geometric parameters of four variant holoenzymes and ternary complexes are presented in Tables 4.1 and 4.2, respectively. Two of these variants were discussed in the previous chapter, but are included here to facilitate an analysis of the effects of amino acid substitutions. The two novel variants are Y241 β F and Y241 β W, introduced to test the hypothesis that the geometric constraints observed in the WT holoenzyme are due to the encroachment of Y241 β on the cofactor's DMB ligand. As the Y241 β A variant had already been shown to relieve these constraints (i.e., AdoCbl bound to Y241 β A had a longer Co–N_{DMB} bond and larger DMB tilt angle than AdoCbl bound to WT EAL), the two new Y241 β variants were expected to induce cofactor geometries with similar (Y241 β F) or even greater (Y241 β W) perturbations to the lower axial ligand, relative to WT EAL. While this is true for the Y241 β F variant, which binds AdoCbl with a Co–N_{DMB} bond length and DMB tilt angle intermediate between those of WT EAL and the Y241 β A variant, the Y241 β W variant defies the trend. Instead of causing the Co–N_{DMB} bond to become even shorter than in the WT holoenzyme, the Y241 β W substitution results in a substantially elongated Co–N_{DMB} bond and a tilt angle exceeding that observed for the Y241 β F holoenzyme.

Table 4.1. Key geometric parameters of AdoCbl-bound WT EAL and four variant holoenzymes. All distances are in Å and all angles in degrees.

	WT ^a	Y241βA ^a	Y241βF	Y241βW	N193αA ^a
r(Co-C)	2.03	2.03	2.03	2.03	2.02
r(Co-N_{DMB})	2.27	2.40	2.34	2.40	2.32
DMB tilt	160.3	163.9	161.2	161.9	160.6
θ(Co-C-C)	125.6	125.5	125.2	123.5	126.2
r(O_{Ado,3'}-O_{N193})	3.39	3.82	3.74	4.04	N/A
r(X241β-DMB)_{min}^b	3.38	5.64	3.61	3.16	3.49

^aAlso reported in Chapter 3.

^bThe r(X241β-DMB)_{min} parameter is the shortest distance between heavy atoms of those two groups.

Table 4.2. Key geometric parameters of AdoCbl-bound WT EAL and four variant ternary complexes. All distances are in Å and all angles in degrees.

	WT ^a	Y241βA	Y241βF	Y241βW	N193αA ^a
r(Co-C)	2.12	2.02	2.01	2.01	2.02
r(Co-N_{DMB})	2.45	2.32	2.33	2.36	2.32
DMB tilt	163.4	161.4	160.9	160.3	168.6
θ(Co-C-C)	137.8	125.9	125.8	125.1	127.0
r(O_{Ado,3'}-O_{N193})	2.98	3.51	3.56	3.80 ^c	N/A
r(X241β-DMB)_{min}^b	3.45	5.89	3.30	3.18	3.26

^aAlso reported in Chapter 3.

^bThe r(X241β-DMB)_{min} parameter is the shortest distance between heavy atoms of those two groups

^cThe distortion of the AdoCbl geometry in response to Y241βW substitution brings N193α closer to the 2'-OH group of the Ado ligand (3.63 Å).

Inspection of the active-site structures of AdoCbl-bound WT and Y241βW EAL reveals that in the variant the combined bulk of the tryptophan side chain and DMB ligand may be too large for both to simultaneously occupy the space beneath the corrin ring. Instead, the tryptophan displaces the DMB ligand rather than just tilting it. To test whether the Y241βW variant can accommodate AdoCbl analogues possessing smaller lower axial ligands, we optimized the structures of Ado(BIm)Cbl and Ado(Im)Cbl both *in vacuo* and in the WT EAL and Y241βW EAL active sites. As summarized in Table 4.3, the WT EAL active site affects the axial ligands of these

analogues differently than the native DMB. While AdoCbl binding to WT EAL induces a 0.11 Å decrease in the Co–N_{DMB} bond length, the Co–N_{Im} bond length of Ado(Im)Cbl decreases by only 0.06 Å, and the Co–N_{BIm} bond of Ado(BIm)Cbl actually lengthens by 0.05 Å. Both analogues exhibit tilt angles ~3° smaller in WT EAL than *in vacuo*, but this change is less than half of the 6.4° decrease observed for AdoCbl. Contrary to the case of AdoCbl, binding of the analogues to the Y241βW EAL variant causes larger changes to the axial ligand's tilt angle but only moderate changes to the Co–N_{ax} bond lengths.

Table 4.3. Key geometric parameters of AdoCbl, Ado(BIm)Cbl, and Ado(Im)Cbl as free species and bound to WT and Y241βW EAL. All distances are in Å and all angles are in deg.

Cofactor (Analogue)	State	r(Co–C)	r(Co–N _{DMB})	L _{ax} tilt ^c	r(X241β–L _{ax}) _{min} ^b
AdoCbl ^a	Free	2.03	2.38	166.7	N/A
	WT	2.03	2.27	160.3	3.38
	Y241βW	2.03	2.40	162.0	3.16
Ado(BIm)Cbl	Free	2.02	2.27	166.3	N/A
	WT	2.03	2.32	163.3	3.49
	Y241βW	2.03	2.33	161.9	3.22
Ado(Im)Cbl	Free	2.05	2.25	165.3	N/A
	WT	2.02	2.19	162.1	3.51
	Y241βW	2.03	2.23	157.1	3.08

^aAlso reported in Chapter 3.

^bL_{ax} refers to the lower axial ligand

^cThe r(X241β–L_{ax})_{min} parameter is the shortest distance between heavy atoms of these groups.

The proposed role for N193α is to distort the Ado ligand's conformation in the ternary complex through a hydrogen bond with the Ado 3'-OH group, so as to force the Co–C bond to grow longer. In Chapter 3, the disruption of this interaction in the N193αA variant was hypothesized to be responsible for the unchanged Co–C bond length in the QM/MM optimized structure of the N193αA ternary complex. In the present study, this hypothesis was tested computationally through the investigation of three additional cofactor analogues that lack either or both of the Ado ligand's hydroxyl groups. The relevant geometric parameters of these analogues

in the WT holoenzyme and ternary complex are summarized in Table 4.4. Compared to AdoCbl, the free analogues feature appreciably shorter Co–N_{DMB} bonds and slightly smaller DMB tilt angles. Upon binding to WT EAL, all three analogues undergo large changes to their DMB tilt angles and Co–N_{DMB} bond lengths, adopting a similar geometry as AdoCbl in the WT holoenzyme. Similarly, all three of these analogues – even 2',3'-ddAdoCbl – assume a conformation like that of AdoCbl in the ternary complex, including the presence of an elongated Co–C bond.

Table 4.4. Key geometric parameters of AdoCbl, 2'-dAdoCbl, 3'-dAdoCbl, and 2',3'-ddAdoCbl as free species and bound to the WT EAL holoenzyme and ternary complex. All distances are in Å and all angles are in degrees.

Cofactor (Analogue)	State	r(Co-C)	r(Co-N _{DMB})	DMB tilt	θ(Co-C-C)
AdoCbl^a	Free	2.03	2.38	166.7	128.4
	Holoenzyme	2.03	2.27	160.3	125.6
	Ternary	2.12	2.45	163.4	137.8
2'-dAdoCbl	Free	2.02	2.27	165.7	121.9
	Holoenzyme	2.04	2.28	160.2	124.8
	Ternary	2.13	2.37	164.9	137.8
3'-dAdoCbl	Free	2.02	2.28	164.2	126.8
	Holoenzyme	2.04	2.30	160.2	124.1
	Ternary	2.13	2.40	164.4	138.6
2',3'-ddAdoCbl	Free	2.02	2.27	165.2	125.8
	Holoenzyme	2.02	2.27	160.7	125.3
	Ternary	2.13	2.38	163.6	138.4

^aAlso reported in Chapter 3.

4.3.2. Predicted Abs spectra. To assess if the spectral characterization of the EAL variants investigated computationally is worthwhile, we used TD-DFT to predict the Abs spectrum of AdoCbl bound to each N193α and Y241β variant holoenzyme (Figure 4.4) and ternary complex (Figure 4.5). (Note that TD-DFT spectra of AdoCbl bound to three E287α variants were reported in Chapter 3.) Detailed analyses of the electronic structure of Co(III)Cbl species have been published elsewhere,⁴² and spectro-structural correlations that relate shifts in specific features of

the AdoCbl Abs spectrum to geometric perturbations were described in Chapter 3. These studies have identified several key regions of the AdoCbl Abs spectrum for identifying changes in cofactor structure. These include the lowest-energy features, or α/β bands, the high-intensity features in the near-UV, collectively called the γ region, and the intermediate features referred to as the D/E bands (Figure 4.5). Shifts in the α/β bands are particularly informative because they can be readily observed and interpreted, while the poor resolution of the D/E bands and the large number of transitions contributing to the γ region features make it difficult to correlate changes in these regions with specific structural perturbations of AdoCbl.

The TD-DFT-computed holoenzyme and ternary complex spectra for several of the EAL variants investigated show substantial blue-shifting of the α/β bands from their WT counterparts, especially compared to the relatively small shifts ($<200\text{ cm}^{-1}$) observed experimentally for most E287 α variants. For example, when AdoCbl binds to N193 α A, the α/β bands shift by over 1000 cm^{-1} in both the absence and presence of substrate, while several smaller changes also occur to the D/E bands and γ region. Much smaller shifts in the α/β positions are predicted for the binding of AdoCbl to the holoenzymes of Y241 β variants (all $<50\text{ cm}^{-1}$, with the exception of the Y241 β A variant). While spectral shifts of features at higher energy are predicted for these models, including substantial perturbations to the γ region, it is not immediately clear whether those can be observed experimentally. However, for each Y241 β variant, a shift of $\sim 500\text{ cm}^{-1}$ of the α/β bands is predicted upon formation of the ternary complex.

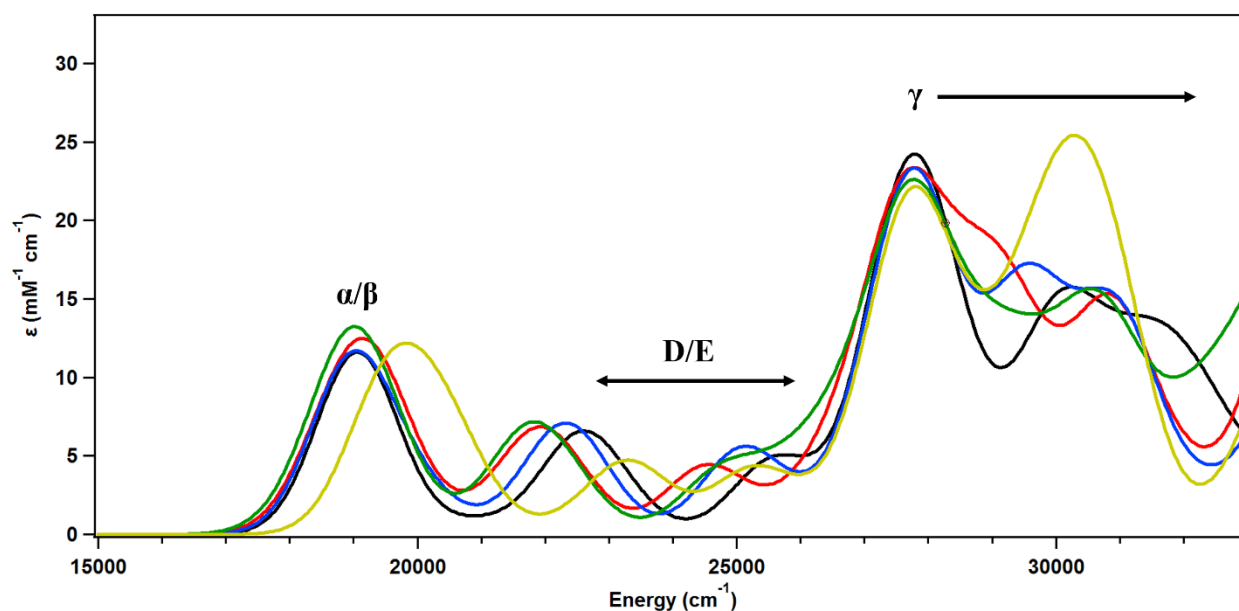


Figure 4.4. TD-DFT-computed Abs spectra for AdoCbl bound to the WT (black), Y241 β A (red), Y241 β F (blue), Y241 β W (green), and N193 α A (gold) EAL holoenzymes. The spectra were shifted to align the most intense feature at 27 786 cm^{-1} , the computed band maximum for AdoCbl-bound WT EAL.

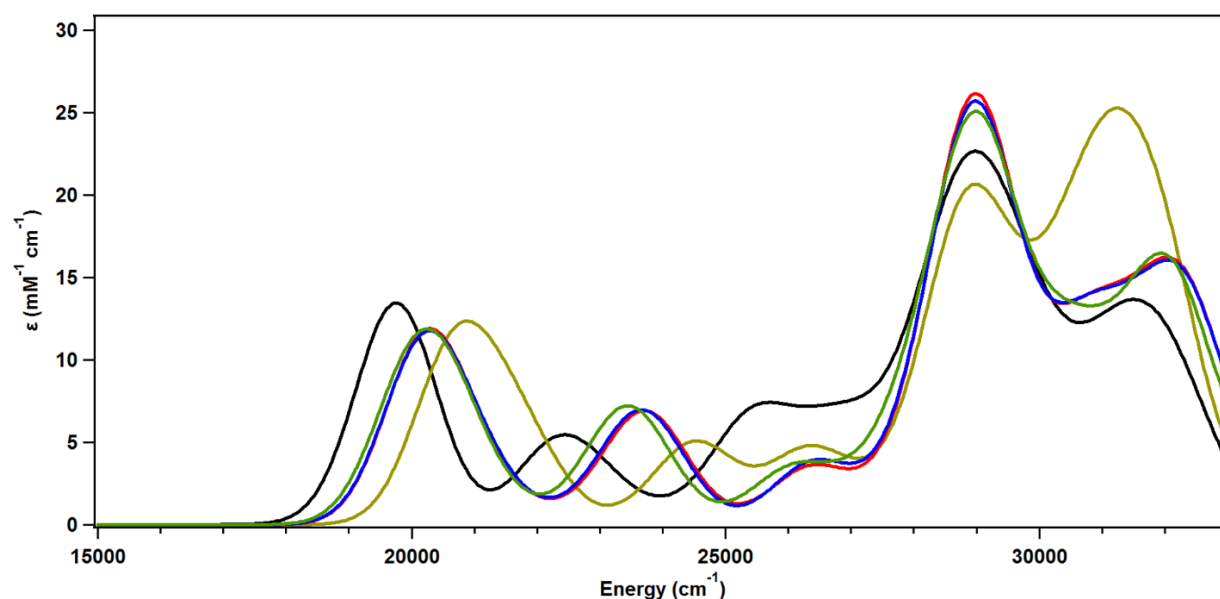


Figure 4.5. TD-DFT-computed Abs spectra for AdoCbl bound to the WT (black), Y241 β A (red), Y241 β F (blue), Y241 β W (green), and N193 α A (gold) EAL ternary complexes. The spectra were shifted to align the most intense feature at 28 983 cm^{-1} , the computed band maximum for AdoCbl in the WT ternary complex.

4.4 Discussion

4.4.1. QM/MM-Optimized Geometries. In our previous study, presented in Chapter 3, we proposed that Y241 β of the WT EAL holoenzyme imposes significant constraints on the conformational flexibility of the AdoCbl DMB ligand, causing decreases in both the Co–N_{DMB} bond length and the DMB tilt angle. The results of our current investigation of Y241 β variants and AdoCbl analogues with modified DMB ligands support this proposal (Tables 4.1 – 4.3). The Y241 β A variant holoenzyme lacks any substantial interaction between the A241 β side chain and the DMB ligand, and as a result AdoCbl adopts a geometry more similar to that of free AdoCbl (Co–N_{DMB} bond length of 2.38 Å, DMB tilt angle of 166.7°) than WT EAL-bound AdoCbl. Alternatively, in the Y241 β F holoenzyme, the Co–N_{DMB} bond lengths and DMB tilt angles are intermediate between those of the WT and Y241 β A holoenzymes. The 0.07 Å difference in lower axial bond length between the WT and Y241 β F holoenzymes does seem unusually large given the similar size of tyrosine and phenylalanine side chains. However, we note that the hydroxyl group of Y241 β in WT EAL is correctly oriented to hydrogen bond with a nitrogen atom of one of the AdoCbl corrin side chains. Although the long O–N distance of 3.77 Å (Figure A.4.1) suggests that the interaction is weak, it may help to properly orient the Y241 β side chain and thus explain the greater impact of WT EAL.

While the long Co–N_{DMB} bond length in the Y241 β A holoenzyme was attributed to a lack of interaction between the alanine side chain and the DMB ligand, a similarly long bond is observed in the Y241 β W variant holoenzyme due to significant steric repulsion between the DMB and the tryptophan side chain. The nature of this interaction causes a qualitatively different perturbation to the DMB ligand than in the WT and Y241 β F holoenzymes; i.e., Y241 β W partially displaces the lower axial ligand, whereas the latter merely change the ligand's orientation by tilting

it. This difference in enzyme-DMB interaction affects the entire cofactor, as revealed by the overlay plot of WT- and Y241 β W-bound AdoCbl shown in Figure 4.6, which shows significant differences between the orientations of corrin side chains and the Ado ligand in these models. Similar overlay plots of the other Y241 β variant holoenzymes (Figure A.4.1) fail to show such large-scale distortion.

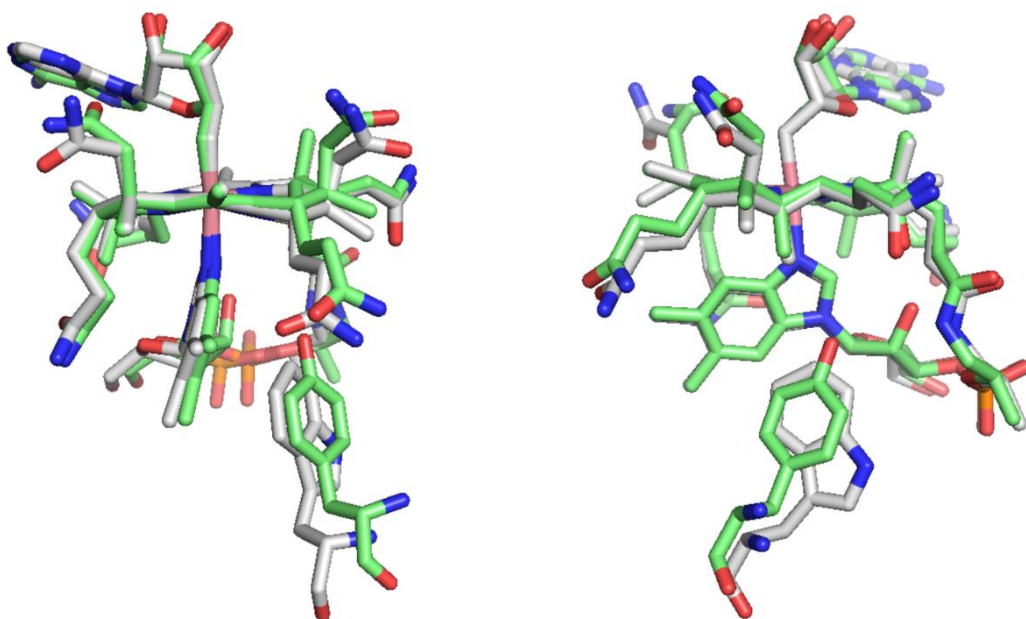


Figure 4.6. Two perspectives of an overlay of optimized geometries of WT-bound (green) and Y241 β W-bound (gray) AdoCbl. Hydrogen atoms are omitted for clarity.

The interaction between the DMB ligand and Y241 β was also investigated through the use of two cofactor analogues featuring BIm or Im in the lower axial position. Interestingly, both of these analogues support partial EAL activity (91% and 9% of activity for Ado(BIm)Cbl and Ado(Im)Cbl, respectively).⁴³ Based on our proposal that EAL achieves Co–C bond activation through the imposition of geometric constraints on the cofactor, the loss in activity exhibited by these analogues may be attributed to the decreased steric interaction between the smaller BIm/Im ligand and Y241 β . Indeed, our QM/MM-optimized model confirms that the influence of Y241 β on these analogues is diminished, as changes in the positioning of their lower axial ligands caused

by binding to WT EAL are more subtle than in the case of AdoCbl. The steric interaction between Y241 β of WT EAL and these cofactor analogues can be enhanced by Y241 β W substitution, which leads to a significant decrease in the lower axial ligand's tilt angle similar to what is observed upon binding of AdoCbl to WT EAL. Thus, if it is truly the encroachment of EAL upon the cofactor's lower axial ligand that is essential for Co–C bond activation, it is possible that Ado(Im)Cbl is a more competent cofactor in Y241 β W EAL than in the WT enzyme.

The computationally predicted effect of the N193 α A substitution on the AdoCbl geometry has been discussed previously (Chapter 3). Here, we explore the effect of removing one or both of the two –OH groups of the Ado ligand, one of which is expected to form a hydrogen bond with N193 α . Interestingly, the corresponding analogues (2'-dAdoCbl, 3'-dAdoCbl, and 2',3'-ddAdoCbl) all exhibit geometries similar to each other and to those of AdoCbl in the WT EAL holoenzyme and ternary complex. The activation of the analogues' Co–C bonds in the ternary complex, as inferred by the substantial increase in Co–C bond lengths, suggests that all of them are competent cofactors. Hence, the hydrogen bond between N193 α and the Ado 3'-OH group does not appear to be crucial for Co–C bond activation. In support of this notion is the fact that 2'-dAdoCbl and 3'-dAdoCbl retain 31% and 19%, respectively, of the WT EAL activity observed with AdoCbl incorporation.⁴⁴ (To the best of our knowledge, the activity of 2',3'-ddAdoCbl has not yet been determined.) Alternatively, the N193 α A EAL variant shows <1% activity of WT EAL,⁴⁵ demonstrating that the N193 α residue is more essential than either of the –OH groups of the Ado ligand. One possible interpretation of this result is that N193 α assists in Co–C bond activation by “pushing” the Ado ligand out of the way in order for it to reach a position where it can interact with the substrate, instead of “pulling” on the Ado ligand through a hydrogen bond. In the “pushing” mechanism, the hydrogen bond between N193 α and the Ado ligand's 3'-OH group plays

a secondary role by mitigating the energetic cost of Co–C bond elongation, but is not absolutely necessary for retention of some activity.

4.4.2. Predicted Abs Spectra. One goal of the current work was to identify EAL variants and AdoCbl analogues that merit future spectroscopic characterization. For them to be useful, these variants and analogues should afford species that are spectroscopically distinct from the free, WT EAL-bound, and ternary complex-bound AdoCbl. As the sensitivity of the electronic structure to geometric changes is difficult to predict qualitatively, we used TD-DFT to compute the Abs spectra of AdoCbl bound to each of the N193 α and Y241 β variant holoenzymes and ternary complexes. To assist in the analysis of these spectra, we first briefly summarize the relevant findings from the spectro-structural correlation studies outlined in Chapter 3.

First, the α/β bands are sensitive to the identity, distance, and orientation of the axial ligands. Blue-shifts of these bands are expected when the Co–N_{DMB} bond length increases, the Co–C bond length decreases, or the DMB tilt angle decreases; structural changes in the opposite direction are associated with red-shifts. Second, the binding of AdoCbl to WT EAL induces a red-shift of a transition that appears as a low-energy shoulder of the intense feature at $\sim 26\,500\text{ cm}^{-1}$. This feature has been assigned as the Co $3d_{xz} \rightarrow$ LUMO (corrin π^*) transition, and its red-shifting was attributed to a decrease of the Co–N_{DMB} bond lengths. Lastly, an additional low-intensity feature found at $\sim 23\,500\text{ cm}^{-1}$ in the Abs spectrum of WT ternary complex-bound AdoCbl has been attributed to the HOMO (corrin π) \rightarrow Co $3d_{z^2}$ transition. The Co $3d_{z^2}$ -based acceptor MO, which is formally antibonding with respect to both axial ligands, is greatly stabilized by the elongation of the axial bonds of AdoCbl in the ternary complex. In the Abs spectrum of free AdoCbl, the corresponding feature occurs at higher energy and is therefore obscured by more intense transitions contributing to the γ region.

The TD-DFT-computed Abs spectra for AdoCbl bound to the N193 α A holoenzyme and ternary complex agree well with the prediction emerging from our spectro-structural correlation studies. In the holoenzyme, the long Co–N_{DMB} bond causes the α/β bands to appear around 1000 cm⁻¹ higher in energy than they do in the computed spectrum for the WT holoenzyme, where this bond is 0.05 Å shorter. The same geometric change is also responsible for the red-shift of the Co 3d_{xz} → LUMO transition to ~25 500 cm⁻¹. Similarly, the large geometric differences between AdoCbl bound to the WT and N193 α EAL ternary complexes are responsible for significant differences in the corresponding Abs spectra. Specifically, the much shorter Co–C bonds in all variant ternary complex models cause a large blue-shift of the α/β bands from their positions in the WT EAL spectrum, most noticeably in the case of the N193 α A variant. The short Co–C bond lengths also prevent the red-shifting of the HOMO → Co 3d_{z²} transition predicted for the WT ternary complex.

The computed Abs spectra for the Y241 β variant holoenzymes are more difficult to interpret within the framework of our spectro-structural correlations. Although the nearly unshifted positions of the α/β bands can be attributed to the competing effects of longer Co–N_{DMB} bond paired with larger DMB tilt angles, the positions of the features found at 24 000 – 25 500 cm⁻¹ cannot be explained on the basis of simple structural changes. That is, even though the Co 3d_{xz} → LUMO transition is expected to be found at lower energies when the Co–N_{DMB} bond is short, the corresponding feature appears at lower energies for Y241 β variant-bound AdoCbl models with long Co–N_{DMB} bonds. A possible cause for this discrepancy is that although most Abs features of AdoCbl are predicted to experience a uniform blue-shift upon the inclusion of EAL point charges, the feature due to the Co 3d_{xz} → LUMO transition is especially sensitive to the X241 β side chain's point charges (See Chapter 3.4.2). While this sensitivity proved essential for the correct prediction

of the WT-bound AdoCbl Abs spectrum, it also led to an erroneous blue-shifting of this transition in the computed Abs spectrum for the WT ternary complex. Since both the steric and electronic properties of the X241 β side chain vary greatly among the variants investigated, computation of these spectra test the limits of our methodology, and predictions made on the basis of this particular transition energy should be considered tentative.

4.5 Conclusion

A computational evaluation of several AdoCbl analogues and EAL variants was undertaken in order to identify useful species for future spectroscopic characterization. According to our results, we expect that both Y241 β and N193 α variants are promising candidates, as they are predicted in many cases to induce different geometric and electronic structures in AdoCbl than WT EAL does. The TD-DFT-computed spectra for the N193 α A variant holoenzyme and ternary complex are distinct from those of WT EAL, suggesting that the effect of making this substitution would be spectroscopically observable. The same is true for the Y241 β variant ternary complexes, although the corresponding holoenzymes may exhibit features quite similar to those of WT EAL. Similarly, as the predicted geometric changes to Ado(BIm)Cbl and Ado(Im)Cbl upon binding to EAL were fairly subtle, it is unlikely that studies of these analogues in WT EAL will offer substantial insight into the importance of the lower axial ligand. However, we do note that the change in tilt angle for both of these species upon binding to the Y241 β W variant was significant. It is possible that the pairing of a BIm or Im ligand with the bulky tryptophan residue might produce an effect similar to that caused by the interaction between the DMB ligand and Y241 β in WT EAL, which has been observed spectroscopically. The predicted susceptibility of 2'-dAdoCbl, 3'-dAdoCbl, and 2',3'-ddAdoCbl to Co–C bond elongation in the EAL ternary complex, while intriguing, may make the characterization of these species' interaction with EAL less revealing,

on account of the similarity in behavior of these analogues and AdoCbl itself. One exception would be the study of these analogues bound to the N193 α A variant. If, as predicted here, the analogues display behavior similar to AdoCbl while the variant changes the native cofactor's spectrum substantially, those results would provide experimental support for the mixed steric and electronic roles of N193 α postulated here.

4.6 References

1. Banerjee, R.; Ragsdale, S. W., *Annual Review of Biochemistry* **2003**, 72, 209-247.
2. Brown, K. L., *Chemical Reviews* **2005**, 105, 2075-2149.
3. Toraya, T., *Archives of Biochemistry and Biophysics* **2014**, 544, 40-57.
4. Banerjee, R., *Chemistry and Biochemistry of B₁₂*. Wiley-Interscience: New York, NY, 1999.
5. Babior, B. M., *Journal of Biological Chemistry* **1970**, 245, 6125-&.
6. Babior, B. M.; Woodams, A. D.; Brodie, J. D., *Journal of Biological Chemistry* **1973**, 248, 1445-1450.
7. Chowdhury, S.; Banerjee, R., *Biochemistry* **1999**, 38, 15287-15294.
8. Marsh, E. N. G.; Ballou, D. P., *Biochemistry* **1998**, 37, 11864-11872.
9. Banerjee, R., *Chemical Reviews* **2003**, 103, 2083-2094.
10. Marsh, E. N. G.; Holloway, D. E., *Febs Letters* **1992**, 310, 167-170.
11. Ratnatilleke, A.; Vrijbloed, J. W.; Robinson, J. A., *Journal of Biological Chemistry* **1999**, 274, 31679-31685.
12. Beatrix, B.; Zelder, O.; Linder, D.; Buckel, W., *European Journal of Biochemistry* **1994**, 221, 101-109.
13. Yamanishi, M.; Yamada, S.; Ishida, A.; Yamauchi, J.; Toraya, T., *Journal of Biochemistry* **1998**, 124, 598-601.
14. Yamanishi, M.; Yamada, S.; Muguruma, H.; Murakami, Y.; Tobimatsu, T.; Ishida, A.; Yamauchi, J.; Toraya, T., *Biochemistry* **1998**, 37, 4799-4803.
15. Yamanishi, M.; Yunoki, M.; Tobimatsu, T.; Sato, H.; Matsui, J.; Dokiya, A.; Iuchi, Y.; Oe, K.; Suto, K.; Shibata, N.; Morimoto, Y.; Yasuoka, N.; Toraya, T., *European Journal of Biochemistry* **2002**, 269, 4484-4494.
16. Akita, K.; Hieda, N.; Baba, N.; Kawaguchi, S.; Sakamoto, H.; Nakanishi, Y.; Yamanishi, M.; Mori, K.; Toraya, T., *Journal of Biochemistry* **2010**, 147, 83-93.
17. Brooks, A. J.; Fox, C. C.; Marsh, E. N. G.; Vlasie, M.; Banerjee, R.; Brunold, T. C., *Biochemistry* **2005**, 44, 15167-15181.
18. Brooks, A. J.; Vlasie, M.; Banerjee, R.; Brunold, T. C., *Journal of the American Chemical Society* **2005**, 127, 16522-16528.
19. Stich, T. A.; Buan, N. R.; Brunold, T. C., *Journal of the American Chemical Society* **2004**, 126, 9735-9749.
20. Brooks, A. J.; Vlasie, M.; Banerjee, R.; Brunold, T. C., *Journal of the American Chemical Society* **2004**, 126, 8167-8180.
21. Chen, Z. G.; Zietek, M. A.; Russell, H. J.; Tait, S.; Hay, S.; Jones, A. R.; Scrutton, N. S., *Chembiochem* **2013**, 14, 1529-1533.
22. Shibata, N.; Tamagaki, H.; Hieda, N.; Akita, K.; Komori, H.; Shomura, Y.; Terawaki, S.; Mori, K.; Yasuoka, N.; Higuchi, Y.; Toraya, T., *Journal of Biological Chemistry* **2010**, 285, 26484-26493.
23. The PyMOL Molecular Graphics System, Version 1.5.0.4 Schrodinger, LLC.

24. Dolinsky, T. J.; Nielsen, J. E.; McCammon, J. A.; Baker, N. A., *Nucleic Acids Research* **2004**, *32*, W665-W667.
25. Word, J. M.; Lovell, S. C.; Richardson, J. S.; Richardson, D. C., *Journal of Molecular Biology* **1999**, *285*, 1735-1747.
26. Gaussian 09; Revision D.01; Frisch, M. J.; Trucks, G. W.; Schlegel, H. B.; Scuseria, G. E.; Robb, M. A.; Cheeseman, J. R.; Scalmani, G.; Barone, V.; Mennucci, B.; Petersson, G. A.; Nakatsuji, H.; Caricato, M.; Li, X.; Hratchian, H. P.; Izmaylov, A. F.; Bloino, J.; Zheng, G.; Sonnenberg, J. L.; Hada, M.; Ehara, M.; Toyota, K.; Fukuda, R.; Hasegawa, J.; Ishida, M.; Nakajima, T.; Honda, Y.; Kitao, O.; Nakai, H.; Vreven, J. A.; Montgomery, J. A.; Peralta, J. E.; Ogliaro, F.; Bearpark, M.; Heyd, J. J.; Brothers, E.; Kudin, K. N.; Staroverov, V. N.; Kobayashi, R.; Normand, J.; Raghavachari, K.; Rendell, A.; Burant, J. C.; Iyengar, S. S.; Tomasi, J.; Cossi, M.; Rega, N.; Millam, J. M.; Klene, M.; Knox, J. E.; Cross, J. B.; Bakken, V.; Adamo, C.; Jaramillo, J.; Gomperts, R.; Stratmann, R. E.; Yazyev, O.; Austin, A. J.; Cammi, R.; Pomelli, C.; Ochterski, J. W.; Martin, R. L.; Morokuma, K.; Zakrzewski, V. G.; Voth, G. A.; Salvador, P.; Danneberg, J. J.; Dapprich, S.; Daniels, A. D.; Farkas, O.; Foresman, J. B.; Ortiz, J. V.; Cioslowski, J.; Fox, D. G. Gaussian Inc.: Wallingford, CT, 2009.
27. Cornell, W. D.; Cieplak, P.; Bayly, C. I.; Gould, I. R.; Merz, K. M.; Ferguson, D. M.; Spellmeyer, D. C.; Fox, T.; Caldwell, J. W.; Kollman, P. A., *Journal of the American Chemical Society* **1995**, *117*, 5179-5197.
28. Marques, H. M.; Ngoma, B.; Egan, T. J.; Brown, K. L., *Journal of Molecular Structure* **2001**, *561*, 71-91.
29. Perdew, J. P., *Physical Review B* **1986**, *33*, 8822-8824.
30. Becke, A. D., *Physical Review A* **1988**, *38*, 3098-3100.
31. Kuta, J.; Patchkovskii, S.; Zgierski, M. Z.; Kozlowski, P. M., *Journal of Computational Chemistry* **2006**, *27*, 1429-1437.
32. Hay, P. J.; Wadt, W. R., *Journal of Chemical Physics* **1985**, *82*, 299-310.
33. Hay, P. J.; Wadt, W. R., *Journal of Chemical Physics* **1985**, *82*, 270-283.
34. Wadt, W. R.; Hay, P. J., *Journal of Chemical Physics* **1985**, *82*, 284-298.
35. Neese, F., *Wiley Interdisciplinary Reviews-Computational Molecular Science* **2012**, *2*, 73-78.
36. Neese, F.; Olbrich, G., *Chemical Physics Letters* **2002**, *362*, 170-178.
37. Hirata, S.; Head-Gordon, M., *Chemical Physics Letters* **1999**, *314*, 291-299.
38. Becke, A. D., *Journal of Chemical Physics* **1993**, *98*, 1372-1377.
39. Lee, C. T.; Yang, W. T.; Parr, R. G., *Physical Review B* **1988**, *37*, 785-789.
40. Schafer, A.; Huber, C.; Ahlrichs, R., *Journal of Chemical Physics* **1994**, *100*, 5829-5835.
41. Schafer, A.; Horn, H.; Ahlrichs, R., *Journal of Chemical Physics* **1992**, *97*, 2571-2577.
42. Stich, T. A.; Brooks, A. J.; Buan, N. R.; Brunold, T. C., *Journal of the American Chemical Society* **2003**, *125*, 5897-5914.
43. Fukuoka, M.; Yamada, S.; Miyoshi, S.; Yamashita, K.; Yamanishi, M.; Zou, X.; Brown, K. L.; Toraya, T., *Journal of Biochemistry* **2002**, *132*, 935-943.
44. Ichikawa, M.; Toraya, T., *Biochimica Et Biophysica Acta* **1988**, *952*, 191-200.
45. Mori, K.; Oiwa, T.; Kawaguchi, S.; Kondo, K.; Takahashi, Y.; Toraya, T., *Biochemistry* **2014**, *53*, 2661-2671.

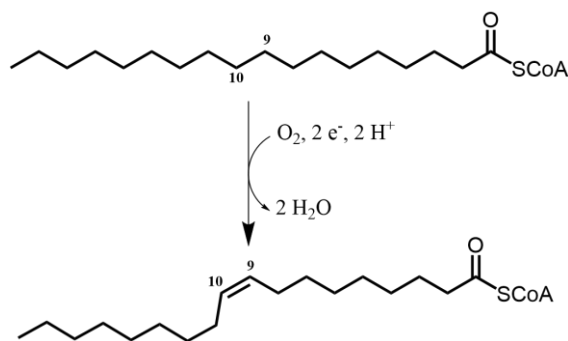
CHAPTER 5

Computational Investigation of the Dioxygen Binding Site and a Putative Reaction Mechanism of Stearoyl-CoA Desaturase

5.1 Introduction

Fatty acids are ubiquitous components of living organisms, being essential for the proper construction of lipid membranes and the biosynthesis of hormones and prostaglandins.¹⁻⁶ Monounsaturated, polyunsaturated, and otherwise functionalized fatty acids are typically formed by successive modifications of a parent saturated fatty acid or acyl-CoA. For example, stearoyl-CoA is used to construct many eukaryotic fatty acyl-CoAs, beginning with its desaturation (Scheme 5.1) by stearoyl-CoA desaturase (SCD).^{7,8} SCD is a membrane-bound dimer that belongs to a class of desaturases known as $\Delta 9$ desaturases ($\Delta 9$ DSs), so named because of their ability to introduce a double bond between C₉ and C₁₀ of fatty acid or acyl-CoA substrates.⁵ SCD has been implicated in the development of metabolic diseases such as obesity and diabetes in mammals, making it and other $\Delta 9$ DSs potential pharmacological targets.⁹⁻¹² Moreover, the ready availability of fatty acids and their derivatives from plant and animal sources has inspired interest in their use as industrial feedstocks and encouraged further investigation of the pathways that lead to their formation and the enzymatic mechanisms that enable their syntheses.¹³⁻¹⁵ The ability of $\Delta 9$ DSs and other desaturases to selectively break aliphatic, seemingly unactivated C–H–bonds has also fascinated the chemical community,¹⁶ and an understanding of the enzyme mechanisms may hold meaningful implications for catalytic C–H bond activation.

Scheme 5.1. Desaturation of stearoyl-CoA to form oleyl-CoA.



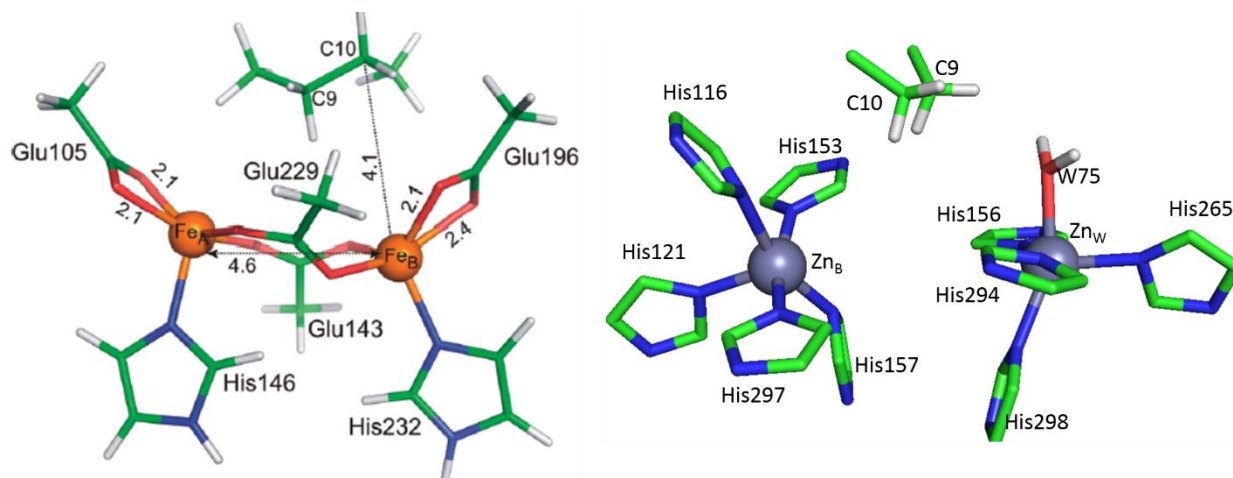
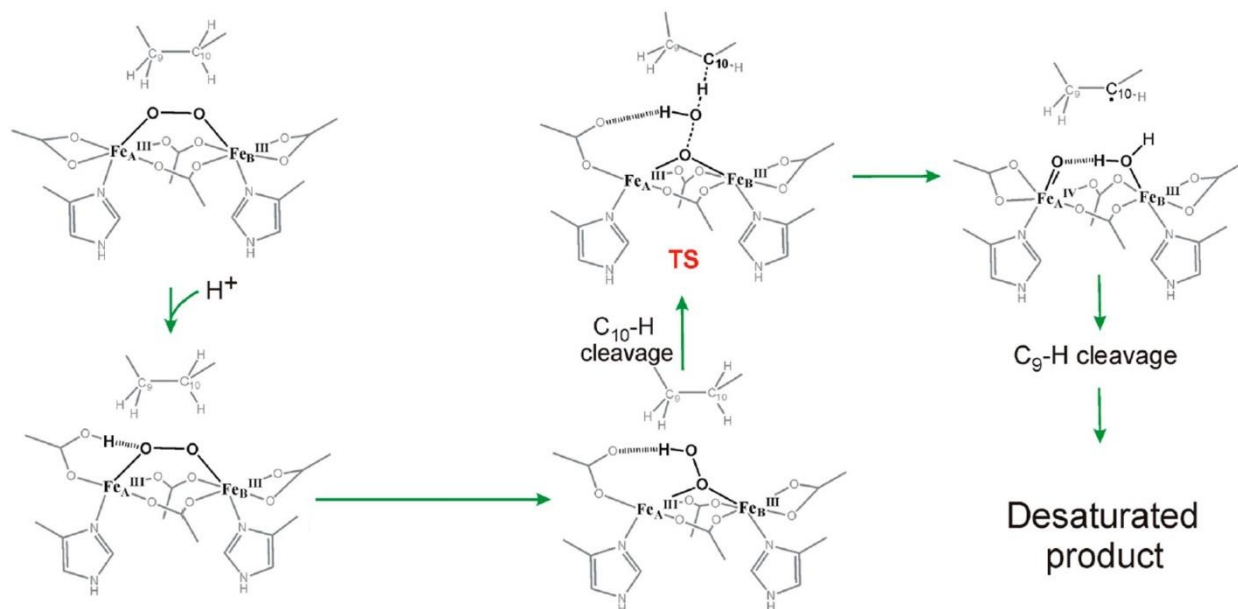


Figure 5.1. Active-site regions of cytosolic (left, PDB: 1AFR,¹⁷ figure adapted from ref 20) and membrane-bound (right, PDB: 4YMK²²) $\Delta 9$ Ds.

All known $\Delta 9$ Ds contain a non-heme diiron (NHFe₂) active site and catalyze the desaturation of their substrates alongside the four-electron reduction of O₂ to two H₂O molecules.⁵ However, two classes of evolutionarily distinct $\Delta 9$ Ds are known: the membrane-bound $\Delta 9$ Ds, found throughout eukaryotic kingdoms, and cytosolic $\Delta 9$ Ds, found exclusively in plants.¹⁸ X-ray crystal structures of the latter revealed the iron ions to be roughly 3–4 Å apart and bridged by two conserved, bidentate glutamate residues (Figure 5.1, left).¹⁷ Subsequent spectroscopic and computational investigations have led to the identification of **P**, a putative *cis*- μ -1,2-peroxodiferrous intermediate generated from the binding of O₂ to a diferrous active site.^{19, 20} Computational investigation of several possible mechanisms led to the proposal that this intermediate is activated by protonation to form a μ -1,1-hydroperoxodiferrous species (Scheme 5.2).²¹ In the proposed mechanism, this intermediate performs a hydrogen atom abstraction (HAA) from the fatty acid substrate concomitant with homolytic O–O bond cleavage to form an Fe(III)/Fe(IV)-oxo species and a water molecule in the rate-determining step. This high-valent species quickly abstracts a second hydrogen atom from the substrate, forming the desaturated product and a diferrous NHFe₂

site. The catalytic cycle is completed upon two-electron reduction of the latter by an exogenous source.



Scheme 5.2. Proposed mechanism for the activation of **P** and subsequent desaturation of substrate in cytosolic $\Delta 9$ Ds. Adapted from ref 21.

Very recently, Bai et al. reported the crystal structure of Zn_2 -bound *Mus musculus* SCD complexed with stearoyl-CoA (PDB: 4YMK),²² the first structure of any membrane-bound $\Delta 9$ D. Shortly thereafter, another group solved a crystal structure of Zn_2 -bound human SCD, also with substrate bound (PDB: 4ZYO).²³ These structures both revealed an unusual active site in which one Zn ion (here, “ Zn_B ”) is coordinated by five histidine (His) residues, while the other (“ Zn_W ”) is coordinated by four His side chains and one solvent molecule (Figure 5.1, right). Intriguingly, the intermetallic distance was found to be ~ 6.5 Å, which is too far for O_2 to serve as a bridging ligand in the O_2 activation mechanism. Although a potential shortcoming of these crystal structures is the presence of non-native metal ions in the active site, Bai et al. noted that the uniformity of B-values and the reasonable position of substrate relative to the Zn_2 binding site imply that the metal substitution had at most a minor effect on the active-site geometry.²² Eight of the nine coordinating

His residues are part of three highly-conserved “His boxes” in membrane-bound but not cytosolic desaturases.²⁴ Alanine substitution of any of these His residues causes a complete loss of desaturase activity. A more recent analysis of desaturases across 56 eukaryotic genomes confirmed that these His residues, as well as several of the other residues within these boxes, are highly conserved in all desaturases with saturated substrates (Figure 5.2).²⁵

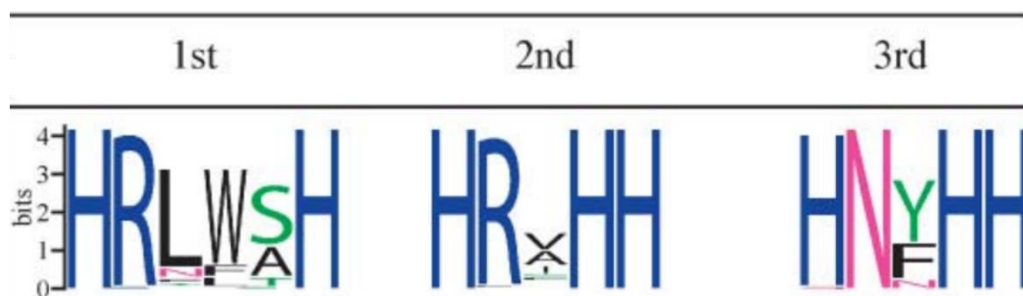


Figure 5.2. Sequence logo representation of conserved residues in the three His boxes of fatty acid desaturases. The height of the one-letter amino acid code represents the frequency of that residue’s occurrence in desaturases throughout the genomes studied. Only those desaturases with saturated substrates were included in this analysis. Figure adapted from ref 25.

The uniqueness of the SCD active-site geometry has led to a host of new questions regarding the mechanisms of SCD and other membrane-bound Δ^9 Ds. The long Fe–Fe distance implicated by the observed Zn–Zn separation is unprecedented among NHFe_2 enzymes,²⁶ and the means by which the two Fe ions bind and activate O_2 is as of yet unclear. Obtaining this information is a necessary first step in proposing a reasonable mechanism, yet the inherent difficulty of working with membrane-bound proteins makes the experimental characterization of SCD more challenging than that of the cytosolic Δ^9 Ds. As an alternative, the SCD crystal structure allows for the computational exploration of putative O_2 binding sites and reaction mechanisms.

In this chapter, we describe the use of combined quantum mechanics/molecular mechanics (QM/MM) geometry optimizations to accomplish three objectives. First, we demonstrate that the active-site structure of SCD is largely unperturbed by the *in silico* substitution of Zn with Fe.

Following this, we apply the same computational methods to investigate several possible O₂ binding sites. We then conclude our analysis by proposing a reaction mechanism on the basis of one promising O₂-bound model, using the computed energies and geometries of the intermediates to show the mechanism's plausibility.

5.2 Computational Methods

All SCD models considered in this study were generated from the crystallographic coordinates provided by Bai et al., which were recently deposited in the Protein Data Bank.²² Hydrogen atoms were added to the SCD crystal structure with the pdb2pqr program,²⁷ assuming a pH of 7, while Reduce²⁸ was used to add hydrogen atoms to the stearyl-CoA substrate. All nine metal-coordinating His residues were protonated to ensure a neutral charge. An initial molecular mechanics (MM) geometry optimization of the Zn₂-bound structure was performed in Gaussian09²⁹ with the AMBER force field.³⁰ AMBER parameters of aliphatic carbons were used for the fatty acyl moiety of the substrate. The CoA moiety was frozen as a rigid fragment; only non-bonding terms (e.g., those modeling van der Waals and electrostatic forces) were included for the constituent atoms. The Zn ions were also frozen during the MM optimization. Charges were assigned to the substrate by Gaussian09, using the QEq formalism.³¹ One of the SCD monomers (Chain D in the PDB file), along with its corresponding substrates and Zn ions, was frozen in this and all subsequent optimizations.

This MM-optimized SCD model was used as an initial geometry for subsequent QM/MM optimizations of both Zn₂- and high-spin Fe^{II}₂-bound SCD models in the absence of O₂, performed with the ONIOM module of Gaussian09.³² The QM regions of all models included both metal ions, all nine coordinating His side chains, the coordinating solvent molecule, and most of the fatty acid portion of the substrate (Figure 5.3). The coordinates of the QM regions of all models in this study

are reported at the end of Appendix A.5. Covalent bonds spanning the QM/MM boundary were capped with hydrogen link atoms, replacing C_α of each of the nine coordinating His and C_2 of the substrate in the QM steps of all calculations. Bond lengths for bonds to link atoms were scaled to 0.709 times their original length. Optimizations were performed using three different density functionals: BP86,^{33,34} B3LYP,^{35,36} and M-06L.³⁷ The MM region was treated with the same force field and choice of frozen atoms as in the initial MM optimization. Ahlrichs' triple zeta with polarization (TZVP) basis set³⁸ was used for the metal atoms and the coordinating atoms of all ligands, and his split-valence polarized (SVP) basis set³⁹ was employed for the remaining QM atoms. During many of these optimizations, maximum and root-mean-square (RMS) forces failed to reach the default ONIOM convergence criteria despite the convergence of the maximum and RMS displacements and the lack of any further motion of the QM atoms. These models were considered optimized if no further movement was observed after restarting the optimization. Optimizations using the BP86 functional experienced SCF convergence problems with the Fe^{II} -bound SCD models. For this reason, only the optimizations carried out with the B3LYP and M-06L functionals are described below.

The B3LYP-optimized model of substrate-bound Fe^{II}_2 -SCD was used in subsequent QM/MM computations to test putative O_2 binding sites. Initial coordinates for O_2 were generated by assuming an Fe–O bond length of 2.00 Å, an O–O bond length of 1.35 Å, and an Fe–O–O bond angle of 135°, with the latter two being intermediate between typical values for Fe-bound superoxo and peroxo ligands. A multiplicity of 9 ($S=4$) was used for each of these models, consistent with the combination of a high-spin, mixed-valence Fe^{II}/Fe^{III} system in which the Fe^{III} bears an antiferromagnetically coupled superoxide ligand. (Note that this multiplicity does not preclude the possibility of convergence to an Fe^{II}/Fe^{IV} -peroxo species.) Models featuring an additional solvent

molecule bound to the Fe ion lacking the O₂-derived ligand were also tested. Both O₂ and the additional solvent (when present) were placed in the QM region and treated with the TZVP basis set. For each model, several initial O₂ orientations relative to the stearyl-CoA substrate were evaluated. Initial coordinates for the putative intermediates in the mechanism proposed on the basis of these computations (Section 5.3.3) were generated from the optimized geometry of the appropriate O₂-bound models. The solvent-derived ligand on Fe_w was modeled as hydroxide throughout. The intermediate directly following the water-forming step was optimized both with and without the nascent water molecule present; all subsequent intermediates did not include this water molecule. To calculate the relative energies of the putative reaction intermediates, single-point calculations using ONIOM's electronic embedding method⁴⁰ were performed on the optimized structures.

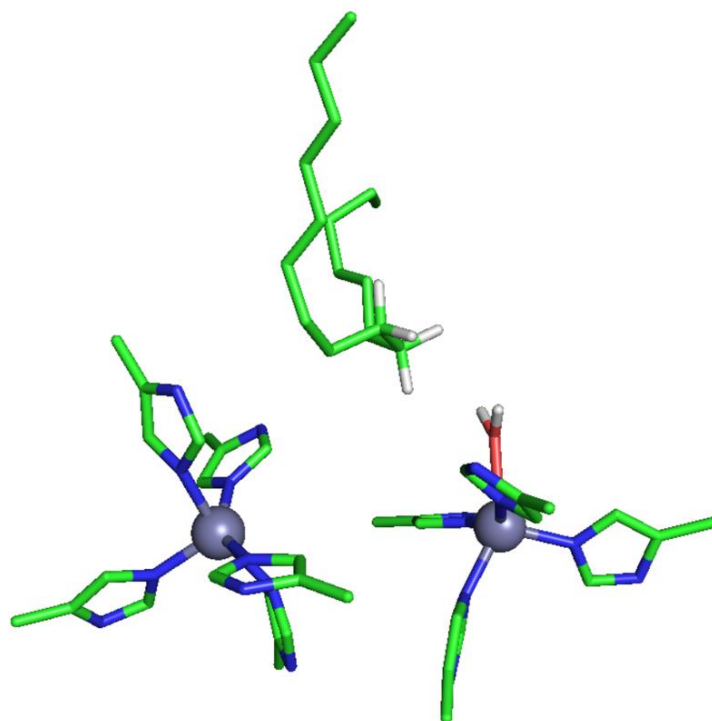


Figure 5.3. QM region used for all QM/MM optimizations in this study. All hydrogen atoms are omitted for clarity, except for those attached to C₉ and C₁₀ of the substrate and the solvent ligand.

5.3 Results

5.3.1. Geometry Optimizations of Zn₂- and Fe₂-bound SCD. The B3LYP- and M-06L-optimized geometries of Zn₂-bound SCD complexed with stearyl-CoA are shown in Figure 5.4, with relevant geometric parameters summarized in Table 5.1. The optimized Zn–Zn distances of 7.55 Å and 7.09 Å, respectively, are both longer than the 6.45 Å distance observed in the crystal structure. Despite this lengthening, the coordination environments of both Zn^{II} ions are relatively unperturbed, with all metal-ligand bond distances remaining reasonable (Table A.5.1). Of particular interest is the distance between the metal ions and the pro*R* hydrogens of C₉ and C₁₀ of the substrate (H_{9R} and H_{10R}, respectively), as these atoms must be abstracted at some point during SCD turnover. Abstraction of H_{9R} is known to be rate-limiting on the basis of kinetic isotope effect studies.^{41, 42} In both models, H_{9R} is found to point at the open cavity in the active site, significantly closer to Zn_W than to Zn_B.

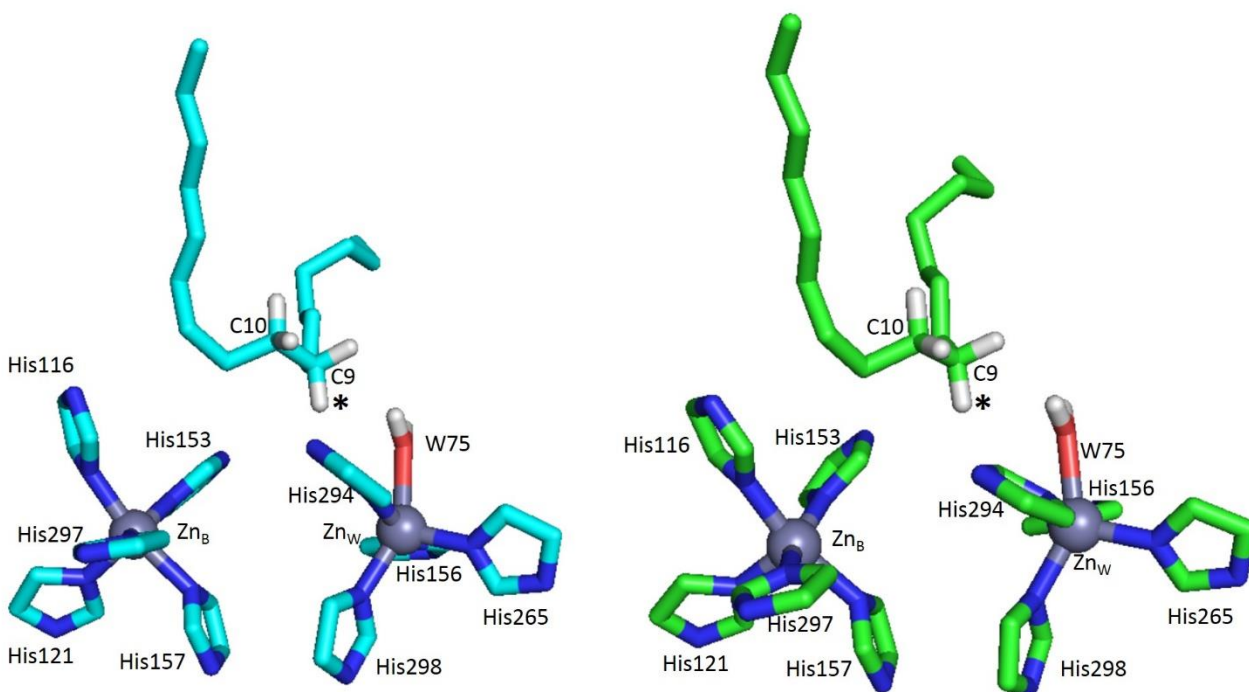


Figure 5.4. QM regions of QM/MM-optimized models of Zn^{II}₂-bound SCD obtained with B3LYP (left) and M-06L (right). H_{9R} is indicated with a star.

Table 5.1. Key geometric parameters of the QM/MM-optimized geometries of Zn^{II} - and Fe^{II} -bound SCD. All distances are in Å.

Model	$r(\text{M-M})$	$r(\text{M}_\text{B}-\text{H}_{9\text{R}})$	$r(\text{M}_\text{W}-\text{H}_{9\text{R}})$	$r(\text{M}_\text{B}-\text{H}_{10\text{R}})$	$r(\text{M}_\text{W}-\text{H}_{10\text{R}})$
$\text{Zn}^{\text{II}}_2/\text{B3LYP}$	7.55	6.33	4.37	7.06	5.95
$\text{Zn}^{\text{II}}_2/\text{M-06L}$	7.09	5.52	4.21	6.45	5.55
$\text{Fe}^{\text{II}}_2/\text{B3LYP}$	6.80	4.94	4.23	4.28	5.17
$\text{Fe}^{\text{II}}_2/\text{M-06L}$	6.88	5.05	4.04	4.28	5.03

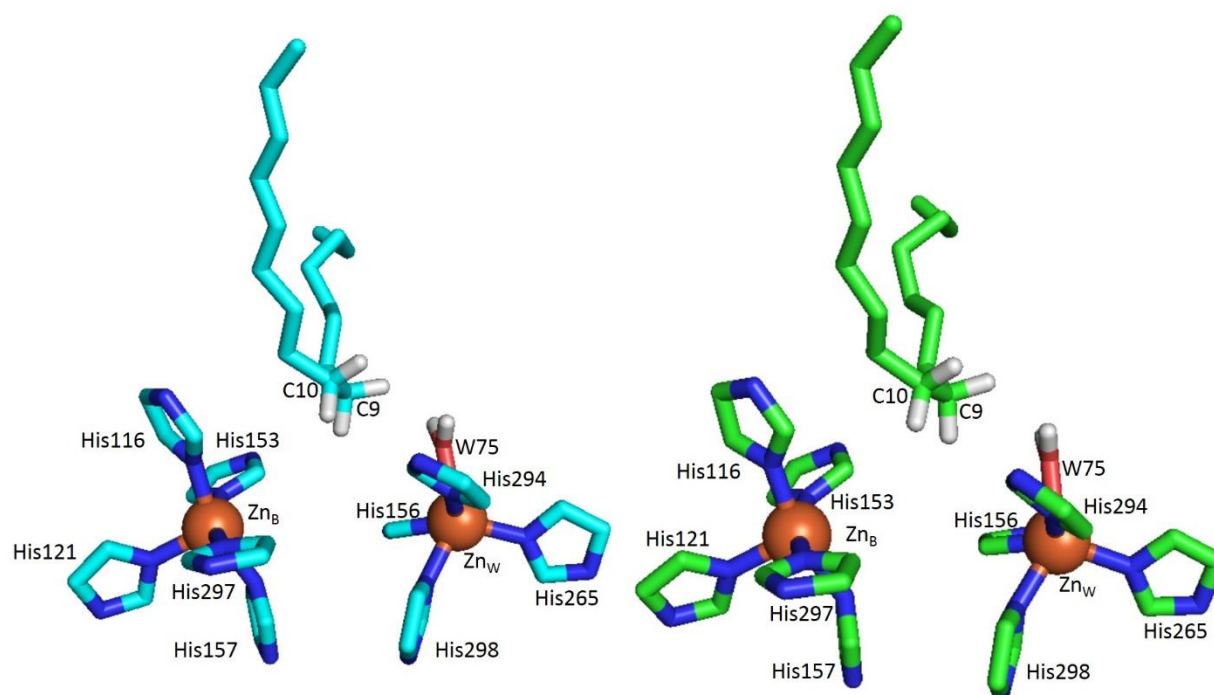


Figure 5.5. QM regions of QM/MM-optimized geometries of Fe^{II}_2 -bound SCD obtained with B3LYP (left) and M-06L (right).

While the SCD active site can readily accommodate incorporation of Fe (Table A.5.1), as claimed by Bai et al., two significant changes in the active-site geometry are predicted computationally upon substitution of Fe for Zn (Figure 5.5, Table 5.1). First, both B3LYP and M-06L predict the intermetallic distance to decrease to slightly less than 6.9 Å. Second, a significant rotation around the substrate's C_9 – C_{10} bond positions $\text{H}_{10\text{R}}$ so that it points towards the

metal ions' empty coordination sites, much like H_{9R} in the Zn_2 -bound models. The combination of these two events brings H_{10R} significantly closer to Fe_B than Fe_W , while H_{9R} remains closer to Fe_W .

5.3.2. Exploration of putative O_2 binding sites. The SCD crystal structure reveals open coordination sites on both metal ions, making it impossible to determine the O_2 binding site on the basis of visual inspection alone. Therefore, we carried out QM/MM optimizations of the following viable models of the O_2 -bound reaction intermediate: O_2 bound to Fe_W , in the absence (1) and presence (2) of an additional solvent (H_2O) ligand on Fe_B ; and O_2 bound to Fe_B , in the absence (3) and presence (4) of an additional solvent ligand on Fe_W . In each case, several different initial conformations of the O_2 moiety were evaluated. Representative models for each of these states are shown in Figure 5.6, and a comparison of relevant geometric parameters is provided in Table 5.2.

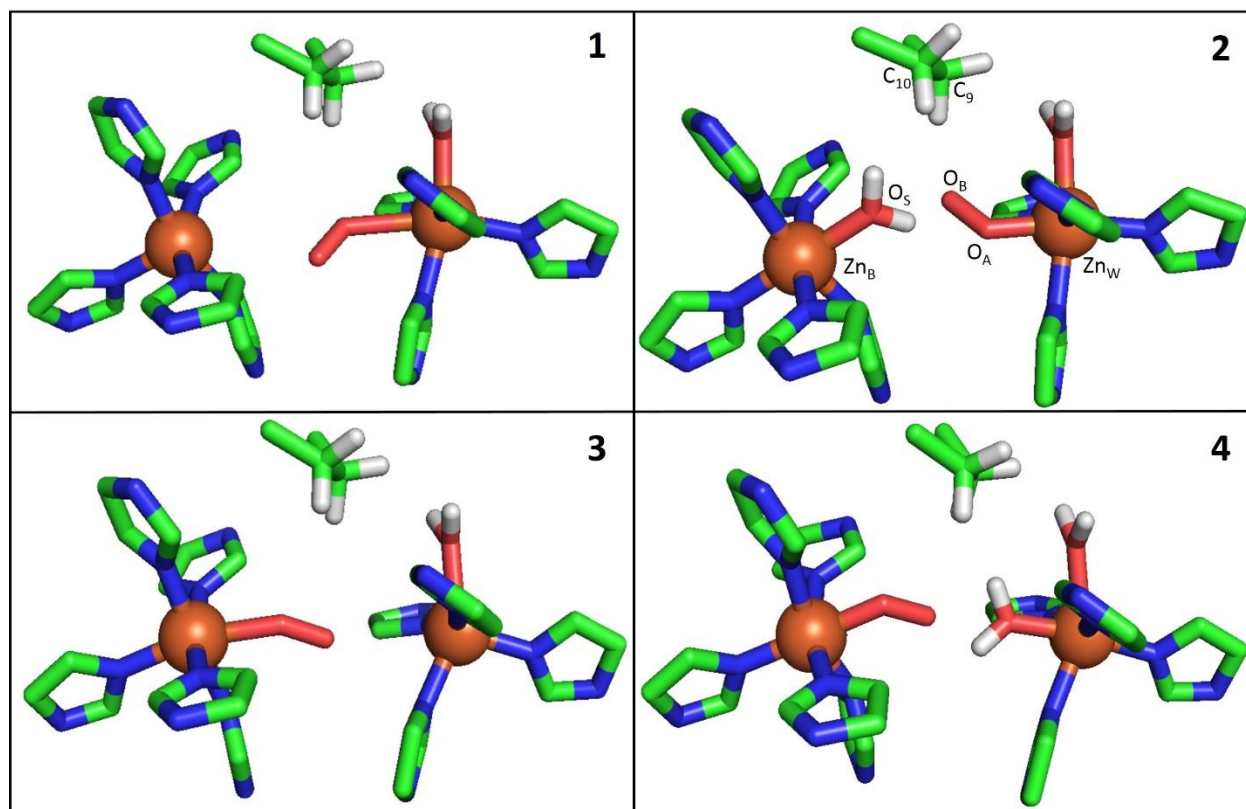
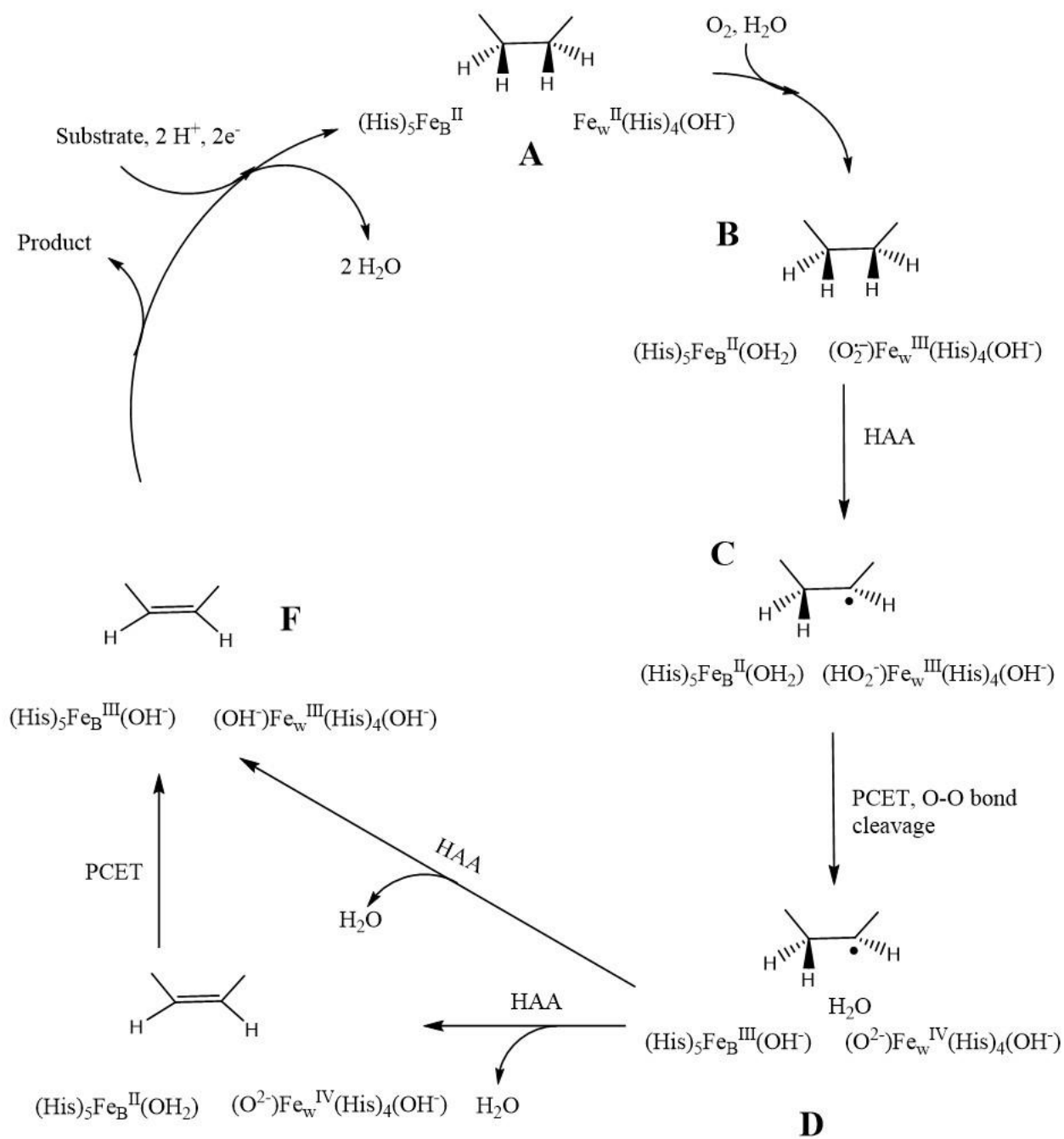


Figure 5.6. QM/MM-optimized geometries of four putative O_2 -bound reaction intermediates of SCD. See text for details.

Table 5.2. Key geometric parameters of the B3LYP-optimized O₂-bound models of SCD. All distances are in Å and angles are in degrees. See Figure 5.6 for definitions of O_A, O_B, and O_S.

Parameter	1	2	3	4
r(Fe–Fe)	6.91	6.72	6.79	7.32
r(Fe–O _A)	2.24	1.95	1.98	1.99
r(O _A –O _B)	1.23	1.30	1.28	1.24
θ(Fe–O _A –O _B)	127.1	126.1	118.9	129.6
r(O _A –H _{9R})	2.78	3.19	3.52	3.50
r(O _B –H _{9R})	3.64	2.37	3.39	2.99
r(Fe–O _S)	--	2.17	--	2.13
r(O _S –O _B)	--	2.65	--	2.41

The determination of a likely O₂ binding site is a necessary prerequisite for proposal of a reasonable catalytic mechanism for SCD. Evaluation of models **1-4** leads us to conclude that model **2** provides the best description of the O₂-bound SCD intermediate. Because formation of Fe^V species is extremely unlikely given the neutral His coordination environments provided by the enzyme, we expect that the two metal ions must work in concert to accomplish substrate oxidation. However, the combination of long Fe–Fe distances and the absence of a solvent ligand in models **1** and **3** seems to preclude any meaningful interaction between Fe_B and Fe_W. Models **2** and **4**, however, allow for a hydrogen-bonding interaction between the O₂-derived ligand on one Fe ion and the solvent ligand on the other, with the close contact between the two ligands shown by O_S–O_B distances of under 3 Å. (See Figure 5.6 for definitions of O_A, O_B, and O_S. Furthermore, as O_B is significantly closer to H_{9R} in model **2** than in model **4**, and the abstraction of H_{9R} is known to be rate-limiting, we consider model **2** superior and use it to propose the mechanism in Scheme 5.3.

Scheme 5.3. Proposed SCD mechanism.

5.3.3. SCD Mechanistic Intermediates. A possible enzymatic reaction mechanism for SCD based on this model is presented in Scheme 5.3. The diferrous, substrate-bound state, designated as **A**, corresponds to the Fe^{II}_2 -bound models investigated in Section 5.3.1, but with the Fe_W -bound solvent modeled as a hydroxide ligand. The addition of O_2 and H_2O ligands to Fe_W and Fe_B , respectively, leads to the formation of intermediate **B**. Aside from the deprotonation of the solvent ligand on Fe_W , this species is identical to **2** and is described as an $\text{Fe}_\text{B}^{\text{II}}(\text{OH}_2)/\text{Fe}_\text{W}^{\text{III}}(\text{O}_2^{\bullet-})$ species on account of the $\text{O}_\text{A}-\text{O}_\text{B}$ bond length of 1.30 Å, typical for a superoxo ligand. This intermediate may perform a HAA on the substrate to form an $\text{Fe}_\text{B}^{\text{II}}(\text{OH}_2)/\text{Fe}_\text{W}^{\text{III}}(\text{O}_2\text{H}^-)$ intermediate (**C**), after which we propose O–O cleavage occurs concomitant with proton-coupled electron transfer from the $\text{Fe}_\text{B}^{\text{II}}(\text{OH}_2)$ site to form an $\text{Fe}_\text{B}^{\text{III}}(\text{OH}^-)/\text{Fe}_\text{W}^{\text{IV}}(\text{O}^{2-})$ species (**D**). This intermediate then abstracts a second hydrogen atom from the substrate to make the final product. This second HAA may be accomplished by either the $\text{Fe}_\text{W}^{\text{IV}}(\text{O}^{2-})$ site to directly form the diferric species **F**. However, if $\text{H}_{10\text{R}}$ is significantly closer to Fe_B , HAA may be carried out by the $\text{Fe}_\text{B}^{\text{III}}(\text{OH}^-)$ site to form an $\text{Fe}_\text{B}^{\text{II}}(\text{OH}_2)/\text{Fe}_\text{W}^{\text{IV}}(\text{O}^{2-})$ mixed-valent intermediate **E**, which could readily form **F** via PCET. The computed energies (relative to **B**) of all of the species in Scheme 5.3 are presented in Figure 5.7, and the QM/MM-optimized active-site geometries of **C-F** are shown in Appendix 5, Figures A.5.1 –A.5.5.

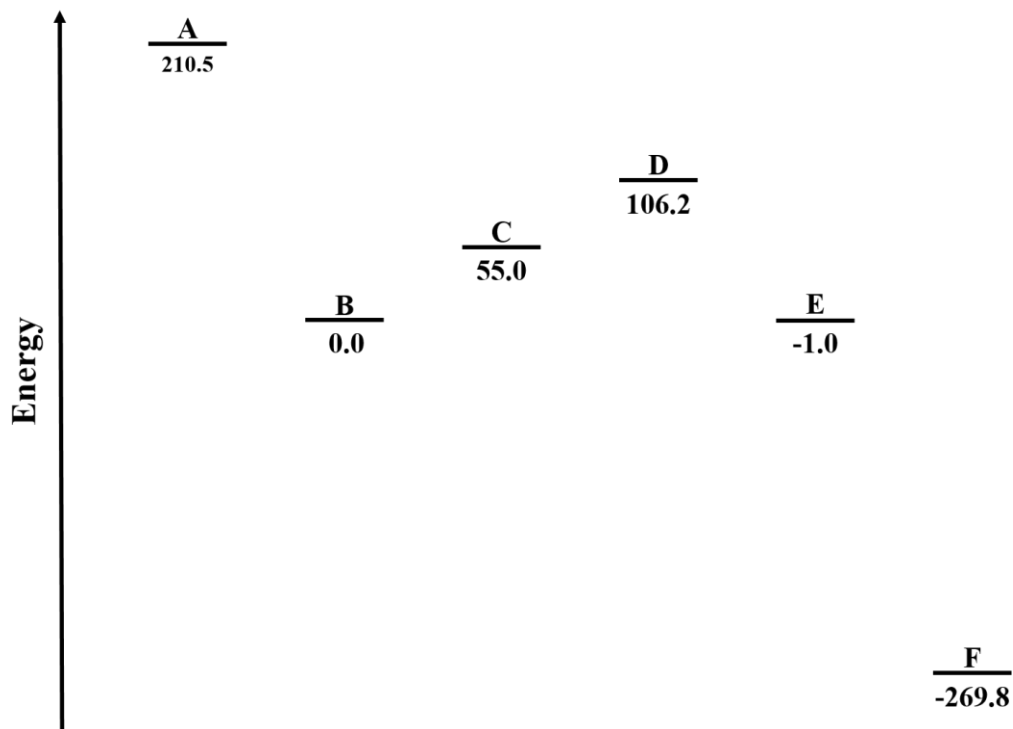


Figure 5.7. Computed QM energies (kJ/mol) of putative reaction intermediates in the proposed SCD mechanism, relative to state **B**.

5.4 Discussion

5.4.1. Metal substitution in the SCD active site. Both crystal structures of SCD reported to date were solved with Zn rather than Fe incorporated in the enzyme active site.^{22, 23} The QM/MM-optimized structures presented in Section 5.3.1 reinforce the compelling argument of Bai et al. that the presence of a non-native metal does not substantially distort the active-site architecture. Nevertheless, B3LYP and M-06L predict, on average, a decrease in the M–M distance and a moderate increase of the M–N_{His} bond lengths upon iron substitution of zinc, as well as a shorter Fe_W–OH₂ bond. Another, more substantial change involves the position of the substrate, as a rotation around the C₉–C₁₀ bond causes H_{10R} to point more directly toward the cavity between the two metal ions in the Fe₂^{II}-bound structure. This is likely a secondary effect of the shorter Fe–Fe distance. In the Zn₂-bound structure (Figure 5.5), C₁₁ is not substantially further from the open

Fe_B and Fe_W coordination sites than C_9 and C_{10} . However, the movement of Fe_B and its His ligands (specifically His121 and His153) reduces the amount of space available for the substrate, and pushes C_{11} away from the metal ions. The positions assumed by $\text{H}_{9\text{R}}$ and $\text{H}_{10\text{R}}$ after this rotation suggests that these atoms are now properly oriented for abstraction.

5.4.2. Evaluation of proposed mechanism. In the absence of detailed kinetic and/or spectroscopic data regarding reaction intermediates, and given the limitations of the computational methods used in this chapter (described below), we cannot conclusively demonstrate that the mechanism presented in Scheme 5.3 is the one by which SCD functions. However, even in the absence of transition state geometries and free energy barriers for each step, we can examine whether or not the proposed intermediates are energetically accessible. To that end, we note that the binding of water and O_2 to form **B** is energetically favorable, as would be expected. The subsequent formation of **C** and **D** by abstraction of $\text{H}_{9\text{R}}$ of the substrate and PCET from the $\text{Fe}_\text{B}^\text{II}(\text{OH}_2)$ moiety are both endothermic by about ~50-55 kJ/mol. Although the energetic costs of these steps are steep, they do not preclude consistency with the experimental activation energy of ~80 kJ/mol.⁴¹ By comparison, the HAA step of cytosolic $\Delta 9\text{Ds}$, for which a free energy barrier of ~60 kJ/mol has been determined experimentally,⁴³ was computed to have reaction and activation energies of 8 kJ/mol and 90 kJ/mol, respectively, with B3LYP.²¹ Interestingly, it is also possible to consider reversing the order of the HAA and PCET steps. This alternative mechanism would create an $\text{Fe}_\text{B}(\text{III})(\text{OH}^-)/\text{Fe}_\text{W}(\text{III})(\text{O}_2\text{H}^-)$ intermediate (**C***), which may then abstract $\text{H}_{9\text{R}}$ of the substrate. The formation of **D** from **C*** would more closely parallel the HAA proposed for the cytosolic $\Delta 9\text{Ds}$ and merits further investigation. However, as of the time of this writing, a model for **C*** has not yet been optimized.

A previous computational study of the cytosolic $\Delta 9$ Ds also revealed the importance of applying multiple functionals to reaction mechanisms of NHFe_2 enzymes to see where they agree and/or disagree.²¹ When nine functionals – including generalized gradient approximation (GGA), meta-GGA, and hybrid functionals – were used to investigate several different putative reaction pathways, they demonstrated a high degree of quantitative and qualitative disagreement. The authors overcame this difficulty by using complete active space 2nd-order perturbation theory as a benchmark by which the different DFT methods were judged. Such an intricate method may not be necessary for evaluating possible SCD mechanisms because of the expected lack of electronic coupling between its two metal centers. However, the results of that study still serve as a cautionary tale for the use of only one functional in the computational analysis of such a complicated system.

The research summarized in this chapter should also be extended to computations of the transition state energies and structures in the putative reaction mechanism, as well as the free energy barrier of each step to generate a reaction profile. Activation energies are paramount to any claim that our proposed mechanism is supported by experimental data, and can also be used to answer important mechanistic questions. For example, from Figure 5.7 it is clear that the formation of either **E** or **F** from **D** is thermodynamically favorable. However, it is the energetic barrier to each reaction step that will ultimately determine which pathway is actually used by SCD. The distance between the Fe_W -bound oxo ligand and $\text{H}_{10\text{R}}$ in the optimized geometry of **D** is over 1.3 Å longer than that between the Fe_B -bound hydroxide and $\text{H}_{10\text{R}}$. Thus, HAA of $\text{H}_{10\text{R}}$ by the Fe_B -bound hydroxide to form **E** may occur due to a low kinetic barrier even though **F** is thermodynamically favored.

The spin state of the SCD NHFe_2 active site also warrants further computational investigation. The computations reported here were performed assuming ferromagnetic coupling between high-spin Fe ions, an assumption that seems justified on the basis of the weak-field histidine ligands and the long Fe–Fe distance. However, both high-spin⁴⁴ and low-spin⁴⁵ biomimetic mononuclear Fe(III)-hydroperoxo complexes with first coordination spheres similar to those in SCD have recently been shown to abstract hydrogen atoms from organic substrates. Thus, while the computations performed provide valuable qualitative insights, it will be necessary to perform parallel analyses of different active-site spin states for a quantitative evaluation of the SCD mechanism.

5.4.3. Roles of conserved active-site residues. Extensive studies of NHFe_2 enzymes, such as soluble methane monooxygenase,⁴⁶ ribonucleotide reductase,⁴⁷ and even the cytosolic $\Delta 9$ Ds^{17, 19-21} that are isofunctional with SCD have uniformly led to the proposal that O_2 is activated by binding as a bridging ligand to the bimetallic active site. The unusually long Fe–Fe distance in SCD, which precludes such an O_2 binding mode, requires the proposal of a unique mechanism for O_2 activation. While both cytosolic and membrane-bound $\Delta 9$ Ds are now proposed to achieve O–O bond cleavage through the transfer of a hydrogen atom to a hydroperoxo intermediate, the distinct ways by which they accomplish this step reflect the differences between their active-site structures.

By binding O_2 as a bridging ligand, cytosolic $\Delta 9$ Ds are able to reduce it to a peroxo ligand by transferring one electron from each of the two Fe^{II} centers. Thus, a simple proton transfer to the peroxo ligand is required to reach the reactive hydroperoxo species. By contrast, when SCD binds O_2 , the resulting superoxo ligand needs activation by a hydrogen atom from either the $\text{Fe}_\text{B}^{\text{II}}(\text{OH}_2)$ site or substrate to form the hydroperoxo species **C** or **C***. In keeping with this

distinction, cytosolic $\Delta 9$ Ds possess an active site with numerous potential proton donors, while the active site of membrane-bound SCD is relatively hydrophobic, consistent with its close proximity to the enzyme's transmembrane helices and the cell membrane surface.²² Although the requirement for protons to complete the catalytic cycle after product dissociation suggests that they are not entirely excluded from the SCD active site, it is possible that the difference in $\Delta 9$ D mechanisms is related to the different cellular environments of these enzymes.

In order to accomplish a PCET involving ligands bound to both Fe_B and Fe_W , the enzyme must maintain strict control over the intermetallic distance during turnover. When constrained to the distances observed in our computational models, the Fe_B - and Fe_W -bound ligands are at an ideal distance to interact with each other. Yet if the metal ions approach distances of less than 4 Å, O_2 may bind in a μ -1,2 fashion, similar to what is seen in the cytosolic $\Delta 9$ Ds. This species, which apparently requires proton activation of a coordinating glutamate residue, would instead be a dead end in SCD, given its exclusive use of His ligands. However, an increase in the Fe–Fe distance to lengths greater than those observed in our computational models would diminish the likelihood of PCET between the two metal sites. Thus, the validity of the proposed mechanism depends on the ability of SCD to exert this control over the Fe–Fe distance.

Such control may hint at the reason for the strict conservation of the three His boxes of membrane-bound desaturases. These His boxes impose two sets of constraints on the SCD active-site (shown in Figure 5.8 for state **A**). First, the alternating coordination between Fe_B and Fe_W shown by the second (pink) and third (teal) His boxes places a limit on how closely the Fe ions may approach each other. This is best demonstrated by the binding of consecutive side chains to different metal ions, a motif observed twice (His156/His157 and His297/His298) in the SCD active site. Any hypothetical rearrangement of the active site that brings the two Fe ions to within less

than ~ 5 Å of each other would result in significant strain on the geometry of the adjacent His residues. Second, the conserved residues within the His boxes (e.g., Arg117, Arg154, and Asn295) point away from the active site and form strong hydrogen bonding or ionic contacts with other parts of the protein. Thus, these residues serve as anchors for the His boxes, preventing any significant movement of Fe_B relative to Fe_W during turnover. By constraining the variations in the Fe–Fe distance to within 2–3 Å, these residues ensure that any Fe_B -bound solvent ligand will always be in close proximity to Fe_W -bound O_2 . It is also possible that by exerting this control over the relative positioning of the Fe_B and Fe_W ligands, SCD minimizes entropic costs associated with the free energy barrier to PCET and O–O bond homolysis and suppresses undesired side reactions.

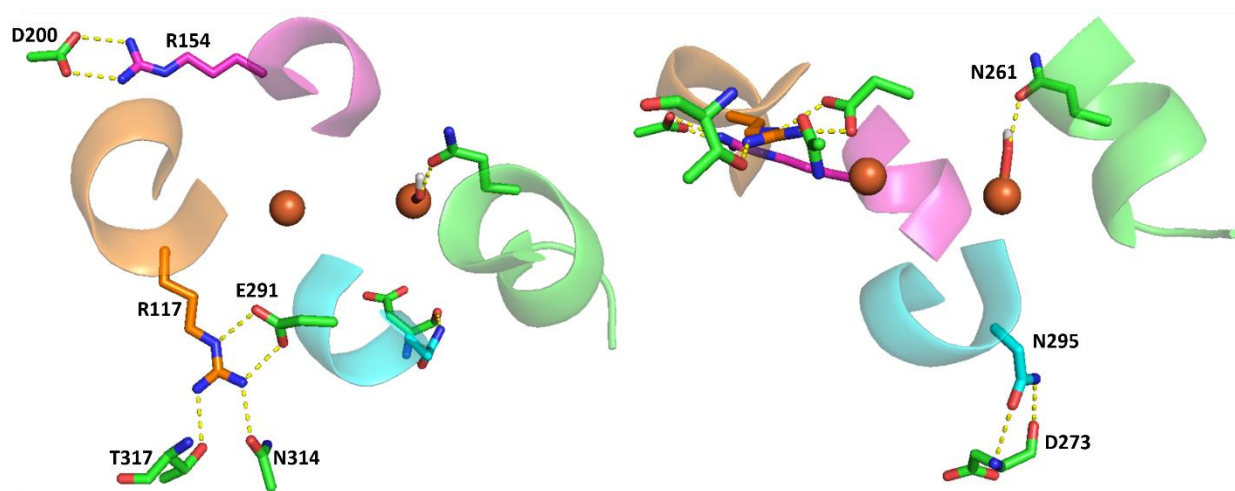


Figure 5.8. Cartoon of QM/MM-optimized SCD active site in state **A** viewed from the top (left) and the side (right). The four cartoon segments represent the three conserved His boxes and the conserved sequences containing H265, and include residues 116–121 (orange), 153–157 (pink), 259–267 (green), and 294–298 (teal). Hydrogen-bonding contacts between conserved non-histidine residues in these sequences and other SCD residues or Fe_W -bound solvent are shown as yellow dashes. Substrate and coordinating His residues are omitted for clarity.

5.5 Conclusion

We have presented a preliminary computational analysis of SCD, a membrane-bound fatty acid desaturase with an active-site architecture unique among NHFe_2 enzymes. Our research suggests that the SCD active site can accommodate incorporation of Zn or Fe without significant deformation. Study of four putative O_2 binding modes led to the conclusion that O_2 likely binds to Fe_W as a superoxo ligand, and that an additional solvent ligand binds to Fe_B . The resulting intermediate was used to propose a reaction mechanism in which the $\text{Fe}_\text{W}^{\text{III}}(\text{O}_2^{\bullet-})$ site first abstracts a hydrogen atom from the substrate and then engages in PCET with the $\text{Fe}_\text{B}^{\text{II}}(\text{OH}_2)$ site. These putative reaction steps lead to O–O bond cleavage without the need for coordination of O_2 as a bridging ligand. The PCET event, which has not been proposed in the isofunctional cytosolic $\Delta 9$ Ds, requires the unusually long Fe–Fe distance adopted in the SCD active site. Maintenance of this distance may be the role of some conserved active-site residues.

5.6 References

1. Powell, W. S.; Rokach, J., *Biochimica Et Biophysica Acta-Molecular and Cell Biology of Lipids* **2015**, 1851, 340-355.
2. Milne, G. L.; Dai, Q.; Roberts, L. J., *Biochimica Et Biophysica Acta-Molecular and Cell Biology of Lipids* **2015**, 1851, 433-445.
3. Arish, M.; Husein, A.; Kashif, M.; Sandhu, P.; Hasnain, S. E.; Akhter, Y.; Rub, A., *Biochimie* **2015**, 113C, 111-124.
4. Galano, J. M.; Lee, J. C. Y.; Gladine, C.; Comte, B.; Le Guennec, J. Y.; Oger, C.; Durand, T., *Biochimica Et Biophysica Acta-Molecular and Cell Biology of Lipids* **2015**, 1851, 446-455.
5. Buist, P. H., *Natural Product Reports* **2004**, 21, 249-262.
6. Tootle, T. L., *International Journal of Biochemistry & Cell Biology* **2013**, 45, 1629-1632.
7. Paton, C. M.; Ntambi, J. M., *American Journal of Physiology-Endocrinology and Metabolism* **2009**, 297, E28-E37.
8. Sperling, P.; Ternes, P.; Zank, T. K.; Heinz, E., *Prostaglandins Leukotrienes and Essential Fatty Acids* **2003**, 68, 73-95.
9. Fekete, K.; Gyorei, E.; Lohner, S.; Verduci, E.; Agostoni, C.; Decsi, T., *Obesity Reviews* **2015**, 16, 488-497.

10. Ntambi, J. M.; Miyazaki, M.; Stoeck, J. P.; Lan, H.; Kendziorowski, C. M.; Yandell, B. S.; Song, Y.; Cohen, P.; Friedman, J. M.; Attie, A. D., *Proceedings of the National Academy of Sciences of the United States of America* **2002**, *99*, 11482-11486.
11. Gutierrez-Juarez, R.; Pocai, A.; Mulas, C.; Ono, H.; Bhanot, S.; Monia, B. P.; Rossetti, L., *Journal of Clinical Investigation* **2006**, *116*, 1686-1695.
12. Zhang, Z.; Dales, N. A.; Winther, M. D., *Journal of Medicinal Chemistry* **2014**, *57*, 5039-5056.
13. Sakuradani, E.; Shimizu, S., *Journal of Biotechnology* **2009**, *144*, 31-36.
14. Armenta, R. E.; Valentine, M. C., *Journal of the American Oil Chemists Society* **2013**, *90*, 167-182.
15. Pfleger, B. F.; Gossing, M.; Nielsen, J., *Metabolic Engineering* **2015**, *29*, 1-11.
16. Buist, P. H., *Natural Product Reports* **2007**, *24*, 1110-1127.
17. Lindqvist, Y.; Huang, W. J.; Schneider, G.; Shanklin, J., *Embo Journal* **1996**, *15*, 4081-4092.
18. Fox, B. G.; Shanklin, J.; Ai, J. Y.; Loehr, T. M.; Sandersloehr, J., *Biochemistry* **1994**, *33*, 12776-12786.
19. Yang, Y. S.; Broadwater, J. A.; Pulver, S. C.; Fox, B. G.; Solomon, E. I., *Journal of the American Chemical Society* **1999**, *121*, 2770-2783.
20. Srnc, M.; Rokob, T. A.; Schwartz, J. K.; Kwak, Y.; Rulisek, L.; Solomon, E. I., *Inorganic Chemistry* **2012**, *51*, 2806-2820.
21. Chalupsky, J.; Rokob, T. A.; Kurashige, Y.; Yanai, T.; Soomon, E. I.; Rulisek, L.; Srnc, M., *Journal of the American Chemical Society* **2014**, *136*, 15977-15991.
22. Bai, Y.; McCoy, J. G.; Levin, E. J.; Sobrado, P.; Rajashankar, K. R.; Fox, B. G.; Zhou, M., *Nature* **2015**.
23. Wang, H.; Klein, M. G.; Lane, W.; Snell, G.; Levin, I.; Li, K.; Sang, B.-C., *To Be Published* **2015**.
24. Shanklin, J.; Whittle, E.; Fox, B. G., *Biochemistry* **1994**, *33*, 12787-12794.
25. Hashimoto, K.; Yoshizawa, A. C.; Okuda, S.; Kuma, K.; Goto, S.; Kanehisa, M., *Journal of Lipid Research* **2008**, *49*, 183-191.
26. Ray, K.; Pfaff, F. F.; Wang, B.; Nam, W., *Journal of the American Chemical Society* **2014**, *136*, 13942-13958.
27. Dolinsky, T. J.; Nielsen, J. E.; McCammon, J. A.; Baker, N. A., *Nucleic Acids Research* **2004**, *32*, W665-W667.
28. Word, J. M.; Lovell, S. C.; Richardson, J. S.; Richardson, D. C., *Journal of Molecular Biology* **1999**, *285*, 1735-1747.
29. Gaussian 09; Revision D.01; Frisch, M. J.; Trucks, G. W.; Schlegel, H. B.; Scuseria, G. E.; Robb, M. A.; Cheeseman, J. R.; Scalmani, G.; Barone, V.; Mennucci, B.; Petersson, G. A.; Nakatsuji, H.; Caricato, M.; Li, X.; Hratchian, H. P.; Izmaylov, A. F.; Bloino, J.; Zheng, G.; Sonnenberg, J. L.; Hada, M.; Ehara, M.; Toyota, K.; Fukuda, R.; Hasegawa, J.; Ishida, M.; Nakajima, T.; Honda, Y.; Kitao, O.; Nakai, H.; Vreven, J. A.; Montgomery, J., A.; Peralta, J. E.; Ogliaro, F.; Bearpark, M.; Heyd, J. J.; Brothers, E.; Kudin, K. N.; Staroverov, V. N.; Kobayashi, R.; Normand, J.; Raghavachari, K.; Rendell, A.; Burant, J. C.; Iyengar, S. S.; Tomasi, J.; Cossi, M.; Rega, N.; Millam, J. M.; Klene, M.; Knox, J. E.; Cross, J. B.; Bakken, V.; Adamo, C.; Jaramillo, J.; Gomperts, R.; Stratmann, R. E.; Yazyev, O.; Austin, A. J.; Cammi, R.; Pomelli, C.; Ochterski, J. W.; Martin, R. L.; Morokuma, K.; Zakrzewski, V. G.; Voth, G. A.; Salvador, P.;

- Danneberg, J. J.; Dapprich, S.; Daniels, A. D.; Farkas, O.; Foresman, J. B.; Ortiz, J. V.; Cioslowski, J.; Fox, D. G. Gaussian Inc.: Wallingford, CT, 2009.
30. Cornell, W. D.; Cieplak, P.; Bayly, C. I.; Gould, I. R.; Merz, K. M.; Ferguson, D. M.; Spellmeyer, D. C.; Fox, T.; Caldwell, J. W.; Kollman, P. A., *Journal of the American Chemical Society* **1995**, *117*, 5179-5197.
 31. Rappe, A. K.; Goddard, W. A., *Journal of Physical Chemistry* **1991**, *95*, 3358-3363.
 32. Chung, L. W.; Sameera, W. M. C.; Ramozzi, R.; Page, A. J.; Hatanaka, M.; Petrova, G. P.; Harris, T. V.; Li, X.; Ke, Z.; Liu, F.; Li, H.-B.; Ding, L.; Morokuma, K., *Chemical Reviews* **2015**.
 33. Becke, A. D., *Physical Review A* **1988**, *38*, 3098-3100.
 34. Perdew, J. P., *Physical Review B* **1986**, *33*, 8822-8824.
 35. Becke, A. D., *Journal of Chemical Physics* **1993**, *98*, 1372-1377.
 36. Lee, C. T.; Yang, W. T.; Parr, R. G., *Physical Review B* **1988**, *37*, 785-789.
 37. Zhao, Y.; Truhlar, D. G., *Journal of Chemical Physics* **2006**, *125*, 18.
 38. Schafer, A.; Huber, C.; Ahlrichs, R., *Journal of Chemical Physics* **1994**, *100*, 5829-5835.
 39. Schafer, A.; Horn, H.; Ahlrichs, R., *Journal of Chemical Physics* **1992**, *97*, 2571-2577.
 40. Vreven, T.; Byun, K. S.; Komaromi, I.; Dapprich, S.; Montgomery, J. A.; Morokuma, K.; Frisch, M. J., *Journal of Chemical Theory and Computation* **2006**, *2*, 815-826.
 41. Enoch, H. G.; Catala, A.; Strittmatter, P., *Journal of Biological Chemistry* **1976**, *251*, 5095-5103.
 42. Behrouzian, B.; Fauconnot, L.; Daligault, F.; Nugier-Chauvin, C.; Patin, H.; Buist, P. H., *European Journal of Biochemistry* **2001**, *268*, 3545-3549.
 43. Lyle, K. S.; Haas, J. A.; Fox, B. G., *Biochemistry* **2003**, *42*, 5857-5866.
 44. Cho, J.; Jeon, S.; Wilson, S. A.; Liu, L. V.; Kang, E. A.; Braymer, J. J.; Lim, M. H.; Hedman, B.; Hodgson, K. O.; Valentine, J. S.; Solomon, E. I.; Nam, W., *Nature* **2011**, *478*, 502-505.
 45. Liu, L. V.; Hong, S.; Cho, J.; Nam, W.; Solomon, E. I., *Journal of the American Chemical Society* **2013**, *135*, 3286-3299.
 46. Shu, L. J.; Nesheim, J. C.; Kauffmann, K.; Munck, E.; Lipscomb, J. D.; Que, L., *Science* **1997**, *275*, 515-518.
 47. Sturgeon, B. E.; Burdi, D.; Chen, S. X.; Huynh, B. H.; Edmondson, D. E.; Stubbe, J.; Hoffman, B. M., *Journal of the American Chemical Society* **1996**, *118*, 7551-7557.

CHAPTER 6

*Development and Implementation of an Interactive
Program for Setup and Analysis of Computations on
Large Biomolecules*

6.1 Introduction

Over the past several decades, the fields of theoretical and computational chemistry have evolved at an accelerated pace, driven by the increasing availability of incredible amounts of computational power. Such resources have led to the development of a broad array of new methods for solving many diverse problems of interest to the chemistry community. The rapid growth of this field occurred alongside rising institutional trends toward interdisciplinary research in academia, a phenomenon which has helped many experimental chemists become aware of theoretical tools and the insight they can provide. In addition to encouraging many fruitful collaborative partnerships, this philosophical shift also encouraged an increasing number of experimentalists to employ computational chemistry tools in order to supplement and/or analyze data that on their own may appear complicated, confusing, or contradictory. Indeed, a cursory inspection reveals that in the last five years, around two-thirds of the chemistry faculty at the University of Wisconsin-Madison (excluding those in the Theoretical Chemical Institute) are co-authors of papers that make use of computational methods.¹⁻²⁰

Implementation of advanced theoretical techniques to study complicated systems, however, is not a trivial process. One major problem is that the most accurate *ab initio* methods do not scale efficiently with increasing system size; for example, the CCSD(T) “gold standard” scales as N^7 ,²¹ where N is the number of basis functions. This makes such methods prohibitively slow for many systems of chemical interest. These systems require the use of more approximate methods such as density functional theory or semi-empirical methods, which scale as N^3 or even less.^{22, 23} Thus, the scientific community’s ability to perform computations in many instances comes with the price of using less accurate methods, with less confidence in the results. As such, there is a vital need for scientists to integrate experiment and theory. Experiments provide the

data necessary for validating the use of a given theory, while that theory provides atomic-level insight inaccessible to most experiments.

Despite the complementary nature of theory and experiment, the difficulty of using most computational chemistry packages serves as a barrier to those who wish to begin performing computations of their own. These programs, which often come with long, jargon-filled instruction manuals, require users to create and analyze text-based input and output files, or use of an accessory graphical interface such as WebMO²⁴ or GaussView.²⁵ These skills must be acquired in addition to the technical knowledge necessary for building, maintaining, and troubleshooting the associated computational infrastructure. Thus, even as resources have become more broadly available, there is still a steep learning curve for their use.

The previous five chapters of this thesis described in detail a combined spectroscopic/computational investigation of several bioinorganic systems. Two theoretical methods in particular were essential to the successful completion of these studies: (1) quantum mechanical/molecular mechanical (QM/MM) geometry optimizations;²⁶ and (2) time-dependent density functional theory (TD-DFT),²⁷ used to compute electronic absorption spectra. When performed on systems of this size, both types of computations pose unique challenges for input construction and output analysis. An additional complication presented by this work was the use of two different computational chemistry packages: the Gaussian09²⁸ implementation of the ONIOM algorithm^{29,30} for the QM/MM jobs and Orca 2.9/3.0³¹ for the TD-DFT jobs. Despite the fact that similar computations had been performed within the Brunold group for several years, it became apparent early in my research that the difficulty of performing these analyses, and the time required to do so, could potentially limit the scope and efficiency of my research. Moreover, there are a number of pitfalls that await the inexperienced theorist who does not know the correct

questions to consider, be they large (“What density functional or force field is appropriate?”) or small (“How should histidine side chains be protonated?”). Although helpful considerations of these questions are available in recent reviews,^{30, 32} the process of actually making the decision and implementing subsequent changes in the input file is still daunting.

With this in mind, I have written a short Python program called “bulb,” which assists in the setup and analysis of the types of computational analyses commonly used in the Brunold lab at UW-Madison. The primary use of bulb is to assist users in the preparation of input files for QM/MM geometry optimizations in Gaussian09, starting with the crystallographic coordinates from a PDB (“Protein Data Bank”) or PQR file.³³ To do this, users work interactively with bulb, responding to its questions instead of supplying a list of keywords, a feature that distinguishes bulb from other programs available for QM/MM setup.³⁴ Add-ons to the original code now also allow for the quick setup of TD-DFT jobs in Orca 2.0/3.0 that use the optimized QM/MM geometries from Gaussian09 log files. Bulb can also be used to analyze the TD-DFT output, make small adjustments to the protonation of several amino acids, rotate and translate coordinates, create PDB/PQR files with optimized coordinates, and perform other small tasks.

In addition to the work presented in this thesis and related publications, bulb has been used by the members of the Brunold group to help study a number of other proteins, including ATP:corrinoid adenosyltransferase, cysteine dioxygenase, Fe/Mn-containing superoxide dismutase, homoprotocatechuate dioxygenase, and calprotectin. Members of the Burstyn group at UW-Madison have also used bulb to investigate human cystathionine β -synthase, and Dr. Elizabeth Blaesi, now a post-doctoral researcher at Pennsylvania State University, is currently using bulb to study Class 1B ribonucleotide reductases and PhnZ, a dioxygenase with a diiron active site. In the coming years, I also plan to use bulb in undergraduate research projects at St.

Mary's University of Minnesota. However, more rigorous documentation of bulb is required in order to make it more accessible to a larger number of users. In the following sections, I will briefly describe bulb's architecture and provide a rationale for the manner in which it constructs input files.

6.2 Program Architecture

To interactively construct QM/MM input, bulb must accomplish three distinct tasks: it must collect structural information (i.e., Cartesian coordinates) from an external source, modify them according to the user's wishes, and construct a Gaussian09 input file with appropriate syntax and keywords. To a large extent, bulb accomplishes these tasks sequentially, as described in the following subsections. From a coding perspective, however, it is clear that many of the tasks bulb must accomplish are independent of the others. For example, the code that bulb requires to reorient a protein in Cartesian space is quite distinct from that which is needed to protonate a histidine (His) side chain. Thus, the nature of bulb's purpose inherently makes the program well-suited for modular programming. During normal program flow, bulb asks users a series of straightforward questions, the answers to which may cause bulb to call short sections of code ("functions") suitable for the task at hand. An example from the user's point of view is shown in Figure 1. The user's answer to the initial question about reading coordinates from an alternative file causes bulb to ask a few additional questions before calling a function whose sole purpose is to find Cartesian coordinates in a Gaussian log file. Had the user answered differently, bulb would skip the follow-up questions and that function would never have been called. The majority of bulb's code (~80%) is in these functions, which are only accessed when the user requests that function's specific task to be accomplished.

```

#####
#                                     #
#               DEFINING PROGRAM OPTIONS               #
#                                     #
#####

Would you like to read in coordinates from a file other than your PDB/PQR file? (y/n)
y

What type of file would you like to read coordinates from?
    1 Converged Gaussian geometry optimization
    2 Failed Gaussian geometry optimization
    3 XYZ file
1

Please provide the name of a Gaussian log file with coordinates to use.
n193a_qmmm.log

Would you like to explicitly include solvent molecules in your model? (y/n)
y

Please define a threshold distance (in A). All water molecules within this
distance of any atom in your QM region.
1000

#####
#                                     #
#               PROCESSING STRUCTURE               #
#                                     #
#####

WARNING: CHAIN B DOES NOT START AT RESIDUE 1.

*****

NOW READING IN GEOMETRY FROM GAUSSIAN OUTPUT FILE.
THIS MAY TAKE SOME TIME....

GEOMETRY SUCCESSFULLY READ.

*****

Would you like to print an XYZ file with this geometry? (y/n)
|

```

Figure 6.1. Screenshot of interactive bulb session demonstrating the use of alternative coordinates.

6.2.1 Structure Reading and Modification. The most challenging barrier to performing quantum chemical computations on biomolecules like proteins is the generation of a reasonable initial geometry. Fortunately for the theoretical community, over 100 000 solved crystal structures of large biomolecules have been deposited in the worldwide Protein Data Bank (wwPDB) since its establishment in 1971.³⁵ While these structures can occasionally be ambiguous and typically lack the resolution necessary to locate hydrogen atoms, they provide a crucially important starting

point for any QM/MM optimization. The wwPDB has also performed a useful service to the rest of the scientific community by standardizing the format in which these structures are reported in PDB files. The uniformity of these files makes it possible to construct short yet robust programs or scripts that can quickly read the geometry of any solved structure. Several programs that can add protons to a PDB file, a necessary first step for the construction of any QM/MM input with bulb, are freely available.^{36, 37}

Bulb begins its work by reading in a protonated structure from a PDB/PQR file specified in the command prompt and storing each atom's coordinates, atom type (e.g., C _{α}), residue type (e.g., His), residue number, and chain ID. For residues represented by multiple conformations in the crystal structure, bulb selects the "A" conformer and neglects the "B" conformer. All of this "atom-specific" information is then used to generate "residue-specific" arrays of data, such as the charge of each amino acid and its position in the protein's primary sequence. After reading in this information, bulb asks the user a series of questions designed to identify any necessary changes to the structure (Figure 6.1). This can be done in three main ways, two of which are trivial to implement. Users can read in the coordinates from an alternative source, such as an XYZ file or any step in a Gaussian09 log file of a successful or unsuccessful geometry optimization. Alternatively, users are given the option of reorienting their molecule in Cartesian space, which can be useful in analyzing the results of later calculations the user might wish to perform.

A less trivial modification is the addition or removal of protons from amino acid side chains. While histidine is the only amino acid with a pK_a implying variable protonation at a biological pH, other amino acid residues can be deprotonated in order to coordinate to metal ions or react with substrates and/or other amino acid side chains (e.g., to form disulfide bridges). While the simplicity of programs that add protons wholesale to proteins is advantageous in that the

programs are robust and efficient, it also limits their ability to recognize unusual situations. For example, the `pdb2pqr` program³⁶ used to add protons to a fatty acid desaturase in the work described in Chapter 5 of this thesis incorrectly protonates all nine His residues coordinated to the enzyme's Fe₂ active site. Thus, researchers – especially those concerned with bioinorganic systems – often need to make further adjustments to a number of amino acids.

To ensure that users are aware of and have considered these concerns, `bulb` uses the number of hydrogen atoms associated with each amino acid to calculate its charge. All anomalous charges are reported to the user, who is then asked whether any of these should be changed (Figure 6.2). Should the user desire to do so, he or she is then guided through a series of questions to identify first the amino acid to adjust and then the proton to add or remove (Figure 6.3). `Bulb` then proceeds to loop through the code until the user is satisfied with the structure. After giving the user an opportunity to reorient the final structure, `bulb` prints an updated PDB/PQR file and exits the structure modification section.

```
WARNING: Unusual charge found on MET1 on chain A. Charge is 1
WARNING: Unusual charge found on GLU179 on chain A. Charge is 0
WARNING: Unusual charge found on HIS317 on chain A. Charge is 1
WARNING: Unusual charge found on ASP348 on chain A. Charge is 0
WARNING: Unusual charge found on PHE453 on chain A. Charge is -1
WARNING: Unusual charge found on ALA44 on chain B. Charge is 1
WARNING: Unusual charge found on HIS62 on chain B. Charge is 1
WARNING: Unusual charge found on GLU210 on chain B. Charge is 0
WARNING: Unusual charge found on ARG295 on chain B. Charge is 0

Note that the first and last residues in a chain will often have unusual
charges because of the terminal N and O, respectively.

Would you like Bulb to print all residue charges to a .chg file? (Y/N)
n

Do you wish to change the protonation state of any of the residues? (y/n)
y
```

Figure 6.2. Screenshot of `bulb` showing the communication of unusually charged amino acids to the user and the option to adjust protonation state.

6.2.2 QM/MM Input File Construction. After the structure of the protein has been finalized, bulb asks the user a series of questions that will allow the program to construct an appropriate Gaussian09 input file. Users are first asked whether they are doing a 1-level or 2-level computation. A 1-level, all-MM optimization is often used to ensure a reasonable starting geometry for a subsequent 2-level, QM/MM job. Users who choose this option may then read in the coordinates from the finished MM job as well as a PQR file printed during their initial use of bulb to set up the QM/MM job. The user's choice of theory and basis set (if applicable) for these levels is also required. If the AMBER force field is used, bulb will automatically include the atom types and partial charges for each atom in the protein according to the definitions provided by Cornell et al.³⁸ For 2-level jobs, users are given the option of specifying amino acid side chains to include in the QM region. The charge and multiplicity of each region must also be provided by the user, although bulb does provide the total charge of all protein chains in the PDB/PQR file. Finally, the user is given the choice of freezing the coordinates of the protein or excluding solvent molecules further than user-selected threshold distances from non-solvent QM atoms. The final input file printed by bulb contains the minimum number of keywords required for submission to Gaussian09, as well as the coordinate block for all atoms chosen for inclusion by the user (Figure 6.4).

```

%chk=mod_pcetB2_int
%NProcShared=8
#P ONIOM(BP86/Gen:AMBER) Opt

COMMENT: First QM/MM job with E287A variant, starting from final MM geometry.

-11 1 1 1
O-O--0.5819   -1   14.750  -20.334   -5.893   L !   40A  GLU  1
N-N--0.5163   -1   12.702  -22.300   -6.437   L !   40A  GLU  2
C-CT-0.0397   -1   13.326  -21.471   -7.477   L !   40A  GLU  3
C-C-0.5366    -1   14.650  -20.842   -7.013   L !   40A  GLU  4
C-CT-0.056    -1   12.366  -20.346   -7.897   L !   40A  GLU  5
C-CT-0.0136   -1   11.193  -20.848   -8.749   L !   40A  GLU  6
C-C-0.8054    -1    9.934  -20.025   -8.472   L !   40A  GLU  7
O-O2--0.8188  -1    8.974  -20.600   -7.908   L !   40A  GLU  8

```

Figure 6.4. Screenshot of the first 15 lines of a QM/MM Gaussian09 input file generated by bulb, with no additional modifications. The first 7 lines of text include all user-specified job options. The coordinate block contains for each atom, from left to right: its element name, AMBER atom type, and partial charges; a “freeze-code” designating whether its coordinates should be frozen (-1) or optimized (0); its Cartesian coordinates; its placement in the QM (“H”) or MM (“L”) region; and a comment identifying its amino acid and indexed position in the input file.

6.2.3 TD-DFT Input Construction and Command-Line Shortcuts. Unlike the process of constructing the QM/MM input files, setup of subsequent properties calculations should require no major structural modifications. Thus, in building the TD-DFT input file, bulb does not run interactively. Instead, users call bulb with a “command-line shortcut,” which prompts it to circumvent normal program flow in order to call the functions necessary for producing a TD-DFT input file. Users provide both the location of the Gaussian09 log file that contains the optimized coordinates and the desired name for the TD-DFT input file, which bulb then produces automatically. This file is in principle ready for submission to Orca 2.9/3.0, but includes by default some keywords that are typically used by researchers in the Brunold group (Section 6.3.3) and may merit extensive modification. Other shortcuts can be used by researchers who would like bulb to perform one specific task without generating a new QM/MM or TD-DFT input file. These include the reorientation of coordinates, the printing of PDB/PQR files from the converged

coordinates from a QM/MM optimization, the identification of amino acid side chains in close proximity to the QM region, and much more.

6.3 Chemical Considerations

Computational chemistry cannot be practiced responsibly in a “black-box” manner. All would-be theorists need to carefully consider their choice of methodology in light of that methodology’s limitations regarding accuracy and efficiency. That said, in order for bulb to ease the process of input construction, the program does make some decisions on behalf of its users that they should be aware of. These decisions can be loosely grouped into two categories: those regarding protein modifications and those regarding the keywords placed into input files by bulb. Knowledge of how bulb divides QM and MM regions or identifies amino acids with unusual charges is necessary for the majority of users, who will have to make post-bulb adjustments to their Gaussian inputs to account for chemically unusual nuances of their systems.

6.3.1 Structural Modifications. The current version of bulb is designed to facilitate removal or addition of protons from the side chains of histidine, lysine, arginine, aspartic acid/aspartate, and glutamic acid/glutamate residues. To add a proton to an atom, bulb first identifies its coordinates and those of two nearby heavy atoms, and then places the proton in a predefined position relative to them. For example, when the user asks bulb to connect a proton to N_ϵ of a His side chain, the program finds the coordinates of N_ϵ , C_ϵ , and C_γ . It then calculates new coordinates for the proton such that the $H_\epsilon-N_\epsilon$ distance is 1.01 Å, the $H_\epsilon-N_\epsilon-C_\epsilon$ angle is 120°, and the $H_\epsilon-N_\epsilon-C_\delta-C_\gamma$ dihedral is 180°. This relatively straightforward computation can be easily adapted to work for other protons (or even heavy atoms) on other amino acids, so long as appropriate internal coordinates can be robustly defined. However, this procedure clearly does not consider the three-dimensional environment into which the proton is being placed. Because it

is quite possible that the new proton will be added unreasonably close to a solvent molecule, substrate, or the side chain of another residue, users may wish to perform a sanity check with molecular viewer software (such as PyMol³⁹) to ensure newly added protons are placed reasonably.

Before users are given the opportunity to add or remove protons to/from their PDB/PQR file, they are warned about any amino acids with unusual charges. These charges are calculated by comparing the number of hydrogen atoms present in the PDB/PQR file to the number needed for a neutral amino acid of that type. While typically trustworthy, this system will fail to recognize bonds between amino acid side chains, such as the fairly common disulfide bridge motif or the tyrosine-cysteine crosslink in cysteine dioxygenase.⁴⁰ Similarly, terminal amino acids typically have charges because of the free carboxylate (C-terminal) or amine (N-terminal) functional groups. Thus, when bulb reports charges as “unusual” to the user, it is best for the user to understand why the charge is unusual rather than to assume that each amino acid must be modified in some way.

Users should also be aware of how bulb divides the QM and MM regions in the Gaussian09 input file. The choice is made for each atom based on its label as either an “ATOM” or “HETATM” in the PDB/PQR file. The HETATM label signifies the atom is not part of the protein, and thus is likely part of a substrate, cofactor, or solvent molecule. Since such parts of the system are often of most interest to the user, bulb automatically places these atoms in the QM region. The ATOM label designates an atom as part of the protein, and bulb places such atoms in the MM region unless instructed otherwise by the user. The user has the choice of defining the QM region in the “Input Construction” section of bulb’s program flow, and can identify amino acid residues by their chain and residue number. Once identified, bulb automatically places the

side chain, starting at C β , in the QM region, while leaving atoms in the polypeptide backbone in the MM region. This causes a covalent bond to span the QM/MM boundary, which bulb communicates to Gaussian09 by making C α a link atom.

6.3.2 Post-bulb Modifications. The input files generated by bulb are rarely ready for immediate submission to Gaussian09, and often require some back-end modifications by the user. This is largely because of the presence of HETATM atoms in the PDB/PQR file. Since there are many compounds that could potentially be co-crystallized with proteins, bulb neglects everything but the coordinates of these atoms. Thus, it cannot calculate the charge of the QM region if any HETATM atoms carry a charge, nor can it provide the AMBER parameters or partial charges for these atoms, aside from H₂O molecules. Users need to consider their system carefully and determine whether these atoms belong in the QM or MM regions, what their MM parameters should be, and whether or not link atoms will be necessary. Sometimes, as in the case of adenosylcobalamin (Chapters 2-4), entire force fields may have to be appended onto those hardwired into Gaussian09 to model complex cofactors. Other changes, such as keywords that adjust Gaussian09's default settings, are often necessary as well.

6.3.3. TD-DFT Setup and Analysis. Despite the fact that the Brunold group traditionally performs QM/MM and TD-DFT computations in different programs, the fact that the latter are 1-level, "QM-only" jobs makes the construction and modification of their input files relatively simple. However, bulb contributes to their construction by automatically finding the converged coordinates from a Gaussian09 log file and transferring them to an Orca 2.9/3.0 input file. When doing so, it keeps the coordinates of atoms in the QM and MM regions separate, as only those for the QM region will be included in the TD-DFT input. Bulb also identifies all link atoms, and replaces them in the TD-DFT input with hydrogen atoms, using the same default scaled bond

lengths that Gaussian09's ONIOM method uses for computations on the QM region during the QM/MM optimization.²⁹ A separate point charge file containing the coordinates and AMBER partial charges of all non-link atoms in the MM region is also printed. These may be passed along to Orca 2.9/3.0, which can include them as a way of allowing the MM region of the system to polarize the computed wavefunction in the TD-DFT computation.

By default, the TD-DFT input file printed by bulb in this operation uses the same theory as the QM calculations in the QM/MM geometry optimization. The charge and multiplicity of the QM system is also read from the Gaussian09 log file and placed into the Orca input, and the multiplicity is also used to identify whether a restricted or unrestricted formalism should be requested. Like the Gaussian09 input files, these files typically require some post-bulb modifications, as the desired TD-DFT settings, such as the energy window to sample and number of roots to calculate, can vary from system to system.

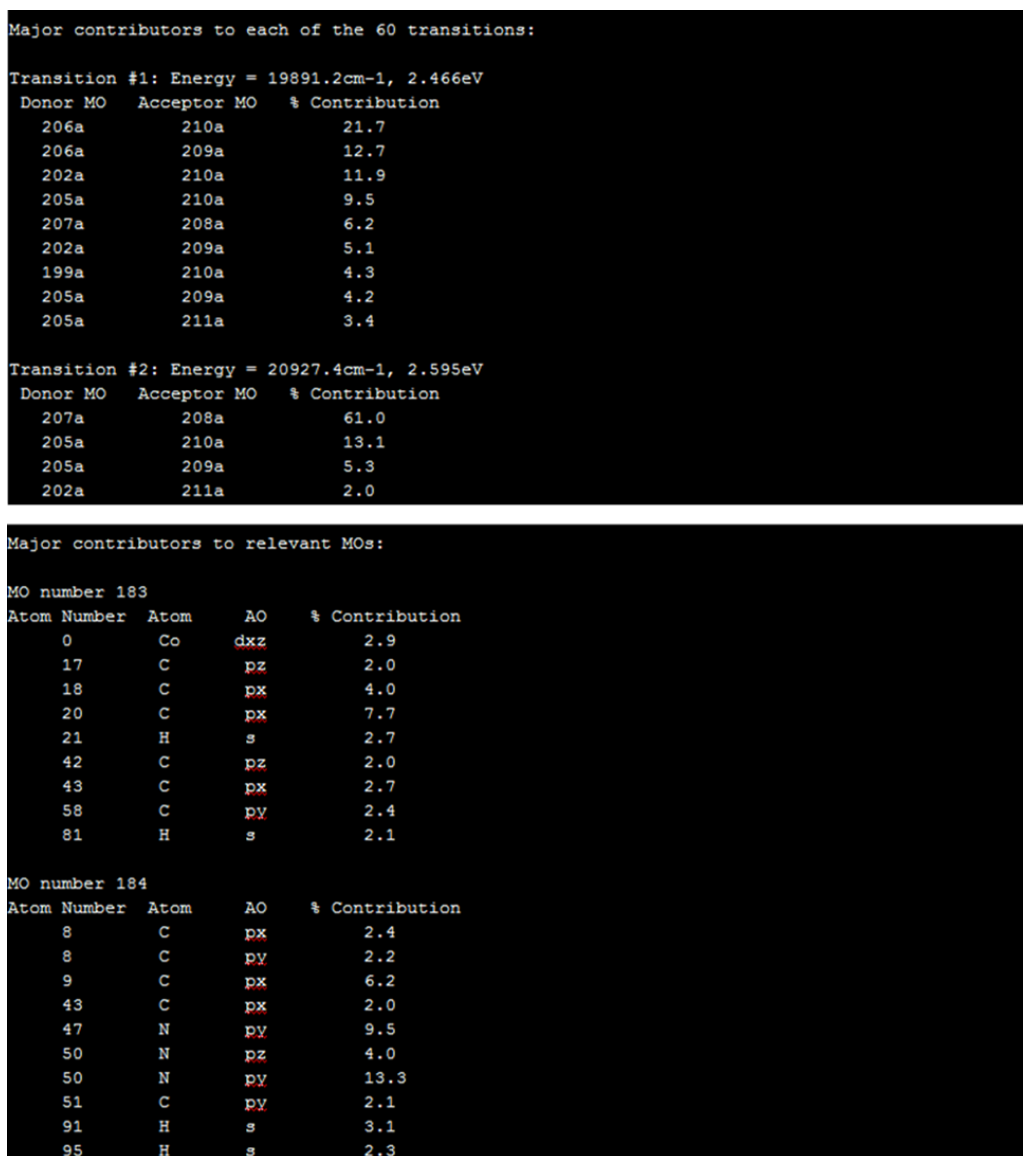


Figure 6.5. Screenshot of TD-DFT-computed transition compositions (top) and DFT-computed MO compositions (bottom), as extracted from an Orca 2.9/3.0 log file by bulb.

Finally, bulb also contributes to the analysis of the TD-DFT output file. In brief, the relevant information produced by a typical TD-DFT computation (i.e., those presented in the previous chapters of this thesis) includes the energies, intensities, and compositions of the lowest-energy predicted transitions. While the former two can be summarized graphically by either a stick spectrum or a curve calculated from assigning a width to each transition (see, for example, Figure 2.4), the compositions of the computed transitions are harder to describe. TD-DFT

transitions are linear combinations of one-electron excitations between occupied and virtual MOs of the computed ground-state wavefunction, which are themselves linear combinations of basis set functions representing individual atomic orbitals. For systems like cobalamin species, which have many MOs near the HOMO/LUMO gap, including some with mixed metal/ligand character, identifying the nature of individual computed transitions is not trivial. To make this task easier, *bulb* reads Orca TD-DFT log files and prints all one-electron excitations that contribute more than a user-defined amount (e.g., 5%) for each computed transition. It then finds the composition of each MO in this list and prints all atomic orbitals that contribute more than another user-defined amount to it. An example of *bulb*'s output file, which was used in the construction of Table 2.2, is shown in Figure 6.5.

6.4 Summary

In order to assist researchers in the setup and analysis of computations on large proteins, I have written a short Python program, *bulb*. *Bulb* assists users in constructing input files for QM/MM optimizations with the ONIOM module of Gaussian09. Specifically, it helps assess and modify the protonation of amino acid side chains, and automatically constructs the thousands of lines of text required for atomic coordinates, force field atom types, partial charges, and more. *Bulb* is also capable of using the optimized coordinates from a converged QM/MM optimization to construct an input file for an Orca 2.9/3.0 TD-DFT calculation, as well as providing a brief analysis of that calculation's output. Together, these functionalities have vastly improved the efficiency of computational research in the Brunold group, and have contributed to the quality and quantity of research presented in this thesis.

6.5 References

1. Cantu, P.; Andrew, T. L.; Menon, R., *Applied Physics Letters* **2013**, *103*, 4.
2. Brogden, D. W.; Christian, J. H.; Dalal, N. S.; Berry, J. F., *Inorganica Chimica Acta* **2015**, *424*, 241-247.
3. Preston, T. J.; Shaloski, M. A.; Crim, F. F., *Journal of Physical Chemistry A* **2013**, *117*, 2899-2907.
4. Hill, J. C.; Ping, Y.; Galli, G. A.; Choi, K. S., *Energy & Environmental Science* **2013**, *6*, 2440-2446.
5. Jennaro, T. S.; Beaty, M. R.; Kurt-Yilmaz, N.; Luskin, B. L.; Cavagnero, S., *Proteins-Structure Function and Bioinformatics* **2014**, *82*, 2318-2331.
6. Berns, V. M.; Engelkemier, J.; Guo, Y. M.; Kilduff, B. J.; Fredrickson, D. C., *Journal of Chemical Theory and Computation* **2014**, *10*, 3380-3392.
7. Lin, P. H.; Lyubimov, I.; Yu, L.; Ediger, M. D.; de Pablo, J. J., *Journal of Chemical Physics* **2014**, *140*.
8. Marsh, B. M.; Zhou, J.; Garand, E., *Physical Chemistry Chemical Physics* **2015**.
9. Mori, T.; Hamers, R. J.; Pedersen, J. A.; Cui, Q., *Journal of Physical Chemistry B* **2014**, *118*, 8210-8220.
10. Zhang, X. W.; Meng, F.; Christianson, J. R.; Arroyo-Torres, C.; Lukowski, M. A.; Liang, D.; Schmidt, J. R.; Jin, S., *Nano Letters* **2014**, *14*, 3047-3054.
11. Landis, C. R.; Weinhold, F., *Inorganic Chemistry* **2013**, *52*, 5154-5166.
12. Mondal, J.; Mahanthappa, M.; Yethiraj, A., *Journal of Physical Chemistry B* **2013**, *117*, 4254-4262.
13. Stanton, J. F.; Garand, E.; Kim, J.; Yacovitch, T. I.; Hock, C.; Case, A. S.; Miller, E. M.; Lu, Y. J.; Vogelhuber, K. M.; Wren, S. W.; Ichino, T.; Maier, J. P.; McMahon, R. J.; Osborn, D. L.; Neumark, D. M.; Lineberger, W. C., *Journal of Chemical Physics* **2012**, *136*.
14. Wiens, J. P.; Nathanson, G. M.; Alexander, W. A.; Minton, T. K.; Lakshmi, S.; Schatz, G. C., *Journal of the American Chemical Society* **2014**, *136*, 3065-3074.
15. Newberry, R. W.; Raines, R. T., *Acs Chemical Biology* **2014**, *9*, 880-883.
16. Ma, L.; Pegram, L.; Record, M. T.; Cui, Q., *Biochemistry* **2010**, *49*, 1954-1962.
17. Ryland, B. L.; McCann, S. D.; Brunold, T. C.; Stahl, S. S., *Journal of the American Chemical Society* **2014**, *136*, 12166-12173.
18. Mondal, J.; Bratton, B. P.; Li, Y. J.; Yethiraj, A.; Weisshaar, J. C., *Biophysical Journal* **2011**, *100*, 2605-2613.
19. Boyle, E. S.; Neff-Mallon, N. A.; Handali, J. D.; Wright, J. C., *Journal of Physical Chemistry A* **2014**, *118*, 3112-3119.
20. Buchanan, L. E.; Carr, J. K.; Fluit, A. M.; Hoganson, A. J.; Moran, S. D.; de Pablo, J. J.; Skinner, J. L.; Zanni, M. T., *Proceedings of the National Academy of Sciences of the United States of America* **2014**, *111*, 5796-5801.
21. Pople, J. A.; Headgordon, M.; Raghavachari, K., *Journal of Chemical Physics* **1987**, *87*, 5968-5975.
22. Thiel, W., *Wiley Interdisciplinary Reviews-Computational Molecular Science* **2014**, *4*, 145-157.
23. Hohenberg, P.; Kohn, W., *Physical Review* **1964**, *136*, B864-B871.
24. Schmidt, J. R.; Polik, W. F. *WebMO Enterprise, Version 15.0*, WebMO, LLC: Holland, MI, USA, 2014.
25. Dennington, R.; Keith, T.; Millam, J. *Gaussview, Version 5*; Semichem Inc.: Shawnee Mission, KS, 2009.
26. Warshel, A.; Levitt, M., *Journal of Molecular Biology* **1976**, *103*, 227-249.
27. Bauernschmitt, R.; Ahlrichs, R., *Chemical Physics Letters* **1996**, *256*, 454-464.

28. Gaussian 09; Revision D.01; Frisch, M. J.; Trucks, G. W.; Schlegel, H. B.; Scuseria, G. E.; Robb, M. A.; Cheeseman, J. R.; Scalmani, G.; Barone, V.; Mennucci, B.; Petersson, G. A.; Nakatsuji, H.; Caricato, M.; Li, X.; Hratchian, H. P.; Izmaylov, A. F.; Bloino, J.; Zheng, G.; Sonnenberg, J. L.; Hada, M.; Ehara, M.; Toyota, K.; Fukuda, R.; Hasegawa, J.; Ishida, M.; Nakajima, T.; Honda, Y.; Kitao, O.; Nakai, H.; Vreven, J. A.; Montgomery, J. A.; Peralta, J. E.; Ogliaro, F.; Bearpark, M.; Heyd, J. J.; Brothers, E.; Kudin, K. N.; Staroverov, V. N.; Kobayashi, R.; Normand, J.; Raghavachari, K.; Rendell, A.; Burant, J. C.; Iyengar, S. S.; Tomasi, J.; Cossi, M.; Rega, N.; Millam, J. M.; Klene, M.; Knox, J. E.; Cross, J. B.; Bakken, V.; Adamo, C.; Jaramillo, J.; Gomperts, R.; Stratmann, R. E.; Yazyev, O.; Austin, A. J.; Cammi, R.; Pomelli, C.; Ochterski, J. W.; Martin, R. L.; Morokuma, K.; Zakrzewski, V. G.; Voth, G. A.; Salvador, P.; Danneberg, J. J.; Dapprich, S.; Daniels, A. D.; Farkas, O.; Foresman, J. B.; Ortiz, J. V.; Cioslowski, J.; Fox, D. G. Gaussian Inc.: Wallingford, CT, 2009.
29. Vreven, T.; Byun, K. S.; Komaromi, I.; Dapprich, S.; Montgomery, J. A.; Morokuma, K.; Frisch, M. J., *Journal of Chemical Theory and Computation* **2006**, 2, 815-826.
30. Chung, L. W.; Sameera, W. M. C.; Ramozzi, R.; Page, A. J.; Hatanaka, M.; Petrova, G. P.; Harris, T. V.; Li, X.; Ke, Z.; Liu, F.; Li, H.-B.; Ding, L.; Morokuma, K., *Chemical Reviews* **2015**.
31. Neese, F., *Wiley Interdisciplinary Reviews-Computational Molecular Science* **2012**, 2, 73-78.
32. Senn, H. M.; Thiel, W., *Angewandte Chemie-International Edition* **2009**, 48, 1198-1229.
33. PQR files differ from PDB files in that they replace the latter's occupancy and B-factors with atomic charges (Q) and radii (R). Since bulb does not use those columns of data, it does not distinguish between the two file types.
34. Tao, P.; Schlegel, H. B., *Journal of Computational Chemistry* **2010**, 31, 2363-2369.
35. Berman, H. M.; Kleywegt, G. J.; Nakamura, H.; Markley, J. L., *Journal of Computer-Aided Molecular Design* **2014**, 28, 1009-1014.
36. Dolinsky, T. J.; Nielsen, J. E.; McCammon, J. A.; Baker, N. A., *Nucleic Acids Research* **2004**, 32, W665-W667.
37. Word, J. M.; Lovell, S. C.; Richardson, J. S.; Richardson, D. C., *Journal of Molecular Biology* **1999**, 285, 1735-1747.
38. Cornell, W. D.; Cieplak, P.; Bayly, C. I.; Gould, I. R.; Merz, K. M.; Ferguson, D. M.; Spellmeyer, D. C.; Fox, T.; Caldwell, J. W.; Kollman, P. A., *Journal of the American Chemical Society* **1995**, 117, 5179-5197.
39. The PyMOL Molecular Graphics System, Version 1.5.0.4 Schrodinger, LLC.
40. Ito, N.; Phillips, S. E. V.; Stevens, C.; Ogel, Z. B.; McPherson, M. J.; Keen, J. N.; Yadav, K. D. S.; Knowles, P. F., *Nature* **1991**, 350, 87-90.

CHAPTER 7

Conclusions and Future Directions

7.1 Adenosylcobalamin-Dependent Enzymes

The mode of Co–C bond activation employed by B₁₂-dependent isomerases and eliminases has been investigated in a series of studies using a combined spectroscopic and computational methodology. A particular goal of these studies was to better understand the consequences of the different adenosylcobalamin (AdoCbl) binding modes exhibited by these two classes of enzymes. The importance of His-on coordination and the conserved DXHXGXX motif in the isomerases was investigated indirectly through the use of AdoCbl and cob(II)alamin [Co(II)Cbl] analogues with variable lower axial ligation (Chapter 2). It was demonstrated in this study that replacement of the native dimethylbenzimidazole (DMB) ligand with weaker electron donors causes blue-shifts of electronic transitions with predominantly metal-to-ligand charge transfer (MLCT) character,¹ similar to the MCD shifts exhibited by Co(II)Cbl upon binding to the isomerases glutamate mutase (GM)² and methylmalonyl-CoA mutase (MMCM).³ These shifts were attributed to a stabilization of the occupied Co 3d-based MOs in response to reduced charge donation from the lower axial ligand in these species. No such reduction in charge donation is observed upon AdoCbl binding to GM or MMCM, suggesting that the electron-donating strength of the His ligand is different before and after Co–C bond homolysis. This modulation in His charge donation could be achieved through proton uptake into the DXHXGXX hydrogen-bonding network during Co–C bond homolysis, which would help stabilize Co(II)Cbl relative to AdoCbl.

The inability of the native DMB ligand to participate in hydrogen-bonding networks necessitates a different mechanism for Co–C bond activation by AdoCbl-dependent eliminases such as ethanolamine ammonia lyase (EAL). A spectroscopic and computational investigation of EAL (Chapter 3) revealed that unlike GM and MMCM, EAL induces subtle but important changes to the electronic structure of AdoCbl in both the holoenzyme and the ternary complex. Our

experimentally-validated computational models of the EAL holoenzyme and ternary complex permitted us to attribute these changes to specific geometric constraints imposed on the cofactor. Two active-site residues, N193 α and Y241 β , were proposed to be largely responsible for the changes to the AdoCbl geometric and electronic structures. In the holoenzyme, Y241 β limits the cofactor's conformational flexibility by imposing steric constraints on the DMB ligand, while the subsequent addition of substrate causes N193 α to displace the Ado ligand in order to form hydrogen bonds with both the substrate and the 3'-OH group of the Ado ligand. As a result of these constraints, AdoCbl adopts a significantly longer Co–C bond in the ternary complex than in the holoenzyme, implying that the addition of substrate activates this bond. Extension of our computational methodology to the study of Y241 β variants and AdoCbl analogues with modified DMB ligands (Chapter 4) confirmed that Y241 β is responsible for the geometry assumed by AdoCbl in the native holoenzyme. A similar analysis showed that compared to the removal of the Ado hydroxyl groups, the N193 α A substitution has a much larger effect on the geometry of AdoCbl in the EAL ternary complex. This result suggests that instead of using the Ado/N193 α hydrogen bond to “pull” the Ado ligand away from the rest of the cofactor, EAL uses the bulk of the N193 α side chain to “push” the ligand away.

A comparison of the results of Chapter 2 with those of Chapters 3-4 highlights an intriguing difference in the role of the lower axial ligand in AdoCbl-dependent enzymes. By adopting a His-on binding mode in the isomerases, AdoCbl acquires a lower axial ligand capable of engaging in strong hydrogen bonding interactions with other active-site residues. This provides the isomerases with a means of tuning the reactivity of the Co–C bond via the preferential stabilization of the Co(II)Cbl state. By contrast, the eliminases can only interact with the AdoCbl DMB ligand through weaker non-bonding interactions, and thus lack the ability to fine-tune the cofactor's electronic

structure. Without the means to directly stabilize Co(II)Cbl, the eliminases instead use the substrate to selectively destabilize the AdoCbl state. Thus, despite the fact that the isomerases and eliminases achieve a similar degree of Co–C bond activation, they appear to do so via two fundamentally different mechanisms.

The proposed mechanisms for Co–C bond activation in Chapters 2-4 should be refined in future studies. The importance of the DXHXGXX motif in the isomerases has already been demonstrated by site-directed mutagenesis of the conserved aspartate residue in several isomerases.^{4, 5} Interestingly, a former member of the Brunold group performed a preliminary spectroscopic characterization of the D14E variant of GM,⁶ but the computational modeling of this enzyme has proved difficult. The results of Chapter 2 and other recent cofactor analogue studies should inspire future researchers to investigate this variant with renewed vigor. The study of other, less conservative variants that are sure to disrupt the conserved hydrogen bonding network may also provide useful information.

The proposal of putative roles for N193 α and Y241 β in the Co–C bond activation mechanism employed by EAL also suggests that characterization of select variants with substitutions of these residues will be informative. As discussed in Chapter 4, AdoCbl in the N193 α A holoenzyme and ternary complex should show significant spectral differences from WT EAL-bound AdoCbl. Studies of the AdoCbl analogues without key hydroxyl groups should help to assess further the importance of the N193 α –Ado hydrogen bond. Meanwhile, the spectral changes in response to Y241 β substitution or DMB modification are expected to be more subtle. Yet, a promising research direction to pursue involves the study of the interactions of cofactor analogues with Y241 β variants. For example, WT EAL reconstituted with adenosyl(imidazole)cobalamin [Ado(Im)Cbl] is 9% as active as it is with AdoCbl bound.⁷ If the

reduced catalytic activity is due to the decrease in ligand bulk, enzyme activity can perhaps be restored by the Y241 β W substitution. Thus, the importance of steric crowding of the lower axial ligand can be investigated by assessing how similar the AdoCbl/WT EAL interaction is to that between Ado(Im)Cbl and Y241 β W EAL.

7.2 Stearoyl-CoA Desaturase

A preliminary computational investigation of the unique active site of stearoyl-CoA desaturase (SCD), a non-heme diiron (NHFe₂) enzyme that converts stearoyl-CoA to oleyl-CoA was presented in Chapter 5. The QM/MM-optimized geometries of Zn^{II}₂- and Fe^{II}₂- bound SCD demonstrated that the substitution of Zn for Fe in two recently resolved crystal structures^{8, 9} did not dramatically alter the active-site architecture. The optimized Fe^{II}₂-bound structure was used to investigate several putative O₂ binding sites, and it was concluded that the best model features a solvent ligand on Fe_B and a terminally bound superoxo ligand on Fe_W. This model was used to propose a novel O₂ activation mechanism in which the unusually long intermetallic distance is used to promote proton-coupled electron transfer (PCET) from the Fe_B^{II}(OH₂) site to the O₂-derived ligand on Fe_W.

Because SCD is a membrane-bound protein, isolation of the Fe₂-bound form presents a major challenge for the testing of the proposed mechanism. Should this species become available, it will be amenable to a wide variety of sophisticated techniques, including MCD, EPR, and Mössbauer spectroscopies. Although the characterization of reaction intermediates will be extremely challenging, it may be possible to take advantage of the complete loss of activity shown by all alanine variants of the coordinating His residues.¹⁰ For example, our proposed mechanism implies that alanine substitution of one Fe_B-coordinating His residue is unlikely to affect the ability of Fe_W to bind O₂. However, this variant would not properly position Fe_B for PCET during O₂

activation, allowing for the trapping and characterization of an O₂-bound, dead-end species. Furthermore, the use of NO as an O₂ analogue may provide confirmation of the proposed O₂ binding site, as the EPR spectrum of a {FeNO}⁷ species should be straightforward to interpret in the absence of coupling between the Fe centers. Our analysis of SCD also led us to propose specific roles for several conserved amino acids within the histidine boxes, namely R117, R154, and N295. These residues were proposed to be essential for imposing the proper intermetallic distance for efficient PCET. Substitution of these residues should, according to our model, drastically slow the rate of formation of the Fe_B^{III}/Fe_W^{IV}-oxo species.

7.3 Bulb

Bulb is an interactive program that facilitates the construction of input files and the analysis of output files for various computations on whole-protein models (Chapter 6). Bulb substantially reduces the barriers that can discourage experimentalists from performing QM/MM computations by automatically manipulating large numbers of Cartesian coordinates and helping users through input file construction with a series of guided questions. It also helps users to utilize the optimized coordinates of QM/MM optimizations in subsequent property calculations and to analyze the corresponding results. While currently used only by students and graduates of this department, bulb will soon be used by undergraduate researchers at Saint Mary's University of Minnesota to make the computational study of proteins accessible to undergraduate researchers. Furthermore, the modular architecture of bulb makes the grafting of additional small scripts onto the program a straightforward process. The writing of such scripts, a reasonable goal of possible short-term undergraduate research projects, can thus be educationally beneficial while still serving a pragmatic purpose. Such modifications may even lead to the fulfillment of a long-desired graphical

user interface for bulb, which would allow users to point and click their way through input file construction instead of relying solely on keyboard input.

7.4 Concluding Remarks

The research presented in the preceding chapters has demonstrated the utility of a combined spectroscopic and computational methodology for the study of two bioinorganic systems. These techniques have helped us answer some very old questions (the isolation of the first cobalamin was published 67 years ago^{11, 12}) and some very new questions (the first crystal structures of SCD were published less than five weeks before the defense of this thesis). Even as this research helps refine our understanding of AdoCbl-dependent enzymes and SCD, it also poses important new questions to the scientific community. I hope that these questions will guide future research and serve as inspiration for the development of creative experiments designed to test the mechanistic proposals presented in this thesis.

7.5 References

1. Stich, T. A.; Buan, N. R.; Brunold, T. C., *Journal of the American Chemical Society* **2004**, *126*, 9735-9749.
2. Brooks, A. J.; Fox, C. C.; Marsh, E. N. G.; Vlasie, M.; Banerjee, R.; Brunold, T. C., *Biochemistry* **2005**, *44*, 15167-15181.
3. Brooks, A. J.; Vlasie, M.; Banerjee, R.; Brunold, T. C., *Journal of the American Chemical Society* **2005**, *127*, 16522-16528.
4. Pierik, A. J.; Ciceri, D.; Lopez, R. F.; Kroll, F.; Broker, G.; Beatrix, B.; Buckel, W.; Golding, B. T., *Biochemistry* **2005**, *44*, 10541-10551.
5. Chen, H. P.; Marsh, E. N. G., *Biochemistry* **1997**, *36*, 7884-7889.
6. Conrad, K. S. Spectroscopic and Computational Insights into the Transport and Utilization of B12 in Biological Systems. University of Wisconsin-Madison, Madison, WI, 2010.
7. Fukuoka, M.; Yamada, S.; Miyoshi, S.; Yamashita, K.; Yamanishi, M.; Zou, X.; Brown, K. L.; Toraya, T., *Journal of Biochemistry* **2002**, *132*, 935-943.
8. Bai, Y.; McCoy, J. G.; Levin, E. J.; Sobrado, P.; Rajashankar, K. R.; Fox, B. G.; Zhou, M., *Nature* **2015**.
9. Wang, H.; Klein, M. G.; Lane, W.; Snell, G.; Levin, I.; Li, K.; Sang, B.-C., *To Be Published* **2015**.
10. Shanklin, J.; Whittle, E.; Fox, B. G., *Biochemistry* **1994**, *33*, 12787-12794.
11. Rickes, E. L.; Brink, N. G.; Koniuszy, F. R.; Wood, T. R.; Folkers, K., *Science* **1948**, *107*, 396-397.
12. Smith, E. L.; Parker, L. F. J., *The Biochemical journal* **1948**, *43*, viii.

CHAPTER 8

How to Break a Bond:

A Brief, Non-Technical Account of Coenzyme B₁₂, One Enzyme that Uses It, and the Last Six Years of My Life

8.1 Introduction and Motivation

Over the past six years, I've had the privilege of devoting much of my working life to studying one of nature's most fascinating molecules, coenzyme B₁₂. Over those same six years, I have been surrounded by an incredibly supportive network of friends and family who have frequently, out of curiosity or politeness, asked about my research. The answers they have received have often been rambling, circuitous, and disjointed: it turns out that distilling the essence of years of research into a few talking points over dinner or a cup of coffee is challenging. But despite this barrier, I am still excited at the thought of sharing the work I do with these supporters and with the general public. For that reason, I am including this brief, non-technical explanation of my favorite part of the following thesis (Chapter 3). My hope is that this short chapter will be able to rectify some of my past struggles to communicate my research and its significance to those people who kept me sane throughout the process.

Of course, a major challenge in communicating any scientific work to a non-scientific audience is the matter of translating precise technical jargon into words better suited for general communication. In chemistry, however, there are many concepts for which the technical term is the **only** term I can use. To keep this from posing too large of a problem, we'll begin this chapter with two short reviews for non-chemists. The first will help readers understand what exactly coenzyme B₁₂ is, its biological role, and why chemists are fascinated by it. The second will explain the experimental and theoretical tools we use to investigate it. Following those sections, I will present some of my data and explain how these results have improved the scientific community's understanding of B₁₂.

8.2 From Atoms to Enzymes: Bonding, Biochemistry, and Catalysis

When I teach freshman chemistry students, I like to begin the first day of class by asking them to take 30 seconds to write down a definition of the word *chemistry*. I don't do this to be cruel to the students, but because it can be instructive to realize how broad a field chemistry is. Any one-sentence definition of chemistry is unlikely to include the work of everyone who self-identifies as a chemist. With that caveat in place, I'll suggest that most chemists are mainly interested in finding out one of two things: (1) why some type of "stuff" has the properties it has, or (2) how to convert one type of "stuff" into another type of "stuff" via what is called a chemical reaction.¹ Even fairly simple chemical questions fall into these two categories. For example, a budding chemist interested in the properties of stuff may try to answer the questions, "Why don't oil and water mix?" or "Why do metals conduct electricity?" Another chemist interested in changing one type of stuff to another might ask, "How does my body use food and oxygen to provide me with energy?"

If chemistry encompasses any question that fits into either of these two categories, then it is an absolutely enormous discipline. Everything we do requires stuff, and everything we see is made of stuff. Stuff makes up our computers, our cars, our food, our environment, our clothes, and, most importantly, ourselves. What ties the study of all of these things together is an audacious two-part claim. First, chemists think that all stuff is made of very small components called atoms. Second, chemists believe that if we understand how atoms are constructed and interact with each other, then we can explain and predict the properties and behaviors of all kinds of stuff. In the remainder of this section, we'll briefly discuss the components of atoms, how atoms come together

¹ If you want to sound more scientific, replace "stuff" with "matter" in the previous sentence. I will continue using "stuff."

to form molecules, the special types of molecules involved in my research, and the chemical reactions they perform.

8.2.1. Atoms are made of protons, neutrons, and electrons. Atoms consist of some number and arrangement of three **sub-atomic particles** called protons, neutrons, and electrons. These particles differ in three significant ways. First, in the electrical charge they carry: protons have a positive charge, electrons have a negative charge, and neutrons are, well, neutral. Overall, the atoms themselves are also neutral, since they have an equal number of protons and electrons, causing their charges to cancel out. Sub-atomic particles also differ in mass: protons and neutrons have similar weights (neutrons are just a pinch heavier), but both are about 2000 times heavier than electrons. Third, they are found in different places inside the atom. All of the protons and neutrons are very densely packed in a nucleus at the center of the atom, while the tiny electrons swarm about the nucleus at some distance. The distance at which the furthest electrons are found from the nucleus tells us the size of the atom, which is typically about 0.000 000 000 200 meters, or 200 “picometers.” The nucleus itself is about 100,000 times smaller: 0.000 000 000 000 000 002 meters, or 0.002 picometers.

That’s more than just a nice trivia fact. It’s an important observation because it tells us that an atom’s electrons are what communicate with the rest of the world – the nucleus is too small and tucked away to be of primary importance. So if we want to understand how atoms come together to form different types of materials, we need to understand where the electrons are inside of atoms, and how electrons from one atom can interact with electrons from other atoms. This is a very challenging problem to solve, since electrons can behave in very counterintuitive ways. Thankfully, chemists have discovered useful patterns that help us predict how atoms behave based on how many electrons they have. To show the importance of the number of electrons in each

atom, consider this: if you gather a bunch of atoms that each have six electrons and six protons, you'll find that you have carbon (C) in one of its various forms (e.g., graphite, charcoal, diamond). Or, collect a bunch of atoms with seven electrons and you'll have nitrogen (N); choose eight, and you'll get oxygen (O). These materials – carbon, nitrogen, oxygen, and anything else you find on chemistry's periodic table – are examples of **elements**, or materials consisting of only one type of atom. There are about 115 known elements, many of which do not occur naturally. Each element contains only atoms with a characteristic number of electrons and protons.

8.2.2. Atoms can combine to make molecules by sharing electrons. There are way more than 115 different types of stuff in the universe, however, so we're going to need to understand materials other than elements. These other materials are called **compounds**, and they contain atoms of more than one kind of element. A common example is water. Many people know its chemical **formula**, H_2O , which describes the ratio of hydrogen to oxygen atoms (2:1) in any sample of water. Water is an example of a **molecular compound**, which means that there are very small distinct units of water called **molecules**, each of which has two hydrogen atoms and one oxygen atom. All of the compounds that I study are also molecular compounds, but they have many more atoms than water. For example, coenzyme B_{12} has the formula $\text{C}_{72}\text{H}_{100}\text{CoN}_{18}\text{O}_{17}\text{P}$, and ethanolamine ammonia lyase (EAL), another important molecule in this chapter, has the formula $\text{C}_{3415}\text{H}_{5158}\text{N}_{905}\text{O}_{887}\text{S}_{26}$.²

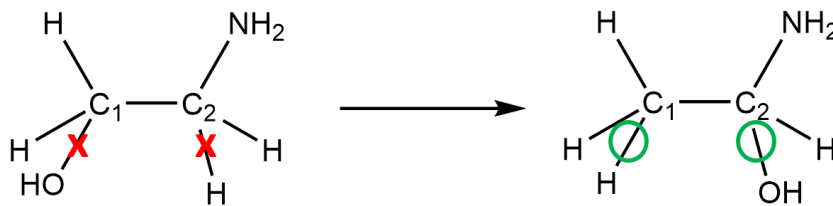
A major focus of my research is understanding how the many atoms in my molecules are held together. We call the connection between two atoms a **chemical bond**, and bonds within molecules are typically formed when two atoms share a pair of electrons. These electrons benefit

² In these formulas, Co stands for cobalt, P stands for phosphorous, and S stands for sulfur.

from the arrangement because as negatively charged particles they are attracted to the positively charged nuclei of both atoms. By spending some time near both nuclei, they force the nuclei to stay close together, and in doing so form a bond between the two atoms. The number of electrons in individual atoms determines how many bonds they will form, how strong those bonds are, and how far apart the bonded atoms sit. Carbon, for example, has atoms that like to form a lot of strong bonds, a property that makes it the centerpiece of a huge class of stable molecules that make up the basis of all living things. On the other hand, helium atoms completely refuse to form bonds at all.

When molecules engage in a **chemical reaction**, bonds may be broken and new bonds may be formed, changing the connections between atoms. For example, when hydrogen (H_2) and oxygen (O_2) molecules are reacted to form water (H_2O), the bond between the two hydrogen atoms is broken, as is the bond between the two oxygen atoms. As this happens, new bonds are formed between oxygen and hydrogen atoms – it is these bonds that hold the new water molecule together. Other chemical reactions may be more subtle. This chapter is about a rearrangement reaction, which changes which atoms within a molecule are bound to each other. In Scheme 8.1 below, the molecule on the left is called **ethanolamine**, and it has two carbon atoms, which I’ve labeled C_1 and C_2 . Before the reaction happens, there is an “OH” on C_1 and an “ NH_2 ” on C_2 . After the reaction happens, both the “OH” and the “ NH_2 ” are on C_2 . It looks like a simple reaction, but it actually is very challenging for two “groups” on one molecule to switch places on their own. This reaction is one step in a multi-reaction sequence that some bacteria use to take carbon dioxide (CO_2) and use it as a source of carbon for all of the complicated molecules they plan to build. Unfortunately, because the reaction is so difficult, it takes a very long time to occur, which poses a big problem

for these bacteria. However, organisms have evolved their own complicated machinery called **proteins** that can **catalyze** reactions. Let's talk about those bolded terms next.



Scheme 8.1. The rearrangement of ethanolamine. Lines represent bonds between two atoms. Not all bonds involving hydrogen atoms are drawn. On the left, a red “X” is placed over bonds that are broken during the reaction. Bonds formed during the reaction are circled on the right.

8.2.3. Proteins: nature’s modular architecture. In the previous section, I told you that the formula for EAL was $C_{3415}H_{5158}N_{905}O_{887}S_{26}$: add up all those subscripts, and you’ll find that this molecule has 10,391 atoms in it. That’s a lot to keep track of, but proteins are constructed in a very regular pattern that helps us understand how they function. Take a look at Figure 8.1A below, where I’ve drawn a small segment of a protein, and note how the sections in black are repeated over and over again. This is the protein’s backbone, a sequence of carbon, nitrogen, and hydrogen atoms that goes on and on and on. The only variation is found in the colored “side chains,” where different groups of atoms containing carbon, hydrogen, nitrogen, oxygen, and sulfur dangle off of the backbone. Living things construct proteins by joining together smaller molecules called **amino acids**: each set of brackets encloses a different amino acid. The three amino acids I included in this figure – histidine, asparagine, and tyrosine – are very important to my research.

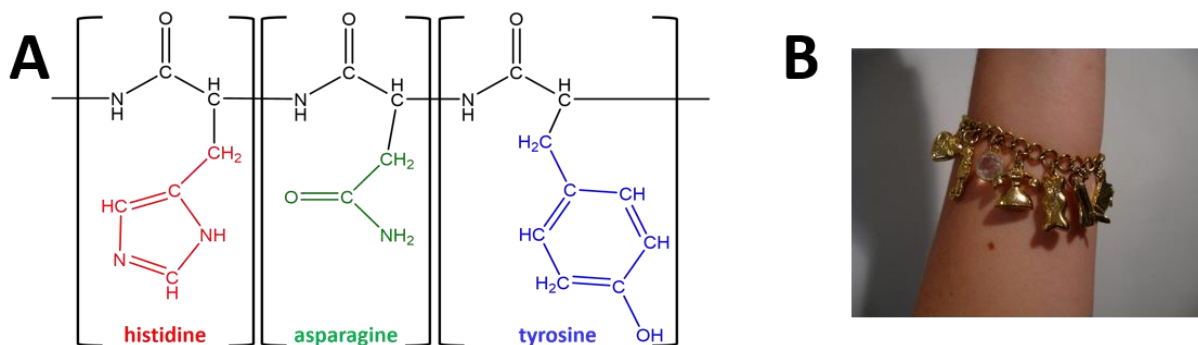


Figure 8.1. General organization of a protein. (A) Each segment in brackets represents an individual amino acid. Colored groups of atoms are amino acid side chains. Lines extending to the left and right of the figure indicate that more amino acids may be added to either side. (B) A charm bracelet is an analogy for the protein.³ The charms represent the protein's amino acid side chains, and the links are the backbone that connects the amino acids together.

One way to think of a protein is like a charm bracelet, where each amino acid represents one link in the bracelet's chain (Figure 8.1B). Just as different charms dangle from the jewelry, different amino acids have different groups of atoms that branch off from the protein's backbone. And just like the same individual charms can be reorganized into many different sequences, each different from the other, a vast array of proteins can be built from the same building blocks. In fact, the function of a protein depends on what amino acids are present and what order they are found in. There are twenty different amino acids found commonly in nature, and proteins can be anywhere from a few dozen to thousands of amino acids in length. Although the structure in Figure 8.1A is drawn in roughly a straight line, proteins tend to fold into very complicated three-dimensional structures with lots of nooks and crannies.

Proteins serve a wide variety of functions for healthy organisms. Some of them, like keratin, provide structure for the organism's cells and are responsible for the texture of hair and nails in mammals. Others are responsible for transporting small molecules or nutrients throughout

³ Image credit: Wikipedia.

the organism – right now, a protein called hemoglobin is picking up oxygen from your lungs and will soon deliver it to the rest of your body. But EAL, the protein I work with, is an **enzyme**, which means it is a protein that serves as a **catalyst** for a chemical reaction. Specifically, EAL is the catalyst for the reaction in Scheme 8.1, which means that it helps the reaction go much, much faster – up to 1,000,000,000,000 times faster, to be precise. In technical terms, we say that ethanolamine is EAL's **substrate**. Enzymes and substrates often have a very special relationship in which the substrate fits somewhere into or onto its enzyme, and the enzyme does *something* to make the substrate more reactive.

8.2.4. EAL, coenzyme B₁₂, and ethanolamine. Despite the crash-course in chemistry you just received, there is one lingering matter that we haven't addressed – the role of coenzyme B₁₂ (Figure 8.2A). Coenzyme B₁₂ is a type of molecule called a **cofactor**. While in many ways an enzyme is like a car's engine, chugging away and efficiently converting reactants to products, a cofactor is more like a key in the car's ignition. EAL can't begin to do its work unless coenzyme B₁₂ is present. For anything to happen in this biochemical machine, then the trio of EAL, coenzyme B₁₂, and ethanolamine must all be present. That sentence right there is the inspiration for my research: **Something about the way these three molecules interact with each other allows catalysis to occur, but nobody has a good explanation of what this interaction is.**

It's not at all unusual for enzymes to require cofactors, and EAL is not the only protein that uses coenzyme B₁₂, but I care about this particular cofactor for one specific reason. Coenzyme B₁₂ and a very closely related compound called methylcobalamin possess bonds between a carbon atom and a metal atom (in this case, cobalt, Co), the only known examples of **organometallic**

bonds in all of nature.⁴ Moreover, we know that the Co–C bond breaks in the very first step of any reaction for which coenzyme B₁₂ is required. The breaking of the Co–C bond creates two fragments called an “adenosyl radical” and “cobalt (II) cobalamin,” or “Co(II)Cbl” for short (Figure 8.2A). The former is an extremely reactive molecular fragment that goes on to react with the ethanolamine. We know that the rate at which the Co–C bond breaks controls the rate of catalysis for the overall reaction.

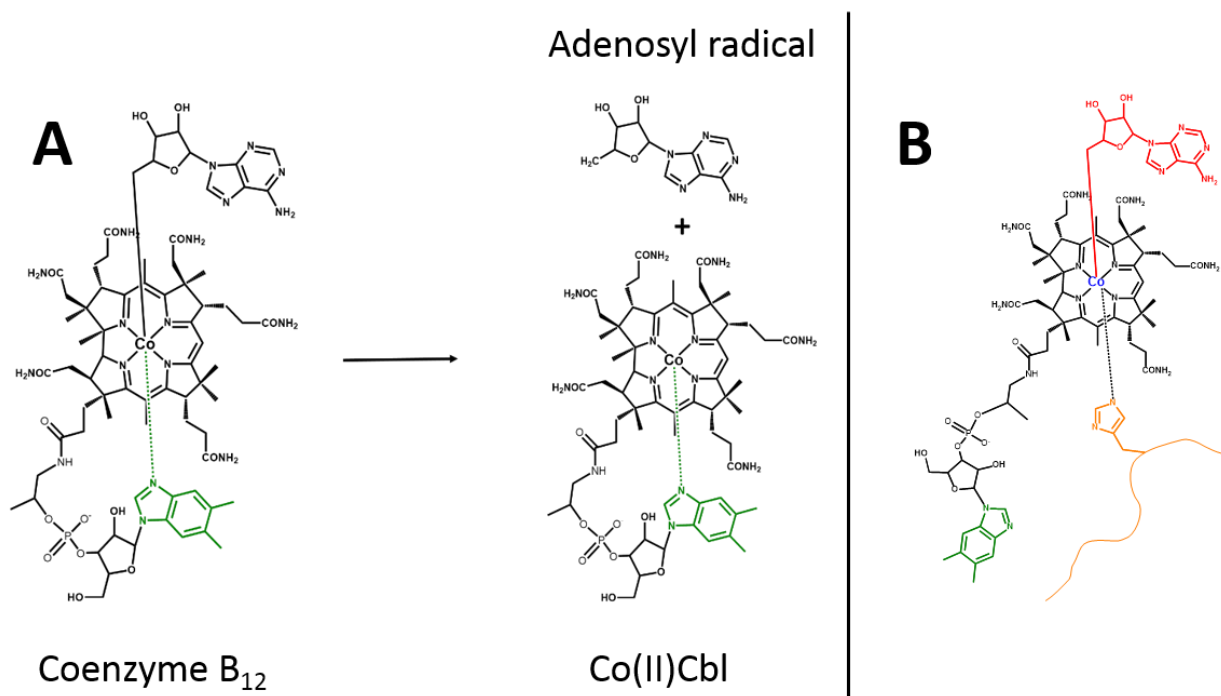


Figure 8.2. (A) Coenzyme B₁₂ (left), and the first step of the reactions it helps catalyze. In this structure, hydrogen atoms are omitted for clarity, and bonds between carbon atoms are drawn without the elemental symbol “C”. The DMB group (see text) is colored green. The products of this reaction step are an adenosyl radical (top, right) and Co(II)Cbl (bottom, right). (B) Coenzyme B₁₂ bound to an enzyme through replacing the DMB (green) with a histidine side chain (orange). The curvy line represents the protein backbone, and other amino acids are not shown.

⁴ In the interest of full disclosure, several years ago researchers discovered a carbon atom surrounded by six iron atoms in an enzyme called nitrogenase. Coenzyme B₁₂ is different in that the carbon bound to the cobalt atom is part of a bigger organic “group”, instead of just being a lone atom.

There is one feature of the enzyme-cofactor relationship that is particularly puzzling. First, there are several dozen known enzymes that utilize coenzyme B₁₂ as a cofactor, and they can be loosely grouped into two classes. One, which contains the only human coenzyme B₁₂-dependent enzyme, is known to bind the cofactor by breaking the Co—N bond opposite the Co—C bond, displacing a part of B₁₂ we call “DMB.”⁵ The DMB is replaced by forming a new Co—N bond between the Co and a nitrogen atom from a histidine side chain (Figure 8.2B). For a long time, many scientists thought that this must play a key role in helping enzymes break the Co—C bond, and a lot of work was put into researching how the Co—C bond’s strength depended on the strength of the Co—N bond across from it. Then, the unexpected happened. Researchers discovered that the other class of B₁₂-dependent enzymes does not break any Co—N bonds when the cofactor binds. Despite this fact, enzymes in this class are equally effective at weakening the Co—C bond as the others. EAL belongs to this latter class.

Thus, we have a conundrum. Two different classes of enzymes catalyze the same types of reactions, and do so with similar efficiencies. Both classes of enzymes use the same cofactor, and the key step in all reactions using this cofactor is the breaking of its Co—C bond. And yet, one of these classes absolutely requires a histidine side chain to attach to the Co atom to function, and the other has absolutely no need for this. The research presented informally here (and formally in Chapter 3) offers a possible explanation for this.

8.2.5. Why bother? Finally, let me address a more important question I’ve been asked many times since beginning this research. **Why?** Why do chemists bother studying things like

⁵ Short for “**dimethylbenzimidazole**.” I don’t want to type that word out over and over again, and I suspect you don’t want to read it over and over again.

this? The questions I want to answer are very esoteric, and it's taken the better part of six years⁶ to gather enough evidence to propose some answers to them. This seems like a very difficult thing to study, and it seems very far removed from other, more practical things we could study, like the nutritional effects of B₁₂. In other words, why are we working so hard to understand *how* B₁₂ works if we already have a good grasp on *what* it can do?

To answer, humor me with this scenario: pretend you've never seen a car before, and that you've stumbled across one in the woods. You find the owner's manual in the glove compartment, and after perusing that you have a general idea of what a car does and how to operate it. Excellent – good for you! But no matter how closely you study the owner's manual, you will never get a real idea of how everything under the hood comes together to make the car work. It would take years of monkeying around, testing out many failed theories of what each component does before you would gain a working knowledge of the car's engine.

Would those years be well-spent? I can think of three possible reasons to answer “Yes,” and each one is directly analogous to a reason for research like my own. First, you might study that car's engine so that you know how to fix it if it breaks down. Similarly, many biochemists and molecular biologists study how coenzyme B₁₂ functions so that they can think of ways to treat disorders related to its malfunction. For example, some men and women suffer from a genetic disease that affects the human enzyme that uses coenzyme B₁₂. When that happens, this particular enzyme becomes unable to bind the cofactor, and the result is a disease called methylmalonic acidemia caused by the toxicity of the unreacted substrate. Currently the best way to treat the disease is a liver transplant. Wouldn't it be nice if, based on our understanding of the interaction

⁶ To be fair to myself, those other six years did include a lot of coursework, teaching, research related to the other chapters of this thesis, a year away from campus, and – occasionally – a little bit of family time.

between enzymes and coenzyme B₁₂, we could design an analogue of the cofactor that was still capable of binding despite this mutation and add that as a supplement to patients' diets? Such lofty goals are unfeasible in the absence of an understanding of how catalysis works.

Second, you might study your mystery car's engine in order to use its technology to accomplish an unrelated purpose. That is, if you want to build a lawnmower, you might take the things you learned from your study of the car engine and adapt them to make them suitable for your new tool. Coenzyme B₁₂ may be the only known organometallic cofactor, but organometallic catalysts in general have become incredibly useful industrially. To give a sense of this, the American Chemical Society has an entire journal devoted solely to the study of organometallic compounds. Last year alone, nearly 850 articles were published in this journal, and the journal was cited over 42,000 times (cite). Most of the research in this journal is related to the synthesis of new catalysts, and the measurement and explanation of their properties. When it comes to designing these catalysts, however, there are likely some very important lessons that can be taken from coenzyme B₁₂. This cofactor, and the enzymes that utilize it, are the products of billions of years of evolutionary pressures that reward those organisms best adapted to their environment and the resources they have available. In other words, the cofactor/enzyme combination is already a well-engineered machine, and its study should bear fruit in fields other than medicine or biochemistry.

Last, many of you might study the car's engine because it's cool. There is something about the human mind that is fascinated by machines. Studying cars or enzymes for this reason isn't pragmatic or utilitarian, but those who lack this inspiration will find it impossible to dedicate years of their lives to study. Nearly every scientist who survives the rigors and setbacks of research is a person who is captivated by a problem, and is willing to devote his or her career to solving it. The scientist in the lab is not all that different from the grease monkey who tinkers for hours late at

night in the garage. Both have a passion that inspires them to a better understanding of their work, which in turn further fuels that passion. For me, B₁₂ is the most fascinating puzzle I've been exposed to (and subjected to) in my life. Without its inspiration, I would never have spent the countless hours in the lab and in front of the computer necessary to do this research, and I would never have bothered writing this summary for you. Since we're on the subject, let's move on and talk about exactly how these hours were invested.

8.3 Matter, Light, and Energy

8.3.1. Introduction to Light. Molecules are far too small for us to see, and the motions of their atoms are far too fast for us to observe directly. To actually understand what happens to coenzyme B₁₂ when bound to EAL, we need something to act as a probe, something that will interact with B₁₂ and produce some sort of effect that we can measure. Thankfully, there is a whole field of science on the interface of chemistry and physics called **spectroscopy**, the study of the interaction of light and matter. We can literally shine light on our problem, and use it to interrogate our molecules. The experiments I will describe to you here are types of **absorption** spectroscopy, in which the amount of light absorbed by a sample is measured. Unless you are colorblind, your eyes perform experiments like this all the time. For example, look at the vial in Figure 8.3 below, which contains a dilute solution of coenzyme B₁₂. The lights in the room are shining white light on it, which consists of all colors of light. Some of these colors are absorbed by the solution, while others are transmitted. Your eye detects the latter, and interprets that combination of colors as “red.”

It is possible to make this measurement of color more quantitative, but to do so we'll first have to talk about what light is. The technical term for light is **electromagnetic radiation**, a fancy phrase that tells us that light behaves a lot like waves in the ocean or ripples in a pond. For example,

if you drop a rock into a pond, you will see ripples “radiating” away from the point where the rock hits the water. If we want to describe one of these ripples, we might talk about its **amplitude** (how high and low the water’s crests and troughs are), **wavelength** (the distance between one crest and another), or **frequency** (how many times the wave goes up and down in a certain amount of time). We use the same terms to describe light waves, which are oscillations of an electric field.⁷ In the early 20th century, Einstein made the revolutionary suggestion that the energy of light is proportional to its frequency and inversely proportional to its wavelength. Put more simply, high-energy light has a high frequency and a short wavelength, while low-energy light has a low frequency and a long wavelength. When your eye distinguishes different colors of light, it is really identifying what wavelengths of light are reaching it. Red light has the longest wavelength of light you can detect, and violet light has the shortest.⁸



Figure 8.3. A dilute solution of coenzyme B₁₂.

So why does the sample in Figure 8.3 absorb some colors of light and not others? The best answers we have come from the field of quantum mechanics. One of the most important results that follows from the fundamental postulates of quantum mechanics is that electrons can only exist

⁷ Technically, there are two fields oscillating: one electric and one magnetic. But to keep this chapter from growing too long, we’ll just talk about the electric field.

⁸ There are wavelengths of light much longer and shorter than these. While they’re important for other interesting types of spectroscopy, the experiments discussed in this chapter use primarily visible light.

in certain configurations called **states**, and that each state has a characteristic energy associated with it.⁹ Ordinarily, the electrons in atoms and molecules are in their lowest-energy state (called the **ground state**), but if something provides them with energy, an electron can be moved into a higher-energy **excited state**. Under no circumstances, however, should an electron have any amount of energy that doesn't correspond to one of its possible states.

If that last paragraph was a doozy, just know that it was meant to provide a short introduction to this statement: **electrons are only allowed to have certain energies**. To get from a ground state to an excited state, they need something to provide that extra energy, which is what happens when light is absorbed. Light that has energy equal to the difference between an electron's ground and excited states **may** be absorbed by the electron to move it into an excited state. But if the light that shines on a sample does not have the right amount of energy, it won't be absorbed and instead will pass through. Since different colors of light have different energies, this gives a general explanation for why solutions like the one in Figure 8.3 have color – red light just doesn't have the right energy to be absorbed.

8.3.2 Spectroscopic and Computational Techniques. Since we are now equipped with some knowledge about how light and matter interact, we can talk about how to design an experiment to better understand why the solution appears a certain color. Figure 8.4A below shows a simplified sketch of a **spectrophotometer**, the instrument we use to collect this type of data. White light is emitted from a source (1) and is reflected off a “diffraction grating” (2) which, like a prism, separates the different wavelengths (colors). Only light from a very narrow range of colors is able to pass through a slit (3) and make it to our sample (4). Some of that light will be absorbed

⁹ If that doesn't make sense at first, try repeating it a few times. It may never sound reasonable, but eventually you may convince yourself that it's true.

by the sample, and the rest will make it to a detector (5). The detector measures the intensity of this light relative to the intensity at the source, and uses that to calculate the **absorbance**, a measure of how much light is absorbed by the sample. After the absorbance has been measured at one wavelength, the angle of the diffraction grating is changed to allow a different wavelength of light through the slit. The actual instrument we use to perform this measurement is shown in Figure 8.4B.

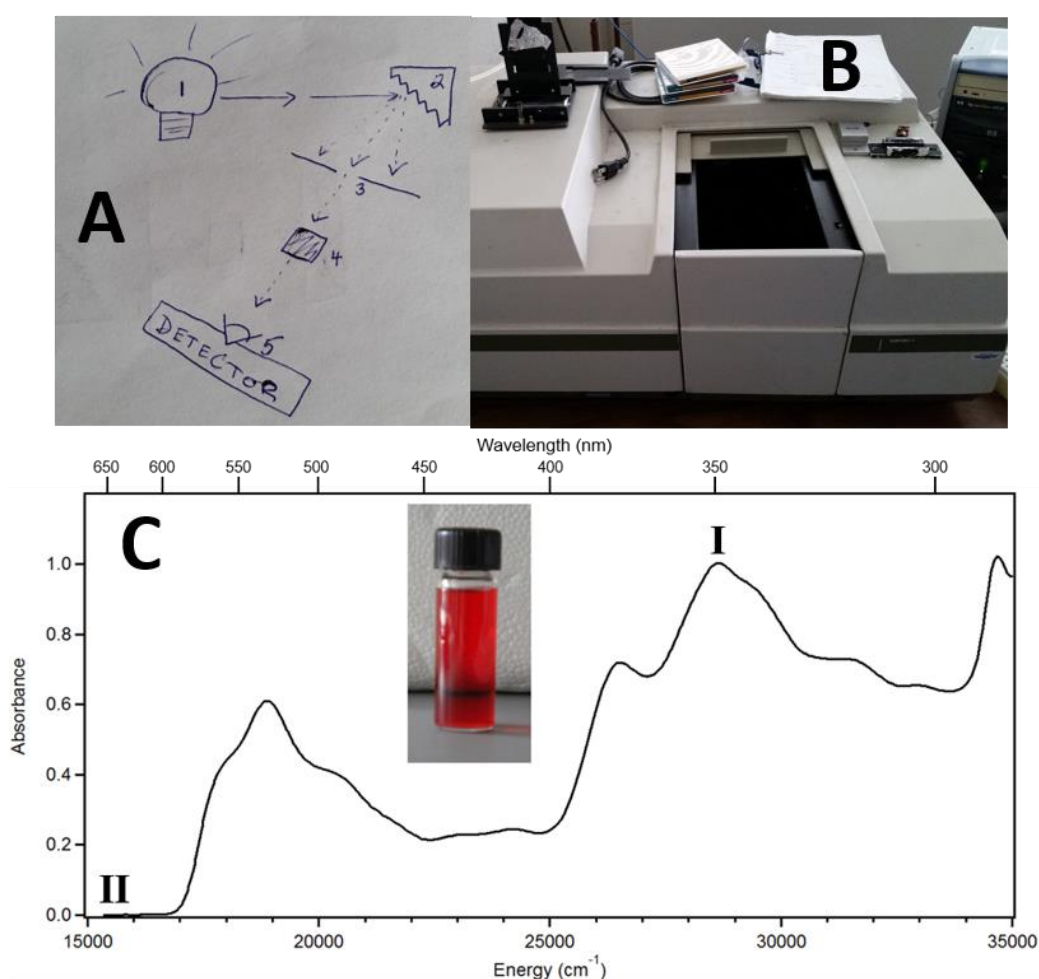


Figure 8.4. (A) Sketch of how an absorption spectrophotometer works. (B) A picture of the spectrophotometer in our lab. (C) An absorption spectrum of coenzyme B₁₂ produced by this instrument.

The end result of this experiment is an absorption spectrum (Figure 8.4C). This plot has absorbance on the y-axis plotted versus wavelength, frequency, or energy on the x-axis.¹⁰ If the incoming light has the appropriate amount of energy to move any of a molecule's electrons into a higher-energy state, the molecule **may** absorb that energy, in which case there will be a correspondingly high absorbance. For example, light with a wavelength of 350 nm (energy $\approx 28,500\text{ cm}^{-1}$) is very easily absorbed by coenzyme B₁₂, so at that point (I) on our plot we have a high absorbance and a “peak” in the spectrum. However, light at 650 nm (point II, energy $\approx 15,400\text{ cm}^{-1}$) does not have the right amount of energy to excite an electron, and so it is not absorbed at all.

There is clearly a lot of information about coenzyme B₁₂ in this figure, but there are also two major obstacles preventing us from obtaining and using that information. First, even though we can find the peaks on the spectrum, we don't know for sure how many possible transitions there are. That's because each peak has some width to it. It's certainly possible that each peak is due to one and only one transition, but it's also possible that there are multiple transitions very close in energy that overlap with one another. In other words, our absorption spectrum suffers from poor resolution. Second, even if we knew how many transitions we had and what the corresponding energies were, we don't know how to interpret that information. We may know that the energy is a difference between two states an electron may be in, but the spectrum itself can't tell us where the electron is coming from and where it is going to for any individual transition.

To resolve our first issue, we use a complementary technique called magnetic circular dichroism (MCD) spectroscopy, which requires us to do two things. First, we'll conduct our

¹⁰ In our group, we usually use energy, in the unusual unit of “wavenumbers” (cm^{-1}). In Figure 0.4, I also included wavelength in “nanometers” (nm) as an upper x-axis.

experiment inside a high magnetic field. Next, instead of ordinary light, we use “circularly polarized” light, in which the electric field looks more like a corkscrew than a wave (Figure 8.5A). This light can be either “right” or “left” circularly polarized light, depending on whether it is turning in a clockwise or counterclockwise direction. The rest of the experiment follows the same principles as absorption spectroscopy, which we talked about earlier, but the setup is much more challenging. Our instrument is shown in Figure 8.5B: circularly polarized light is generated by the beige box on the far left and passes through the metal tube to a sample chamber beneath the blue cylinder. That cylinder is a magnetocryostat, which contains a superconducting magnet and a liquid helium cryostat to keep it and our samples very, very cold. The sample itself is injected into a small cell and screwed onto a rod (Figure 8.5C), which is lowered through the magnetocryostat and into the sample chamber. After the light passes through the sample, it goes all the way to a detector at the far end of the gray box. Unlike an absorption spectrum, which can be collected in a few minutes, it takes hours to collect MCD spectra, and the instrument requires frequent maintenance while it runs.

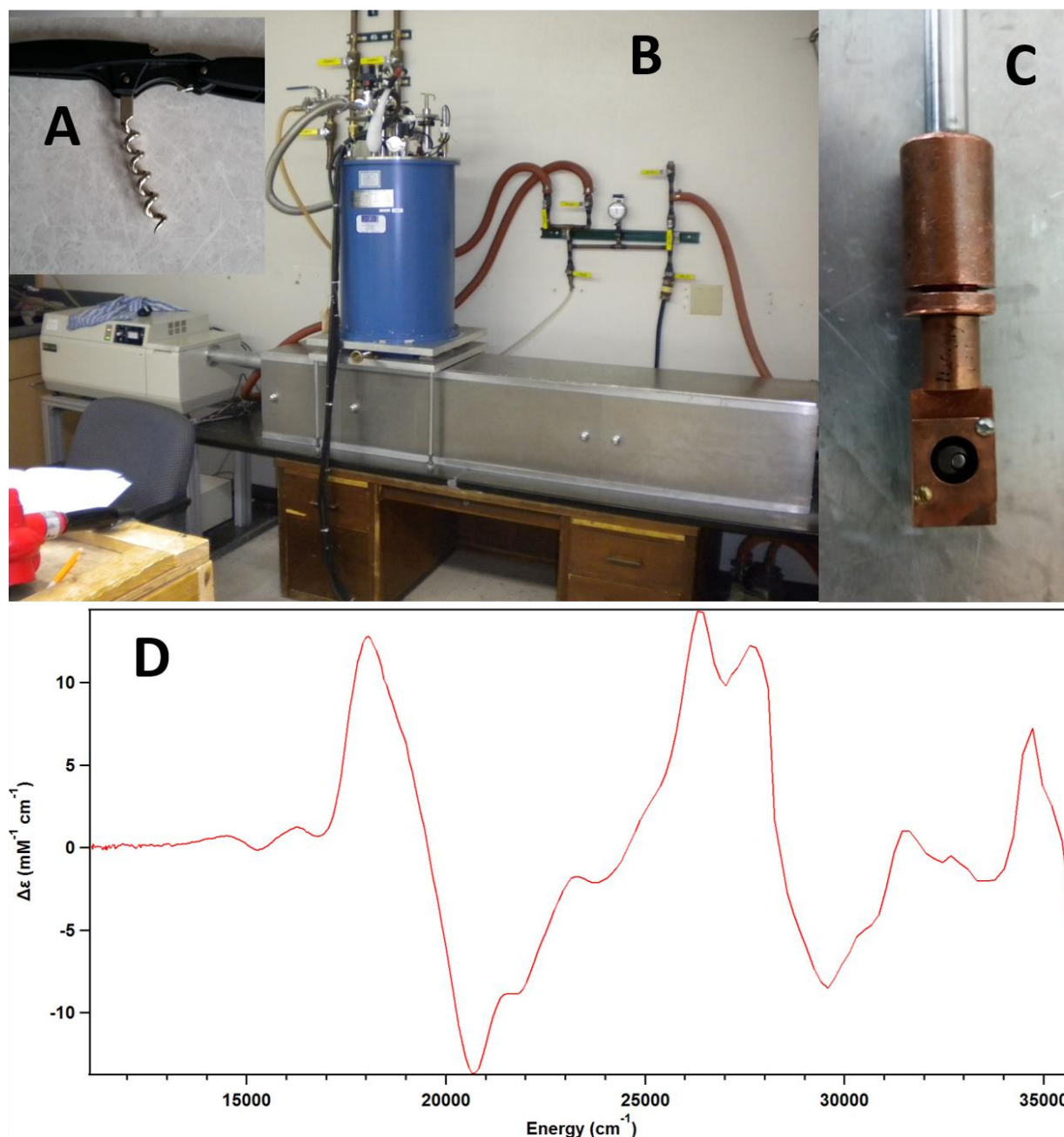


Figure 8.5. Setup and results of an MCD experiment. (A) Circularly polarized light has an electric field that oscillates and rotates, which makes it look like it's traveling along a corkscrew. An observer watching the light come down this corkscrew toward her would see it rotating counterclockwise, so this would be "left" circularly polarized light. (B) The MCD instrument used to collect data in this chapter. (C) Close-up of the sample cell and rod. (D) An MCD spectrum of coenzyme B₁₂.

So why do we go to all this trouble? You may have noticed that the features of the absorption spectrum in Figure 8.4C have different intensities. This is a result of what chemists call “selection rules”, rules that determine how likely a transition will be based on the initial and final states of the electron.¹¹ Interestingly, these selection rules can change when we impose certain conditions on our experiment – conditions like the use of circularly polarized light or an external magnetic field. That means that prominent features in the absorption spectrum may be much less intense in an MCD spectrum, and vice versa. We can also play a clever trick by using both right- and left-circularly polarized light, since our molecules will sometimes absorb one better than the other. That’s a huge aid to our problem of resolution, since we can take the difference in absorbance between the two polarizations of light and get a spectrum with both positive and negative features, as shown in the MCD spectrum in Figure 8.5D. Two transitions that might overlap in the absorption spectrum will be easily distinguished in the MCD spectrum if one is positive and the other is negative. Again, the same transitions are being probed in both absorption and MCD spectroscopy; by using both simultaneously we have a better chance of finding all of the transitions and precisely determining their energies.

Overcoming our second obstacle, the one of interpretation, requires another complementary technique, but this one doesn’t involve going into the lab. Instead, we attempt to use the theories of quantum mechanics to predict the energies at which we should observe transitions, and how intense those transitions will be. Unfortunately, the equations involved can’t be solved exactly for atoms or molecules with more than one electron – and we have tens of thousands of them! In the past few decades, however, a number of very good approximate methods

¹¹ I’m being deliberately vague here in order to save you another mini-lecture on quantum mechanics.

have been developed that can be applied to systems of our size. These methods allow us to predict the **geometric structure** (the relative positions of atoms and their nuclei) and **electronic structure** (the arrangement and energies of electrons) of EAL, coenzyme B₁₂, and ethanolamine. Despite the fact that these methods aren't exact, it can take a large computer cluster weeks to finish computing the final position of all the atoms of just one of my models, after which it takes about a week for a separate calculation of the absorption spectrum to run.

These computations are worth all this time because of the huge wealth of easily interpretable information they contain. When the computer predicts that an electron in B₁₂ will absorb light of a certain energy, it can also tell me where the electron is coming from and where it is going to. This information gives me clues about what EAL does to B₁₂ to affect the electron's energies. We can also use our computational model to correlate changes in the computed spectrum to changes in the molecule's geometry. For example, if we see that binding to EAL causes one of the bonds in B₁₂ to get longer, we can investigate whether or not that change is responsible for a corresponding change in the computed spectra. In the computer models, I can manipulate that bond length to any arbitrary distance and see the effect on the absorption spectrum, which is something I could never do to my real molecules in the lab.

The wealth of the information we get should be taken with a grain of salt, however, since these methods are approximate. Every time we use one of these models to explain something about B₁₂'s behavior, we must be sure that the theory has been experimentally verified. That is, we calculate something with that theory that can be compared to our experimental data. If experiment and theory agree, then it's evidence that the theory can be trusted. This shouldn't be mistaken for ironclad proof that our theories are perfect: on the fringes of science, we seek adequacy, not perfection. To further demonstrate that the theory is good enough, we can use the computational

results to propose hypotheses about how B₁₂ functions, and then design further experiments to test those hypotheses. When everything works right, this approach is circular, since good computations will inspire new experiments, which will in turn require further computations to interpret.

8.4 Results

8.4.1. A mechanism for EAL: to stabilize or destabilize? Now that you've been introduced to the systems I study and the techniques I use, let's get to the data. As I suggested earlier, the first thing we want to determine is how EAL affects the Co–C bond. In principle, it could do this by either weakening the bond directly or by stabilizing Co(II)Cbl to make it easier to reach that state. We can determine this by comparing the absorption and MCD spectra of coenzyme B₁₂ before and after we bind it to EAL. We can also do the same to Co(II)Cbl. Those are the comparisons shown in Figure 8.6 below. The top two overlays show the absorption and MCD spectra of coenzyme B₁₂ by itself, with EAL, and with EAL and ethanolamine. The bottom part of the figure shows the corresponding MCD spectra of Co(II)Cbl. It's possible to talk about the gritty details about this spectra – and I do in Chapter 3 – but to get the main point, we only need to look at these spectra very qualitatively. Here's what I mean: when EAL and ethanolamine are added to coenzyme B₁₂, there are some pretty noticeable changes (see the red boxes in particular). We'll talk about what causes these in Section 8.4.2, but for now, note that there are almost no changes to the MCD spectrum of Co(II)Cbl when we do the same to it.

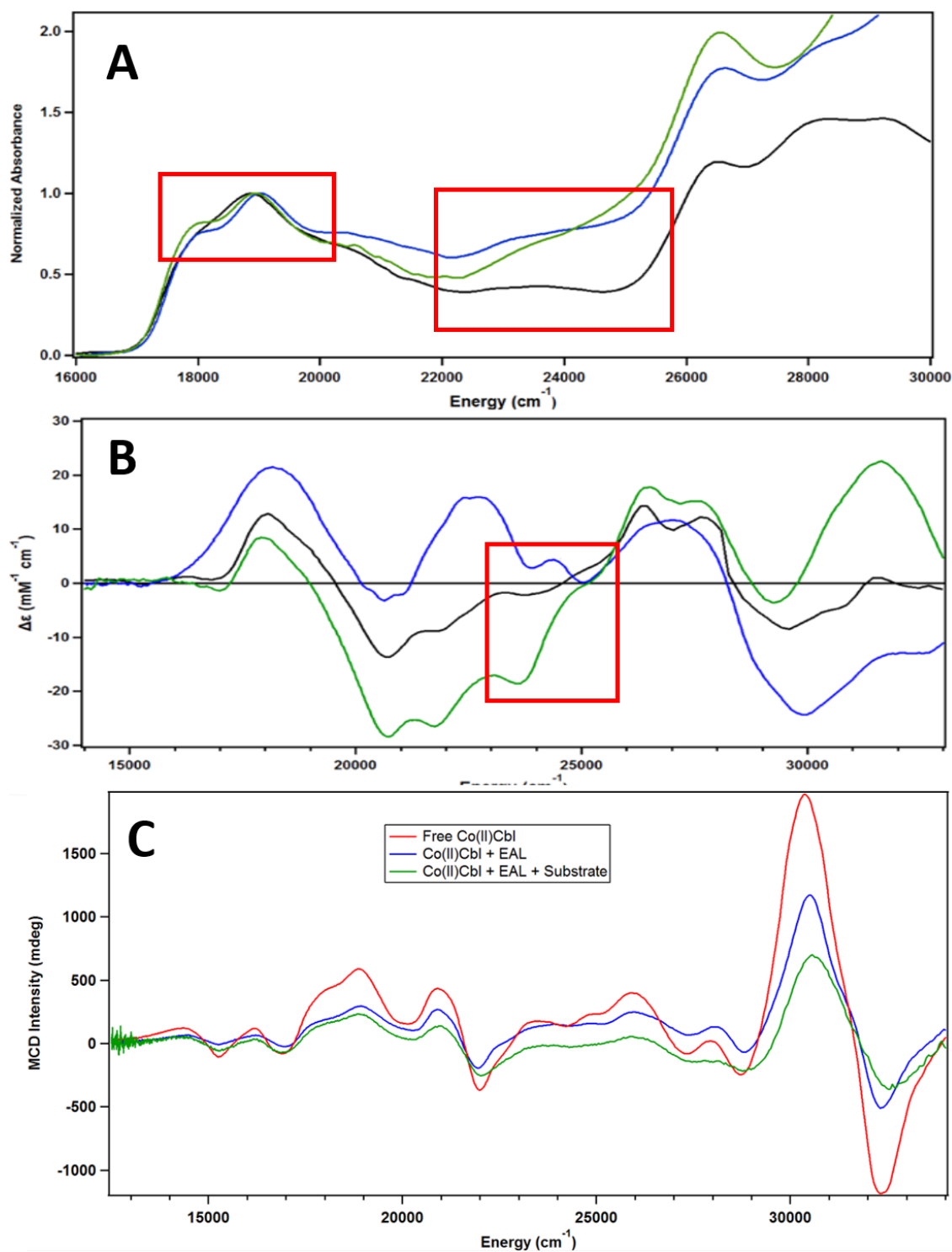


Figure 8.6. Absorption (A) and MCD (B) spectra of coenzyme B₁₂ and MCD spectra of Co(II)Cbl (C) in the following three states: by itself (red), with the addition of EAL (blue), and with the addition of EAL and ethanolamine (green). Key changes induced by the protein and substrate are indicated by red boxes.

That's really important, because it tells us that EAL must function by weakening the Co–C bond directly. What's interesting is that this is the exact opposite of what we would observe if we did this experiment with the histidine-binding class of coenzyme B₁₂-dependent enzymes. In those enzymes, nothing happens to the spectra of the coenzyme B₁₂ form, but a lot happens to the Co(II)Cbl form. This strongly suggests that for some reason, whether or not the enzyme uses a histidine side chain to bind our cofactor is related to whether the enzyme works by destabilizing coenzyme B₁₂ or by stabilizing Co(II)Cbl. That alone is a worthwhile thing to know, but we can extend our analysis to find out what parts of EAL are important and why.

8.4.2. Proposed roles for amino acids. The results from the previous experiment can only give us information about the total effect of the protein on the cofactor. To dig deeper, we need to use a computational model. I'll spare you the details of the model and show you the results of the absorption spectra I compute in Figure 8.7A. Compare that figure to the spectra to the coenzyme B₁₂ absorption spectra in Figure 8.6A above, and judge for yourself whether or not the model reproduces the major effects of EAL and ethanolamine on the cofactor's spectrum. I hope you'll agree with me that theory and experiment are in good agreement here.¹² We can now use the results of our computations to propose reasons for why the spectra are changing.

¹² If not, then in principle you shouldn't accept the model I'm about to present to you – but thank you for reading this far!

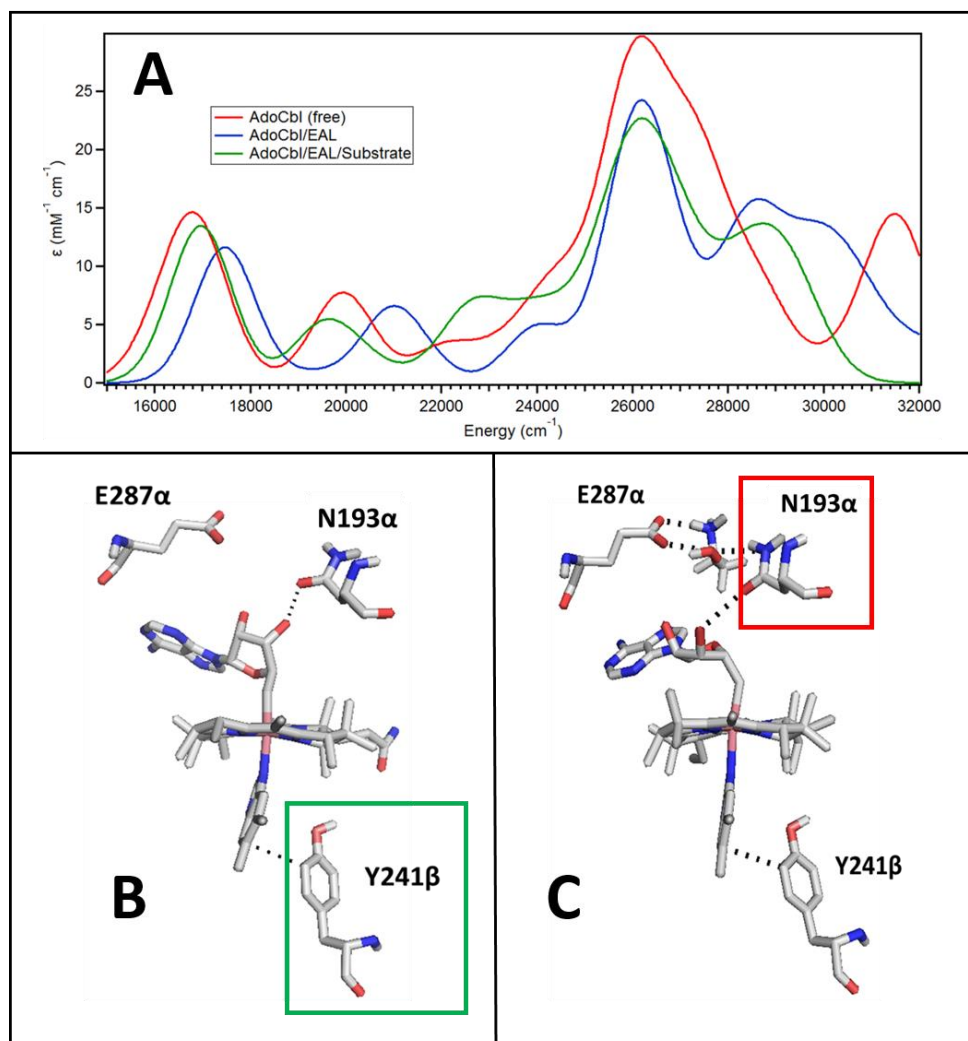


Figure 8.7. Results from my computational models. (A) Absorption spectra for coenzyme B₁₂ in three states: by itself (red), with the addition of EAL (blue), and with the addition of EAL and ethanolamine. (B) Geometric structures of coenzyme B₁₂ bound to EAL. (C) Geometric structure of coenzyme B₁₂ bound to EAL in the presence of ethanolamine.

Figures 8.7B and 8.7C show the molecular geometry of coenzyme B₁₂ used to compute the blue and green spectra in Figure 8.7A. (They also include three side chains of EAL's amino acids, identified by an alphanumeric code.) Since these models have been validated, we can ask ourselves: what parts of the protein are causing our cofactor's shape to change? And that brings us to the final part of the study. It turns out that when we only include B₁₂ and EAL (Figure 8.7B), the major changes all involve the lower half of the cofactor. And it appears that the amino acid

responsible for that movement is the one in the green box. That's the side chain of tyrosine – a big, bulky amino acid – that looks to be imposing on the DMB of B₁₂. When we add ethanolamine to the mix (Figure 8.7C) we see all the changes happening to the upper half of the cofactor. Here, the culprit is the one in the red box, another big amino acid called asparagine. Asparagine has both a strong attraction to the ethanolamine molecule and to the cofactor, and in order to stay close to both, it needs to distort the cofactor's geometry, causing the Co–C bond to grow longer. In general, longer bonds are weaker bonds, so this is a tell-tale sign of coenzyme B₁₂ being destabilized in the presence of EAL and ethanolamine. Thus, the specific changes caused by these tyrosine and asparagine side chains in the model's prediction agree with the general mode of coenzyme B₁₂ destabilization that we qualitatively expect based on our experiments.

8.5 Conclusion

An important step in the scientific method is the formulation of theories that tie together a series of observations. In the previous section, I showed you the following:

1. The absorption and MCD spectra of coenzyme B₁₂ are changed by EAL and ethanolamine, meaning they affect the cofactor's electronic structure.
2. The absorption and MCD spectra of Co(II)Cbl are not affected by EAL and ethanolamine.
3. Our computer models are verified by reproducing the changes to the spectra observed experimentally in #1.
4. These computer models predict changes to the geometric structure of coenzyme B₁₂ when EAL and ethanolamine are added.
5. The structural changes in #4 appear to be a result of the effects of two specific amino acids that are near the cofactor.

I would like to tie these observations together in a conclusion by using my favorite analogy, one that makes it into my informal presentations but not (usually) into my papers: **coenzyme B₁₂ is like a bottle of beer, and EAL and ethanolamine together act as a bottle opener.** In this analogy, the goal of EAL and ethanolamine is to take the top off of coenzyme B₁₂'s "bottle" by breaking the Co–C bond. This happens in two steps. First, before ethanolamine arrives, EAL binds the cofactor in a very rigidly defined position, just as you might firmly grasp a bottle that you plan to open. This is one possible role of the tyrosine side chain we identified: by imposing a certain position on the DMB group, it prevents the cofactor from wiggling around inside the enzyme. Then, when ethanolamine arrives, it provides a motive for the asparagine side chain to drag across the cofactor's upper face and pull on the Co–C bond, thus weakening it. Once the bond is broken, the strain that was placed on the cofactor is removed, explaining why we see no evidence of major changes to the Co(II)Cbl spectra.

That is the conclusion of this study, and although I hope it has helped you get a glimpse of my research, I also hope that it leaves you hanging a little bit. What I've told you about should be seen not as a complete work, but as just one rung of a ladder. It is only possible because of the countless hours of work put in by biologists, biochemists, chemists, and physicists, not to mention the funding support provided by my university, the taxpayers that fund it, and the federal agencies that deemed it worthy of pursuit. And it is clearly not the culmination of our work on B₁₂. Like any conclusion on the fringes of our scientific knowledge, mine are supported by evidence and yet to some extent speculative. That's a good thing! My hypothesis regarding these tyrosine and asparagine side chains is that both are necessary for EAL to function, and I hope that some young researcher comes along and designs new experiments to test this. This is how scientific progress

tends to happen, with every small project giving us a little more understanding of how the world works, and a lot more questions to answer.

APPENDIX

Appendix Table of Contents:

Chapter 2	200
Chapter 3	223
Chapter 4	244
Chapter 5	279

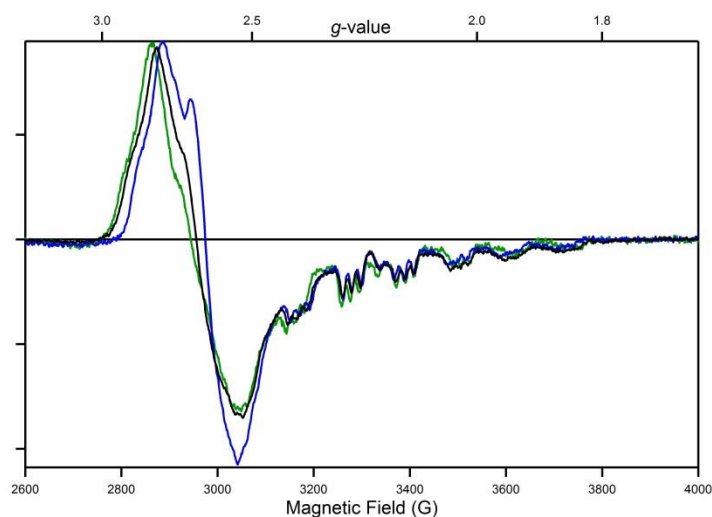


Figure A.2.1. EPR spectra of Co(II)pyCbi^+ (black), $\text{Co(II)(Me}_2\text{N-py)Cbi}^+$ (blue), and $\text{Co(II)(CN-py)Cbi}^+$ (green), collected at 77 K.

Table A.2.1. EPR parameters derived from fits of the EPR spectra in Figure S1. Parameters for Co(II)Cbl (from reference 39 in the main text) are provided for comparison

Cofactor	g_x	g_y	g_z	$A_x(\text{Co})$	$A_y(\text{Co})$	$A_z(\text{Co})$
Co(II)Cbl^{39}	2.230	2.272	2.004	30.00	40.00	305.00
$\text{Co(II)(CN-py)Cbi}^+$	2.270	2.270	2.006	50.00	50.00	320.00
Co(II)(py)Cbi^+	2.260	2.265	2.260	45.00	45.00	310.00
$\text{Co(II)(Me}_2\text{N-py)Cbi}^+$	2.255	2.260	2.006	42.00	42.00	295.00

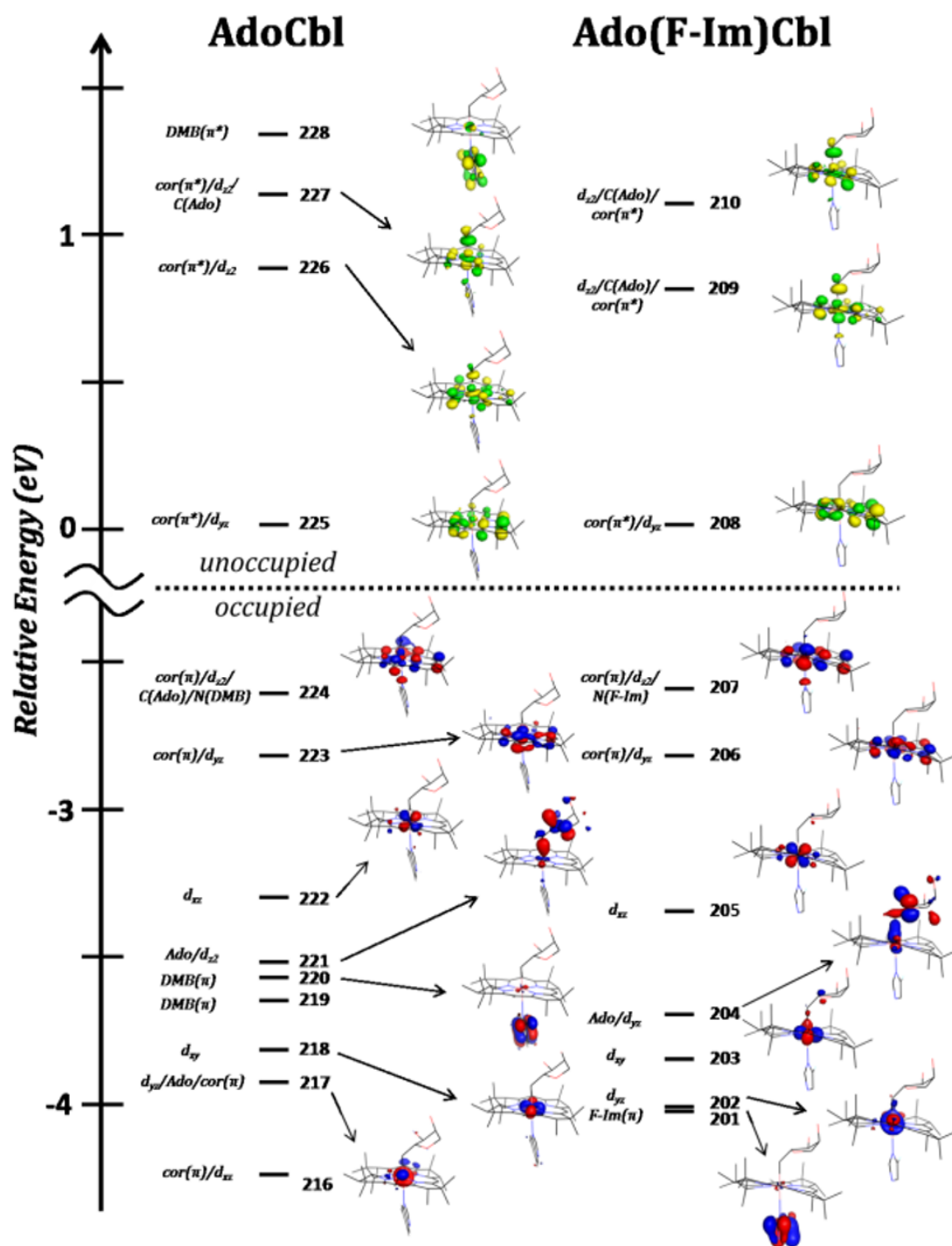


Figure A.2.2. DFT/TPSSH computed MO diagrams for AdoCbl and Ado(F-Im)Cbl. MOs were shifted vertically to align the LUMOs at 0 eV. Occupied orbitals are shown in red and blue; unoccupied orbitals in green and yellow.

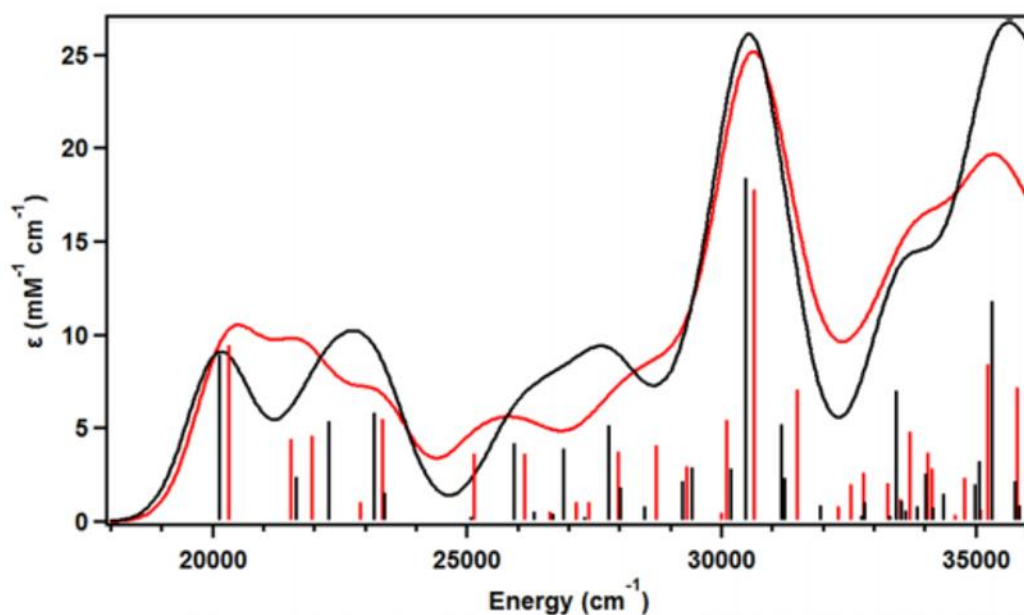


Figure A.2.3. TD-DFT/TPSSh computed Abs spectra for AdoCbl (black) and Ado(F-Im)Cbl (red). The computed energies and intensities of individual transitions are shown as sticks.

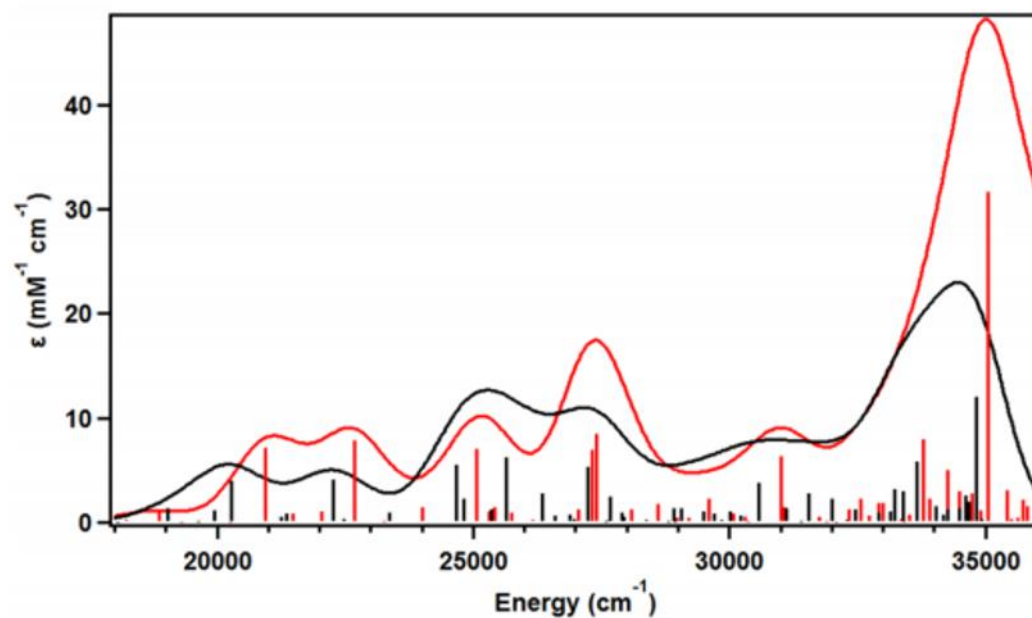


Figure A.2.4. TD-DFT/TPSSh computed Abs spectra for Co(II)Cbl (black) and Co(II)(F-Im)Cbl (red). The computed energies and intensities of individual transitions are shown as sticks.

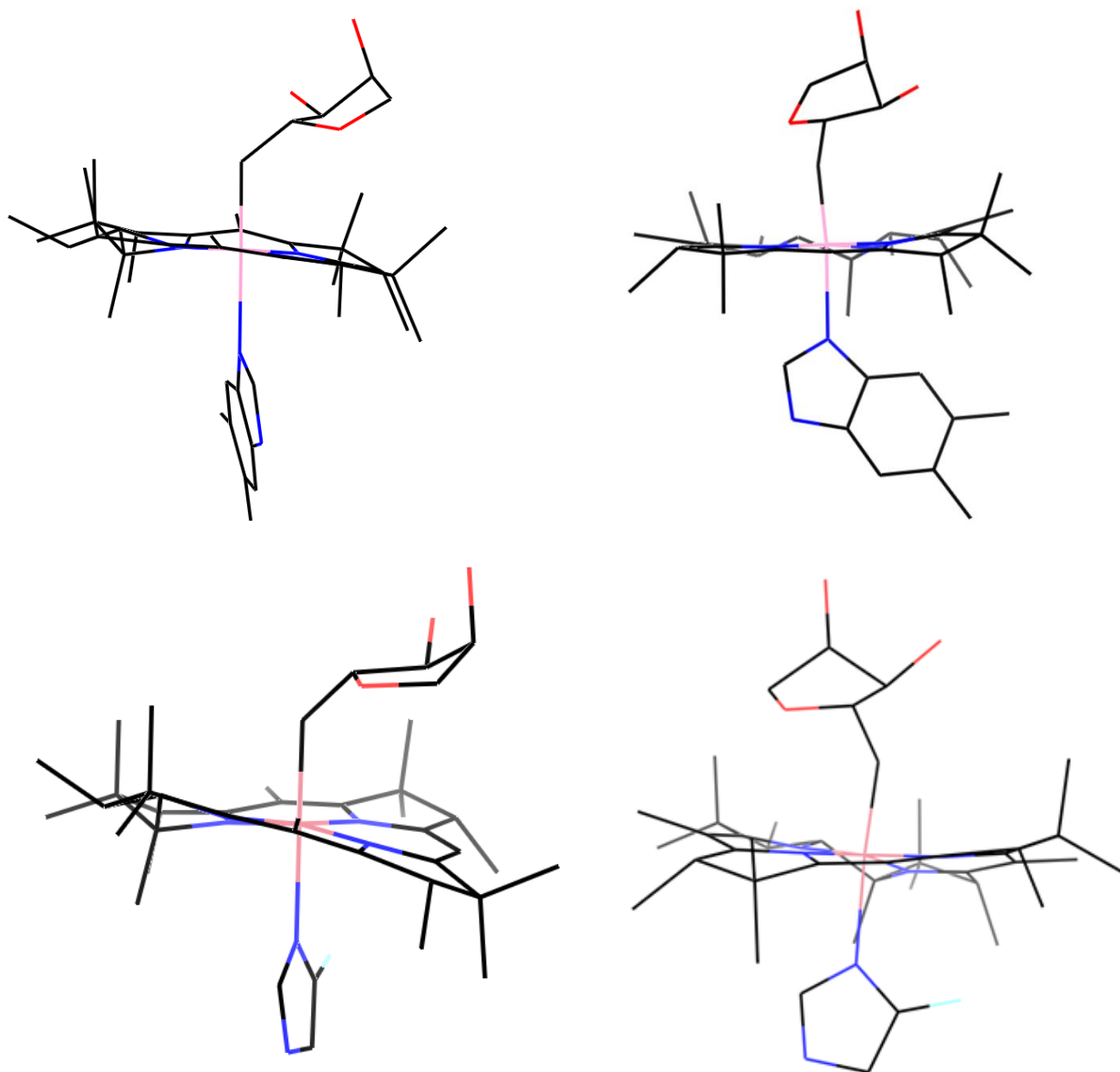


Figure A.2.5. Two perspectives of the QM/MM-optimized geometries for AdoCbl (top) and Ado(F-Im)Cbl (bottom). Only non-hydrogen atoms in the QM regions are shown.

Table A.2.2. Geometric parameters describing corrin ring deformation in the computed structures of AdoCbl and Ado(F-Im)Cbl

Species	Fold Angle ^a (deg)	Plane Fit RMSD (Å) ^b
AdoCbl	14.4	0.0235
Ado(F-Im)Cbl	7.2	0.0653

^aThe fold angle is the normal measure used to describe the ruffling of the corrin ring, and is defined as the angle formed by two planes of best fit. One plane contains N21, C4, C5, C6, N22, C9, and C10; the other contains C10, C11, N23, C14, C15, C16, and N24. Large lower axial ligands (such as the native DMB) typically lie directly underneath the C5···C15 axis and thus cause both planes to tilt “upwards” and the fold angle to increase. In Ado(F-Im)Cbl, however, the rotation of the F-Im ligand relaxes this pressure on the plane that includes C5, causing it to tilt “downwards” instead. This causes the fold angle to decrease.

^bThe root-mean-square displacement of the four coordinating nitrogen atoms in the corrin ring from the plane of best fit. Despite the low fold angle in Ado(F-Im)Cbl, the model suggests a larger out-of-plane distortion than in AdoCbl.

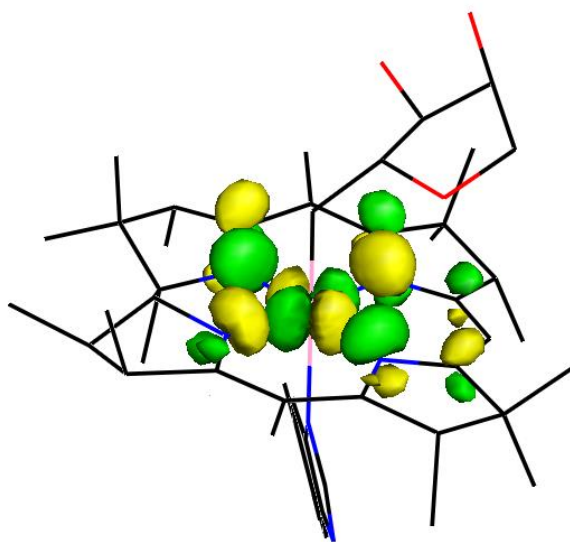


Figure A.2.6. Isosurface plot of the Co $3d_{x^2-y^2}$ -based MO of AdoCbl (MO #230), as obtained from a spin-restricted DFT computation.

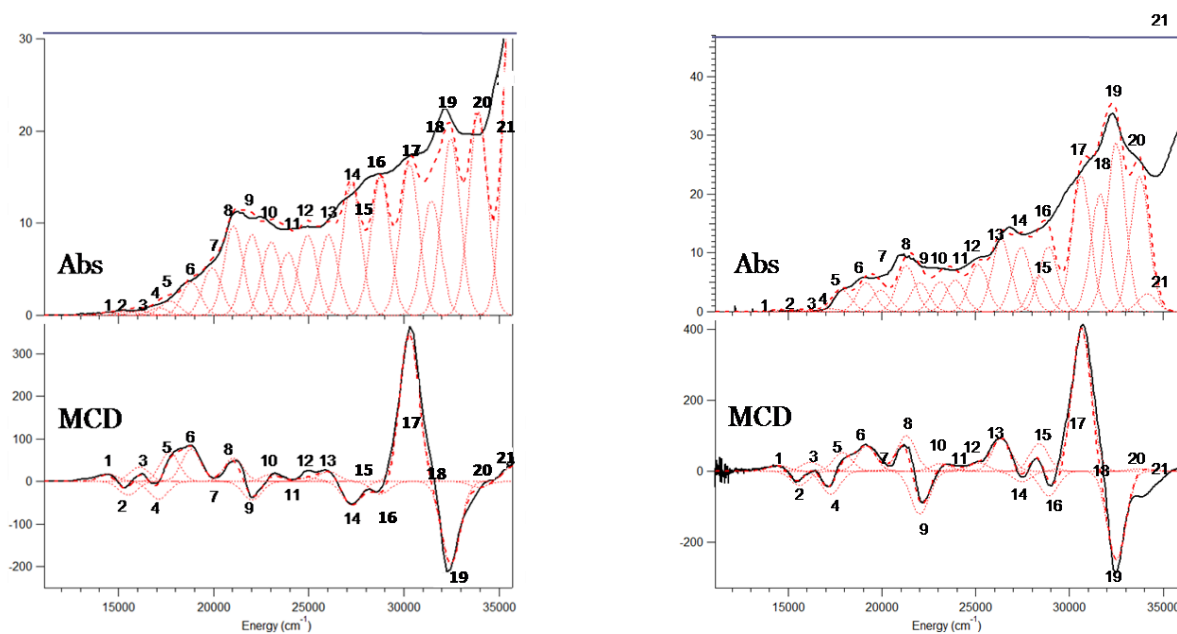


Figure A.2.7. Gaussian deconvolutions of the Abs and MCD spectra of Co(II)Cbl (left) and Co(II)(F-Im)Cbl (right).

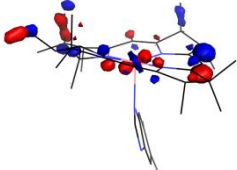
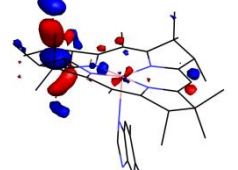
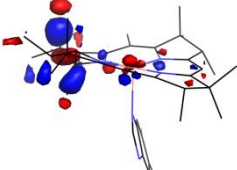
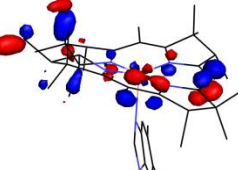
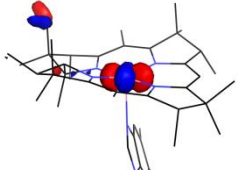
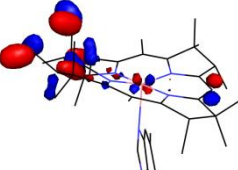
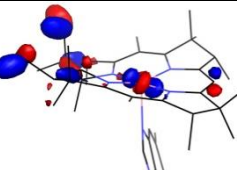
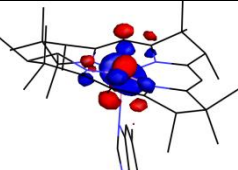
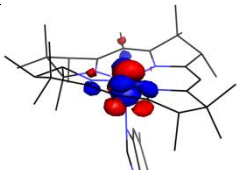
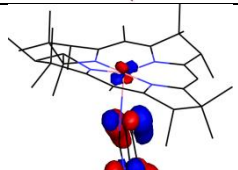
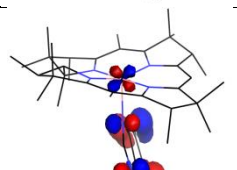
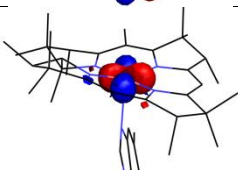
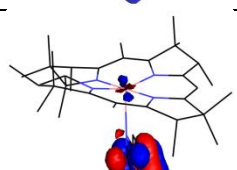
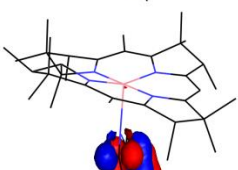
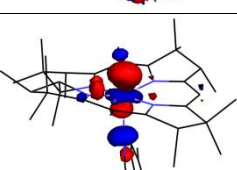
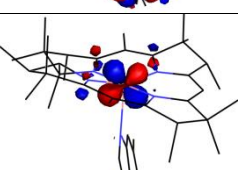
Table A.2.3. Fit parameters from the Gaussian deconvolutions of the Co(II)Cbl Abs and MCD spectra shown in Figure A.2.7.

Band	Energy (cm ⁻¹)	ϵ (M ⁻¹ cm ⁻¹)	$\Delta\epsilon$ (M ⁻¹ cm ⁻¹)
1	14 470	0.3	17
2	15 510	0.4	-31
3	16 110	0.5	34
4	17 110	0.8	-42
5	17 700	1.6	69
6	18 830	3.6	76
7	19 930	5.2	0
8	21 050	9.7	55
9	22 030	8.8	-44
10	23 040	8.0	17
11	23 930	6.8	0
12	24 950	8.7	9
13	26 040	8.8	24
14	27 260	14.2	-56
15	-	-	-
16	28 770	15.1	-29
17	30 300	16.4	349
18	31 450	12.4	0
19	32 470	19.1	-194
20	33 910	22.1	-14
21	35 770	40.9	37

Table A.2.4. Fit parameters from the Gaussian deconvolutions of the Co(II)(F-Im)Cbl Abs and MCD spectra shown in Figure A.2.7.

Band	Energy (cm ⁻¹)	ϵ (M ⁻¹ cm ⁻¹)	$\Delta\epsilon$ (M ⁻¹ cm ⁻¹)
1	14 470	0.3	17
2	15 590	0.2	-40
3	16 180	0.2	25
4	17 260	0.5	-66
5	17 900	3.6	52
6	19 170	4.9	70
7	19 940	3.6	2
8	21 300	7.8	100
9	22 030	4.9	-121
10	23 130	5.1	21
11	23 930	5.4	5
12	25 150	8.0	23
13	26 390	12.3	94
14	27 460	11.0	-30
15	28 380	6.0	77
16	28 900	11.0	-70
17	30 650	23.1	402
18	31 670	20.0	0
19	32 510	28.7	-251
20	33 770	23.0	7
21	37 170	3.0	13

Table A.2.5. Isosurface plots of frontier MOs of Co(II)Cbl, as obtained from a spin-unrestricted DFT computation. Assignments for MOs that contribute to the dominant features of the computed Abs spectrum are presented in Table 4 of the main text

MO #	Spin-Up MOs	Spin-Down MOs
183		
184		
185		
186		
187		
188		
189		
190		

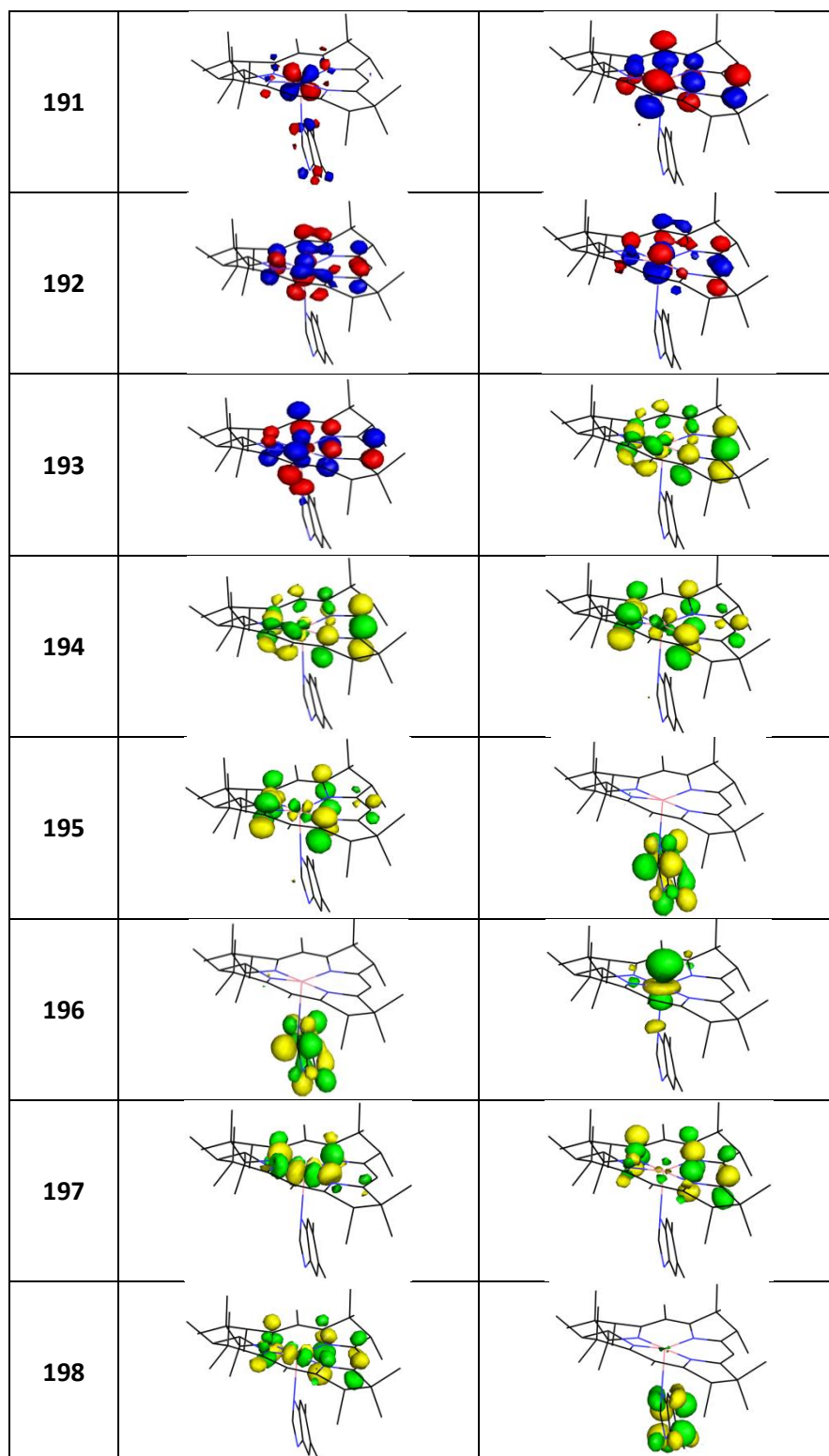
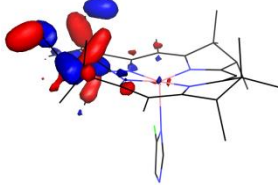
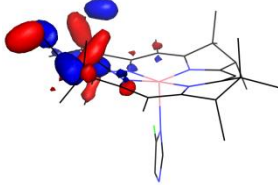
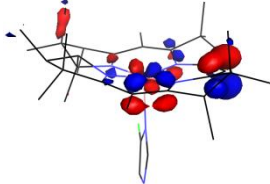
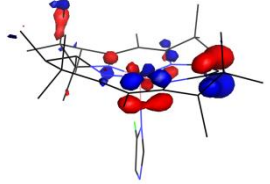
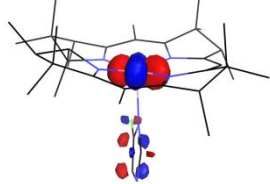
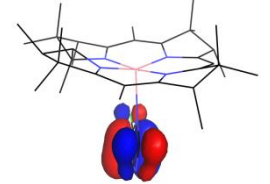
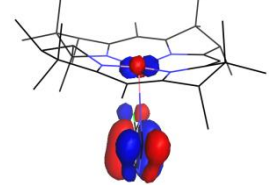
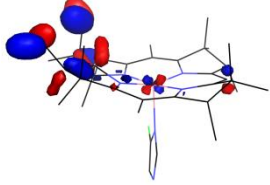
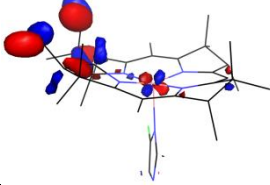
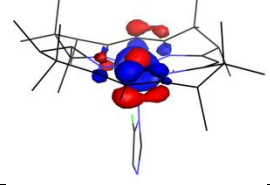
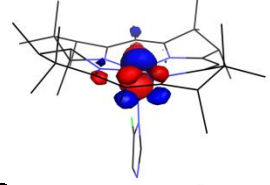
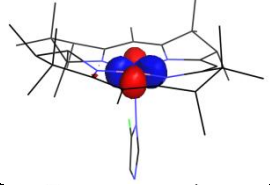
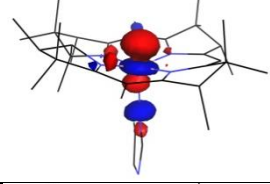
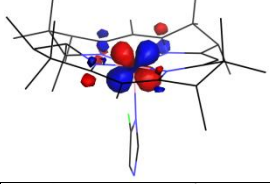
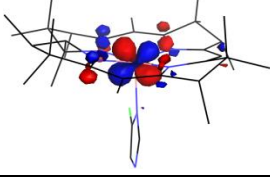
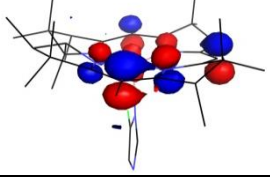


Table A.2.6. Isosurface plots of frontier MOs of Co(II)(F-Im)Cbl, as obtained from a spin-unrestricted DFT computation. Assignments for MOs that contribute to the dominant features of the computed Abs spectrum are presented in Table 5 of the main text

MO #	Spin-Up MOs	Spin-Down MOs
167		
168		
169		
170		
171		
172		
173		
174		

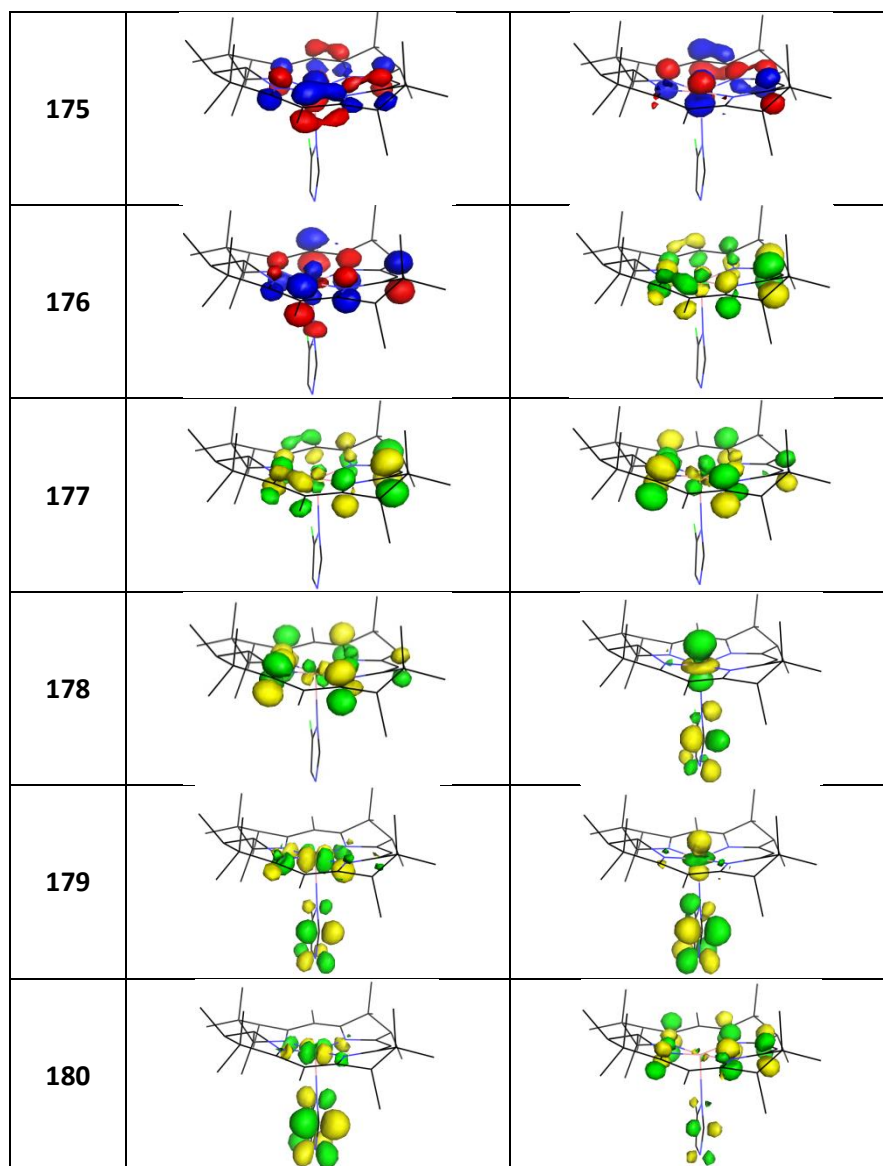


Table A.2.7. Optimized Cartesian Coordinates for AdoCbl (QM Region)

Atom	X (Å)	Y (Å)	Z (Å)	Atom	X (Å)	Y (Å)	Z (Å)
Co	0.000	0.000	0.000	C	-1.060	-0.414	3.025
N	1.894	0.000	0.000	N	-0.033	0.113	2.379
N	0.021	1.954	-0.000	C	0.675	0.837	3.339
N	-1.920	-0.201	0.134	C	1.850	1.608	3.227
N	0.229	-1.868	0.028	C	2.331	2.304	4.347
C	2.595	-1.307	0.267	C	3.568	3.165	4.223
C	2.742	-1.527	1.786	C	1.632	2.227	5.601
C	3.988	-1.098	-0.492	C	2.127	3.019	6.788
C	5.165	-1.923	0.056	C	0.474	1.440	5.722
C	3.779	-1.413	-1.998	C	-0.090	-0.242	-2.018
H	4.625	-1.187	-2.682	C	-0.837	0.591	-3.028
C	4.190	0.453	-0.308	O	-2.249	0.667	-2.822
C	4.944	0.957	0.962	C	-2.771	1.762	-3.611
H	6.027	1.272	0.850	C	-0.436	2.047	-3.298
C	2.750	0.950	-0.308	C	-1.566	2.471	-4.257
C	2.397	2.333	-0.523	H	-3.609	1.379	-4.368
C	3.515	3.260	-0.973	H	3.177	2.763	7.045
C	1.105	2.790	-0.253	H	2.112	4.110	6.576
C	0.676	4.277	-0.194	H	1.502	2.843	7.684
C	1.629	5.075	0.736	H	4.409	2.786	4.842
C	0.626	4.862	-1.655	H	3.923	3.203	3.175
H	0.859	5.946	-1.717	H	3.382	4.210	4.548
C	-0.805	4.180	0.347	H	2.396	-5.314	-1.254
C	-1.191	4.767	1.736	H	3.502	-4.004	-0.899
H	-0.949	4.161	2.662	H	-1.280	-5.800	0.587
C	-1.095	2.699	0.212	H	0.410	-6.090	1.015
C	-2.387	2.187	0.308	H	-1.064	-4.949	-1.834
C	-2.770	0.844	0.249	H	0.483	-4.166	-2.258
C	-4.232	0.430	0.394	H	0.470	-5.816	-1.564
C	-5.104	1.079	-0.704	H	-3.356	-4.326	0.735
C	-4.707	0.919	1.784	H	-3.867	-3.567	-0.802
C	-4.139	-1.140	0.230	H	-2.485	-4.665	-0.768
C	-4.899	-1.982	1.301	H	-4.237	-2.777	1.690
H	-5.881	-2.481	1.021	H	-5.101	-1.338	2.178
C	-2.625	-1.399	0.132	H	-4.055	0.538	2.595
C	-2.061	-2.674	0.007	H	-4.665	2.025	1.832
C	-2.986	-3.863	-0.203	H	-5.752	0.625	2.004
C	-0.625	-2.873	0.004	H	-5.003	2.184	-0.692
C	0.113	-4.241	-0.078	H	-4.811	0.718	-1.708
C	-0.015	-4.821	-1.512	H	-6.177	0.857	-0.545
C	-0.367	-5.297	0.963	H	-0.732	5.773	1.829
H	-0.572	-4.940	2.025	H	-2.287	4.944	1.734
C	1.606	-3.792	0.174	H	1.297	4.302	-2.333
C	2.736	-4.655	-0.435	H	-0.385	4.722	-2.082
H	3.258	-5.247	0.344	H	1.907	4.502	1.640
C	1.596	-2.340	-0.306	H	2.571	5.345	0.225
H	-1.823	-0.360	5.084	H	1.163	6.026	1.062
N	-1.095	-0.087	4.365	H	4.196	3.555	-0.147
C	0.009	0.744	4.590	H	4.144	2.770	-1.743

Atom	X (Å)	Y (Å)	Z (Å)	Atom	X (Å)	Y (Å)	Z (Å)
H	3.131	4.189	-1.422	H	4.704	0.867	-1.195
H	4.389	1.835	1.354	H	-1.807	-1.004	2.492
H	4.890	0.198	1.765	H	1.757	-3.737	1.266
H	3.580	-2.498	-2.114	H	-4.528	-1.378	-0.786
H	2.867	-0.911	-2.377	H	-3.189	2.926	0.444
H	5.285	-1.858	1.152	H	-3.269	2.468	-2.908
H	5.048	-2.994	-0.201	H	-0.342	2.115	-5.696
H	6.118	-1.599	-0.405	H	1.519	2.014	-3.285
H	3.221	-0.671	2.289	H	-0.455	-1.277	-2.107
H	1.747	-1.669	2.246	H	0.973	-0.238	-2.326
H	3.351	-2.429	1.989	H	-0.636	0.059	-4.000
H	1.671	-2.318	-1.413	H	-1.706	3.580	-4.262
H	-1.444	4.734	-0.373	O	-1.305	1.976	-5.561
H	-0.055	1.411	6.686	H	-0.506	2.632	-2.361
H	2.359	1.693	2.258	O	0.819	2.218	-3.938

Table A.2.8. Optimized Cartesian Coordinates for Ado(F-Im)Cbl (QM Region)

Atom	X (Å)	Y (Å)	Z (Å)	Atom	X (Å)	Y (Å)	Z (Å)
Co	0.000	0.000	0.000	C	-3.951	0.538	2.821
N	1.885	0.000	0.000	C	-3.982	-1.275	0.918
N	-0.023	1.946	-0.000	C	-4.442	-2.279	2.017
N	-1.879	-0.259	0.340	H	-5.416	-2.802	1.906
N	0.235	-1.868	-0.158	C	-2.538	-1.475	0.434
C	2.588	-1.331	0.129	C	-2.026	-2.712	0.031
C	2.723	-1.766	1.602	C	-3.003	-3.842	-0.238
C	3.992	-1.016	-0.568	C	-0.615	-2.878	-0.233
C	5.163	-1.902	-0.108	C	0.106	-4.185	-0.670
C	3.806	-1.130	-2.108	C	-0.129	-4.367	-2.195
H	4.653	-0.863	-2.736	C	-0.346	-5.489	0.043
C	4.179	0.501	-0.172	H	-0.449	-5.512	1.149
C	4.888	0.842	1.178	C	1.613	-3.799	-0.394
H	5.967	1.103	1.118	C	2.696	-4.463	-1.257
C	2.735	0.986	-0.175	H	2.873	-5.506	-1.020
C	2.369	2.373	-0.369	C	1.591	-2.279	-0.587
C	3.535	3.294	-0.682	H	-0.483	-1.309	5.228
C	1.043	2.799	-0.308	N	-0.221	-0.678	4.405
C	0.513	4.228	-0.600	C	0.204	0.643	4.516
C	1.281	5.423	0.003	C	-0.266	-0.980	3.069
C	0.339	4.366	-2.147	N	0.128	0.054	2.324
H	1.219	4.515	-2.770	C	0.436	1.039	3.213
C	-0.967	4.138	-0.030	F	0.928	2.211	2.820
C	-1.452	5.016	1.153	H	0.327	1.169	5.466
H	-1.183	4.762	2.201	C	-0.037	0.070	-2.034
C	-1.159	2.653	0.179	C	-1.277	0.072	-2.922
C	-2.391	2.109	0.569	O	-2.217	-0.958	-2.598
C	-2.707	0.753	0.694	C	-3.543	-0.428	-2.616
C	-4.026	0.260	1.296	C	-2.095	1.380	-3.049
C	-5.252	0.999	0.719	C	-3.506	0.865	-3.427

Atom	X (Å)	Y (Å)	Z (Å)	Atom	X (Å)	Y (Å)	Z (Å)
O	-3.576	0.607	-4.813	H	4.259	3.338	0.155
O	-1.663	2.248	-4.095	H	4.100	2.940	-1.571
H	-4.254	-1.162	-2.936	H	3.233	4.329	-0.890
H	2.489	-4.332	-2.335	H	4.364	1.703	1.646
H	3.657	-3.944	-1.075	H	4.774	0.005	1.892
H	-1.310	-5.805	-0.395	H	3.571	-2.183	-2.357
H	0.362	-6.297	-0.240	H	2.922	-0.546	-2.432
H	-1.202	-4.468	-2.436	H	5.315	-1.904	0.986
H	0.259	-3.507	-2.778	H	5.019	-2.954	-0.428
H	0.387	-5.280	-2.551	H	6.111	-1.568	-0.575
H	-3.205	-4.509	0.625	H	3.125	-0.965	2.244
H	-3.975	-3.438	-0.571	H	1.741	-2.061	2.010
H	-2.640	-4.486	-1.058	H	3.390	-2.648	1.676
H	-3.669	-3.063	2.138	H	1.667	-2.078	-1.675
H	-4.466	-1.747	2.986	H	-1.635	4.437	-0.868
H	-3.091	0.025	3.301	H	4.719	1.019	-0.986
H	-3.829	1.626	2.998	H	-0.624	-1.917	2.632
H	-4.881	0.222	3.337	H	1.825	-4.004	0.675
H	-5.164	2.094	0.867	H	-4.614	-1.393	0.010
H	-5.378	0.811	-0.365	H	-3.191	2.828	0.789
H	-6.183	0.694	1.234	H	-3.832	-0.142	-1.575
H	-1.163	6.070	0.961	H	-2.978	1.276	-5.218
H	-2.563	5.017	1.094	H	-0.691	2.345	-4.055
H	-0.249	3.512	-2.536	H	0.580	-0.792	-2.323
H	-0.313	5.250	-2.325	H	0.562	0.972	-2.254
H	1.612	5.232	1.041	H	-0.889	-0.132	-3.957
H	2.177	5.704	-0.578	H	-4.296	1.583	-3.093
H	0.634	6.321	-0.005	H	-2.137	1.920	-2.077

Table A.2.9. Optimized Cartesian Coordinates for Co(II)Cbl (QM Region)

Atom	X (Å)	Y (Å)	Z (Å)	Atom	X (Å)	Y (Å)	Z (Å)
Co	0.000	0.000	0.000	C	0.558	4.175	-0.657
N	1.880	-0.000	-0.000	C	1.356	5.434	-0.252
N	-0.007	1.944	-0.000	C	0.448	4.030	-2.218
N	-1.917	-0.194	-0.129	H	0.349	4.972	-2.754
N	0.213	-1.771	-0.615	C	-0.881	4.167	-0.044
C	2.543	-1.352	-0.050	C	-1.130	4.872	1.322
C	2.513	-2.043	1.327	H	-0.684	4.400	2.223
C	4.011	-0.988	-0.567	C	-1.153	2.682	0.017
C	5.119	-1.949	-0.101	C	-2.441	2.163	0.145
C	3.976	-0.892	-2.120	C	-2.796	0.815	0.088
H	4.893	-0.588	-2.620	C	-4.237	0.340	0.260
C	4.183	0.460	0.016	C	-5.196	1.039	-0.730
C	4.686	0.642	1.482	C	-4.646	0.688	1.714
H	5.746	0.927	1.645	C	-4.105	-1.200	-0.064
C	2.757	0.982	-0.074	C	-4.662	-2.190	1.006
C	2.416	2.377	-0.214	H	-5.606	-2.741	0.800
C	3.540	3.364	-0.486	C	-2.606	-1.382	-0.332
C	1.086	2.790	-0.226	C	-2.058	-2.574	-0.813

Atom	X (Å)	Y (Å)	Z (Å)	Atom	X (Å)	Y (Å)	Z (Å)
C	-3.017	-3.658	-1.273	H	-3.887	-2.948	1.247
C	-0.627	-2.735	-0.956	H	-4.812	-1.624	1.945
C	0.125	-3.964	-1.544	H	-3.957	0.237	2.458
C	-0.008	-3.924	-3.090	H	-4.603	1.786	1.859
C	-0.374	-5.352	-1.047	H	-5.678	0.368	1.952
H	-0.521	-5.518	0.047	H	-5.203	2.138	-0.581
C	1.605	-3.639	-1.106	H	-4.903	0.843	-1.782
C	2.749	-4.189	-1.973	H	-6.236	0.684	-0.585
H	2.918	-5.250	-1.824	H	-0.784	5.924	1.250
C	1.599	-2.110	-1.022	H	-2.227	4.923	1.479
H	-1.846	-1.643	4.640	H	1.333	3.485	-2.604
N	-1.211	-1.069	3.997	H	-0.424	3.395	-2.478
C	-0.428	0.027	4.385	H	1.707	5.417	0.795
C	-1.013	-1.228	2.642	H	2.237	5.600	-0.897
N	-0.166	-0.344	2.137	H	0.706	6.324	-0.375
C	0.259	0.436	3.212	H	3.686	4.090	0.338
C	1.237	1.445	3.281	H	4.504	2.849	-0.638
C	1.486	2.081	4.506	H	3.349	3.945	-1.409
C	2.560	3.142	4.602	H	4.060	1.433	1.948
C	0.724	1.723	5.671	H	4.479	-0.271	2.073
C	0.931	2.477	6.964	H	3.725	-1.885	-2.537
C	-0.223	0.684	5.613	H	3.153	-0.223	-2.444
H	1.988	2.437	7.301	H	5.134	-2.096	0.994
H	0.680	3.553	6.837	H	5.011	-2.948	-0.572
H	0.295	2.077	7.776	H	6.116	-1.568	-0.397
H	3.366	2.844	5.306	H	2.916	-1.399	2.127
H	3.036	3.322	3.618	H	1.472	-2.297	1.600
H	2.163	4.110	4.971	H	3.102	-2.981	1.302
H	2.607	-3.951	-3.045	H	1.744	-1.685	-2.037
H	3.691	-3.689	-1.680	H	-1.575	4.645	-0.767
H	-1.318	-5.575	-1.574	H	-0.781	0.420	6.522
H	0.332	-6.128	-1.412	H	1.794	1.731	2.377
H	-1.066	-3.973	-3.413	H	4.845	1.034	-0.657
H	0.428	-2.997	-3.515	H	-1.516	-1.961	2.007
H	0.521	-4.785	-3.544	H	1.735	-4.008	-0.070
H	-3.306	-4.372	-0.476	H	-4.616	-1.370	-1.037
H	-3.949	-3.213	-1.670	H	-3.255	2.896	0.234
H	-2.586	-4.253	-2.097				

Table A.2.10. Optimized Cartesian Coordinates for Co(II)(F-Im)Cbl (QM Region)

Atom	X (Å)	Y (Å)	Z (Å)	Atom	X (Å)	Y (Å)	Z (Å)
Co	0.000	0.000	0.000	H	4.727	-0.488	-2.872
N	1.891	0.000	-0.000	C	4.205	0.462	-0.112
N	0.001	1.940	-0.000	C	4.894	0.583	1.282
N	-1.894	-0.188	-0.359	H	5.997	0.718	1.283
N	0.215	-1.805	-0.556	C	2.771	0.983	-0.046
C	2.556	-1.336	-0.169	C	2.432	2.383	-0.090
C	2.611	-2.070	1.186	C	3.560	3.387	-0.255
C	3.977	-0.948	-0.771	C	1.102	2.790	-0.145
C	5.075	-1.980	-0.458	C	0.607	4.205	-0.527
C	3.828	-0.729	-2.307	C	1.364	5.447	-0.020

Atom	X (Å)	Y (Å)	Z (Å)
C	0.496	4.289	-2.099
H	0.356	3.354	-2.645
C	-0.848	4.153	0.058
C	-1.110	4.692	1.490
H	-0.707	4.130	2.362
C	-1.138	2.680	-0.058
C	-2.430	2.186	-0.257
C	-2.752	0.859	-0.520
C	-4.066	0.406	-1.148
C	-3.850	0.461	-2.689
C	-5.277	1.278	-0.792
C	-4.088	-1.095	-0.696
C	-4.819	-1.420	0.643
H	-5.781	-1.975	0.600
C	-2.587	-1.375	-0.576
C	-2.040	-2.653	-0.692
C	-2.985	-3.835	-0.797
C	-0.606	-2.807	-0.815
C	0.131	-4.020	-1.455
C	-0.290	-4.080	-2.946
C	-0.136	-5.413	-0.802
H	-0.212	-5.478	0.307
C	1.643	-3.588	-1.304
C	2.613	-3.989	-2.431
H	2.886	-5.039	-2.418
C	1.564	-2.067	-1.107
H	-1.471	-1.592	4.824
N	-0.908	-1.028	4.107
C	0.173	-0.202	4.404
C	-1.105	-0.970	2.752
N	-0.211	-0.172	2.166
C	0.567	0.306	3.183
F	1.561	1.160	2.962
H	0.560	-0.039	5.414
H	2.236	-3.688	-3.427
H	3.563	-3.438	-2.297
H	-1.058	-5.843	-1.239
H	0.674	-6.101	-1.125
H	-1.384	-4.210	-3.052
H	-0.007	-3.151	-3.483

Atom	X (Å)	Y (Å)	Z (Å)
H	0.202	-4.931	-3.457
H	-3.336	-4.167	0.204
H	-3.889	-3.593	-1.387
H	-2.518	-4.713	-1.271
H	-4.129	-2.030	1.259
H	-4.986	-0.487	1.219
H	-5.515	1.281	0.289
H	-5.091	2.328	-1.097
H	-6.173	0.952	-1.355
H	-3.650	1.502	-3.018
H	-2.981	-0.154	-2.998
H	-4.750	0.091	-3.220
H	-0.752	5.740	1.547
H	-2.213	4.744	1.615
H	-0.338	4.970	-2.368
H	1.408	4.780	-2.498
H	1.630	5.389	1.052
H	2.286	5.638	-0.596
H	0.713	6.335	-0.162
H	3.643	4.077	0.607
H	4.536	2.887	-0.365
H	3.424	4.001	-1.167
H	4.454	1.458	1.803
H	4.644	-0.292	1.913
H	3.434	-1.648	-2.775
H	3.057	0.043	-2.508
H	5.201	-2.163	0.623
H	4.845	-2.954	-0.937
H	6.056	-1.661	-0.862
H	3.106	-1.461	1.962
H	1.582	-2.288	1.531
H	3.155	-3.030	1.097
H	1.596	-1.562	-2.096
H	-1.519	4.721	-0.619
H	4.773	1.084	-0.829
H	-1.885	-1.498	2.194
H	2.023	-4.019	-0.359
H	-4.494	-1.712	-1.521
H	-3.226	2.936	-0.365

Table A.2.11. Optimized Cartesian Coordinates for Co(II)(Me-Im)Cbl (QM Region)

Atom	X (Å)	Y (Å)	Z (Å)	Atom	X (Å)	Y (Å)	Z (Å)
Co	0.000	0.000	0.000	C	-0.025	-0.552	4.417
N	1.896	-0.000	0.000	C	-1.272	-0.907	2.627
N	0.005	1.943	0.000	N	-0.250	-0.170	2.208
N	-1.926	-0.201	-0.307	C	0.542	0.085	3.325
N	0.214	-1.814	-0.517	C	1.771	0.938	3.301
C	2.577	-1.342	-0.114	H	1.917	1.452	4.271
C	2.682	-2.004	1.273	H	1.704	1.698	2.501
C	3.985	-0.959	-0.760	H	2.685	0.343	3.101
C	5.129	-1.935	-0.437	H	0.291	-0.585	5.465
C	3.801	-0.823	-2.301	H	2.374	-4.571	-2.886
H	4.666	-0.506	-2.880	H	3.540	-3.557	-2.060
C	4.207	0.477	-0.161	H	-1.259	-5.709	-1.075
C	4.938	0.646	1.207	H	0.421	-6.206	-1.170
H	6.031	0.852	1.187	H	-1.160	-4.175	-3.117
C	2.774	0.985	-0.070	H	0.326	-3.214	-3.361
C	2.436	2.385	-0.087	H	0.412	-5.003	-3.298
C	3.560	3.393	-0.258	H	-3.297	-4.373	-0.140
C	1.107	2.802	-0.072	H	-3.881	-3.461	-1.567
C	0.610	4.237	-0.352	H	-2.500	-4.539	-1.718
C	1.368	5.407	0.311	H	-4.327	-2.511	1.086
C	0.615	4.324	-1.922	H	-5.397	-1.115	1.157
H	0.584	5.337	-2.318	H	-4.858	0.851	1.467
C	-0.871	4.154	0.132	H	-5.169	2.175	0.315
C	-1.257	4.643	1.555	H	-6.225	0.750	0.306
H	-0.917	4.060	2.440	H	-4.611	2.024	-2.110
C	-1.139	2.679	-0.036	H	-3.973	0.505	-2.815
C	-2.432	2.176	-0.165	H	-5.684	0.594	-2.272
C	-2.796	0.842	-0.339	H	-0.931	5.698	1.675
C	-4.239	0.432	-0.624	H	-2.368	4.669	1.585
C	-4.649	0.918	-2.038	H	1.506	3.804	-2.327
C	-5.173	1.073	0.428	H	-0.255	3.771	-2.329
C	-4.135	-1.142	-0.611	H	1.625	5.211	1.368
C	-4.994	-1.880	0.467	H	2.300	5.667	-0.219
H	-5.860	-2.514	0.168	H	0.729	6.314	0.280
C	-2.622	-1.392	-0.518	H	3.763	3.976	0.662
C	-2.051	-2.648	-0.724	H	4.505	2.904	-0.547
C	-2.974	-3.811	-1.042	H	3.331	4.118	-1.063
C	-0.614	-2.813	-0.780	H	4.459	1.494	1.739
C	0.143	-4.063	-1.325	H	4.767	-0.241	1.845
C	-0.086	-4.115	-2.860	H	3.513	-1.807	-2.718
C	-0.248	-5.443	-0.718	H	2.947	-0.152	-2.528
H	-0.218	-5.586	0.388	H	5.254	-2.127	0.644
C	1.628	-3.672	-0.997	H	4.967	-2.914	-0.930
C	2.733	-4.293	-1.879	H	6.093	-1.553	-0.826
H	3.200	-5.142	-1.388	H	3.229	-1.371	1.991
C	1.585	-2.142	-0.991	H	1.669	-2.189	1.682
H	-1.846	-1.768	4.566	H	3.214	-2.973	1.205
N	-1.170	-1.193	3.962	H	1.654	-1.757	-2.030

Atom	X (Å)	Y (Å)	Z (Å)
H	-1.504	4.738	-0.571
H	4.749	1.086	-0.907
H	-2.086	-1.199	1.961

Atom	X (Å)	Y (Å)	Z (Å)
H	1.806	-3.950	0.058
H	-4.424	-1.491	-1.625
H	-3.235	2.925	-0.197

Table A.2.12. Optimized Cartesian Coordinates for Co(II)(CN-Im)Cbl (QM Region)

Atom	X (Å)	Y (Å)	Z (Å)
Co	0.000	0.000	0.000
N	1.897	-0.000	0.000
N	0.003	1.937	0.000
N	-1.899	-0.192	-0.374
N	0.212	-1.806	-0.560
C	2.564	-1.336	-0.185
C	2.646	-2.074	1.166
C	3.977	-0.948	-0.809
C	5.088	-1.964	-0.489
C	3.808	-0.757	-2.346
H	4.700	-0.525	-2.924
C	4.210	0.473	-0.173
C	4.948	0.603	1.194
H	6.046	0.769	1.157
C	2.776	0.985	-0.068
C	2.433	2.383	-0.111
C	3.556	3.392	-0.272
C	1.102	2.789	-0.155
C	0.596	4.199	-0.542
C	1.358	5.452	-0.071
C	0.446	4.257	-2.112
H	0.346	3.310	-2.649
C	-0.844	4.148	0.078
C	-1.068	4.677	1.520
H	-0.619	4.122	2.373
C	-1.137	2.675	-0.042
C	-2.429	2.184	-0.246
C	-2.749	0.861	-0.536
C	-4.052	0.421	-1.195
C	-3.801	0.467	-2.731
C	-5.253	1.317	-0.872
C	-4.100	-1.078	-0.738
C	-4.829	-1.377	0.610
H	-5.839	-1.845	0.610
C	-2.597	-1.376	-0.613
C	-2.049	-2.650	-0.745
C	-2.975	-3.838	-0.933
C	-0.610	-2.798	-0.855
C	0.129	-3.980	-1.548
C	-0.229	-3.903	-3.057
C	-0.230	-5.405	-1.039

Atom	X (Å)	Y (Å)	Z (Å)
H	-0.089	-5.658	0.039
C	1.635	-3.584	-1.311
C	2.651	-4.018	-2.382
H	2.866	-5.081	-2.348
C	1.564	-2.065	-1.113
H	-1.629	-2.041	4.516
N	-1.020	-1.382	3.927
C	0.124	-0.749	4.364
C	-1.230	-0.979	2.626
N	-0.269	-0.176	2.199
C	0.583	0.002	3.287
C	1.697	0.891	3.301
N	2.595	1.642	3.388
H	0.528	-0.858	5.377
H	2.338	-3.706	-3.395
H	3.617	-3.511	-2.200
H	-1.282	-5.599	-1.311
H	0.354	-6.141	-1.632
H	-1.316	-4.019	-3.226
H	0.078	-2.932	-3.499
H	0.286	-4.708	-3.619
H	-4.034	-3.549	-0.856
H	-2.850	-4.316	-1.926
H	-2.807	-4.632	-0.180
H	-4.173	-2.063	1.189
H	-4.888	-0.443	1.207
H	-5.514	1.334	0.204
H	-5.036	2.361	-1.178
H	-6.142	1.013	-1.456
H	-3.586	1.505	-3.059
H	-2.928	-0.154	-3.019
H	-4.691	0.100	-3.280
H	-0.734	5.733	1.568
H	-2.167	4.701	1.685
H	-0.429	4.887	-2.371
H	1.321	4.793	-2.537
H	1.651	5.415	0.994
H	2.265	5.637	-0.673
H	0.698	6.333	-0.214
H	3.636	4.071	0.597
H	4.534	2.895	-0.385

Atom	X (Å)	Y (Å)	Z (Å)
H	3.416	4.012	-1.179
H	4.500	1.450	1.753
H	4.747	-0.286	1.822
H	3.410	-1.685	-2.792
H	3.035	0.012	-2.550
H	5.230	-2.120	0.596
H	4.865	-2.951	-0.941
H	6.060	-1.642	-0.910
H	3.172	-1.470	1.928

Atom	X (Å)	Y (Å)	Z (Å)
H	1.623	-2.284	1.536
H	3.178	-3.039	1.060
H	1.589	-1.559	-2.101
H	-1.530	4.723	-0.579
H	4.744	1.093	-0.915
H	-2.079	-1.253	1.992
H	1.950	-4.008	-0.337
H	-4.522	-1.691	-1.557
H	-3.223	2.934	-0.350

Table A.2.13. Optimized Cartesian Coordinates for Co(II)ImCbl (QM Region)

Atom	X (Å)	Y (Å)	Z (Å)
Co	0.000	0.000	0.000
N	1.887	0.000	0.000
N	-0.018	1.940	0.000
N	-1.891	-0.205	-0.239
N	0.217	-1.741	-0.709
C	2.569	-1.283	-0.393
C	2.736	-2.212	0.826
C	3.941	-0.749	-1.005
C	5.085	-1.775	-0.981
C	3.662	-0.260	-2.457
H	4.483	0.206	-2.999
C	4.194	0.512	-0.090
C	4.954	0.334	1.262
H	6.048	0.533	1.247
C	2.757	0.985	0.117
C	2.406	2.378	0.213
C	3.549	3.375	0.305
C	1.099	2.786	-0.042
C	0.663	4.113	-0.701
C	1.378	5.422	-0.322
C	0.830	3.762	-2.233
H	0.969	4.609	-2.901
C	-0.859	4.148	-0.369
C	-1.349	4.979	0.846
H	-1.118	4.610	1.869
C	-1.149	2.668	-0.235
C	-2.448	2.156	-0.293
C	-2.795	0.804	-0.288
C	-4.215	0.274	-0.488
C	-4.493	0.237	-2.019
C	-5.295	1.130	0.188
C	-4.033	-1.202	0.020
C	-4.295	-1.469	1.539
H	-5.187	-2.076	1.807
C	-2.556	-1.426	-0.292
C	-2.005	-2.662	-0.630

Atom	X (Å)	Y (Å)	Z (Å)
C	-2.922	-3.872	-0.690
C	-0.600	-2.740	-0.990
C	0.092	-3.818	-1.871
C	-0.456	-3.629	-3.310
C	-0.117	-5.306	-1.469
H	-0.082	-5.604	-0.397
C	1.608	-3.385	-1.767
C	2.498	-3.591	-3.005
H	2.782	-4.624	-3.173
C	1.532	-1.905	-1.368
H	-0.716	-2.515	4.490
N	-0.530	-1.667	3.866
C	-0.423	-0.352	4.300
C	-0.395	-1.649	2.501
N	-0.186	-0.414	2.064
C	-0.194	0.409	3.171
H	-0.032	1.487	3.089
H	-0.510	-0.069	5.355
H	2.042	-3.150	-3.912
H	3.446	-3.041	-2.854
H	-1.082	-5.650	-1.892
H	0.643	-5.913	-2.006
H	-1.554	-3.768	-3.338
H	-0.234	-2.615	-3.703
H	-0.001	-4.367	-4.002
H	-3.073	-4.341	0.307
H	-3.927	-3.610	-1.071
H	-2.530	-4.662	-1.351
H	-3.409	-1.984	1.970
H	-4.357	-0.505	2.085
H	-5.183	1.190	1.288
H	-5.263	2.168	-0.201
H	-6.308	0.746	-0.045
H	-4.463	1.260	-2.448
H	-3.737	-0.375	-2.552
H	-5.495	-0.193	-2.216

Atom	X (Å)	Y (Å)	Z (Å)
H	-0.965	6.015	0.742
H	-2.454	5.063	0.766
H	1.687	3.071	-2.361
H	-0.053	3.191	-2.586
H	1.456	5.575	0.769
H	2.395	5.486	-0.750
H	0.805	6.277	-0.739
H	3.272	4.273	0.881
H	4.424	2.932	0.811
H	3.895	3.717	-0.698
H	4.502	1.021	2.008
H	4.795	-0.684	1.665
H	3.358	-1.127	-3.075
H	2.789	0.424	-2.472

Atom	X (Å)	Y (Å)	Z (Å)
H	5.305	-2.158	0.032
H	4.849	-2.648	-1.624
H	6.020	-1.335	-1.383
H	3.195	-1.692	1.685
H	1.749	-2.581	1.158
H	3.359	-3.092	0.576
H	1.508	-1.280	-2.284
H	-1.391	4.555	-1.257
H	4.729	1.277	-0.683
H	-0.499	-2.502	1.827
H	2.052	-3.938	-0.917
H	-4.649	-1.873	-0.607
H	-3.257	2.889	-0.419

Table A.2.14. Optimized Cartesian Coordinates for Co(II)pyCbi⁺ (QM Region)

Atom	X (Å)	Y (Å)	Z (Å)
Co	0.000	0.000	0.000
N	1.893	-0.000	0.000
N	0.001	1.951	0.000
N	-1.893	-0.184	-0.318
N	0.215	-1.776	-0.620
C	2.560	-1.325	-0.240
C	2.638	-2.119	1.080
C	3.975	-0.907	-0.837
C	5.076	-1.952	-0.589
C	3.813	-0.616	-2.358
H	4.707	-0.346	-2.918
C	4.210	0.469	-0.107
C	4.920	0.506	1.281
H	6.022	0.645	1.284
C	2.776	0.982	0.005
C	2.438	2.384	0.023
C	3.578	3.385	-0.091
C	1.113	2.799	-0.101
C	0.644	4.204	-0.551
C	1.370	5.461	-0.032
C	0.668	4.239	-2.133
H	0.753	3.286	-2.658
C	-0.848	4.170	-0.072
C	-1.217	4.789	1.305
H	-0.887	4.270	2.232
C	-1.134	2.691	-0.124
C	-2.428	2.192	-0.278
C	-2.768	0.850	-0.438
C	-4.141	0.367	-0.901
C	-4.115	0.367	-2.458
C	-5.312	1.238	-0.431

Atom	X (Å)	Y (Å)	Z (Å)
C	-4.089	-1.117	-0.398
C	-4.620	-1.389	1.049
H	-5.559	-1.973	1.153
C	-2.586	-1.384	-0.470
C	-2.034	-2.647	-0.672
C	-2.963	-3.845	-0.759
C	-0.605	-2.776	-0.880
C	0.122	-3.978	-1.538
C	-0.355	-4.084	-3.009
C	-0.106	-5.346	-0.825
H	-0.117	-5.384	0.289
C	1.639	-3.528	-1.456
C	2.552	-3.870	-2.648
H	2.797	-4.925	-2.729
C	1.558	-2.016	-1.198
H	2.138	-3.485	-3.599
H	3.521	-3.351	-2.515
H	-1.052	-5.794	-1.189
H	0.686	-6.042	-1.180
H	-1.449	-4.228	-3.075
H	-0.101	-3.168	-3.581
H	0.129	-4.942	-3.517
H	-3.172	-4.290	0.239
H	-3.940	-3.576	-1.202
H	-2.546	-4.655	-1.381
H	-3.839	-1.932	1.620
H	-4.752	-0.426	1.586
H	-5.407	1.293	0.671
H	-5.195	2.275	-0.808
H	-6.269	0.868	-0.850
H	-3.977	1.396	-2.847

Atom	X (Å)	Y (Å)	Z (Å)	Atom	X (Å)	Y (Å)	Z (Å)
H	-3.284	-0.254	-2.851	H	3.154	-1.548	1.872
H	-5.070	-0.032	-2.858	H	1.618	-2.349	1.439
H	-0.857	5.837	1.336	H	3.181	-3.073	0.936
H	-2.325	4.852	1.343	H	1.580	-1.467	-2.164
H	-0.210	4.794	-2.518	H	-1.468	4.701	-0.824
H	1.549	4.836	-2.449	H	4.762	1.133	-0.796
H	1.545	5.454	1.060	H	2.080	-3.991	-0.553
H	2.339	5.610	-0.539	H	-4.606	-1.761	-1.135
H	0.749	6.348	-0.274	H	-3.225	2.932	-0.384
H	3.516	4.189	0.662	N	-0.170	-0.256	2.123
H	4.559	2.901	0.035	C	-0.920	-1.238	2.671
H	3.591	3.859	-1.097	C	-1.053	-1.405	4.058
H	4.482	1.345	1.863	C	-0.381	-0.519	4.916
H	4.684	-0.409	1.860	C	0.406	0.495	4.347
H	3.418	-1.515	-2.865	C	0.487	0.587	2.950
H	3.039	0.159	-2.518	H	-1.425	-1.914	1.963
H	5.210	-2.198	0.478	H	-1.677	-2.222	4.452
H	4.847	-2.896	-1.127	H	-0.468	-0.620	6.009
H	6.054	-1.606	-0.978	H	0.956	1.213	4.975
				H	1.098	1.363	2.463

Table A.2.15. Optimized Cartesian Coordinates for Co(II)(Me₂N-py)Cbi⁺ (QM Region)

Atom	X (Å)	Y (Å)	Z (Å)	Atom	X (Å)	Y (Å)	Z (Å)
Co	0.000	0.000	0.000	C	-1.132	2.692	-0.116
N	1.892	-0.000	-0.000	C	-2.428	2.194	-0.266
N	0.002	1.950	0.000	C	-2.768	0.854	-0.429
N	-1.894	-0.181	-0.311	C	-4.140	0.371	-0.900
N	0.213	-1.781	-0.605	C	-4.108	0.379	-2.456
C	2.559	-1.328	-0.220	C	-5.313	1.241	-0.431
C	2.634	-2.103	1.111	C	-4.090	-1.115	-0.404
C	3.974	-0.917	-0.824	C	-4.631	-1.395	1.037
C	5.077	-1.959	-0.565	H	-5.576	-1.973	1.131
C	3.812	-0.645	-2.348	C	-2.586	-1.379	-0.468
H	4.704	-0.366	-2.907	C	-2.038	-2.643	-0.671
C	4.210	0.465	-0.108	C	-2.982	-3.827	-0.781
C	4.913	0.516	1.283	C	-0.609	-2.781	-0.863
H	6.016	0.657	1.290	C	0.121	-3.996	-1.495
C	2.775	0.982	-0.005	C	-0.347	-4.130	-2.966
C	2.439	2.383	0.003	C	-0.104	-5.352	-0.756
C	3.578	3.383	-0.129	H	-0.164	-5.358	0.357
C	1.113	2.797	-0.111	C	1.637	-3.548	-1.407
C	0.641	4.202	-0.559	C	2.560	-3.905	-2.586
C	1.374	5.459	-0.053	H	2.810	-4.960	-2.652
C	0.647	4.230	-2.142	C	1.558	-2.031	-1.172
H	0.716	3.274	-2.662	H	2.155	-3.533	-3.547
C	-0.844	4.171	-0.062	H	3.525	-3.379	-2.451
C	-1.194	4.782	1.323	H	-1.019	-5.840	-1.148
H	-0.853	4.255	2.242	H	0.722	-6.032	-1.056

Atom	X (Å)	Y (Å)	Z (Å)	Atom	X (Å)	Y (Å)	Z (Å)
H	-1.440	-4.281	-3.034	H	6.056	-1.610	-0.952
H	-0.093	-3.224	-3.553	H	3.151	-1.522	1.894
H	0.143	-4.995	-3.456	H	1.612	-2.316	1.474
H	-3.374	-4.140	0.210	H	3.169	-3.063	0.981
H	-3.860	-3.597	-1.416	H	1.586	-1.497	-2.145
H	-2.496	-4.713	-1.219	H	-1.473	4.706	-0.804
H	-3.856	-1.945	1.609	H	4.768	1.121	-0.802
H	-4.759	-0.435	1.580	H	2.067	-4.002	-0.494
H	-5.415	1.285	0.671	H	-4.600	-1.759	-1.146
H	-5.190	2.282	-0.794	H	-3.225	2.935	-0.371
H	-6.267	0.879	-0.862	N	-0.164	-0.255	2.121
H	-3.969	1.410	-2.840	C	-0.914	-1.229	2.688
H	-3.272	-0.238	-2.849	C	-1.056	-1.400	4.064
H	-5.060	-0.020	-2.865	C	-0.386	-0.516	4.966
H	-0.831	5.829	1.358	C	0.417	0.496	4.352
H	-2.303	4.847	1.375	C	0.493	0.576	2.963
H	-0.227	4.796	-2.519	H	-1.428	-1.910	1.990
H	1.533	4.815	-2.468	H	-1.688	-2.220	4.428
H	1.565	5.451	1.037	H	0.982	1.223	4.951
H	2.336	5.608	-0.572	H	1.115	1.352	2.488
H	0.749	6.345	-0.285	N	-0.501	-0.632	6.324
H	3.532	4.187	0.627	C	0.202	0.299	7.201
H	4.560	2.897	-0.023	C	-1.331	-1.686	6.901
H	3.574	3.859	-1.134	H	1.306	0.240	7.067
H	4.471	1.359	1.855	H	-0.024	0.052	8.254
H	4.676	-0.394	1.867	H	-0.111	1.352	7.024
H	3.434	-1.555	-2.846	H	-0.973	-2.699	6.614
H	3.027	0.117	-2.519	H	-2.395	-1.594	6.584
H	5.208	-2.198	0.505	H	-1.299	-1.614	8.002
H	4.855	-2.907	-1.097				

Table A.2.16. Optimized Cartesian Coordinates for Co(II)(CN-py)Cbi⁺ (QM Region)

Atom	X (Å)	Y (Å)	Z (Å)	Atom	X (Å)	Y (Å)	Z (Å)
Co	0.000	0.000	0.000	C	1.115	2.799	-0.117
N	1.896	-0.000	-0.000	C	0.642	4.197	-0.583
N	0.004	1.953	0.000	C	1.374	5.463	-0.098
N	-1.895	-0.183	-0.319	C	0.642	4.204	-2.166
N	0.218	-1.773	-0.637	H	0.721	3.243	-2.676
C	2.565	-1.327	-0.238	C	-0.843	4.173	-0.082
C	2.635	-2.125	1.079	C	-1.191	4.805	1.293
C	3.985	-0.908	-0.827	H	-0.845	4.297	2.220
C	5.090	-1.948	-0.566	C	-1.132	2.694	-0.116
C	3.833	-0.629	-2.351	C	-2.428	2.194	-0.255
H	4.728	-0.347	-2.903	C	-2.768	0.854	-0.424
C	4.213	0.471	-0.102	C	-4.141	0.380	-0.894
C	4.906	0.512	1.295	C	-4.116	0.401	-2.450
H	6.008	0.651	1.311	C	-5.312	1.246	-0.411
C	2.778	0.984	-0.001	C	-4.093	-1.111	-0.412
C	2.441	2.387	0.006	C	-4.619	-1.403	1.032
C	3.581	3.385	-0.119	H	-5.561	-1.982	1.136

Atom	X (Å)	Y (Å)	Z (Å)
C	-2.590	-1.381	-0.493
C	-2.035	-2.639	-0.724
C	-2.957	-3.837	-0.860
C	-0.603	-2.763	-0.924
C	0.126	-3.946	-1.614
C	-0.303	-3.959	-3.105
C	-0.157	-5.344	-0.992
H	-0.142	-5.467	0.116
C	1.641	-3.523	-1.466
C	2.598	-3.874	-2.621
H	2.822	-4.933	-2.699
C	1.566	-2.010	-1.205
H	2.236	-3.472	-3.587
H	3.570	-3.377	-2.441
H	-1.135	-5.707	-1.361
H	0.580	-6.057	-1.420
H	-1.397	-4.075	-3.217
H	-0.012	-3.019	-3.616
H	0.181	-4.798	-3.642
H	-3.021	-4.439	0.072
H	-3.988	-3.535	-1.115
H	-2.629	-4.526	-1.658
H	-3.838	-1.963	1.587
H	-4.739	-0.448	1.585
H	-5.407	1.284	0.692
H	-5.195	2.287	-0.771
H	-6.269	0.883	-0.836
H	-3.984	1.436	-2.827
H	-3.282	-0.211	-2.852
H	-5.069	0.002	-2.855
H	-0.830	5.854	1.306
H	-2.299	4.870	1.348
H	-0.241	4.755	-2.547
H	1.519	4.796	-2.503
H	1.562	5.477	0.992
H	2.338	5.601	-0.618
H	0.751	6.346	-0.348
H	3.506	4.211	0.609
H	4.560	2.907	0.038
H	3.610	3.829	-1.137
H	4.462	1.354	1.868
H	4.662	-0.401	1.872
H	3.458	-1.538	-2.854
H	3.048	0.132	-2.525
H	5.214	-2.195	0.502
H	4.874	-2.892	-1.108
H	6.069	-1.591	-0.943
H	3.144	-1.556	1.877
H	1.613	-2.362	1.430
H	3.182	-3.077	0.936
H	1.598	-1.458	-2.169

Atom	X (Å)	Y (Å)	Z (Å)
H	-1.474	4.695	-0.830
H	4.773	1.133	-0.788
H	2.038	-3.991	-0.546
H	-4.617	-1.739	-1.158
H	-3.226	2.933	-0.354
N	-0.168	-0.261	2.105
C	-0.923	-1.244	2.646
C	-1.066	-1.424	4.027
C	-0.391	-0.539	4.901
C	0.407	0.482	4.333
C	0.489	0.576	2.939
H	-1.427	-1.917	1.934
H	-1.691	-2.237	4.422
H	0.954	1.191	4.972
H	1.106	1.354	2.461
C	-0.509	-0.678	6.326
N	-0.606	-0.791	7.490

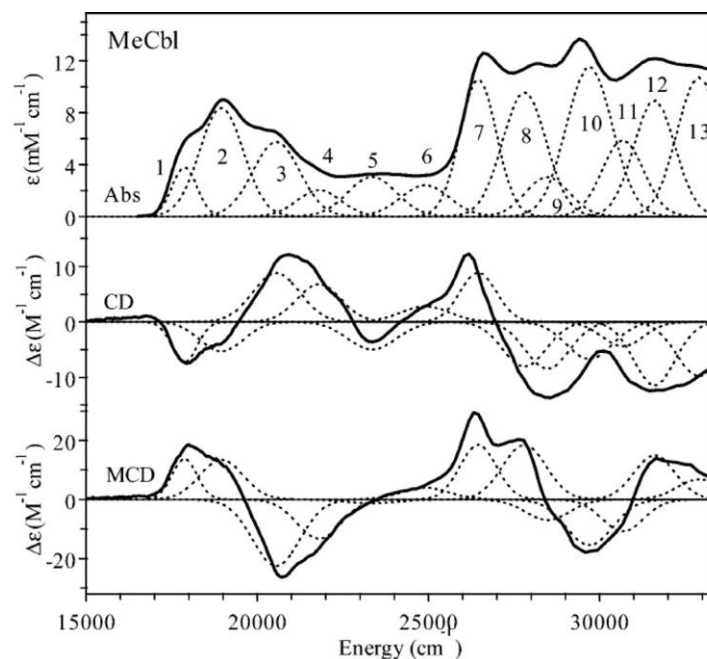


Figure A.3.1. Abs, CD, and MCD spectra of methylcobalamin (MeCbl). The dotted lines represent the results of an iterative Gaussian deconvolution of these spectra. From ref 57.

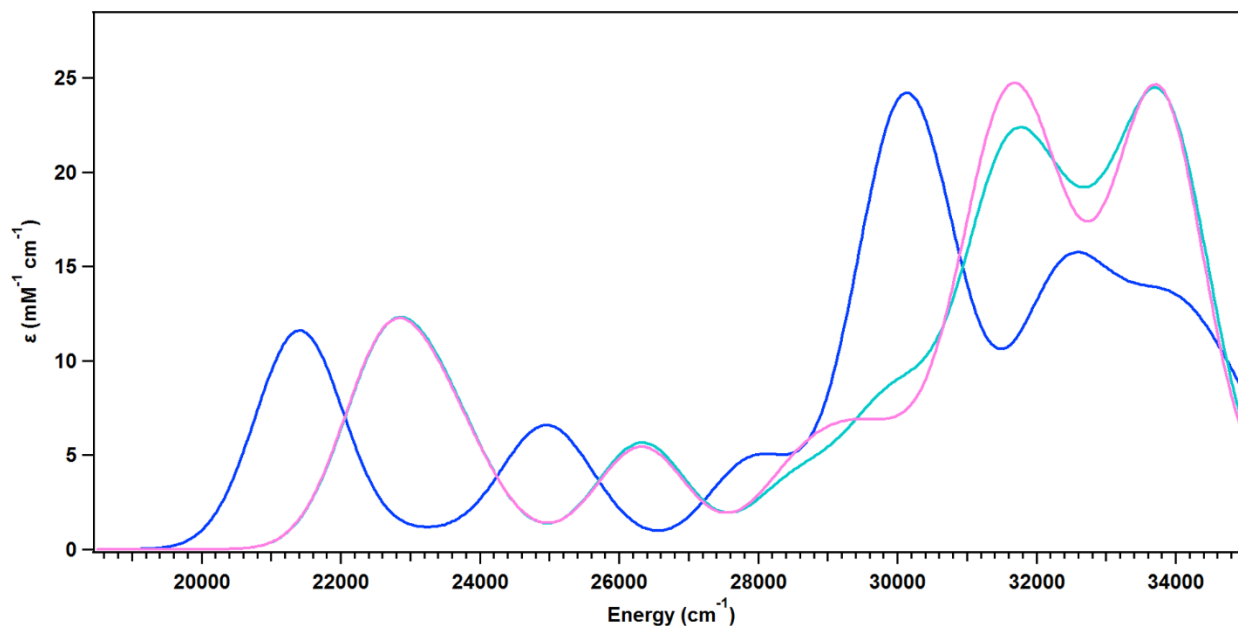


Figure A.3.2. TD-DFT computed Abs spectra for AdoCbl bound to the EAL holoenzyme in the presence of all EAL point charges (blue), no EAL point charges (pink), and only those point charges associated with Y241β (teal).

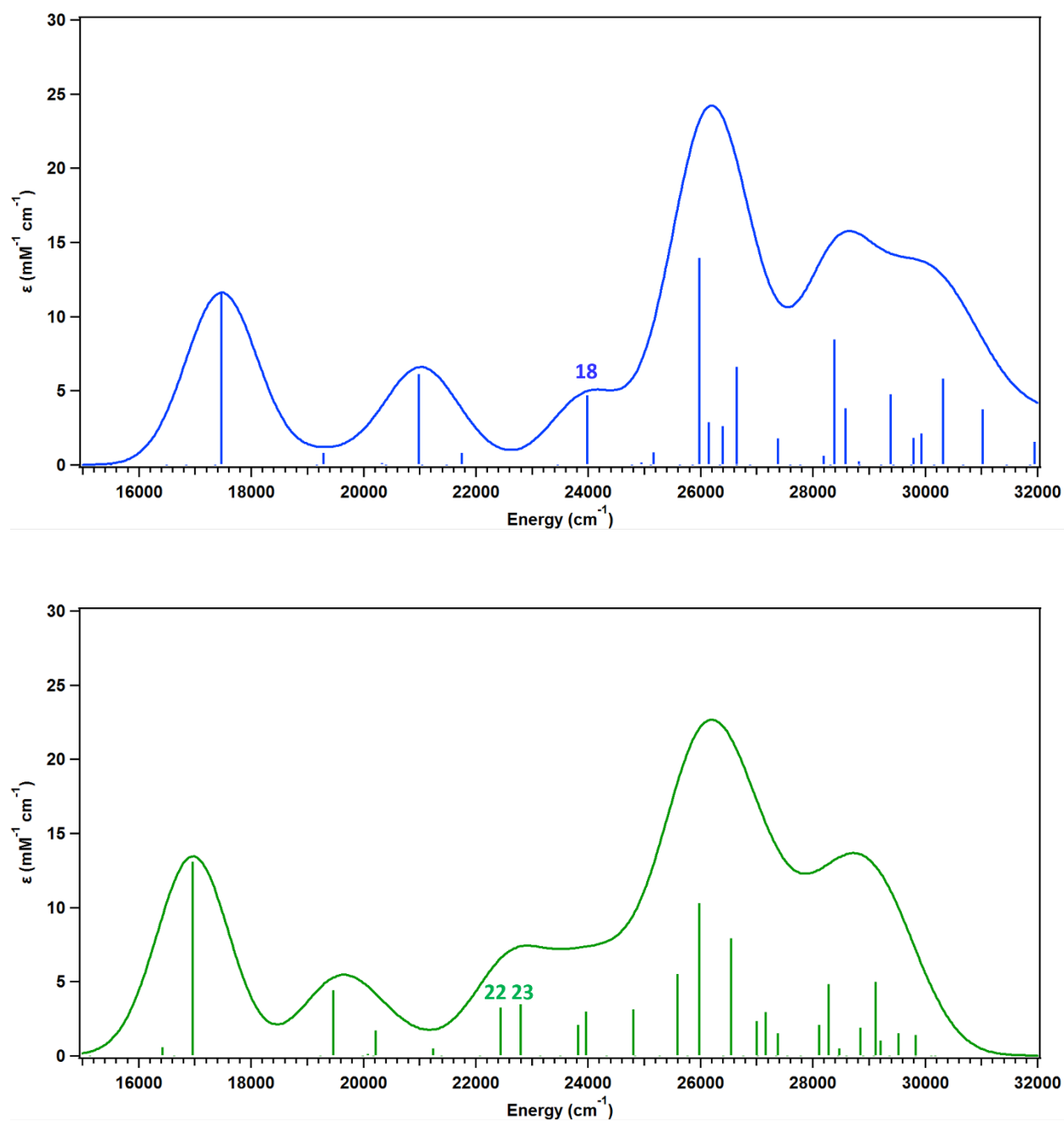


Figure A.3.3. Abs spectra of AdoCbl bound to the EAL holoenzyme (top) and ternary complex (green). Curves are identical to those shown in Figure 3.5. Sticks represent the computed intensity and energy of individual transitions. EDDMs of the three labeled sticks are shown in Figure 3.10.

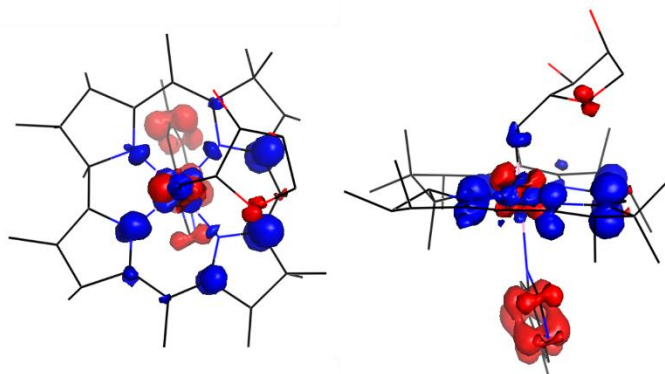


Figure A.3.4. EDDM of the Co $3d_{xz} \rightarrow$ LUMO transition of free AdoCbl viewed from top (left) and side (bottom).

Table A.3.1. One-electron excitations contributing to transition #22 in TD-DFT computed spectrum of the EAL ternary complex.

Transition	%	Donor MO	Acceptor MO
220 \rightarrow 225	29	Co $3d_{z^2}$ /C(Ado)/N(DMB)	corrin π^*
224 \rightarrow 227	25	corrin π /Co $3d_{z^2}$ /N(DMB)	Co $3d_{z^2}$ /C(Ado)/corrin π^*
224 \rightarrow 226	17	corrin π /Co $3d_{z^2}$ /N(DMB)	corrin π^* /Co $3d_{z^2}$
223 \rightarrow 225	5	corrin π /Co $3d_{yz}$	corrin π^*
221 \rightarrow 225	4	DMB π	corrin π^*

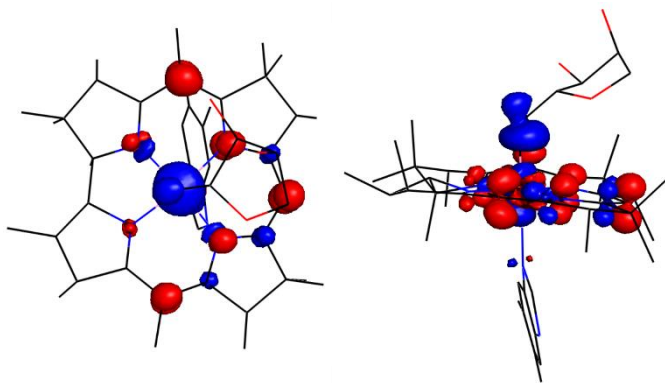


Figure A.3.5. EDDM of the HOMO \rightarrow Co $3d_{z^2}$ transition of free AdoCbl viewed from top (left) and side (bottom).

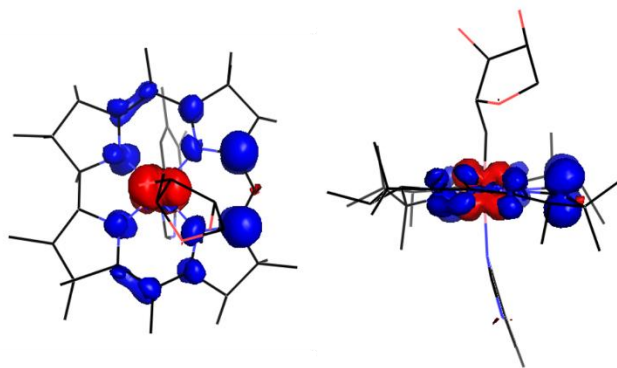


Figure A.3.6. EDDM of the Co $3d_{xz} \rightarrow$ LUMO transition of AdoCbl bound to the EAL holoenzyme. The TD-DFT computation that produced this result was performed in the absence of EAL point charges.

Table A.3.2. Optimized coordinates of QM region for free AdoCbl model.

Atom	X (Å)	Y (Å)	Z (Å)	Atom	X (Å)	Y (Å)	Z (Å)
Co	1.032	-0.400	-0.508	C	1.252	1.632	2.022
N	1.666	-2.126	-0.964	C	0.401	2.015	0.981
N	2.155	-0.433	1.091	C	-0.433	3.291	1.067
N	0.175	1.295	-0.142	C	0.470	4.533	1.242
N	0.022	-0.606	-2.082	C	-1.355	3.148	2.303
C	0.954	-2.865	-2.067	C	-1.175	3.286	-0.329
C	-0.262	-3.623	-1.497	C	-2.713	3.543	-0.282
C	2.108	-3.823	-2.623	H	-3.116	4.556	-0.601
C	1.619	-5.115	-3.301	C	-0.743	1.948	-0.957
C	2.987	-3.010	-3.612	C	-1.189	1.495	-2.204
H	3.912	-3.500	-3.984	C	-2.019	2.433	-3.066
C	2.923	-4.094	-1.303	C	-0.820	0.189	-2.714
C	2.510	-5.308	-0.413	C	-1.293	-0.440	-4.057
H	3.137	-6.251	-0.474	C	-0.591	0.272	-5.245
C	2.725	-2.785	-0.549	C	-2.836	-0.423	-4.270
C	3.558	-2.385	0.560	H	-3.497	-0.677	-3.377
C	4.798	-3.226	0.819	C	-0.726	-1.907	-3.918
C	3.185	-1.323	1.386	C	-0.384	-2.680	-5.214
C	3.845	-0.967	2.740	H	-1.132	-3.471	-5.421
C	3.922	-2.224	3.648	C	0.460	-1.711	-2.972
C	5.258	-0.325	2.476	H	-3.595	-0.831	2.268
H	6.002	-0.518	3.278	N	-2.657	-1.199	1.944
C	2.889	0.160	3.297	C	-1.982	-2.304	2.478
C	2.054	-0.065	4.591	C	-1.827	-0.677	0.973
H	1.094	-0.662	4.515	N	-0.698	-1.350	0.824
C	2.048	0.491	2.082	C	-0.768	-2.396	1.746

Atom	X (Å)	Y (Å)	Z (Å)
C	0.149	-3.426	2.038
C	-0.133	-4.331	3.074
C	0.865	-5.413	3.419
C	-1.350	-4.211	3.828
C	-1.623	-5.156	4.974
C	-2.277	-3.199	3.523
C	2.377	0.515	-1.729
C	3.360	1.606	-1.389
O	2.777	2.807	-0.880
C	3.819	3.600	-0.265
C	4.528	1.341	-0.431
C	5.111	2.762	-0.307
H	3.888	4.678	-0.769
H	-1.611	-6.217	4.644
H	-0.846	-5.063	5.764
H	-2.604	-4.954	5.443
H	0.466	-6.433	3.225
H	1.792	-5.305	2.821
H	1.156	-5.385	4.489
H	-0.260	-2.028	-6.096
H	0.591	-3.191	-5.104
H	-3.147	0.567	-4.658
H	-3.069	-1.147	-5.080
H	-0.774	1.361	-5.264
H	0.508	0.121	-5.213
H	-0.958	-0.141	-6.206
H	-3.111	2.387	-2.871
H	-1.695	3.480	-2.921
H	-1.886	2.215	-4.138
H	-3.237	2.785	-0.893
H	-3.071	3.361	0.749
H	-1.962	2.222	2.253
H	-0.745	3.081	3.226
H	-2.036	4.011	2.427
H	1.125	4.428	2.131
H	1.114	4.682	0.355
H	-0.135	5.447	1.400
H	2.712	-0.529	5.355

Atom	X (Å)	Y (Å)	Z (Å)
H	1.790	0.934	4.999
H	5.671	-0.653	1.504
H	5.160	0.774	2.384
H	3.011	-2.845	3.578
H	4.774	-2.874	3.378
H	4.065	-1.941	4.709
H	4.575	-4.189	1.325
H	5.306	-3.478	-0.133
H	5.537	-2.697	1.442
H	2.532	-4.970	0.643
H	1.457	-5.584	-0.608
H	2.388	-2.773	-4.514
H	3.253	-2.027	-3.176
H	0.875	-5.676	-2.708
H	1.161	-4.895	-4.285
H	2.469	-5.796	-3.502
H	0.010	-4.273	-0.648
H	-1.020	-2.905	-1.135
H	-0.725	-4.254	-2.278
H	1.327	-1.324	-3.545
H	3.533	1.035	3.533
H	-3.193	-3.114	4.126
H	1.095	-3.492	1.484
H	3.996	-4.201	-1.547
H	-2.014	0.228	0.393
H	-1.463	-2.495	-3.343
H	-0.679	4.060	-0.956
H	1.303	2.302	2.891
H	3.528	3.759	0.799
H	6.396	2.242	-1.639
H	5.153	-0.445	-0.921
H	1.731	0.892	-2.537
H	2.966	-0.326	-2.141
H	3.853	1.827	-2.378
H	5.701	2.884	0.635
O	5.894	3.065	-1.451
H	4.136	1.015	0.552
O	5.525	0.459	-0.923

Table A.3.3. Optimized coordinates of QM region for WT EAL holoenzyme model.

Atom	X (Å)	Y (Å)	Z (Å)	Atom	X (Å)	Y (Å)	Z (Å)
Co	6.385	-1.622	3.481	C	7.956	-1.887	-1.818
N	7.801	-0.485	4.007	H	8.455	-2.888	-1.637
N	5.871	-1.805	5.369	C	8.725	-0.463	0.281
N	5.133	-2.905	2.774	C	9.533	0.747	-0.243
N	6.992	-1.253	1.733	H	10.140	0.524	-1.143
C	8.847	-0.135	2.954	C	8.027	-0.167	1.630
C	9.974	-1.196	2.922	H	8.674	-6.466	2.768
C	9.368	1.289	3.476	N	8.524	-5.529	3.240
C	10.811	1.663	3.085	C	8.995	-5.166	4.530
C	8.393	2.382	2.952	C	7.814	-4.421	2.762
H	8.643	3.413	3.261	N	7.801	-3.394	3.629
C	9.204	1.133	5.048	C	8.585	-3.812	4.731
C	10.439	0.602	5.874	C	8.990	-3.105	5.887
H	10.937	1.385	6.520	C	9.761	-3.765	6.864
C	8.009	0.186	5.145	C	10.221	-3.015	8.106
C	7.237	0.020	6.355	C	10.098	-5.154	6.689
C	7.503	0.999	7.501	C	10.877	-5.886	7.757
C	6.257	-0.976	6.446	C	9.724	-5.855	5.521
C	5.340	-1.230	7.683	C	5.033	-0.102	3.517
C	6.069	-1.373	9.046	C	4.223	0.400	2.315
C	4.386	0.044	7.756	O	3.465	-0.667	1.614
H	3.295	-0.094	7.656	C	2.201	-0.795	2.356
C	4.613	-2.578	7.268	C	3.107	1.408	2.800
C	5.028	-3.968	7.883	C	1.729	0.634	2.665
H	6.020	-4.434	7.597	H	1.453	-1.480	1.760
C	4.829	-2.607	5.766	H	11.862	-5.418	7.937
C	4.129	-3.487	4.941	H	10.339	-5.898	8.726
C	4.335	-3.678	3.569	H	11.034	-6.928	7.451
C	3.739	-4.886	2.833	H	11.324	-2.938	8.158
C	2.213	-5.024	3.086	H	9.813	-1.988	8.127
C	4.449	-6.132	3.440	H	9.897	-3.518	9.036
C	4.117	-4.565	1.326	H	8.876	1.615	-0.415
C	4.892	-5.664	0.530	H	10.246	1.059	0.539
H	4.345	-6.321	-0.206	H	7.088	-2.054	-2.474
C	5.007	-3.301	1.431	H	8.637	-1.275	-2.431
C	5.614	-2.695	0.325	H	5.816	-0.137	-1.719
C	5.118	-3.037	-1.081	H	6.379	0.894	-0.375
C	6.655	-1.700	0.516	H	7.342	0.760	-1.866
C	7.515	-1.007	-0.598	H	5.747	-3.751	-1.633
C	6.703	0.198	-1.168	H	4.119	-3.491	-1.052

Atom	X (Å)	Y (Å)	Z (Å)	Atom	X (Å)	Y (Å)	Z (Å)
H	5.046	-2.127	-1.696	H	10.877	1.994	2.033
H	5.688	-5.159	-0.039	H	11.148	2.517	3.699
H	5.405	-6.298	1.267	H	10.423	-1.343	3.917
H	5.549	-6.037	3.405	H	9.579	-2.163	2.583
H	4.173	-6.214	4.505	H	10.772	-0.878	2.230
H	4.149	-7.071	2.946	H	7.470	0.783	1.544
H	1.666	-4.118	2.793	H	3.536	-2.549	7.493
H	1.792	-5.885	2.547	H	10.022	-6.900	5.415
H	2.018	-5.193	4.162	H	8.690	-2.066	6.030
H	4.948	-3.927	8.982	H	8.909	2.113	5.462
H	4.230	-4.661	7.552	H	7.285	-4.367	1.819
H	4.573	0.572	8.707	H	9.428	-1.298	0.456
H	4.681	0.757	6.963	H	3.180	-4.329	0.800
H	6.905	-2.087	9.007	H	3.383	-4.121	5.430
H	6.473	-0.411	9.395	H	2.404	-1.307	3.327
H	5.350	-1.715	9.812	H	1.321	2.062	1.354
H	8.269	0.637	8.213	H	3.497	3.345	2.375
H	7.851	1.970	7.110	H	5.627	0.742	3.926
H	6.590	1.210	8.076	H	4.337	-0.441	4.307
H	10.123	-0.226	6.534	H	4.850	0.880	1.545
H	11.195	0.188	5.187	H	1.158	0.688	3.614
H	8.446	2.379	1.850	O	0.914	1.175	1.581
H	7.348	2.154	3.231	H	3.263	1.706	3.852
H	11.522	0.840	3.234	O	3.018	2.600	1.938

Table A.3.4. Optimized coordinates of QM region for WT EAL ternary complex model.

Atom	X (Å)	Y (Å)	Z (Å)	Atom	X (Å)	Y (Å)	Z (Å)
Co	6.293	-1.114	3.229	C	7.842	0.536	5.119
N	7.715	-0.098	3.948	C	6.946	0.355	6.250
N	5.567	-1.310	5.031	C	7.221	1.168	7.515
N	5.122	-2.412	2.370	C	5.917	-0.595	6.208
N	7.181	-0.827	1.591	C	5.027	-1.054	7.418
C	8.902	0.166	3.025	C	5.843	-1.300	8.716
C	9.880	-1.037	3.030	C	3.935	0.032	7.725
C	9.574	1.479	3.655	H	3.310	-0.188	8.620
C	11.112	1.465	3.502	C	4.317	-2.341	6.825
C	8.979	2.760	2.986	C	4.647	-3.769	7.383
H	9.517	3.705	3.205	H	5.661	-4.194	7.120
C	9.101	1.414	5.179	C	4.599	-2.233	5.337
C	10.143	0.873	6.224	C	3.978	-3.099	4.433
H	10.661	1.679	6.823	C	4.277	-3.233	3.076

Atom	X (Å)	Y (Å)	Z (Å)
C	3.792	-4.450	2.271
C	2.266	-4.700	2.395
C	4.518	-5.680	2.903
C	4.261	-4.069	0.807
C	4.982	-5.197	0.006
H	4.397	-5.834	-0.719
C	5.186	-2.838	1.029
C	5.951	-2.242	0.015
C	5.614	-2.552	-1.450
C	6.991	-1.276	0.345
C	7.963	-0.587	-0.660
C	7.158	0.545	-1.366
C	8.586	-1.511	-1.757
H	9.057	-2.476	-1.410
C	9.033	0.055	0.334
C	9.798	1.316	-0.137
H	10.501	1.101	-0.967
C	8.212	0.269	1.628
H	8.649	-6.176	2.687
N	8.469	-5.237	3.149
C	8.918	-4.847	4.440
C	7.731	-4.153	2.655
N	7.655	-3.126	3.521
C	8.428	-3.519	4.641
C	8.744	-2.806	5.821
C	9.537	-3.424	6.807
C	9.903	-2.679	8.082
C	10.002	-4.771	6.609
C	10.865	-5.435	7.655
C	9.688	-5.487	5.432
C	5.293	0.693	2.741
C	3.936	1.383	3.066
O	2.884	1.019	2.080
C	2.224	-0.128	2.729
C	3.295	1.155	4.467
C	2.011	0.279	4.188
H	1.280	-0.482	2.132
H	11.797	-4.865	7.831
H	10.352	-5.528	8.632
H	11.133	-6.443	7.315
H	10.991	-2.480	8.148
H	9.382	-1.708	8.145
H	9.634	-3.259	8.985

Atom	X (Å)	Y (Å)	Z (Å)
H	9.119	2.139	-0.400
H	10.418	1.693	0.697
H	7.832	-1.753	-2.522
H	9.355	-0.941	-2.298
H	6.256	0.169	-1.868
H	6.849	1.316	-0.644
H	7.793	1.016	-2.127
H	6.298	-3.256	-1.954
H	4.602	-2.972	-1.538
H	5.630	-1.623	-2.042
H	5.796	-4.733	-0.574
H	5.481	-5.863	0.727
H	5.612	-5.544	2.951
H	4.173	-5.803	3.946
H	4.294	-6.617	2.368
H	1.939	-4.548	3.440
H	1.685	-4.035	1.738
H	2.023	-5.746	2.154
H	4.525	-3.780	8.482
H	3.875	-4.453	6.982
H	4.439	1.004	7.880
H	3.256	0.158	6.868
H	6.847	-1.711	8.529
H	5.965	-0.362	9.280
H	5.297	-1.991	9.380
H	7.801	0.606	8.270
H	7.797	2.075	7.284
H	6.291	1.490	8.008
H	9.653	0.189	6.939
H	10.906	0.276	5.697
H	9.024	2.657	1.891
H	7.907	2.863	3.245
H	11.581	0.522	3.806
H	11.376	1.642	2.444
H	11.575	2.258	4.110
H	10.212	-1.288	4.050
H	9.399	-1.922	2.598
H	10.777	-0.802	2.432
H	7.668	1.230	1.574
H	3.226	-2.245	6.942
H	10.085	-6.496	5.311
H	8.369	-1.793	5.971
H	8.786	2.437	5.469

Atom	X (Å)	Y (Å)	Z (Å)
H	7.227	-4.125	1.698
H	9.792	-0.698	0.591
H	3.367	-3.713	0.256
H	3.258	-3.800	4.862
H	2.944	-0.976	2.723
H	1.042	1.877	4.845
H	3.539	2.894	5.505
H	5.330	0.589	1.645

Atom	X (Å)	Y (Å)	Z (Å)
H	6.095	1.372	3.088
H	4.105	2.467	2.902
H	2.001	-0.612	4.842
O	0.784	1.048	4.342
H	4.010	0.650	5.130
O	2.789	2.379	5.109

Table A.3.5. Optimized coordinates of QM region for E287αA holoenzyme model.

Atom	X (Å)	Y (Å)	Z (Å)
Co	6.911	-1.371	3.346
N	8.296	-0.245	3.971
N	6.331	-1.635	5.198
N	5.716	-2.651	2.537
N	7.575	-0.909	1.644
C	9.370	0.140	2.967
C	10.442	-0.973	2.858
C	9.970	1.493	3.59
C	11.471	1.704	3.305
C	9.105	2.678	3.054
H	9.426	3.686	3.287
C	9.685	1.308	5.143
C	10.756	0.650	6.1
H	11.449	1.312	6.66
C	8.457	0.388	5.137
C	7.645	0.158	6.311
C	7.870	1.057	7.528
C	6.665	-0.841	6.316
C	5.666	-1.109	7.484
C	6.261	-1.256	8.907
C	4.709	0.165	7.466
H	3.643	0.016	7.364
C	4.979	-2.454	7.006
C	5.412	-3.846	7.599
H	6.404	-4.262	7.33
C	5.261	-2.440	5.515
C	4.602	-3.294	4.631
C	4.883	-3.451	3.266
C	4.364	-4.661	2.477
C	2.839	-4.884	2.655
C	5.110	-5.887	3.083

Atom	X (Å)	Y (Å)	Z (Å)
C	4.794	-4.288	0.997
C	5.545	-5.377	0.167
H	4.969	-5.994	-0.547
C	5.680	-3.024	1.179
C	6.327	-2.364	0.127
C	5.906	-2.660	-1.316
C	7.317	-1.329	0.401
C	8.190	-0.564	-0.653
C	7.316	0.549	-1.308
C	8.809	-1.449	-1.791
H	9.329	-2.381	-1.493
C	9.284	0.109	0.293
C	9.978	1.411	-0.187
H	10.659	1.228	-1.014
C	8.545	0.240	1.643
H	9.334	-6.248	2.552
N	9.159	-5.308	3.039
C	9.628	-4.949	4.328
C	8.406	-4.219	2.581
N	8.351	-3.211	3.471
C	9.137	-3.630	4.573
C	9.450	-2.968	5.782
C	10.197	-3.647	6.764
C	10.490	-2.974	8.094
C	10.660	-4.989	6.522
C	11.433	-5.730	7.591
C	10.396	-5.631	5.294
C	5.559	0.139	3.405
C	4.775	0.678	2.204
O	4.040	-0.363	1.449
C	2.791	-0.583	2.2

Atom	X (Å)	Y (Å)	Z (Å)	Atom	X (Å)	Y (Å)	Z (Å)
C	3.646	1.651	2.722	H	8.437	0.552	8.331
C	2.290	0.817	2.621	H	8.432	1.964	7.253
H	2.123	-1.173	1.617	H	6.916	1.396	7.961
H	12.401	-5.242	7.81	H	10.173	0.082	6.846
H	10.874	-5.773	8.546	H	11.358	-0.099	5.556
H	11.618	-6.766	7.272	H	9.104	2.638	1.953
H	11.575	-2.871	8.277	H	8.057	2.529	3.376
H	10.042	-1.966	8.138	H	12.064	0.819	3.573
H	10.085	-3.555	8.943	H	11.658	1.937	2.241
H	9.261	2.208	-0.436	H	11.854	2.554	3.894
H	10.594	1.813	0.637	H	10.844	-1.237	3.849
H	8.035	-1.711	-2.531	H	10.013	-1.882	2.416
H	9.529	-0.830	-2.348	H	11.284	-0.636	2.229
H	6.508	0.130	-1.92	H	7.937	1.161	1.668
H	6.869	1.214	-0.549	H	3.893	-2.448	7.191
H	7.941	1.168	-1.968	H	10.830	-6.615	5.103
H	6.578	-3.339	-1.872	H	9.084	-1.957	5.973
H	4.905	-3.112	-1.349	H	9.403	2.301	5.54
H	5.854	-1.725	-1.896	H	7.876	-4.173	1.638
H	6.321	-4.864	-0.424	H	10.087	-0.615	0.488
H	6.085	-6.049	0.856	H	3.875	-4.004	0.459
H	6.206	-5.755	3.06	H	3.837	-3.942	5.066
H	4.825	-5.994	4.146	H	3.020	-1.167	3.122
H	4.849	-6.827	2.572	H	1.848	2.223	1.296
H	2.243	-4.115	2.145	H	3.880	3.623	2.296
H	2.541	-5.873	2.275	H	6.149	0.967	3.849
H	2.565	-4.864	3.727	H	4.848	-0.225	4.168
H	5.310	-3.836	8.698	H	5.414	1.191	1.467
H	4.647	-4.557	7.229	H	1.777	0.790	3.602
H	4.883	0.759	8.379	O	1.379	1.409	1.646
H	5.007	0.823	6.628	H	3.834	1.975	3.764
H	7.109	-1.955	8.951	O	3.493	2.831	1.848
H	6.605	-0.289	9.298				
H	5.475	-1.618	9.593				

Table A.3.6. Optimized coordinates of QM region for E287αD holoenzyme model.

Atom	X (Å)	Y (Å)	Z (Å)	Atom	X (Å)	Y (Å)	Z (Å)
Co	6.838	-1.488	3.178	C	9.301	0.006	2.757
N	8.231	-0.359	3.774	C	10.361	-1.117	2.659
N	6.282	-1.740	5.039	C	9.917	1.358	3.357
N	5.630	-2.766	2.392	C	11.422	1.551	3.073
N	7.486	-1.039	1.463	C	9.084	2.556	2.807

Atom	X (Å)	Y (Å)	Z (Å)
H	9.442	3.551	3.045
C	9.635	1.196	4.913
C	10.749	0.557	5.834
H	11.221	1.238	6.567
C	8.406	0.283	4.931
C	7.607	0.064	6.116
C	7.849	0.983	7.312
C	6.636	-0.942	6.148
C	5.684	-1.230	7.349
C	6.355	-1.405	8.736
C	4.733	0.045	7.412
H	3.665	-0.095	7.337
C	4.972	-2.568	6.877
C	5.393	-3.969	7.463
H	6.366	-4.408	7.161
C	5.226	-2.552	5.380
C	4.551	-3.406	4.506
C	4.802	-3.559	3.135
C	4.253	-4.759	2.349
C	2.728	-4.970	2.553
C	4.992	-5.999	2.938
C	4.666	-4.386	0.864
C	5.390	-5.485	0.018
H	4.790	-6.069	-0.703
C	5.566	-3.134	1.034
C	6.193	-2.476	-0.032
C	5.722	-2.754	-1.463
C	7.197	-1.453	0.224
C	8.057	-0.694	-0.844
C	7.191	0.444	-1.465
C	8.633	-1.577	-2.005
H	9.128	-2.531	-1.733
C	9.189	-0.055	0.080
C	9.907	1.234	-0.399
H	10.556	1.058	-1.253
C	8.471	0.097	1.440
H	9.235	-6.344	2.408
N	9.064	-5.408	2.899
C	9.541	-5.055	4.187
C	8.312	-4.317	2.449
N	8.264	-3.311	3.342
C	9.057	-3.735	4.438
C	9.381	-3.082	5.650

Atom	X (Å)	Y (Å)	Z (Å)
C	10.130	-3.769	6.626
C	10.431	-3.107	7.961
C	10.581	-5.114	6.376
C	11.341	-5.871	7.444
C	10.312	-5.747	5.144
C	5.484	0.022	3.235
C	4.673	0.563	2.050
O	3.923	-0.472	1.298
C	2.698	-0.705	2.083
C	3.553	1.528	2.608
C	2.201	0.686	2.537
H	2.012	-1.298	1.524
H	12.309	-5.388	7.675
H	10.772	-5.915	8.394
H	11.522	-6.908	7.124
H	11.517	-2.977	8.126
H	9.956	-2.112	8.030
H	10.056	-3.711	8.809
H	9.206	2.059	-0.602
H	10.563	1.596	0.413
H	7.846	-1.799	-2.744
H	9.364	-0.967	-2.557
H	6.376	0.047	-2.082
H	6.754	1.096	-0.688
H	7.817	1.074	-2.113
H	6.330	-3.476	-2.034
H	4.696	-3.148	-1.466
H	5.708	-1.820	-2.045
H	6.185	-4.991	-0.563
H	5.903	-6.187	0.698
H	6.090	-5.873	2.919
H	4.703	-6.121	3.998
H	4.725	-6.929	2.410
H	2.126	-4.303	1.921
H	2.447	-6.011	2.331
H	2.440	-4.783	3.604
H	5.332	-3.953	8.567
H	4.599	-4.663	7.124
H	4.935	0.598	8.346
H	5.010	0.737	6.595
H	7.191	-2.120	8.716
H	6.743	-0.452	9.121
H	5.604	-1.765	9.462

Atom	X (Å)	Y (Å)	Z (Å)	Atom	X (Å)	Y (Å)	Z (Å)
H	8.547	0.546	8.050	H	9.360	2.197	5.295
H	8.266	1.948	6.984	H	7.774	-4.265	1.510
H	6.913	1.214	7.841	H	9.976	-0.807	0.248
H	10.288	-0.274	6.395	H	3.745	-4.083	0.340
H	11.548	0.110	5.220	H	3.797	-4.057	4.956
H	9.091	2.513	1.706	H	2.962	-1.292	2.994
H	8.028	2.445	3.120	H	1.691	2.112	1.255
H	12.005	0.643	3.273	H	3.772	3.506	2.196
H	11.608	1.850	2.025	H	6.083	0.852	3.660
H	11.818	2.352	3.721	H	4.789	-0.337	4.017
H	10.787	-1.355	3.647	H	5.296	1.083	1.305
H	9.911	-2.031	2.252	H	1.722	0.642	3.535
H	11.187	-0.803	1.999	O	1.254	1.278	1.600
H	7.875	1.028	1.458	H	3.769	1.840	3.648
H	3.889	-2.548	7.078	O	3.366	2.719	1.756
H	10.739	-6.733	4.948				
H	9.014	-2.072	5.849				

Table A.3.7. Optimized coordinates of QM region for E287αQ holoenzyme model.

Atom	X (Å)	Y (Å)	Z (Å)	Atom	X (Å)	Y (Å)	Z (Å)
Co	6.861	-1.511	3.216	C	4.967	-2.594	6.902
N	8.262	-0.393	3.819	C	5.375	-3.994	7.497
N	6.294	-1.771	5.073	H	6.348	-4.440	7.205
N	5.638	-2.774	2.420	C	5.233	-2.580	5.408
N	7.518	-1.060	1.505	C	4.555	-3.425	4.530
C	9.338	-0.021	2.807	C	4.805	-3.567	3.158
C	10.409	-1.135	2.722	C	4.246	-4.758	2.365
C	9.935	1.338	3.409	C	2.718	-4.952	2.559
C	11.433	1.577	3.119	C	4.971	-6.005	2.955
C	9.085	2.530	2.867	C	4.666	-4.383	0.883
H	9.406	3.526	3.154	C	5.391	-5.479	0.039
C	9.657	1.162	4.966	H	4.791	-6.079	-0.669
C	10.784	0.521	5.870	C	5.572	-3.135	1.061
H	11.190	1.175	6.665	C	6.209	-2.477	0.000
C	8.426	0.250	4.978	C	5.743	-2.744	-1.435
C	7.607	0.040	6.153	C	7.227	-1.469	0.264
C	7.819	0.975	7.342	C	8.097	-0.719	-0.798
C	6.637	-0.969	6.182	C	7.245	0.436	-1.410
C	5.673	-1.255	7.378	C	8.667	-1.595	-1.964
C	6.338	-1.427	8.768	H	9.149	-2.558	-1.701
C	4.711	0.011	7.434	C	9.239	-0.099	0.125
H	3.642	-0.129	7.361	C	9.963	1.181	-0.364

Atom	X (Å)	Y (Å)	Z (Å)
H	10.627	1.009	-1.209
C	8.518	0.065	1.483
H	9.183	-6.395	2.427
N	9.028	-5.455	2.918
C	9.506	-5.112	4.208
C	8.300	-4.348	2.465
N	8.267	-3.344	3.359
C	9.045	-3.784	4.459
C	9.372	-3.138	5.674
C	10.104	-3.840	6.653
C	10.408	-3.185	7.991
C	10.531	-5.193	6.403
C	11.273	-5.963	7.473
C	10.258	-5.819	5.169
C	5.529	0.014	3.289
C	4.730	0.562	2.104
O	3.958	-0.464	1.367
C	2.720	-0.655	2.142
C	3.633	1.559	2.643
C	2.258	0.757	2.572
H	2.030	-1.233	1.576
H	12.248	-5.496	7.707
H	10.701	-5.998	8.421
H	11.439	-7.002	7.153
H	11.495	-3.067	8.160
H	9.942	-2.186	8.062
H	10.025	-3.788	8.837
H	9.260	1.998	-0.579
H	10.606	1.553	0.455
H	7.880	-1.800	-2.707
H	9.412	-0.984	-2.498
H	6.370	0.058	-1.953
H	6.893	1.137	-0.632
H	7.859	1.008	-2.121
H	6.355	-3.459	-2.011
H	4.718	-3.141	-1.447
H	5.732	-1.805	-2.010
H	6.169	-4.978	-0.559
H	5.925	-6.164	0.718
H	6.069	-5.889	2.938
H	4.680	-6.123	4.015
H	4.698	-6.934	2.429
H	2.128	-4.230	1.977

Atom	X (Å)	Y (Å)	Z (Å)
H	2.414	-5.969	2.268
H	2.439	-4.830	3.622
H	5.305	-3.973	8.600
H	4.580	-4.685	7.155
H	4.913	0.572	8.363
H	4.984	0.697	6.611
H	7.170	-2.146	8.754
H	6.728	-0.474	9.151
H	5.582	-1.781	9.493
H	8.512	0.556	8.094
H	8.219	1.945	7.007
H	6.873	1.194	7.857
H	10.373	-0.384	6.352
H	11.629	0.183	5.247
H	9.135	2.524	1.765
H	8.022	2.383	3.136
H	12.062	0.690	3.273
H	11.594	1.925	2.081
H	11.802	2.370	3.792
H	10.843	-1.351	3.712
H	9.965	-2.062	2.335
H	11.231	-0.828	2.052
H	7.933	1.003	1.491
H	3.882	-2.572	7.090
H	10.666	-6.813	4.975
H	9.021	-2.123	5.872
H	9.385	2.159	5.359
H	7.769	-4.284	1.524
H	10.019	-0.858	0.294
H	3.746	-4.082	0.356
H	3.796	-4.074	4.975
H	2.955	-1.240	3.063
H	1.853	2.137	1.212
H	3.876	3.528	2.213
H	6.140	0.836	3.714
H	4.827	-0.333	4.070
H	5.364	1.057	1.350
H	1.764	0.739	3.563
O	1.339	1.379	1.625
H	3.848	1.883	3.678
O	3.485	2.737	1.766

Table A.3.8. Optimized coordinates of QM region for N193 α A holoenzyme model.

Atom	X (Å)	Y (Å)	Z (Å)	Atom	X (Å)	Y (Å)	Z (Å)
Co	6.897	-1.490	3.408	C	9.150	0.133	0.327
N	8.236	-0.317	4.034	C	9.783	1.462	-0.166
N	6.381	-1.823	5.270	H	10.470	1.317	-0.998
N	5.724	-2.789	2.586	C	8.434	0.217	1.700
N	7.501	-0.963	1.701	H	9.349	-6.300	2.534
C	9.270	0.134	3.015	N	9.175	-5.368	3.034
C	10.389	-0.931	2.892	C	9.645	-5.027	4.328
C	9.807	1.504	3.634	C	8.421	-4.273	2.594
C	11.290	1.777	3.317	N	8.376	-3.273	3.492
C	8.917	2.672	3.115	C	9.166	-3.706	4.586
H	9.268	3.663	3.373	C	9.508	-3.052	5.792
C	9.545	1.311	5.195	C	10.252	-3.750	6.764
C	10.750	0.851	6.104	C	10.581	-3.083	8.087
H	11.214	1.673	6.688	C	10.667	-5.107	6.524
C	8.397	0.295	5.212	C	11.376	-5.885	7.612
C	7.604	0.020	6.395	C	10.400	-5.732	5.288
C	7.841	0.903	7.620	C	5.491	-0.046	3.545
C	6.673	-1.027	6.401	C	4.722	0.578	2.380
C	5.777	-1.448	7.612	O	3.990	-0.428	1.569
C	6.557	-1.589	8.950	C	2.740	-0.657	2.309
C	4.640	-0.371	7.735	C	3.589	1.517	2.967
H	3.890	-0.559	8.504	C	2.233	0.736	2.725
C	5.121	-2.791	7.082	H	2.076	-1.254	1.739
C	5.501	-4.179	7.689	H	12.374	-5.467	7.843
H	6.519	-4.559	7.474	H	10.799	-5.873	8.557
C	5.412	-2.739	5.594	H	11.486	-6.936	7.309
C	4.772	-3.599	4.702	H	11.627	-3.246	8.396
C	4.962	-3.656	3.316	H	10.407	-1.994	8.033
C	4.389	-4.812	2.484	H	9.957	-3.480	8.911
C	2.864	-4.991	2.709	H	9.029	2.224	-0.413
C	5.116	-6.087	2.999	H	10.384	1.895	0.655
C	4.766	-4.370	1.010	H	7.919	-1.658	-2.506
C	5.519	-5.410	0.116	H	9.417	-0.782	-2.275
H	4.939	-5.984	-0.630	H	6.297	0.104	-1.786
C	5.633	-3.099	1.216	H	6.705	1.196	-0.439
C	6.238	-2.393	0.169	H	7.699	1.174	-1.914
C	5.782	-2.647	-1.271	H	6.457	-3.280	-1.874
C	7.219	-1.356	0.454	H	4.797	-3.131	-1.293
C	8.051	-0.554	-0.600	H	5.680	-1.694	-1.812
C	7.129	0.541	-1.220	H	6.296	-4.867	-0.445
C	8.682	-1.413	-1.750	H	6.058	-6.120	0.764
H	9.197	-2.352	-1.462	H	6.213	-5.979	2.938

Atom	X (Å)	Y (Å)	Z (Å)	Atom	X (Å)	Y (Å)	Z (Å)
H	4.873	-6.231	4.067	H	9.978	-1.866	2.490
H	4.810	-6.998	2.461	H	11.192	-0.577	2.223
H	2.646	-5.135	3.785	H	7.795	1.117	1.743
H	2.292	-4.115	2.372	H	4.022	-2.726	7.192
H	2.489	-5.883	2.185	H	10.806	-6.727	5.094
H	5.336	-4.177	8.783	H	9.172	-2.031	5.987
H	4.773	-4.901	7.271	H	9.158	2.272	5.582
H	5.090	0.617	7.934	H	7.883	-4.211	1.656
H	4.113	-0.289	6.764	H	9.985	-0.569	0.481
H	7.604	-1.900	8.796	H	3.826	-4.084	0.511
H	6.569	-0.636	9.504	H	4.071	-4.314	5.142
H	6.074	-2.328	9.606	H	2.966	-1.232	3.239
H	8.634	0.508	8.284	H	1.791	2.265	1.522
H	8.144	1.921	7.324	H	4.084	3.459	2.694
H	6.938	1.007	8.238	H	6.033	0.748	4.093
H	10.408	0.083	6.822	H	4.769	-0.514	4.239
H	11.526	0.377	5.482	H	5.362	1.131	1.672
H	8.904	2.653	2.014	H	1.630	0.708	3.654
H	7.870	2.538	3.447	O	1.447	1.336	1.653
H	11.944	0.925	3.541	H	3.743	1.691	4.050
H	11.439	2.049	2.256	O	3.470	2.808	2.269
H	11.638	2.630	3.918				
H	10.837	-1.150	3.876				

Table A.3.9. Optimized coordinates of QM region for Y241βA holoenzyme model.

Atom	X (Å)	Y (Å)	Z (Å)	Atom	X (Å)	Y (Å)	Z (Å)
Co	6.917	-1.174	3.419	C	7.574	1.267	7.640
N	8.221	0.011	4.094	C	6.547	-0.701	6.376
N	6.328	-1.522	5.244	C	5.512	-1.066	7.481
N	5.816	-2.514	2.562	C	6.005	-1.047	8.947
N	7.580	-0.641	1.740	C	4.327	-0.059	7.237
C	9.297	0.479	3.121	H	3.545	-0.115	7.988
C	10.451	-0.550	3.030	C	5.025	-2.491	7.018
C	9.773	1.863	3.780	C	5.574	-3.804	7.665
C	11.248	2.205	3.527	H	6.633	-4.078	7.487
C	8.847	2.994	3.239	C	5.361	-2.454	5.538
H	9.043	4.003	3.583	C	4.798	-3.353	4.635
C	9.486	1.621	5.323	C	5.054	-3.410	3.260
C	10.599	0.999	6.252	C	4.556	-4.584	2.406
H	11.311	1.671	6.774	C	3.035	-4.841	2.590
C	8.312	0.634	5.275	C	5.331	-5.830	2.926
C	7.459	0.358	6.413	C	4.949	-4.111	0.948

Atom	X (Å)	Y (Å)	Z (Å)
C	5.719	-5.129	0.049
H	5.136	-5.700	-0.696
C	5.781	-2.824	1.189
C	6.387	-2.086	0.164
C	5.951	-2.320	-1.286
C	7.342	-1.037	0.483
C	8.210	-0.236	-0.540
C	7.348	0.907	-1.163
C	8.834	-1.077	-1.708
H	9.340	-2.034	-1.466
C	9.296	0.403	0.433
C	10.015	1.695	-0.032
H	10.757	1.503	-0.804
C	8.520	0.536	1.765
H	9.654	-5.939	2.599
N	9.438	-5.011	3.093
C	9.959	-4.604	4.350
C	8.574	-3.987	2.680
N	8.487	-2.981	3.568
C	9.359	-3.337	4.630
C	9.643	-2.672	5.846
C	10.499	-3.285	6.786
C	10.731	-2.630	8.139
C	11.122	-4.547	6.481
C	12.047	-5.218	7.481
C	10.859	-5.203	5.257
C	5.510	0.284	3.484
C	4.731	0.823	2.281
O	4.011	-0.225	1.524
C	2.792	-0.496	2.307
C	3.587	1.775	2.798
C	2.262	0.882	2.775
H	2.127	-1.091	1.733
H	12.797	-5.824	6.948
H	12.580	-4.496	8.121
H	11.476	-5.883	8.161
H	11.804	-2.455	8.338
H	10.214	-1.657	8.207
H	10.360	-3.268	8.961
H	9.310	2.477	-0.350
H	10.569	2.123	0.823
H	8.065	-1.286	-2.467
H	9.572	-0.432	-2.213

Atom	X (Å)	Y (Å)	Z (Å)
H	6.483	0.521	-1.717
H	6.976	1.600	-0.388
H	7.966	1.491	-1.864
H	6.600	-2.988	-1.878
H	4.942	-2.753	-1.324
H	5.912	-1.362	-1.827
H	6.490	-4.574	-0.510
H	6.267	-5.844	0.686
H	6.425	-5.685	2.872
H	5.087	-5.980	3.993
H	5.064	-6.753	2.387
H	2.767	-4.845	3.662
H	2.423	-4.069	2.102
H	2.751	-5.826	2.187
H	5.379	-3.804	8.752
H	4.947	-4.610	7.238
H	4.714	0.974	7.184
H	3.870	-0.262	6.250
H	6.992	-1.526	9.051
H	6.084	-0.026	9.355
H	5.290	-1.593	9.588
H	8.119	0.793	8.478
H	8.101	2.203	7.397
H	6.581	1.550	8.028
H	10.065	0.437	7.041
H	11.185	0.249	5.691
H	8.966	3.038	2.142
H	7.790	2.730	3.431
H	11.920	1.386	3.817
H	11.433	2.451	2.466
H	11.538	3.094	4.113
H	10.854	-0.796	4.023
H	10.105	-1.485	2.566
H	11.274	-0.138	2.420
H	7.891	1.444	1.751
H	3.930	-2.555	7.144
H	11.361	-6.153	5.048
H	9.169	-1.715	6.077
H	9.156	2.583	5.758
H	7.986	-3.992	1.771
H	10.071	-0.351	0.636
H	4.011	-3.824	0.443
H	4.106	-4.090	5.053

Atom	X (Å)	Y (Å)	Z (Å)
H	3.066	-1.093	3.209
H	1.710	2.225	1.428
H	3.568	3.757	2.346
H	6.054	1.120	3.966
H	4.802	-0.133	4.222
H	5.368	1.346	1.549

Atom	X (Å)	Y (Å)	Z (Å)
H	1.815	0.822	3.786
O	1.260	1.451	1.881
H	3.796	2.152	3.816
O	3.378	2.909	1.873

Table A.3.10. Optimized coordinates of QM region for E287 α A ternary complex model.

Atom	X (Å)	Y (Å)	Z (Å)
Co	6.956	-1.825	3.246
N	8.356	-0.679	3.805
N	6.442	-2.064	5.132
N	5.717	-3.089	2.494
N	7.567	-1.373	1.518
C	9.410	-0.308	2.771
C	10.485	-1.417	2.677
C	10.010	1.062	3.352
C	11.498	1.321	3.032
C	9.130	2.241	2.828
H	9.443	3.248	3.085
C	9.770	0.889	4.910
C	10.897	0.231	5.801
H	11.397	0.905	6.522
C	8.542	-0.023	4.952
C	7.752	-0.216	6.145
C	8.004	0.733	7.311
C	6.793	-1.231	6.217
C	5.843	-1.484	7.429
C	6.523	-1.635	8.816
C	4.896	-0.202	7.465
H	3.828	-0.321	7.340
C	5.121	-2.828	6.996
C	5.499	-4.205	7.659
H	6.451	-4.702	7.380
C	5.391	-2.870	5.501
C	4.702	-3.730	4.644
C	4.911	-3.877	3.265
C	4.301	-5.052	2.491
C	2.774	-5.181	2.733
C	4.996	-6.323	3.058
C	4.686	-4.695	0.995
C	5.383	-5.806	0.143

Atom	X (Å)	Y (Å)	Z (Å)
H	4.772	-6.401	-0.560
C	5.609	-3.452	1.138
C	6.228	-2.806	0.058
C	5.744	-3.094	-1.368
C	7.254	-1.794	0.288
C	8.107	-1.049	-0.800
C	7.248	0.096	-1.418
C	8.659	-1.944	-1.962
H	9.153	-2.896	-1.682
C	9.256	-0.410	0.101
C	9.971	0.874	-0.397
H	10.607	0.695	-1.260
C	8.558	-0.241	1.468
H	9.227	-6.709	2.420
N	9.083	-5.767	2.906
C	9.588	-5.419	4.183
C	8.349	-4.664	2.458
N	8.335	-3.653	3.346
C	9.125	-4.092	4.435
C	9.461	-3.441	5.640
C	10.216	-4.137	6.602
C	10.531	-3.477	7.926
C	10.669	-5.482	6.350
C	11.468	-6.215	7.409
C	10.369	-6.119	5.128
C	5.581	-0.352	3.345
C	4.765	0.219	2.187
O	3.982	-0.799	1.438
C	2.711	-0.932	2.169
C	3.676	1.202	2.783
C	2.279	0.505	2.527
H	2.019	-1.514	1.604
H	12.415	-5.691	7.637

Atom	X (Å)	Y (Å)	Z (Å)	Atom	X (Å)	Y (Å)	Z (Å)
H	10.906	-6.283	8.362	H	7.082	0.957	7.866
H	11.698	-7.242	7.090	H	10.430	-0.592	6.371
H	11.619	-3.392	8.084	H	11.675	-0.231	5.170
H	10.091	-2.466	7.990	H	9.142	2.214	1.726
H	10.126	-4.067	8.766	H	8.080	2.081	3.138
H	9.267	1.698	-0.592	H	12.144	0.449	3.209
H	10.640	1.237	0.404	H	11.643	1.639	1.983
H	7.859	-2.174	-2.684	H	11.861	2.143	3.673
H	9.386	-1.343	-2.531	H	10.930	-1.627	3.664
H	6.387	-0.293	-1.974	H	10.039	-2.348	2.301
H	6.881	0.791	-0.642	H	11.299	-1.110	1.998
H	7.865	0.678	-2.120	H	7.965	0.691	1.481
H	6.361	-3.809	-1.941	H	4.036	-2.777	7.177
H	4.725	-3.505	-1.362	H	10.784	-7.110	4.927
H	5.715	-2.163	-1.954	H	9.109	-2.428	5.844
H	6.159	-5.314	-0.464	H	9.510	1.885	5.309
H	5.918	-6.499	0.814	H	7.802	-4.604	1.526
H	6.097	-6.252	2.994	H	10.047	-1.157	0.271
H	4.746	-6.421	4.130	H	3.755	-4.394	0.488
H	4.665	-7.244	2.551	H	3.952	-4.375	5.110
H	2.220	-4.307	2.361	H	2.894	-1.486	3.122
H	2.373	-6.087	2.256	H	2.113	1.909	1.133
H	2.561	-5.275	3.815	H	4.400	3.052	2.444
H	5.449	-4.122	8.762	H	6.153	0.473	3.820
H	4.673	-4.886	7.372	H	4.881	-0.760	4.097
H	5.071	0.338	8.412	H	5.381	0.738	1.430
H	5.219	0.496	6.673	H	1.649	0.541	3.436
H	7.338	-2.374	8.821	O	1.547	1.148	1.435
H	6.944	-0.684	9.168	H	3.829	1.353	3.869
H	5.766	-1.942	9.559	O	3.649	2.503	2.097
H	8.731	0.318	8.033				
H	8.399	1.700	6.961				

Table A.3.11. Optimized coordinates of QM region for E287αD ternary complex model.

Atom	X (Å)	Y (Å)	Z (Å)	Atom	X (Å)	Y (Å)	Z (Å)
Co	6.960	-1.688	3.254	C	9.980	1.232	3.375
N	8.343	-0.529	3.814	C	11.469	1.517	3.072
N	6.419	-1.933	5.120	C	9.090	2.394	2.828
N	5.744	-2.979	2.491	H	9.288	3.393	3.210
N	7.584	-1.247	1.526	C	9.711	1.067	4.935
C	9.412	-0.156	2.793	C	10.849	0.468	5.855
C	10.511	-1.243	2.729	H	11.266	1.169	6.601

Atom	X (Å)	Y (Å)	Z (Å)
C	8.502	0.132	4.963
C	7.696	-0.073	6.146
C	7.922	0.884	7.314
C	6.755	-1.105	6.211
C	5.819	-1.400	7.425
C	6.519	-1.555	8.800
C	4.848	-0.141	7.508
H	3.781	-0.278	7.394
C	5.117	-2.746	6.970
C	5.531	-4.135	7.579
H	6.498	-4.592	7.284
C	5.376	-2.754	5.476
C	4.703	-3.625	4.620
C	4.936	-3.779	3.248
C	4.375	-4.978	2.471
C	2.851	-5.171	2.691
C	5.111	-6.219	3.058
C	4.769	-4.608	0.981
C	5.522	-5.687	0.138
H	4.940	-6.293	-0.577
C	5.648	-3.341	1.137
C	6.245	-2.677	0.059
C	5.734	-2.950	-1.360
C	7.265	-1.666	0.295
C	8.113	-0.927	-0.793
C	7.260	0.244	-1.371
C	8.619	-1.802	-1.990
H	9.101	-2.776	-1.771
C	9.292	-0.338	0.104
C	10.033	0.927	-0.393
H	10.648	0.751	-1.272
C	8.591	-0.126	1.467
H	9.380	-6.467	2.522
N	9.198	-5.531	3.009
C	9.676	-5.162	4.292
C	8.427	-4.456	2.555
N	8.371	-3.445	3.438
C	9.172	-3.848	4.536
C	9.494	-3.178	5.738
C	10.266	-3.841	6.712
C	10.589	-3.148	8.025
C	10.733	-5.183	6.474
C	11.519	-5.909	7.544

Atom	X (Å)	Y (Å)	Z (Å)
C	10.462	-5.835	5.252
C	5.583	-0.211	3.332
C	4.743	0.318	2.171
O	3.965	-0.730	1.461
C	2.716	-0.883	2.226
C	3.649	1.296	2.760
C	2.265	0.546	2.588
H	2.023	-1.472	1.675
H	12.473	-5.395	7.764
H	10.958	-5.959	8.498
H	11.729	-6.943	7.233
H	11.679	-3.036	8.170
H	10.138	-2.141	8.070
H	10.216	-3.718	8.896
H	9.332	1.759	-0.565
H	10.721	1.270	0.401
H	7.795	-1.982	-2.699
H	9.336	-1.193	-2.560
H	6.366	-0.117	-1.895
H	6.940	0.944	-0.579
H	7.864	0.812	-2.093
H	6.316	-3.681	-1.945
H	4.707	-3.339	-1.336
H	5.715	-2.018	-1.944
H	6.296	-5.169	-0.451
H	6.064	-6.366	0.818
H	6.209	-6.104	3.017
H	4.843	-6.325	4.125
H	4.828	-7.154	2.550
H	2.255	-4.401	2.183
H	2.526	-6.162	2.338
H	2.606	-5.124	3.769
H	5.472	-4.092	8.680
H	4.728	-4.830	7.263
H	5.020	0.364	8.474
H	5.147	0.590	6.735
H	7.321	-2.307	8.803
H	6.961	-0.605	9.135
H	5.767	-1.844	9.557
H	8.705	0.514	7.998
H	8.230	1.878	6.950
H	7.010	1.039	7.905
H	10.440	-0.402	6.398

Atom	X (Å)	Y (Å)	Z (Å)	Atom	X (Å)	Y (Å)	Z (Å)
H	11.682	0.089	5.240	H	7.883	-4.415	1.621
H	9.234	2.460	1.735	H	10.046	-1.130	0.256
H	8.028	2.139	3.002	H	3.835	-4.336	0.461
H	12.128	0.647	3.200	H	3.959	-4.279	5.084
H	11.608	1.902	2.045	H	2.933	-1.435	3.172
H	11.826	2.302	3.759	H	1.974	1.934	1.201
H	10.960	-1.425	3.719	H	4.176	3.215	2.430
H	10.091	-2.189	2.365	H	6.161	0.632	3.765
H	11.317	-0.926	2.044	H	4.898	-0.589	4.114
H	8.014	0.816	1.437	H	5.340	0.826	1.394
H	4.033	-2.723	7.164	H	1.683	0.577	3.528
H	10.898	-6.818	5.063	O	1.459	1.145	1.524
H	9.119	-2.172	5.929	H	3.837	1.505	3.831
H	9.414	2.058	5.322	O	3.559	2.562	2.012

Table A.3.13. Optimized coordinates of QM region for N193αA ternary complex model.

Atom	X (Å)	Y (Å)	Z (Å)	Atom	X (Å)	Y (Å)	Z (Å)
Co	7.279	-1.181	3.286	H	6.996	-4.024	7.395
N	8.622	0.031	3.831	C	5.769	-2.279	5.542
N	6.785	-1.429	5.172	C	5.123	-3.180	4.697
N	6.118	-2.523	2.548	C	5.346	-3.340	3.322
N	7.844	-0.698	1.550	C	4.815	-4.562	2.562
C	9.643	0.444	2.778	C	3.302	-4.801	2.807
C	10.745	-0.636	2.642	C	5.604	-5.772	3.141
C	10.217	1.823	3.365	C	5.174	-4.193	1.063
C	11.691	2.093	2.993	C	5.926	-5.264	0.210
C	9.293	2.982	2.878	H	5.339	-5.893	-0.485
H	9.541	3.976	3.236	C	6.024	-2.902	1.196
C	10.010	1.629	4.930	C	6.586	-2.222	0.108
C	11.176	1.021	5.809	C	6.094	-2.543	-1.307
H	11.706	1.738	6.467	C	7.540	-1.143	0.325
C	8.810	0.680	4.983	C	8.321	-0.352	-0.777
C	8.037	0.460	6.187	C	7.366	0.719	-1.391
C	8.256	1.431	7.349	C	8.923	-1.222	-1.934
C	7.106	-0.582	6.257	H	9.470	-2.144	-1.650
C	6.156	-0.871	7.464	C	9.440	0.370	0.100
C	6.808	-0.954	8.867	C	10.049	1.692	-0.433
C	5.130	0.352	7.459	H	10.699	1.540	-1.293
H	4.069	0.156	7.368	C	8.764	0.493	1.487
C	5.518	-2.259	7.038	H	9.837	-5.950	2.498
C	6.000	-3.619	7.665	N	9.648	-5.013	2.984

Atom	X (Å)	Y (Å)	Z (Å)
C	10.132	-4.630	4.263
C	8.855	-3.949	2.536
N	8.792	-2.934	3.416
C	9.612	-3.322	4.505
C	9.930	-2.641	5.702
C	10.699	-3.295	6.685
C	10.991	-2.599	8.004
C	11.175	-4.636	6.456
C	11.922	-5.376	7.548
C	10.924	-5.288	5.228
C	5.821	0.208	3.355
C	4.956	0.663	2.176
O	4.225	-0.432	1.485
C	2.978	-0.626	2.246
C	3.825	1.608	2.737
C	2.477	0.785	2.609
H	2.299	-1.231	1.691
H	12.895	-4.909	7.789
H	11.340	-5.398	8.491
H	12.086	-6.420	7.245
H	12.074	-2.458	8.168
H	10.512	-1.605	8.044
H	10.620	-3.184	8.866
H	9.283	2.451	-0.651
H	10.686	2.131	0.356
H	8.136	-1.498	-2.655
H	9.617	-0.585	-2.503
H	6.498	0.264	-1.886
H	6.997	1.414	-0.617
H	7.902	1.314	-2.145
H	6.738	-3.223	-1.892
H	5.101	-3.011	-1.279
H	5.996	-1.618	-1.895
H	6.672	-4.735	-0.405
H	6.500	-5.923	0.882
H	6.696	-5.618	3.070
H	5.367	-5.875	4.215
H	5.339	-6.720	2.647
H	2.676	-4.030	2.337
H	2.993	-5.787	2.429
H	3.080	-4.793	3.891

Atom	X (Å)	Y (Å)	Z (Å)
H	5.912	-3.578	8.764
H	5.245	-4.357	7.329
H	5.287	0.956	8.371
H	5.388	1.019	6.617
H	7.653	-1.658	8.916
H	7.175	0.026	9.206
H	6.044	-1.278	9.597
H	9.004	1.069	8.080
H	8.609	2.408	6.977
H	7.324	1.626	7.897
H	10.737	0.238	6.452
H	11.925	0.519	5.173
H	9.342	3.044	1.778
H	8.244	2.743	3.139
H	12.319	1.206	3.145
H	11.793	2.408	1.938
H	12.103	2.904	3.614
H	11.209	-0.859	3.617
H	10.320	-1.568	2.248
H	11.539	-0.292	1.958
H	8.127	1.396	1.525
H	4.436	-2.286	7.243
H	11.375	-6.264	5.040
H	9.543	-1.637	5.886
H	9.717	2.610	5.348
H	8.301	-3.922	1.606
H	10.281	-0.323	0.251
H	4.225	-3.942	0.563
H	4.401	-3.852	5.170
H	3.211	-1.175	3.190
H	2.076	2.177	1.268
H	4.096	3.587	2.418
H	6.352	1.090	3.772
H	5.159	-0.198	4.142
H	5.531	1.179	1.389
H	1.917	0.800	3.565
O	1.626	1.334	1.554
H	4.013	1.874	3.795
O	3.678	2.834	1.930

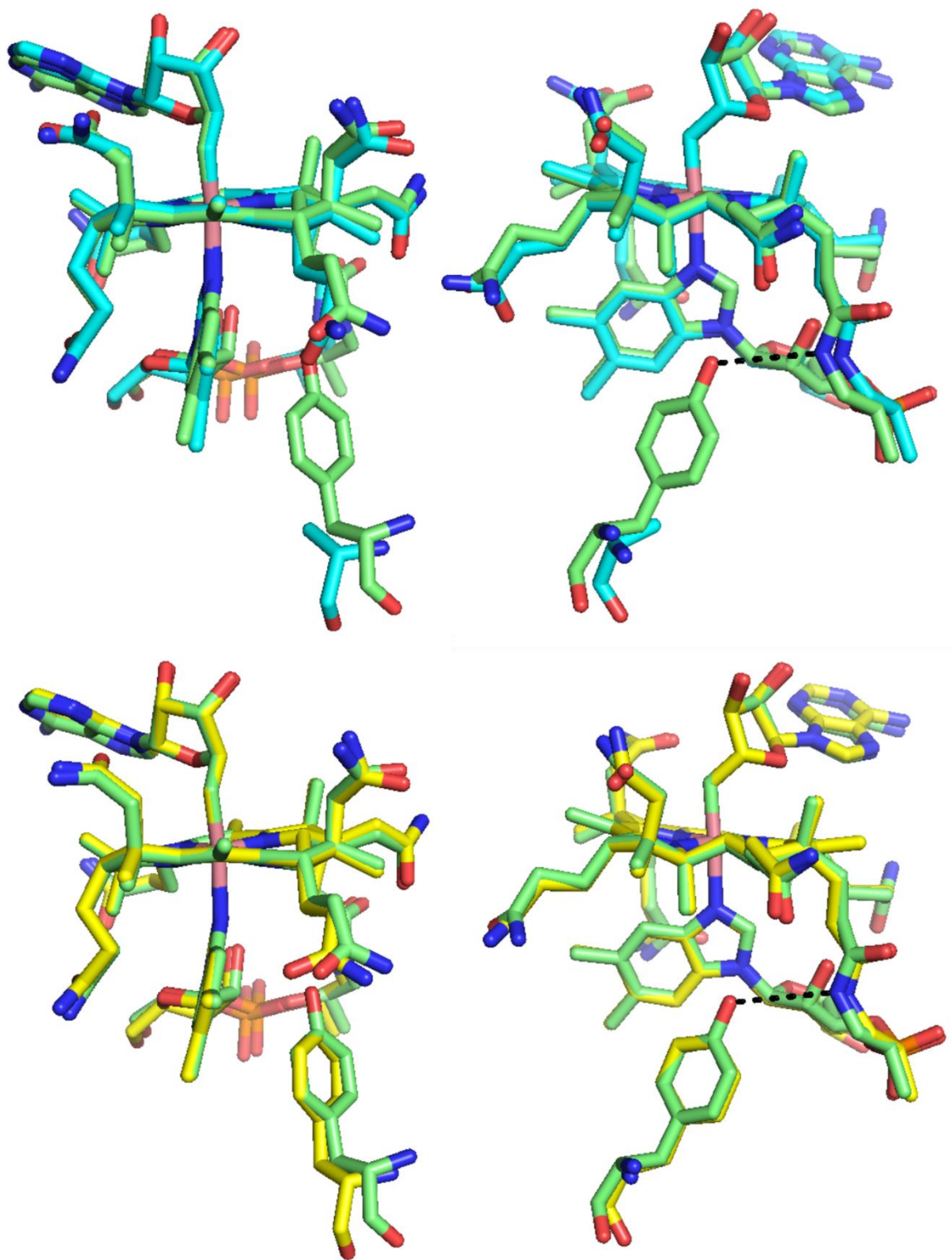


Figure A.4.1. Two perspectives (left and right) of overlay plots of the WT and Y241βA holoenzymes (top) and of the WT and Y241βF holoenzymes (bottom). A potential hydrogen bonding interaction between Y241β and a corrin side chain is shown for the figures on the right.

Table A.4.1. Optimized coordinates of the QM region for the AdoCbl/Y241βF EAL holoenzyme model.

Atom	X (Å)	Y (Å)	Z (Å)	Atom	X (Å)	Y (Å)	Z (Å)
Co	7.010	-1.277	3.449	H	9.236	-2.279	-1.497
N	8.382	-0.109	4.014	C	9.240	0.221	0.296
N	6.503	-1.542	5.329	C	9.895	1.529	-0.221
N	5.814	-2.585	2.691	H	10.602	1.353	-1.028
N	7.599	-0.810	1.718	C	8.546	0.359	1.669
C	9.408	0.303	2.968	H	9.464	-6.126	2.634
C	10.516	-0.773	2.841	N	9.299	-5.183	3.121
C	9.971	1.686	3.559	C	9.796	-4.813	4.400
C	11.437	1.979	3.183	C	8.531	-4.099	2.675
C	9.016	2.823	3.080	N	8.495	-3.084	3.557
H	9.231	3.833	3.409	C	9.307	-3.493	4.645
C	9.781	1.474	5.123	C	9.644	-2.821	5.842
C	10.939	0.839	5.991	C	10.409	-3.489	6.819
H	11.563	1.538	6.579	C	10.732	-2.798	8.135
C	8.578	0.526	5.174	C	10.855	-4.840	6.585
C	7.815	0.289	6.380	C	11.605	-5.591	7.666
C	8.072	1.207	7.577	C	10.578	-5.488	5.361
C	6.850	-0.723	6.427	C	5.613	0.190	3.538
C	5.879	-0.991	7.620	C	4.840	0.746	2.338
C	6.503	-1.090	9.033	O	4.103	-0.289	1.574
C	4.880	0.253	7.589	C	2.851	-0.513	2.323
H	3.819	0.074	7.471	C	3.712	1.725	2.842
C	5.223	-2.369	7.193	C	2.357	0.887	2.759
C	5.680	-3.732	7.840	H	2.182	-1.090	1.728
H	6.660	-4.175	7.568	H	12.600	-5.152	7.867
C	5.476	-2.382	5.695	H	11.054	-5.575	8.628
C	4.810	-3.256	4.836	H	11.726	-6.646	7.380
C	5.025	-3.395	3.457	H	11.821	-2.700	8.302
C	4.453	-4.589	2.681	H	10.298	-1.782	8.170
C	2.928	-4.762	2.916	H	10.332	-3.358	9.001
C	5.192	-5.835	3.250	H	9.156	2.292	-0.505
C	4.831	-4.219	1.186	H	10.483	1.979	0.600
C	5.566	-5.307	0.335	H	7.941	-1.566	-2.505
H	4.974	-5.934	-0.359	H	9.448	-0.697	-2.292
C	5.717	-2.952	1.334	H	6.364	0.206	-1.776
C	6.315	-2.290	0.254	H	6.799	1.309	-0.444
C	5.833	-2.584	-1.171	H	7.789	1.255	-1.922
C	7.300	-1.241	0.487	H	6.511	-3.197	-1.788
C	8.118	-0.465	-0.602	H	4.871	-3.113	-1.163
C	7.206	0.638	-1.221	H	5.677	-1.640	-1.718
C	8.720	-1.333	-1.762	H	6.321	-4.790	-0.280

Atom	X (Å)	Y (Å)	Z (Å)	Atom	X (Å)	Y (Å)	Z (Å)
H	6.134	-5.968	1.010	H	10.961	-1.007	3.821
H	6.289	-5.727	3.175	H	10.110	-1.703	2.421
H	4.956	-5.936	4.324	H	11.322	-0.408	2.181
H	4.887	-6.768	2.751	H	7.923	1.270	1.692
H	2.715	-4.911	3.991	H	4.141	-2.378	7.395
H	2.359	-3.881	2.582	H	10.991	-6.484	5.183
H	2.544	-5.651	2.394	H	9.281	-1.808	6.028
H	5.615	-3.668	8.943	H	9.499	2.453	5.553
H	4.898	-4.455	7.534	H	7.974	-4.059	1.747
H	5.031	0.857	8.501	H	10.052	-0.503	0.459
H	5.169	0.914	6.752	H	3.892	-3.941	0.679
H	7.342	-1.801	9.076	H	4.074	-3.920	5.298
H	6.866	-0.115	9.385	H	3.076	-1.111	3.237
H	5.724	-1.417	9.744	H	1.897	2.280	1.429
H	8.720	0.741	8.344	H	3.856	3.706	2.403
H	8.563	2.140	7.261	H	6.171	1.015	4.026
H	7.133	1.500	8.073	H	4.899	-0.228	4.272
H	10.463	0.142	6.703	H	5.486	1.260	1.608
H	11.609	0.229	5.361	H	1.864	0.853	3.750
H	9.049	2.867	1.978	O	1.422	1.482	1.810
H	7.982	2.552	3.365	H	3.903	2.074	3.875
H	12.078	1.107	3.361	O	3.562	2.886	1.936
H	11.540	2.268	2.121				
H	11.834	2.819	3.777				

Table A.4.2. Optimized coordinates of the QM region for the AdoCbl/Y241βW EAL holoenzyme model.

Atom	X (Å)	Y (Å)	Z (Å)	Atom	X (Å)	Y (Å)	Z (Å)
Co	6.655	-1.549	3.238	C	8.131	0.235	5.032
N	8.003	-0.401	3.865	C	7.263	0.033	6.177
N	6.085	-1.849	5.079	C	7.429	1.010	7.340
N	5.529	-2.895	2.428	C	6.341	-1.020	6.198
N	7.321	-1.068	1.543	C	5.445	-1.453	7.405
C	9.095	-0.009	2.877	C	6.229	-1.543	8.745
C	10.168	-1.118	2.774	C	4.262	-0.426	7.524
C	9.679	1.341	3.517	H	3.608	-0.598	8.380
C	11.179	1.559	3.222	C	4.837	-2.825	6.897
C	8.844	2.539	2.980	C	5.225	-4.197	7.540
H	9.125	3.507	3.377	H	6.252	-4.573	7.363
C	9.376	1.132	5.067	C	5.151	-2.795	5.414
C	10.473	0.449	5.976	C	4.561	-3.703	4.535
H	11.100	1.133	6.577	C	4.780	-3.778	3.156

Atom	X (Å)	Y (Å)	Z (Å)
C	4.271	-4.971	2.336
C	2.757	-5.250	2.545
C	5.058	-6.201	2.879
C	4.644	-4.525	0.863
C	5.401	-5.561	-0.026
H	4.802	-6.139	-0.752
C	5.483	-3.237	1.065
C	6.083	-2.529	0.017
C	5.614	-2.782	-1.420
C	7.060	-1.489	0.299
C	7.918	-0.720	-0.753
C	7.033	0.405	-1.373
C	8.527	-1.597	-1.901
H	9.012	-2.557	-1.627
C	9.029	-0.059	0.180
C	9.712	1.238	-0.321
H	10.418	1.068	-1.131
C	8.293	0.086	1.537
H	9.194	-6.439	2.547
N	9.001	-5.499	3.030
C	9.443	-5.128	4.328
C	8.239	-4.420	2.559
N	8.166	-3.404	3.436
C	8.942	-3.808	4.552
C	9.241	-3.131	5.758
C	9.973	-3.798	6.762
C	10.277	-3.096	8.076
C	10.421	-5.152	6.552
C	11.135	-5.903	7.659
C	10.186	-5.802	5.320
C	5.305	-0.037	3.249
C	4.484	0.374	2.020
O	3.747	-0.739	1.384
C	2.582	-0.984	2.250
C	3.340	1.349	2.459
C	2.095	0.402	2.763
H	1.872	-1.567	1.720
H	12.093	-5.427	7.943
H	10.519	-5.948	8.579
H	11.330	-6.939	7.346
H	11.365	-2.978	8.239
H	9.823	-2.089	8.109
H	9.888	-3.661	8.944

Atom	X (Å)	Y (Å)	Z (Å)
H	8.982	2.011	-0.597
H	10.304	1.673	0.507
H	7.762	-1.809	-2.664
H	9.285	-0.983	-2.412
H	6.144	0.005	-1.877
H	6.697	1.115	-0.597
H	7.613	0.974	-2.112
H	6.224	-3.489	-2.008
H	4.587	-3.174	-1.425
H	5.599	-1.837	-1.984
H	6.170	-5.024	-0.603
H	5.949	-6.266	0.621
H	6.148	-6.030	2.857
H	4.783	-6.358	3.937
H	4.824	-7.129	2.333
H	2.120	-4.555	1.983
H	2.510	-6.279	2.238
H	2.488	-5.164	3.614
H	5.030	-4.175	8.629
H	4.515	-4.933	7.118
H	4.675	0.596	7.593
H	3.642	-0.456	6.608
H	7.274	-1.860	8.598
H	6.243	-0.567	9.257
H	5.745	-2.253	9.436
H	8.300	0.770	7.977
H	7.573	2.040	6.964
H	6.547	1.030	7.993
H	9.954	-0.227	6.679
H	11.140	-0.185	5.367
H	8.981	2.613	1.887
H	7.765	2.366	3.154
H	11.784	0.684	3.493
H	11.349	1.776	2.151
H	11.573	2.423	3.783
H	10.556	-1.402	3.765
H	9.741	-2.012	2.303
H	11.017	-0.761	2.167
H	7.696	1.016	1.547
H	3.735	-2.777	6.991
H	10.617	-6.791	5.149
H	8.875	-2.115	5.925
H	9.111	2.109	5.511

Atom	X (Å)	Y (Å)	Z (Å)
H	7.716	-4.382	1.612
H	9.826	-0.796	0.357
H	3.701	-4.241	0.367
H	3.889	-4.441	4.981
H	2.910	-1.588	3.126
H	1.214	1.538	1.413
H	3.108	3.180	1.628
H	5.912	0.828	3.584

Atom	X (Å)	Y (Å)	Z (Å)
H	4.636	-0.328	4.080
H	5.105	0.818	1.226
H	1.891	0.379	3.847
O	0.886	0.905	2.122
H	3.612	1.947	3.341
O	2.943	2.246	1.351

Table A.4.3. Optimized coordinates of the QM region for the AdoCbl/Y241βA EAL ternary complex model.

Atom	X (Å)	Y (Å)	Z (Å)
Co	7.103	-1.503	3.322
N	8.428	-0.302	3.941
N	6.587	-1.831	5.183
N	5.954	-2.827	2.510
N	7.691	-0.966	1.613
C	9.460	0.166	2.921
C	10.608	-0.867	2.807
C	9.960	1.557	3.547
C	11.419	1.916	3.202
C	9.004	2.686	3.060
H	9.225	3.684	3.423
C	9.745	1.315	5.108
C	10.970	0.792	5.968
H	11.388	1.526	6.685
C	8.585	0.309	5.121
C	7.781	0.036	6.298
C	7.999	0.929	7.518
C	6.856	-1.016	6.308
C	5.924	-1.419	7.502
C	6.636	-1.531	8.872
C	4.775	-0.348	7.554
H	3.980	-0.519	8.280
C	5.322	-2.789	6.992
C	5.761	-4.151	7.622
H	6.782	-4.520	7.393
C	5.628	-2.754	5.510
C	5.012	-3.640	4.627
C	5.208	-3.705	3.244
C	4.645	-4.867	2.420
C	3.126	-5.075	2.669

Atom	X (Å)	Y (Å)	Z (Å)
C	5.399	-6.129	2.923
C	4.997	-4.418	0.943
C	5.730	-5.455	0.033
H	5.126	-6.034	-0.689
C	5.855	-3.139	1.141
C	6.430	-2.413	0.090
C	5.944	-2.655	-1.342
C	7.404	-1.365	0.367
C	8.227	-0.560	-0.693
C	7.322	0.562	-1.291
C	8.827	-1.402	-1.872
H	9.338	-2.357	-1.633
C	9.343	0.100	0.234
C	10.013	1.413	-0.248
H	10.713	1.250	-1.064
C	8.626	0.215	1.601
H	9.634	-6.271	2.421
N	9.457	-5.338	2.921
C	9.962	-4.977	4.198
C	8.665	-4.263	2.498
N	8.618	-3.261	3.396
C	9.446	-3.673	4.471
C	9.775	-3.016	5.679
C	10.558	-3.691	6.637
C	10.877	-3.026	7.965
C	11.028	-5.028	6.375
C	11.776	-5.789	7.448
C	10.766	-5.655	5.137
C	5.667	-0.094	3.438
C	4.840	0.439	2.271

Atom	X (Å)	Y (Å)	Z (Å)
O	4.065	-0.608	1.559
C	2.820	-0.767	2.326
C	3.742	1.423	2.841
C	2.363	0.661	2.690
H	2.128	-1.357	1.776
H	12.757	-5.330	7.676
H	11.203	-5.807	8.396
H	11.927	-6.833	7.139
H	11.948	-3.095	8.223
H	10.601	-1.956	7.953
H	10.327	-3.499	8.802
H	9.284	2.195	-0.508
H	10.612	1.829	0.583
H	8.046	-1.614	-2.620
H	9.556	-0.760	-2.391
H	6.450	0.156	-1.819
H	6.963	1.244	-0.502
H	7.900	1.162	-2.011
H	6.561	-3.346	-1.944
H	4.926	-3.068	-1.343
H	5.907	-1.705	-1.897
H	6.487	-4.912	-0.556
H	6.292	-6.161	0.666
H	6.494	-6.003	2.852
H	5.169	-6.276	3.994
H	5.104	-7.046	2.388
H	2.929	-5.207	3.749
H	2.527	-4.220	2.325
H	2.767	-5.987	2.170
H	5.621	-4.129	8.720
H	5.037	-4.897	7.240
H	5.216	0.643	7.766
H	4.304	-0.275	6.554
H	7.635	-1.980	8.773
H	6.746	-0.548	9.354

Atom	X (Å)	Y (Å)	Z (Å)
H	6.046	-2.155	9.562
H	8.776	0.526	8.196
H	8.311	1.943	7.221
H	7.086	1.041	8.119
H	10.657	-0.098	6.544
H	11.786	0.466	5.301
H	9.077	2.753	1.961
H	7.957	2.420	3.299
H	12.081	1.046	3.284
H	11.509	2.310	2.173
H	11.797	2.703	3.877
H	11.066	-1.067	3.790
H	10.239	-1.818	2.402
H	11.398	-0.484	2.137
H	7.993	1.121	1.619
H	4.223	-2.773	7.095
H	11.191	-6.643	4.941
H	9.393	-2.015	5.889
H	9.390	2.271	5.538
H	8.098	-4.219	1.577
H	10.146	-0.635	0.395
H	4.047	-4.136	0.462
H	4.327	-4.367	5.074
H	3.039	-1.320	3.272
H	2.050	1.990	1.248
H	4.275	3.326	2.448
H	6.211	0.748	3.910
H	4.984	-0.527	4.193
H	5.446	0.944	1.499
H	1.798	0.693	3.639
O	1.518	1.252	1.653
H	3.928	1.658	3.906
O	3.643	2.666	2.064

Table A.4.4. Optimized coordinates of the QM region for the AdoCbl/Y241 β F EAL ternary complex model.

Atom	X (Å)	Y (Å)	Z (Å)	Atom	X (Å)	Y (Å)	Z (Å)
Co	7.107	-1.453	3.295	H	9.358	-2.308	-1.638
N	8.425	-0.245	3.913	C	9.334	0.170	0.203
N	6.591	-1.784	5.156	C	9.976	1.496	-0.285
N	5.965	-2.783	2.484	H	10.672	1.351	-1.108
N	7.695	-0.916	1.586	C	8.618	0.275	1.572
C	9.452	0.234	2.892	H	9.645	-6.228	2.411
C	10.609	-0.790	2.780	N	9.467	-5.293	2.908
C	9.935	1.631	3.518	C	9.955	-4.937	4.191
C	11.388	2.007	3.165	C	8.687	-4.212	2.476
C	8.963	2.749	3.036	N	8.639	-3.210	3.372
H	9.165	3.747	3.410	C	9.451	-3.627	4.457
C	9.728	1.384	5.079	C	9.779	-2.971	5.666
C	10.960	0.874	5.935	C	10.548	-3.653	6.630
H	11.376	1.614	6.648	C	10.866	-2.989	7.960
C	8.579	0.366	5.093	C	11.004	-4.995	6.375
C	7.782	0.084	6.272	C	11.753	-5.757	7.447
C	8.004	0.970	7.497	C	10.740	-5.625	5.140
C	6.860	-0.970	6.282	C	5.666	-0.050	3.413
C	5.932	-1.377	7.478	C	4.838	0.480	2.246
C	6.653	-1.496	8.843	O	4.069	-0.572	1.534
C	4.785	-0.306	7.542	C	2.827	-0.741	2.304
H	3.995	-0.482	8.271	C	3.734	1.457	2.816
C	5.326	-2.744	6.964	C	2.360	0.683	2.670
C	5.761	-4.109	7.589	H	2.139	-1.337	1.756
H	6.783	-4.474	7.360	H	12.731	-5.294	7.674
C	5.631	-2.706	5.482	H	11.179	-5.780	8.394
C	5.015	-3.591	4.600	H	11.909	-6.799	7.134
C	5.217	-3.659	3.218	H	11.929	-3.089	8.237
C	4.664	-4.829	2.396	H	10.622	-1.911	7.939
C	3.147	-5.049	2.640	H	10.289	-3.441	8.790
C	5.427	-6.082	2.910	H	9.229	2.263	-0.539
C	5.021	-4.383	0.919	H	10.573	1.924	0.542
C	5.767	-5.420	0.020	H	8.076	-1.576	-2.646
H	5.172	-6.008	-0.702	H	9.580	-0.714	-2.402
C	5.871	-3.100	1.116	H	6.446	0.174	-1.855
C	6.446	-2.374	0.065	H	6.938	1.276	-0.542
C	5.965	-2.626	-1.368	H	7.880	1.199	-2.048
C	7.412	-1.320	0.341	H	6.582	-3.324	-1.962
C	8.229	-0.512	-0.721	H	4.945	-3.036	-1.369
C	7.310	0.595	-1.326	H	5.933	-1.681	-1.931
C	8.846	-1.356	-1.889	H	6.523	-4.875	-0.569

Atom	X (Å)	Y (Å)	Z (Å)	Atom	X (Å)	Y (Å)	Z (Å)
H	6.331	-6.116	0.661	H	11.068	-0.986	3.763
H	6.520	-5.945	2.848	H	10.244	-1.745	2.379
H	5.188	-6.228	3.979	H	11.396	-0.406	2.109
H	5.145	-7.003	2.375	H	7.976	1.174	1.589
H	2.945	-5.166	3.721	H	4.226	-2.724	7.069
H	2.540	-4.207	2.279	H	11.163	-6.613	4.944
H	2.801	-5.973	2.154	H	9.408	-1.964	5.870
H	5.620	-4.093	8.687	H	9.363	2.334	5.512
H	5.040	-4.855	7.202	H	8.131	-4.164	1.548
H	5.227	0.683	7.757	H	10.153	-0.549	0.359
H	4.309	-0.227	6.545	H	4.073	-4.110	0.431
H	7.663	-1.918	8.733	H	4.329	-4.317	5.046
H	6.741	-0.518	9.341	H	3.053	-1.292	3.249
H	6.083	-2.145	9.525	H	2.029	2.018	1.237
H	8.797	0.574	8.159	H	4.229	3.373	2.434
H	8.295	1.992	7.204	H	6.206	0.795	3.886
H	7.098	1.063	8.112	H	4.985	-0.486	4.167
H	10.658	-0.016	6.516	H	5.441	0.988	1.474
H	11.776	0.554	5.265	H	1.798	0.711	3.621
H	9.040	2.827	1.938	O	1.507	1.269	1.636
H	7.920	2.464	3.268	H	3.921	1.695	3.879
H	12.059	1.145	3.244	O	3.624	2.697	2.035
H	11.467	2.404	2.137				
H	11.759	2.799	3.839				

Table A.4.5. Optimized coordinates of the QM region for the AdoCbl/Y241βW EAL ternary complex model.

Atom	X (Å)	Y (Å)	Z (Å)	Atom	X (Å)	Y (Å)	Z (Å)
Co	7.112	-1.216	3.458	C	8.541	0.632	5.254
N	8.393	0.026	4.071	C	7.762	0.321	6.438
N	6.614	-1.571	5.318	C	7.984	1.197	7.670
N	6.013	-2.583	2.649	C	6.870	-0.758	6.447
N	7.687	-0.660	1.748	C	5.980	-1.206	7.655
C	9.411	0.524	3.051	C	6.743	-1.311	9.004
C	10.565	-0.500	2.928	C	4.808	-0.163	7.756
C	9.888	1.917	3.686	H	4.014	-0.385	8.468
C	11.342	2.291	3.333	C	5.389	-2.581	7.133
C	8.908	3.031	3.210	C	5.817	-3.945	7.762
H	9.100	4.030	3.587	H	6.856	-4.285	7.580
C	9.685	1.655	5.244	C	5.697	-2.534	5.650
C	10.911	1.109	6.083	C	5.109	-3.437	4.767
H	11.372	1.834	6.781	C	5.300	-3.488	3.383

Atom	X (Å)	Y (Å)	Z (Å)
C	4.770	-4.666	2.557
C	3.255	-4.905	2.799
C	5.550	-5.909	3.068
C	5.119	-4.210	1.081
C	5.905	-5.222	0.187
H	5.339	-5.829	-0.542
C	5.928	-2.900	1.280
C	6.482	-2.158	0.229
C	6.012	-2.428	-1.204
C	7.417	-1.076	0.504
C	8.210	-0.248	-0.560
C	7.253	0.824	-1.167
C	8.852	-1.086	-1.720
H	9.391	-2.019	-1.455
C	9.293	0.477	0.357
C	9.890	1.820	-0.148
H	10.591	1.695	-0.971
C	8.576	0.559	1.731
H	9.755	-5.978	2.627
N	9.551	-5.047	3.126
C	9.998	-4.685	4.427
C	8.770	-3.974	2.676
N	8.691	-2.968	3.566
C	9.480	-3.376	4.671
C	9.781	-2.705	5.880
C	10.536	-3.366	6.871
C	10.835	-2.667	8.190
C	11.004	-4.710	6.640
C	11.757	-5.453	7.727
C	10.762	-5.356	5.406
C	5.639	0.151	3.576
C	4.820	0.663	2.395
O	4.079	-0.404	1.677
C	2.838	-0.601	2.442
C	3.690	1.627	2.935
C	2.336	0.815	2.801
H	2.168	-1.213	1.889
H	12.734	-4.985	7.950
H	11.188	-5.471	8.677
H	11.924	-6.498	7.427
H	11.921	-2.579	8.380
H	10.414	-1.645	8.206
H	10.411	-3.211	9.057

Atom	X (Å)	Y (Å)	Z (Å)
H	9.120	2.562	-0.408
H	10.473	2.276	0.675
H	8.088	-1.338	-2.472
H	9.570	-0.430	-2.239
H	6.398	0.372	-1.683
H	6.867	1.496	-0.381
H	7.795	1.446	-1.896
H	6.671	-3.079	-1.805
H	5.020	-2.901	-1.207
H	5.918	-1.482	-1.758
H	6.652	-4.653	-0.391
H	6.483	-5.901	0.835
H	6.641	-5.754	3.007
H	5.315	-6.063	4.136
H	5.285	-6.833	2.531
H	3.059	-5.065	3.877
H	2.643	-4.053	2.473
H	2.911	-5.812	2.279
H	5.621	-3.946	8.852
H	5.134	-4.701	7.331
H	5.223	0.828	8.015
H	4.340	-0.055	6.757
H	7.813	-1.533	8.861
H	6.660	-0.371	9.571
H	6.312	-2.100	9.638
H	8.802	0.818	8.312
H	8.241	2.231	7.386
H	7.088	1.255	8.305
H	10.577	0.239	6.676
H	11.701	0.742	5.406
H	8.983	3.114	2.111
H	7.868	2.734	3.442
H	12.009	1.430	3.448
H	11.425	2.650	2.292
H	11.713	3.102	3.983
H	11.015	-0.723	3.910
H	10.183	-1.438	2.506
H	11.359	-0.108	2.270
H	7.911	1.441	1.755
H	4.287	-2.565	7.225
H	11.203	-6.338	5.225
H	9.402	-1.696	6.060
H	9.331	2.601	5.695

Atom	X (Å)	Y (Å)	Z (Å)
H	8.239	-3.929	1.734
H	10.139	-0.209	0.514
H	4.164	-3.969	0.588
H	4.451	-4.190	5.211
H	3.071	-1.144	3.388
H	1.967	2.124	1.356
H	4.133	3.546	2.501
H	6.157	1.004	4.056

Atom	X (Å)	Y (Å)	Z (Å)
H	4.961	-0.305	4.321
H	5.428	1.176	1.630
H	1.780	0.833	3.756
O	1.461	1.373	1.771
H	3.867	1.903	3.992
O	3.554	2.840	2.116

Table A.4.6. Optimized coordinates of the QM region for the AdoCbl/N193αA EAL ternary complex model.

Atom	X (Å)	Y (Å)	Z (Å)
Co	7.279	-1.181	3.286
N	8.622	0.031	3.831
N	6.785	-1.429	5.172
N	6.118	-2.523	2.548
N	7.844	-0.698	1.550
C	9.643	0.444	2.778
C	10.745	-0.636	2.642
C	10.217	1.823	3.365
C	11.691	2.093	2.993
C	9.293	2.982	2.878
H	9.541	3.976	3.236
C	10.010	1.629	4.930
C	11.176	1.021	5.809
H	11.706	1.738	6.467
C	8.810	0.680	4.983
C	8.037	0.460	6.187
C	8.256	1.431	7.349
C	7.106	-0.582	6.257
C	6.156	-0.871	7.464
C	6.808	-0.954	8.867
C	5.130	0.352	7.459
H	4.069	0.156	7.368
C	5.518	-2.259	7.038
C	6.000	-3.619	7.665
H	6.996	-4.024	7.395
C	5.769	-2.279	5.542
C	5.123	-3.180	4.697
C	5.346	-3.340	3.322
C	4.815	-4.562	2.562
C	3.302	-4.801	2.807

Atom	X (Å)	Y (Å)	Z (Å)
C	5.604	-5.772	3.141
C	5.174	-4.193	1.063
C	5.926	-5.264	0.210
H	5.339	-5.893	-0.485
C	6.024	-2.902	1.196
C	6.586	-2.222	0.108
C	6.094	-2.543	-1.307
C	7.540	-1.143	0.325
C	8.321	-0.352	-0.777
C	7.366	0.719	-1.391
C	8.923	-1.222	-1.934
H	9.470	-2.144	-1.650
C	9.440	0.370	0.100
C	10.049	1.692	-0.433
H	10.699	1.540	-1.293
C	8.764	0.493	1.487
H	9.837	-5.950	2.498
N	9.648	-5.013	2.984
C	10.132	-4.630	4.263
C	8.855	-3.949	2.536
N	8.792	-2.934	3.416
C	9.612	-3.322	4.505
C	9.930	-2.641	5.702
C	10.699	-3.295	6.685
C	10.991	-2.599	8.004
C	11.175	-4.636	6.456
C	11.922	-5.376	7.548
C	10.924	-5.288	5.228
C	5.821	0.208	3.355
C	4.956	0.663	2.176

Atom	X (Å)	Y (Å)	Z (Å)
O	4.225	-0.432	1.485
C	2.978	-0.626	2.246
C	3.825	1.608	2.737
C	2.477	0.785	2.609
H	2.299	-1.231	1.691
H	12.895	-4.909	7.789
H	11.340	-5.398	8.491
H	12.086	-6.420	7.245
H	12.074	-2.458	8.168
H	10.512	-1.605	8.044
H	10.620	-3.184	8.866
H	9.283	2.451	-0.651
H	10.686	2.131	0.356
H	8.136	-1.498	-2.655
H	9.617	-0.585	-2.503
H	6.498	0.264	-1.886
H	6.997	1.414	-0.617
H	7.902	1.314	-2.145
H	6.738	-3.223	-1.892
H	5.101	-3.011	-1.279
H	5.996	-1.618	-1.895
H	6.672	-4.735	-0.405
H	6.500	-5.923	0.882
H	6.696	-5.618	3.070
H	5.367	-5.875	4.215
H	5.339	-6.720	2.647
H	2.676	-4.030	2.337
H	2.993	-5.787	2.429
H	3.080	-4.793	3.891
H	5.912	-3.578	8.764
H	5.245	-4.357	7.329
H	5.287	0.956	8.371
H	5.388	1.019	6.617
H	7.653	-1.658	8.916
H	7.175	0.026	9.206

Atom	X (Å)	Y (Å)	Z (Å)
H	6.044	-1.278	9.597
H	9.004	1.069	8.080
H	8.609	2.408	6.977
H	7.324	1.626	7.897
H	10.737	0.238	6.452
H	11.925	0.519	5.173
H	9.342	3.044	1.778
H	8.244	2.743	3.139
H	12.319	1.206	3.145
H	11.793	2.408	1.938
H	12.103	2.904	3.614
H	11.209	-0.859	3.617
H	10.320	-1.568	2.248
H	11.539	-0.292	1.958
H	8.127	1.396	1.525
H	4.436	-2.286	7.243
H	11.375	-6.264	5.040
H	9.543	-1.637	5.886
H	9.717	2.610	5.348
H	8.301	-3.922	1.606
H	10.281	-0.323	0.251
H	4.225	-3.942	0.563
H	4.401	-3.852	5.170
H	3.211	-1.175	3.190
H	2.076	2.177	1.268
H	4.096	3.587	2.418
H	6.352	1.090	3.772
H	5.159	-0.198	4.142
H	5.531	1.179	1.389
H	1.917	0.800	3.565
O	1.626	1.334	1.554
H	4.013	1.874	3.795
O	3.678	2.834	1.930

Table A.4.7. Optimized coordinates of the QM region for the free Ado(BIm)Cbl model.

Atom	X (Å)	Y (Å)	Z (Å)	Atom	X (Å)	Y (Å)	Z (Å)
Co	1.434	-0.060	0.043	C	0.624	-1.158	-3.866
N	2.789	-1.173	-0.683	C	1.316	-1.260	-5.258
N	2.452	0.027	1.713	H	1.093	-2.209	-5.734
N	-0.087	1.020	0.636	C	1.579	-0.737	-2.729
N	0.671	-0.179	-1.670	H	-2.647	-2.971	1.907
C	2.512	-1.786	-2.056	N	-1.618	-2.821	1.651
C	1.749	-3.127	-1.893	C	-0.539	-3.662	2.028
C	4.007	-1.915	-2.642	C	-1.059	-1.757	0.942
C	4.212	-2.975	-3.747	N	0.276	-1.848	0.820
C	4.440	-0.501	-3.167	C	0.639	-3.055	1.476
H	5.495	-0.353	-3.378	C	1.906	-3.653	1.666
C	4.821	-2.240	-1.317	C	1.969	-4.833	2.432
C	4.976	-3.762	-0.983	H	2.938	-5.304	2.623
H	5.595	-4.033	-0.106	C	0.797	-5.418	2.994
C	4.051	-1.400	-0.289	H	0.890	-6.323	3.602
C	4.634	-0.853	0.917	C	-0.478	-4.846	2.799
C	6.155	-0.858	1.071	C	2.477	1.605	-0.421
C	3.837	-0.201	1.861	C	2.267	2.493	-1.652
C	4.340	0.555	3.133	O	0.956	3.187	-1.688
C	5.479	-0.070	3.980	C	1.110	4.353	-0.793
C	4.835	1.971	2.575	C	3.313	3.661	-1.655
H	4.323	2.870	2.910	C	2.561	4.888	-0.990
C	2.995	0.638	3.963	H	0.331	5.057	-0.968
C	2.701	-0.503	5.002	H	1.050	-0.429	-5.928
H	2.474	-1.512	4.607	H	2.413	-1.205	-5.146
C	1.981	0.679	2.831	H	-2.670	0.070	-4.323
C	0.755	1.335	2.933	H	-1.770	-1.185	-5.180
C	-0.179	1.531	1.903	H	-0.862	2.032	-4.272
C	-1.462	2.338	2.153	H	0.800	1.461	-4.483
C	-1.103	3.786	2.605	H	-0.467	0.965	-5.645
C	-2.239	1.619	3.299	H	-3.543	0.984	-2.151
C	-2.159	2.310	0.723	H	-2.924	2.609	-1.761
C	-3.684	1.934	0.726	H	-2.429	1.813	-3.250
H	-4.431	2.749	0.603	H	-3.886	1.194	-0.064
C	-1.227	1.389	-0.121	H	-3.915	1.422	1.673
C	-1.441	1.052	-1.462	H	-2.452	0.563	3.047
C	-2.649	1.636	-2.190	H	-1.625	1.617	4.217
C	-0.472	0.261	-2.209	H	-3.187	2.125	3.544
C	-0.565	-0.113	-3.724	H	-0.585	4.338	1.801
C	-0.261	1.164	-4.578	H	-2.004	4.351	2.896
C	-1.930	-0.736	-4.180	H	-0.429	3.771	3.481
H	-2.387	-1.514	-3.528	H	3.555	-0.568	5.700

Atom	X (Å)	Y (Å)	Z (Å)	Atom	X (Å)	Y (Å)	Z (Å)
H	1.829	-0.177	5.602	H	2.196	0.105	-3.084
H	5.910	2.085	2.797	H	2.948	1.563	4.564
H	4.762	1.968	1.471	H	-1.358	-5.307	3.256
H	5.325	-1.137	4.206	H	2.804	-3.187	1.258
H	6.459	0.038	3.493	H	5.847	-1.853	-1.424
H	5.536	0.482	4.937	H	-1.593	-0.900	0.554
H	6.519	-1.527	1.868	H	0.235	-2.150	-3.589
H	6.651	-1.151	0.133	H	-2.030	3.320	0.283
H	6.518	0.159	1.305	H	0.549	1.820	3.892
H	3.986	-4.230	-0.850	H	1.009	4.004	0.260
H	5.430	-4.241	-1.870	H	3.013	5.775	-2.708
H	3.908	-0.294	-4.115	H	4.339	3.496	-3.409
H	4.109	0.274	-2.453	H	3.518	1.227	-0.423
H	3.736	-3.941	-3.517	H	2.321	2.201	0.494
H	3.811	-2.620	-4.712	H	2.332	1.939	-2.605
H	5.290	-3.160	-3.906	H	3.020	5.141	-0.016
H	2.234	-3.797	-1.171	O	2.647	6.079	-1.828
H	0.730	-2.927	-1.522	H	4.239	3.397	-1.108
H	1.673	-3.658	-2.856	O	3.643	4.088	-3.029

Table A.4.8. Optimized coordinates of the QM region for the Ado(BIm)Cbl/WT EAL holoenzyme model.

Atom	X (Å)	Y (Å)	Z (Å)	Atom	X (Å)	Y (Å)	Z (Å)
Co	6.591	-1.752	3.650	C	6.256	-1.295	9.217
N	7.991	-0.583	4.122	C	4.570	0.020	7.823
N	6.104	-1.899	5.553	H	3.506	-0.144	7.701
N	5.321	-3.044	2.990	C	4.862	-2.617	7.488
N	7.155	-1.405	1.880	C	5.331	-3.948	8.189
C	9.004	-0.222	3.037	H	6.298	-4.402	7.888
C	10.148	-1.263	2.994	C	5.066	-2.695	5.985
C	9.491	1.225	3.522	C	4.341	-3.573	5.186
C	10.912	1.635	3.094	C	4.498	-3.764	3.808
C	8.471	2.277	3.000	C	3.802	-4.927	3.092
H	8.666	3.298	3.300	C	2.281	-4.975	3.395
C	9.371	1.091	5.099	C	4.455	-6.214	3.670
C	10.630	0.596	5.912	C	4.149	-4.633	1.573
H	11.115	1.386	6.515	C	4.711	-5.836	0.744
C	8.206	0.115	5.242	H	4.052	-6.350	0.018
C	7.455	-0.032	6.468	C	5.148	-3.450	1.650
C	7.715	0.990	7.578	C	5.741	-2.864	0.524
C	6.486	-1.032	6.599	C	5.204	-3.212	-0.863
C	5.555	-1.236	7.836	C	6.779	-1.851	0.671

Atom	X (Å)	Y (Å)	Z (Å)
C	7.571	-1.115	-0.476
C	6.709	0.083	-0.991
C	7.971	-1.955	-1.739
H	8.468	-2.937	-1.607
C	8.808	-0.564	0.363
C	9.582	0.664	-0.174
H	10.150	0.470	-1.078
C	8.151	-0.289	1.738
H	8.827	-6.591	2.824
N	8.725	-5.663	3.348
C	9.261	-5.362	4.633
C	8.021	-4.524	2.940
N	8.068	-3.527	3.837
C	8.888	-4.000	4.894
C	9.357	-3.336	6.053
C	10.121	-4.076	6.976
H	10.475	-3.599	7.895
C	10.431	-5.449	6.744
H	11.005	-6.005	7.495
C	10.022	-6.109	5.564
C	5.207	-0.274	3.678
C	4.443	0.292	2.476
O	3.648	-0.726	1.739
C	2.377	-0.824	2.478
C	3.378	1.321	3.016
C	1.971	0.616	2.837
H	1.673	-1.396	1.923
H	8.918	1.533	-0.313
H	10.318	0.970	0.590
H	7.079	-2.107	-2.367
H	8.625	-1.322	-2.361
H	5.841	-0.268	-1.564
H	6.350	0.729	-0.171
H	7.320	0.705	-1.665
H	5.788	-3.974	-1.402
H	4.187	-3.610	-0.799
H	5.163	-2.309	-1.493
H	5.601	-5.494	0.187
H	5.068	-6.585	1.467
H	5.558	-6.168	3.588
H	4.210	-6.282	4.743
H	4.098	-7.139	3.195
H	1.749	-4.106	2.981

Atom	X (Å)	Y (Å)	Z (Å)
H	1.831	-5.897	2.999
H	2.102	-4.989	4.487
H	5.333	-3.824	9.289
H	4.528	-4.679	7.965
H	4.719	0.588	8.759
H	4.873	0.704	7.007
H	7.067	-2.037	9.262
H	6.678	-0.314	9.486
H	5.509	-1.550	9.991
H	8.485	0.657	8.301
H	8.055	1.950	7.154
H	6.802	1.215	8.149
H	10.336	-0.220	6.598
H	11.382	0.177	5.223
H	8.519	2.278	1.897
H	7.438	1.999	3.276
H	11.642	0.830	3.244
H	10.947	1.952	2.038
H	11.234	2.510	3.686
H	10.652	-1.357	3.969
H	9.747	-2.250	2.725
H	10.903	-0.984	2.239
H	7.560	0.641	1.663
H	3.786	-2.605	7.719
H	10.319	-7.145	5.391
H	9.092	-2.291	6.235
H	9.062	2.073	5.499
H	7.452	-4.430	2.023
H	9.525	-1.396	0.507
H	3.227	-4.263	1.101
H	3.595	-4.185	5.698
H	2.558	-1.377	3.431
H	1.644	2.112	1.580
H	3.819	3.265	2.775
H	5.761	0.549	4.172
H	4.479	-0.685	4.401
H	5.092	0.777	1.727
H	1.389	0.659	3.781
O	1.200	1.232	1.760
H	3.571	1.579	4.072
O	3.361	2.573	2.233

Table A.4.9. Optimized coordinates of the QM region for the Ado(BIm)Cbl/Y241 β W holoenzyme model.

Atom	X (Å)	Y (Å)	Z (Å)	Atom	X (Å)	Y (Å)	Z (Å)
Co	6.416	-1.761	3.465	H	8.651	-2.894	-1.509
N	7.822	-0.685	4.113	C	8.937	-0.510	0.434
N	5.776	-2.025	5.288	C	9.789	0.696	-0.026
N	5.214	-3.031	2.630	H	10.463	0.456	-0.844
N	7.131	-1.334	1.773	C	8.188	-0.262	1.770
C	8.940	-0.335	3.136	H	8.759	-6.668	2.812
C	10.008	-1.454	3.106	N	8.567	-5.739	3.316
C	9.526	1.028	3.750	C	8.921	-5.428	4.660
C	11.041	1.226	3.499	C	7.888	-4.616	2.827
C	8.735	2.227	3.145	N	7.800	-3.619	3.722
H	9.036	3.207	3.497	C	8.484	-4.079	4.876
C	9.173	0.882	5.300	C	8.773	-3.416	6.094
C	10.315	0.360	6.252	C	9.416	-4.146	7.112
H	10.801	1.154	6.853	H	9.642	-3.658	8.067
C	7.960	-0.058	5.285	C	9.769	-5.514	6.924
C	7.092	-0.261	6.434	H	10.241	-6.067	7.744
C	7.341	0.607	7.668	C	9.555	-6.163	5.689
C	6.087	-1.240	6.422	C	5.178	-0.153	3.465
C	5.141	-1.619	7.611	C	4.357	0.325	2.261
C	5.894	-1.796	8.958	O	3.562	-0.733	1.603
C	4.046	-0.501	7.735	C	2.408	-0.956	2.488
H	3.356	-0.646	8.567	C	3.268	1.339	2.758
C	4.429	-2.929	7.074	C	1.972	0.440	3.020
C	4.713	-4.339	7.696	H	1.673	-1.521	1.968
H	5.721	-4.758	7.512	H	9.161	1.566	-0.275
C	4.766	-2.901	5.596	H	10.430	1.020	0.813
C	4.145	-3.778	4.706	H	7.439	-1.985	-2.460
C	4.407	-3.880	3.338	H	9.025	-1.309	-2.248
C	3.883	-5.061	2.507	H	6.072	-0.060	-1.615
C	2.354	-5.291	2.665	H	6.750	0.965	-0.323
C	4.607	-6.314	3.088	H	7.642	0.738	-1.847
C	4.318	-4.633	1.044	H	5.829	-3.676	-1.779
C	5.147	-5.666	0.218	H	4.240	-3.176	-1.215
H	4.621	-6.261	-0.546	H	5.392	-1.963	-1.796
C	5.163	-3.358	1.267	H	5.950	-5.120	-0.303
C	5.790	-2.668	0.223	H	5.654	-6.348	0.918
C	5.303	-2.891	-1.211	H	5.700	-6.169	3.147
C	6.832	-1.705	0.519	H	4.256	-6.481	4.122
C	7.759	-0.999	-0.520	H	4.393	-7.231	2.516
C	7.002	0.232	-1.108	H	2.044	-5.147	3.716
C	8.247	-1.882	-1.718	H	1.763	-4.608	2.044

Atom	X (Å)	Y (Å)	Z (Å)	Atom	X (Å)	Y (Å)	Z (Å)
H	2.092	-6.326	2.390	H	7.659	0.707	1.713
H	4.516	-4.328	8.784	H	3.334	-2.798	7.156
H	3.968	-5.024	7.252	H	9.904	-7.184	5.557
H	4.538	0.480	7.856	H	8.478	-2.377	6.250
H	3.452	-0.449	6.803	H	8.831	1.871	5.661
H	6.914	-2.185	8.813	H	7.433	-4.527	1.848
H	5.969	-0.836	9.494	H	9.618	-1.364	0.605
H	5.351	-2.485	9.625	H	3.402	-4.360	0.491
H	8.018	0.121	8.397	H	3.423	-4.476	5.139
H	7.794	1.572	7.392	H	2.738	-1.572	3.355
H	6.408	0.832	8.205	H	1.169	1.663	1.697
H	9.917	-0.396	6.954	H	3.118	3.222	2.017
H	11.088	-0.147	5.650	H	5.857	0.666	3.773
H	8.895	2.247	2.052	H	4.511	-0.380	4.315
H	7.650	2.087	3.307	H	4.982	0.765	1.469
H	11.651	0.335	3.697	H	1.745	0.405	4.100
H	11.225	1.538	2.455	O	0.801	1.002	2.359
H	11.436	2.033	4.138	H	3.581	1.877	3.672
H	10.432	-1.618	4.109	O	2.920	2.308	1.694
H	9.569	-2.396	2.752				
H	10.834	-1.174	2.428				

Table A.4.10. Optimized coordinates of the QM region for the free Ado(Im)Cbl model.

Atom	X (Å)	Y (Å)	Z (Å)	Atom	X (Å)	Y (Å)	Z (Å)
Co	-0.794	0.653	-0.016	C	-3.836	0.556	3.059
N	-1.400	2.446	-0.166	C	-3.799	1.553	4.249
N	-2.055	0.337	1.437	C	-5.296	0.162	2.612
N	0.051	-1.093	0.040	H	-6.067	0.302	3.367
N	0.354	1.186	-1.435	C	-3.017	-0.767	3.336
C	-0.645	3.376	-1.083	C	-2.413	-1.020	4.749
C	0.533	4.031	-0.336	H	-1.416	-0.623	5.052
C	-1.780	4.419	-1.501	C	-2.054	-0.808	2.168
C	-1.271	5.807	-1.928	C	-1.307	-1.950	1.870
C	-2.629	3.797	-2.644	C	-0.332	-2.087	0.878
H	-3.499	4.359	-2.976	C	0.408	-3.402	0.631
C	-2.636	4.457	-0.176	C	-0.547	-4.413	-0.053
C	-2.265	5.507	0.921	C	0.907	-4.011	1.958
H	-2.918	6.404	0.991	C	1.517	-2.955	-0.402
C	-2.466	3.030	0.334	C	2.996	-3.138	0.067
C	-3.355	2.429	1.300	H	3.650	-3.902	-0.414
C	-4.564	3.258	1.704	C	1.114	-1.514	-0.752
C	-3.070	1.183	1.870	C	1.727	-0.781	-1.774

Atom	X (Å)	Y (Å)	Z (Å)
C	2.791	-1.475	-2.606
C	1.315	0.570	-2.099
C	1.770	1.408	-3.338
C	1.089	0.773	-4.583
C	3.298	1.511	-3.613
H	3.966	1.947	-2.835
C	1.118	2.800	-3.005
C	0.788	3.737	-4.188
H	1.512	4.543	-4.265
C	-0.089	2.406	-2.152
H	3.614	1.194	2.901
N	2.608	1.431	2.613
C	1.854	2.498	3.086
C	1.802	0.734	1.748
N	0.617	1.311	1.615
C	0.625	2.404	2.460
H	-0.246	3.057	2.568
H	2.240	3.216	3.818
C	-2.009	0.014	-1.536
C	-3.158	-0.964	-1.511
O	-2.782	-2.319	-1.253
C	-3.968	-3.073	-0.912
C	-4.367	-0.753	-0.587
C	-5.133	-2.069	-0.821
H	-4.117	-3.892	-1.593
H	0.697	3.203	-5.151
H	-0.199	4.214	-4.034
H	3.675	0.504	-3.868
H	3.431	2.111	-4.538
H	1.388	-0.281	-4.727
H	-0.017	0.799	-4.501
H	1.373	1.327	-5.501
H	3.822	-1.311	-2.226
H	2.610	-2.563	-2.644
H	2.777	-1.132	-3.654
H	3.527	-2.166	0.003
H	2.981	-3.381	1.146
H	1.587	-3.341	2.517
H	0.048	-4.229	2.623
H	1.434	-4.971	1.799
H	-1.383	-4.691	0.621

Atom	X (Å)	Y (Å)	Z (Å)
H	-0.980	-3.979	-0.973
H	0.011	-5.339	-0.307
H	-3.164	-0.649	5.477
H	-2.404	-2.117	4.915
H	-5.583	0.700	1.689
H	-5.320	-0.907	2.326
H	-2.787	1.974	4.393
H	-4.489	2.401	4.090
H	-4.105	1.070	5.197
H	-4.300	4.108	2.368
H	-5.061	3.694	0.813
H	-5.326	2.665	2.228
H	-2.283	5.004	1.911
H	-1.224	5.855	0.782
H	-1.988	3.679	-3.540
H	-2.944	2.769	-2.377
H	-0.545	6.255	-1.226
H	-0.783	5.758	-2.921
H	-2.114	6.517	-2.034
H	0.206	4.533	0.589
H	1.284	3.268	-0.060
H	1.027	4.785	-0.978
H	-0.923	2.102	-2.816
H	-3.730	-1.609	3.204
H	-3.700	4.601	-0.443
H	2.052	-0.197	1.234
H	1.804	3.316	-2.310
H	1.340	-3.532	-1.333
H	-1.478	-2.820	2.517
H	-3.794	-3.519	0.094
H	-6.239	-1.093	-2.056
H	-4.743	1.162	-0.608
H	-1.278	-0.352	-2.274
H	-2.426	0.961	-1.919
H	-3.581	-0.896	-2.552
H	-5.806	-2.309	0.039
O	-5.859	-1.998	-2.039
H	-4.026	-0.714	0.465
O	-5.196	0.350	-0.914

Table A.4.11. Optimized coordinates of the QM region for the Ado(Im)Cbl/WT EAL holoenzyme model.

Atom	X (Å)	Y (Å)	Z (Å)	Atom	X (Å)	Y (Å)	Z (Å)
Co	6.632	-1.819	3.658	H	8.359	-2.987	-1.659
N	8.041	-0.650	4.106	C	8.787	-0.654	0.336
N	6.223	-1.979	5.589	C	9.589	0.557	-0.200
N	5.318	-3.084	3.028	H	10.139	0.356	-1.113
N	7.145	-1.460	1.881	C	8.158	-0.362	1.719
C	9.035	-0.290	3.000	H	8.728	-6.591	2.769
C	10.178	-1.331	2.948	N	8.611	-5.660	3.276
C	9.520	1.165	3.467	C	9.120	-5.353	4.561
C	10.926	1.590	3.010	C	7.916	-4.534	2.843
C	8.479	2.208	2.963	N	7.958	-3.558	3.770
H	8.655	3.230	3.274	C	8.728	-4.045	4.832
C	9.428	1.038	5.044	H	8.970	-3.426	5.689
C	10.701	0.551	5.845	H	9.691	-6.061	5.150
H	11.169	1.349	6.453	C	5.249	-0.352	3.751
C	8.266	0.068	5.213	C	4.482	0.284	2.586
C	7.514	-0.040	6.437	O	3.678	-0.696	1.802
C	7.740	1.036	7.499	C	2.400	-0.797	2.528
C	6.570	-1.054	6.599	C	3.422	1.285	3.190
C	5.627	-1.219	7.830	C	2.009	0.640	2.907
C	6.312	-1.160	9.221	H	1.694	-1.355	1.961
C	4.596	-0.004	7.732	H	8.952	1.449	-0.320
H	3.538	-0.212	7.620	H	10.344	0.831	0.557
C	4.997	-2.654	7.556	H	6.959	-2.128	-2.362
C	5.515	-3.857	8.419	H	8.519	-1.364	-2.397
H	6.492	-4.318	8.168	H	5.815	-0.266	-1.562
C	5.231	-2.811	6.060	H	6.312	0.682	-0.131
C	4.491	-3.693	5.274	H	7.302	0.698	-1.613
C	4.552	-3.829	3.877	H	5.722	-3.960	-1.387
C	3.768	-4.939	3.163	H	4.118	-3.659	-0.760
C	2.258	-4.887	3.525	H	5.045	-2.315	-1.443
C	4.366	-6.271	3.684	H	5.468	-5.512	0.190
C	4.077	-4.639	1.635	H	4.984	-6.610	1.479
C	4.598	-5.850	0.780	H	5.465	-6.269	3.554
H	3.904	-6.354	0.079	H	4.169	-6.359	4.765
C	5.093	-3.466	1.692	H	3.947	-7.163	3.200
C	5.675	-2.887	0.554	H	1.787	-3.958	3.172
C	5.121	-3.226	-0.829	H	1.717	-5.749	3.108
C	6.734	-1.893	0.679	H	2.126	-4.932	4.622
C	7.521	-1.164	-0.481	H	5.551	-3.530	9.473
C	6.677	0.059	-0.967	H	4.738	-4.647	8.386
C	7.874	-1.996	-1.763	H	4.720	0.627	8.630

Atom	X (Å)	Y (Å)	Z (Å)	Atom	X (Å)	Y (Å)	Z (Å)
H	4.880	0.634	6.873	H	3.913	-2.666	7.748
H	7.154	-1.862	9.322	H	9.129	2.023	5.441
H	6.688	-0.149	9.436	H	7.365	-4.431	1.918
H	5.568	-1.395	10.004	H	9.483	-1.508	0.462
H	8.491	0.746	8.257	H	3.146	-4.256	1.191
H	8.087	1.976	7.038	H	3.781	-4.330	5.807
H	6.812	1.286	8.033	H	2.566	-1.363	3.477
H	10.424	-0.277	6.522	H	1.772	2.202	1.716
H	11.461	0.160	5.148	H	3.949	3.207	3.198
H	8.521	2.222	1.860	H	5.776	0.454	4.303
H	7.452	1.909	3.241	H	4.512	-0.809	4.438
H	11.662	0.784	3.126	H	5.124	0.806	1.858
H	10.932	1.926	1.959	H	1.374	0.675	3.818
H	11.256	2.456	3.610	O	1.328	1.310	1.803
H	10.711	-1.400	3.909	H	3.581	1.415	4.275
H	9.771	-2.324	2.711	O	3.465	2.616	2.562
H	10.913	-1.074	2.164				
H	7.580	0.575	1.644				

Table A.4.12. Optimized coordinates of the QM region for the Ado(Im)Cbl/Y241βW holoenzyme model.

Atom	X (Å)	Y (Å)	Z (Å)	Atom	X (Å)	Y (Å)	Z (Å)
Co	6.564	-1.718	3.272	C	4.135	-0.549	7.219
N	7.920	-0.630	4.026	H	3.359	-0.544	7.980
N	5.908	-2.107	5.087	C	4.500	-3.045	6.794
N	5.377	-2.940	2.356	C	4.950	-4.442	7.338
N	7.279	-1.136	1.622	H	5.959	-4.800	7.048
C	8.959	-0.023	3.076	C	4.823	-2.922	5.316
C	10.195	-0.954	3.004	C	4.171	-3.697	4.359
C	9.234	1.370	3.824	C	4.498	-3.765	2.999
C	10.538	2.114	3.490	C	4.003	-4.925	2.122
C	8.024	2.302	3.483	C	2.471	-5.181	2.221
H	7.718	3.076	4.176	C	4.737	-6.175	2.707
C	9.197	0.903	5.338	C	4.501	-4.466	0.689
C	10.519	0.394	6.037	C	5.269	-5.521	-0.162
H	11.044	1.180	6.617	H	4.695	-6.097	-0.908
C	8.095	-0.161	5.272	C	5.394	-3.233	0.981
C	7.288	-0.522	6.415	C	6.083	-2.519	-0.008
C	7.537	0.200	7.740	C	5.691	-2.719	-1.476
C	6.240	-1.435	6.288	C	7.070	-1.510	0.353
C	5.155	-1.738	7.366	C	8.008	-0.738	-0.634
C	5.622	-1.892	8.835	C	7.216	0.421	-1.314

Atom	X (Å)	Y (Å)	Z (Å)
C	8.684	-1.607	-1.754
H	9.108	-2.590	-1.466
C	9.068	-0.129	0.386
C	9.840	1.146	-0.042
H	10.635	0.933	-0.752
C	8.242	0.025	1.688
H	8.864	-6.510	2.477
N	8.679	-5.568	2.952
C	9.030	-5.248	4.279
C	8.029	-4.450	2.430
N	7.945	-3.469	3.353
C	8.589	-3.947	4.502
H	8.665	-3.337	5.398
H	9.531	-5.955	4.936
C	5.198	-0.222	3.314
C	4.540	0.348	2.054
O	3.734	-0.662	1.311
C	2.540	-0.849	2.150
C	3.452	1.424	2.409
C	2.144	0.550	2.694
H	1.805	-1.394	1.610
H	9.181	1.944	-0.418
H	10.340	1.568	0.848
H	7.984	-1.771	-2.590
H	9.502	-1.005	-2.181
H	6.360	0.056	-1.895
H	6.840	1.138	-0.566
H	7.877	0.972	-2.002
H	6.264	-3.488	-2.024
H	4.629	-3.002	-1.553
H	5.816	-1.781	-2.035
H	6.072	-5.004	-0.712
H	5.777	-6.223	0.517
H	5.826	-6.006	2.776
H	4.381	-6.352	3.738
H	4.547	-7.093	2.129
H	2.086	-4.901	3.219
H	1.904	-4.609	1.474
H	2.245	-6.251	2.080

Atom	X (Å)	Y (Å)	Z (Å)
H	4.864	-4.465	8.440
H	4.211	-5.168	6.950
H	4.696	0.402	7.247
H	3.646	-0.588	6.227
H	6.567	-2.451	8.908
H	5.764	-0.919	9.332
H	4.853	-2.434	9.415
H	7.994	-0.458	8.500
H	8.202	1.065	7.614
H	6.600	0.592	8.172
H	10.267	-0.427	6.733
H	11.223	-0.015	5.295
H	8.281	2.807	2.532
H	7.125	1.707	3.268
H	11.432	1.535	3.762
H	10.608	2.382	2.422
H	10.555	3.072	4.042
H	10.542	-1.245	4.005
H	9.939	-1.879	2.464
H	11.030	-0.455	2.477
H	7.641	0.949	1.621
H	3.407	-3.016	6.936
H	8.843	1.742	5.956
H	7.593	-4.349	1.446
H	9.814	-0.905	0.612
H	3.614	-4.121	0.131
H	3.390	-4.369	4.730
H	2.813	-1.483	3.021
H	0.693	1.922	2.387
H	2.396	1.996	0.822
H	5.733	0.580	3.852
H	4.430	-0.620	4.001
H	5.256	0.766	1.329
H	1.911	0.517	3.775
O	0.991	1.086	1.940
H	3.760	2.055	3.257
O	3.204	2.336	1.297

Table A.4.13. Optimized coordinates of the QM region for the free 2'-dAdoCbl model.

Atom	X (Å)	Y (Å)	Z (Å)	Atom	X (Å)	Y (Å)	Z (Å)
Co	1.241	-0.328	0.000	C	0.252	-0.764	-3.996
N	2.266	-1.675	-0.860	C	0.909	-0.935	-5.398
N	2.215	-0.699	1.658	H	0.436	-1.737	-5.954
N	0.069	1.047	0.715	C	1.264	-0.733	-2.832
N	0.509	-0.075	-1.713	H	-3.507	-2.168	1.622
C	1.861	-2.058	-2.282	N	-2.474	-2.283	1.366
C	0.769	-3.156	-2.225	C	-1.666	-3.415	1.653
C	3.261	-2.551	-2.900	C	-1.637	-1.350	0.749
C	3.173	-3.547	-4.081	N	-0.377	-1.791	0.604
C	4.087	-1.289	-3.328	C	-0.367	-3.102	1.145
H	5.114	-1.464	-3.635	C	0.686	-4.032	1.277
C	3.943	-3.186	-1.617	C	0.453	-5.255	1.940
C	3.641	-4.699	-1.292	C	1.597	-6.241	2.124
H	4.501	-5.396	-1.356	C	-0.856	-5.555	2.471
C	3.409	-2.270	-0.507	C	-1.087	-6.846	3.241
C	4.073	-2.086	0.766	C	-1.919	-4.635	2.318
C	5.492	-2.631	0.925	C	2.657	1.066	-0.349
C	3.467	-1.346	1.785	C	2.356	2.351	-1.134
C	4.118	-0.938	3.146	O	1.685	3.383	-0.287
C	4.956	-1.993	3.919	C	2.696	4.366	0.195
C	5.070	0.290	2.766	C	3.654	3.048	-1.613
H	4.858	1.266	3.195	C	4.063	3.911	-0.392
C	2.833	-0.520	3.971	H	2.381	5.362	-0.049
C	2.166	-1.593	4.906	H	-0.772	-7.732	2.660
H	1.641	-2.439	4.421	H	-0.503	-6.851	4.183
C	1.913	-0.069	2.847	H	-2.150	-6.969	3.508
C	0.912	0.887	3.024	H	1.454	-7.160	1.521
C	0.099	1.443	2.024	H	2.557	-5.791	1.817
C	-0.874	2.586	2.344	H	1.700	-6.561	3.177
C	-0.080	3.821	2.868	H	0.902	-0.008	-5.990
C	-1.848	2.091	3.455	H	1.974	-1.205	-5.289
C	-1.522	2.878	0.922	H	-2.543	1.388	-4.346
C	-3.091	2.947	0.900	H	-2.037	-0.033	-5.266
H	-3.569	3.945	0.800	H	-0.273	2.738	-4.115
C	-0.874	1.816	-0.001	H	1.173	1.746	-4.373
C	-1.130	1.712	-1.375	H	-0.154	1.717	-5.568
C	-2.059	2.736	-2.026	H	-3.130	2.475	-1.941
C	-0.432	0.739	-2.201	H	-1.906	3.727	-1.569
C	-0.597	0.557	-3.749	H	-1.845	2.848	-3.096
C	0.074	1.763	-4.488	H	-3.484	2.315	0.087
C	-2.076	0.393	-4.245	H	-3.474	2.497	1.831
H	-2.753	-0.246	-3.634	H	-2.378	1.166	3.159

Atom	X (Å)	Y (Å)	Z (Å)	Atom	X (Å)	Y (Å)	Z (Å)
H	-1.275	1.862	4.371	H	1.085	-4.010	-1.609
H	-2.593	2.858	3.723	H	-0.148	-2.743	-1.780
H	0.609	4.191	2.090	H	0.531	-3.532	-3.233
H	-0.762	4.637	3.161	H	2.092	-0.049	-3.096
H	0.524	3.556	3.757	H	3.049	0.321	4.653
H	2.936	-1.989	5.592	H	-2.896	-4.877	2.747
H	1.426	-1.060	5.536	H	1.683	-3.777	0.909
H	6.112	0.022	3.017	H	5.032	-3.063	-1.708
H	5.059	0.424	1.667	H	-1.911	-0.348	0.451
H	4.454	-2.969	4.015	H	-0.408	-1.625	-3.805
H	5.937	-2.163	3.453	H	-1.091	3.834	0.567
H	5.148	-1.599	4.935	H	0.824	1.307	4.031
H	5.529	-3.574	1.501	H	2.717	4.305	1.301
H	5.953	-2.822	-0.056	H	4.093	4.300	-3.145
H	6.138	-1.897	1.433	H	3.460	0.484	-0.841
H	3.237	-4.763	-0.265	H	2.979	1.335	0.672
H	2.851	-5.078	-1.961	H	1.700	2.197	-2.004
H	3.594	-0.810	-4.194	H	4.611	3.286	0.336
H	4.078	-0.537	-2.519	H	4.732	4.733	-0.698
H	2.409	-4.328	-3.947	H	4.439	2.321	-1.902
H	2.947	-3.019	-5.024	O	3.273	3.887	-2.771
H	4.146	-4.050	-4.227				

Table A.4.14. Optimized coordinates of the QM region for the 2'-dAdoCbl/WT EAL holoenzyme model.

Atom	X (Å)	Y (Å)	Z (Å)	Atom	X (Å)	Y (Å)	Z (Å)
Co	6.388	-1.599	3.490	C	7.520	1.022	7.502
N	7.808	-0.470	4.012	C	6.272	-0.957	6.455
N	5.889	-1.790	5.379	C	5.356	-1.211	7.693
N	5.131	-2.882	2.784	C	6.093	-1.349	9.052
N	6.993	-1.237	1.741	C	4.400	0.060	7.764
C	8.854	-0.122	2.957	H	3.331	-0.075	7.664
C	9.981	-1.184	2.928	C	4.632	-2.562	7.283
C	9.374	1.302	3.477	C	5.040	-3.949	7.908
C	10.815	1.676	3.078	H	6.013	-4.408	7.640
C	8.395	2.394	2.961	C	4.849	-2.596	5.781
H	8.646	3.404	3.257	C	4.146	-3.477	4.958
C	9.218	1.145	5.049	C	4.339	-3.660	3.582
C	10.454	0.610	5.870	C	3.742	-4.869	2.848
H	10.943	1.375	6.503	C	2.220	-5.024	3.105
C	8.021	0.202	5.150	C	4.462	-6.112	3.450
C	7.251	0.039	6.362	C	4.111	-4.544	1.338

Atom	X (Å)	Y (Å)	Z (Å)
C	4.876	-5.643	0.537
H	4.335	-6.286	-0.180
C	5.003	-3.280	1.442
C	5.610	-2.677	0.334
C	5.111	-3.015	-1.072
C	6.654	-1.684	0.523
C	7.515	-0.996	-0.591
C	6.707	0.210	-1.164
C	7.950	-1.881	-1.811
H	8.433	-2.864	-1.635
C	8.728	-0.457	0.285
C	9.542	0.747	-0.242
H	10.133	0.526	-1.125
C	8.033	-0.154	1.635
H	8.661	-6.471	2.763
N	8.513	-5.523	3.241
C	8.986	-5.162	4.530
C	7.807	-4.413	2.763
N	7.798	-3.384	3.629
C	8.582	-3.807	4.732
C	8.993	-3.098	5.886
C	9.764	-3.761	6.862
C	10.230	-3.012	8.101
C	10.095	-5.152	6.686
C	10.873	-5.885	7.754
C	9.715	-5.852	5.521
C	5.045	-0.070	3.539
C	4.250	0.435	2.329
O	3.484	-0.633	1.644
C	2.264	-0.819	2.449
C	3.143	1.447	2.791
C	1.821	0.605	2.880
H	1.570	-1.401	1.888
H	11.858	-5.417	7.934
H	10.336	-5.896	8.723
H	11.030	-6.927	7.448
H	11.333	-2.941	8.153
H	9.829	-1.982	8.120
H	9.903	-3.510	9.033
H	8.891	1.620	-0.410
H	10.260	1.052	0.539
H	7.079	-2.044	-2.465
H	8.632	-1.273	-2.426

Atom	X (Å)	Y (Å)	Z (Å)
H	5.824	-0.124	-1.723
H	6.377	0.904	-0.373
H	7.350	0.773	-1.857
H	5.730	-3.738	-1.622
H	4.106	-3.454	-1.045
H	5.056	-2.104	-1.689
H	5.670	-5.141	-0.038
H	5.395	-6.279	1.269
H	5.561	-6.005	3.421
H	4.182	-6.202	4.514
H	4.175	-7.051	2.951
H	1.646	-4.169	2.722
H	1.833	-5.946	2.648
H	2.019	-5.101	4.191
H	4.950	-3.902	9.006
H	4.244	-4.642	7.573
H	4.584	0.588	8.716
H	4.696	0.772	6.971
H	6.932	-2.060	9.009
H	6.496	-0.384	9.396
H	5.380	-1.691	9.824
H	8.296	0.668	8.207
H	7.854	1.996	7.104
H	6.611	1.227	8.086
H	10.140	-0.220	6.529
H	11.209	0.197	5.181
H	8.435	2.389	1.859
H	7.351	2.172	3.250
H	11.526	0.852	3.221
H	10.875	2.010	2.028
H	11.157	2.528	3.693
H	10.429	-1.330	3.924
H	9.584	-2.152	2.592
H	10.779	-0.870	2.234
H	7.477	0.796	1.548
H	3.554	-2.531	7.501
H	10.010	-6.899	5.415
H	8.697	-2.057	6.026
H	8.927	2.125	5.463
H	7.276	-4.354	1.821
H	9.426	-1.296	0.463
H	3.172	-4.299	0.818
H	3.408	-4.115	5.452

Atom	X (Å)	Y (Å)	Z (Å)
H	2.518	-1.413	3.356
H	2.565	3.276	2.168
H	5.644	0.765	3.957
H	4.342	-0.412	4.321
H	4.885	0.902	1.558
H	1.387	0.619	3.894

Atom	X (Å)	Y (Å)	Z (Å)
H	1.092	1.038	2.173
H	3.396	1.886	3.773
O	3.055	2.510	1.774

Table A.4.15. Optimized coordinates of the QM region for the 2'-dAdoCbl/WT EAL ternary complex model.

Atom	X (Å)	Y (Å)	Z (Å)
Co	6.322	-1.201	3.200
N	7.757	-0.187	3.874
N	5.621	-1.386	5.011
N	5.123	-2.502	2.373
N	7.162	-0.924	1.533
C	8.934	0.054	2.928
C	9.911	-1.147	2.929
C	9.614	1.374	3.538
C	11.151	1.356	3.380
C	9.026	2.646	2.849
H	9.529	3.578	3.098
C	9.150	1.340	5.067
C	10.198	0.830	6.123
H	10.691	1.636	6.701
C	7.891	0.463	5.033
C	6.997	0.311	6.174
C	7.273	1.162	7.415
C	5.966	-0.637	6.167
C	5.075	-1.069	7.390
C	5.891	-1.273	8.695
C	3.974	0.015	7.673
H	3.339	-0.196	8.535
C	4.383	-2.381	6.830
C	4.708	-3.787	7.440
H	5.712	-4.198	7.222
C	4.682	-2.325	5.343
C	4.077	-3.234	4.467
C	4.329	-3.356	3.101
C	3.848	-4.574	2.293
C	2.344	-4.897	2.474
C	4.642	-5.785	2.875
C	4.232	-4.147	0.818

Atom	X (Å)	Y (Å)	Z (Å)
C	4.981	-5.217	-0.035
H	4.416	-5.850	-0.742
C	5.115	-2.887	1.024
C	5.800	-2.245	-0.018
C	5.324	-2.473	-1.457
C	6.884	-1.326	0.286
C	7.831	-0.654	-0.749
C	7.062	0.555	-1.359
C	8.310	-1.561	-1.930
H	8.737	-2.558	-1.705
C	8.998	-0.127	0.209
C	9.837	1.087	-0.264
H	10.439	0.873	-1.142
C	8.231	0.137	1.534
H	8.712	-6.163	2.657
N	8.510	-5.222	3.134
C	8.954	-4.836	4.426
C	7.746	-4.151	2.653
N	7.656	-3.134	3.527
C	8.445	-3.518	4.640
C	8.764	-2.810	5.823
C	9.570	-3.425	6.800
C	9.933	-2.684	8.078
C	10.046	-4.767	6.591
C	10.916	-5.433	7.630
C	9.735	-5.476	5.410
C	5.331	0.624	2.716
C	4.033	1.380	3.135
O	2.902	1.048	2.236
C	2.366	-0.173	2.862
C	3.478	1.160	4.567
C	2.369	0.086	4.390

Atom	X (Å)	Y (Å)	Z (Å)	Atom	X (Å)	Y (Å)	Z (Å)
H	1.456	-0.463	2.400	H	7.867	0.628	8.180
H	11.852	-4.867	7.797	H	7.832	2.072	7.154
H	10.410	-5.521	8.611	H	6.341	1.484	7.906
H	11.175	-6.443	7.290	H	9.716	0.149	6.845
H	11.021	-2.493	8.150	H	10.974	0.238	5.609
H	9.417	-1.709	8.138	H	9.122	2.548	1.756
H	9.654	-3.262	8.979	H	7.944	2.733	3.064
H	9.212	1.979	-0.430	H	11.617	0.407	3.671
H	10.549	1.364	0.536	H	11.413	1.547	2.324
H	7.480	-1.702	-2.639	H	11.616	2.139	3.997
H	9.056	-0.997	-2.509	H	10.269	-1.388	3.942
H	6.112	0.258	-1.824	H	9.423	-2.036	2.512
H	6.843	1.310	-0.589	H	10.790	-0.912	2.304
H	7.687	1.020	-2.132	H	7.719	1.115	1.461
H	5.924	-3.172	-2.061	H	3.287	-2.285	6.916
H	4.294	-2.861	-1.462	H	10.141	-6.481	5.279
H	5.309	-1.515	-2.001	H	8.379	-1.802	5.986
H	5.758	-4.703	-0.624	H	8.832	2.366	5.339
H	5.528	-5.873	0.658	H	7.232	-4.121	1.701
H	5.729	-5.599	2.901	H	9.693	-0.964	0.401
H	4.327	-5.941	3.923	H	3.298	-3.828	0.312
H	4.444	-6.721	2.327	H	3.388	-3.952	4.920
H	2.062	-4.791	3.537	H	3.092	-0.989	2.660
H	1.704	-4.246	1.859	H	1.440	0.514	4.798
H	2.141	-5.948	2.214	H	3.487	2.993	5.421
H	4.552	-3.770	8.535	H	5.271	0.479	1.626
H	3.953	-4.488	7.036	H	6.182	1.283	2.969
H	4.474	0.987	7.832	H	4.234	2.456	2.956
H	3.314	0.138	6.805	H	2.607	-0.845	4.926
H	6.897	-1.684	8.522	H	4.303	0.862	5.233
H	6.008	-0.316	9.228	O	2.792	2.345	5.124
H	5.345	-1.943	9.380				

Table A.4.16. Optimized coordinates of the QM region for the free 3'-dAdoCbl model.

Atom	X (Å)	Y (Å)	Z (Å)	Atom	X (Å)	Y (Å)	Z (Å)
Co	1.398	0.413	-0.056	C	4.175	-0.850	-2.883
N	2.896	-0.418	-0.866	C	4.527	-1.781	-4.066
N	2.436	0.593	1.602	C	4.389	0.641	-3.310
N	-0.269	1.186	0.624	H	5.416	0.932	-3.507
N	0.616	0.245	-1.757	C	5.048	-1.134	-1.592
C	2.693	-0.996	-2.270	C	5.375	-2.637	-1.253
C	2.194	-2.459	-2.147	H	6.447	-2.864	-1.144

Atom	X (Å)	Y (Å)	Z (Å)
C	4.185	-0.474	-0.504
C	4.707	0.041	0.744
C	6.223	0.153	0.902
C	3.845	0.537	1.732
C	4.268	1.289	3.037
C	5.465	0.735	3.858
C	4.624	2.765	2.549
H	3.989	3.574	2.896
C	2.928	1.213	3.863
C	2.760	0.036	4.883
H	2.642	-0.971	4.454
C	1.900	1.144	2.746
C	0.586	1.590	2.901
C	-0.411	1.630	1.911
C	-1.825	2.150	2.230
C	-1.765	3.617	2.750
C	-2.410	1.234	3.351
C	-2.543	2.047	0.817
C	-3.960	1.379	0.833
H	-4.834	2.049	0.748
C	-1.481	1.360	-0.086
C	-1.677	1.048	-1.432
C	-3.003	1.423	-2.091
C	-0.606	0.489	-2.243
C	-0.684	0.176	-3.775
C	-0.655	1.527	-4.566
C	-1.913	-0.673	-4.230
H	-2.176	-1.540	-3.596
C	0.669	-0.621	-4.005
C	1.319	-0.516	-5.417
H	1.262	-1.461	-5.944
C	1.574	-0.092	-2.866
H	-2.043	-3.266	1.762
N	-1.078	-2.919	1.502
C	0.144	-3.531	1.870
C	-0.758	-1.765	0.794
N	0.571	-1.586	0.661
C	1.168	-2.702	1.314
C	2.527	-3.040	1.513
C	2.854	-4.179	2.283
C	4.315	-4.521	2.535
C	1.809	-4.995	2.857
C	2.167	-6.183	3.738

Atom	X (Å)	Y (Å)	Z (Å)
C	0.450	-4.672	2.641
C	2.133	2.251	-0.444
C	1.782	3.149	-1.640
O	0.343	3.530	-1.721
C	0.183	4.624	-0.749
C	2.509	4.535	-1.502
C	1.458	5.495	-0.843
H	-0.723	5.124	-0.905
H	2.842	-6.890	3.220
H	2.692	-5.850	4.655
H	1.266	-6.736	4.052
H	4.615	-5.453	2.016
H	4.977	-3.713	2.177
H	4.522	-4.673	3.610
H	0.880	0.284	-6.032
H	2.390	-0.264	-5.328
H	-2.806	-0.031	-4.326
H	-1.700	-1.049	-5.250
H	-1.432	2.230	-4.232
H	0.315	2.042	-4.438
H	-0.808	1.341	-5.644
H	-3.762	0.619	-2.040
H	-3.432	2.321	-1.621
H	-2.866	1.661	-3.153
H	-4.039	0.634	0.025
H	-4.080	0.805	1.766
H	-2.415	0.170	3.051
H	-1.784	1.314	4.256
H	-3.435	1.530	3.635
H	-1.371	4.300	1.978
H	-2.764	3.973	3.057
H	-1.104	3.699	3.633
H	3.617	0.037	5.580
H	1.861	0.249	5.492
H	5.666	2.997	2.832
H	4.606	2.800	1.443
H	5.409	-0.352	4.033
H	6.432	0.951	3.378
H	5.476	1.245	4.840
H	6.648	-0.627	1.558
H	6.729	0.084	-0.073
H	6.502	1.134	1.320
H	4.868	-2.931	-0.316

Atom	X (Å)	Y (Å)	Z (Å)	Atom	X (Å)	Y (Å)	Z (Å)
H	4.974	-3.297	-2.040	H	-1.471	-1.041	0.417
H	3.828	0.837	-4.242	H	0.477	-1.684	-3.780
H	3.967	1.322	-2.551	H	-2.631	3.081	0.425
H	4.149	-2.810	-3.949	H	0.333	2.003	3.881
H	4.121	-1.387	-5.014	H	0.146	4.187	0.274
H	5.625	-1.835	-4.191	H	2.010	7.214	-1.752
H	2.852	-3.059	-1.503	H	3.227	2.080	-0.440
H	1.188	-2.465	-1.696	H	1.858	2.770	0.491
H	2.140	-2.947	-3.135	H	2.010	2.676	-2.609
H	2.026	0.861	-3.189	H	1.786	5.825	0.164
H	2.782	2.125	4.470	O	1.178	6.678	-1.681
H	-0.327	-5.292	3.101	H	3.441	4.459	-0.914
H	3.312	-2.393	1.115	H	2.748	4.920	-2.510
H	6.005	-0.597	-1.697				

Table A.4.17. Optimized coordinates of the QM region for the 3'-dAdoCbl/WT EAL holoenzyme model.

Atom	X (Å)	Y (Å)	Z (Å)	Atom	X (Å)	Y (Å)	Z (Å)
Co	6.366	-1.565	3.484	H	5.963	-4.403	7.582
N	7.791	-0.450	4.020	C	4.802	-2.560	5.758
N	5.849	-1.759	5.367	C	4.096	-3.431	4.928
N	5.112	-2.847	2.768	C	4.306	-3.619	3.556
N	6.992	-1.207	1.740	C	3.715	-4.828	2.816
C	8.847	-0.106	2.974	C	2.187	-4.967	3.051
C	9.965	-1.177	2.949	C	4.416	-6.077	3.430
C	9.374	1.313	3.504	C	4.106	-4.509	1.312
C	10.821	1.678	3.119	C	4.881	-5.613	0.524
C	8.406	2.414	2.986	H	4.349	-6.249	-0.206
H	8.667	3.422	3.280	C	5.000	-3.248	1.425
C	9.204	1.152	5.074	C	5.622	-2.650	0.323
C	10.434	0.612	5.903	C	5.139	-2.996	-1.087
H	10.924	1.376	6.537	C	6.666	-1.659	0.522
C	8.003	0.213	5.163	C	7.540	-0.977	-0.586
C	7.228	0.045	6.370	C	6.739	0.226	-1.175
C	7.498	1.017	7.520	C	7.991	-1.866	-1.797
C	6.241	-0.944	6.452	H	8.472	-2.848	-1.610
C	5.322	-1.203	7.687	C	8.742	-0.431	0.301
C	6.048	-1.359	9.049	C	9.551	0.778	-0.223
C	4.375	0.074	7.764	H	10.151	0.557	-1.100
H	3.306	-0.053	7.659	C	8.035	-0.129	1.645
C	4.589	-2.544	7.261	H	8.651	-6.467	2.768
C	4.995	-3.942	7.865	N	8.500	-5.517	3.245

Atom	X (Å)	Y (Å)	Z (Å)
C	8.969	-5.154	4.536
C	7.794	-4.407	2.763
N	7.781	-3.380	3.629
C	8.561	-3.800	4.734
C	8.962	-3.092	5.890
C	9.731	-3.751	6.869
C	10.189	-3.000	8.111
C	10.070	-5.140	6.696
C	10.850	-5.869	7.765
C	9.696	-5.843	5.529
C	5.032	-0.023	3.520
C	4.284	0.496	2.287
O	3.507	-0.562	1.589
C	2.259	-0.688	2.356
C	3.171	1.546	2.680
C	1.814	0.744	2.723
H	1.570	-1.295	1.817
H	11.832	-5.395	7.948
H	10.311	-5.884	8.733
H	11.015	-6.910	7.459
H	11.291	-2.917	8.162
H	9.776	-1.976	8.133
H	9.868	-3.505	9.041
H	8.892	1.642	-0.401
H	10.259	1.095	0.562
H	7.130	-2.032	-2.463
H	8.682	-1.261	-2.406
H	5.859	-0.109	-1.738
H	6.407	0.926	-0.390
H	7.388	0.783	-1.867
H	5.752	-3.741	-1.618
H	4.124	-3.413	-1.069
H	5.112	-2.093	-1.717
H	5.689	-5.112	-0.033
H	5.380	-6.256	1.264
H	5.517	-5.985	3.409
H	4.126	-6.160	4.492
H	4.120	-7.013	2.930
H	1.633	-4.090	2.689
H	1.791	-5.867	2.557

Atom	X (Å)	Y (Å)	Z (Å)
H	1.972	-5.074	4.131
H	4.915	-3.907	8.965
H	4.192	-4.627	7.529
H	4.559	0.594	8.722
H	4.678	0.791	6.979
H	6.879	-2.078	9.008
H	6.456	-0.401	9.405
H	5.324	-1.700	9.812
H	8.260	0.648	8.233
H	7.853	1.988	7.132
H	6.585	1.234	8.093
H	10.112	-0.215	6.562
H	11.189	0.194	5.217
H	8.447	2.406	1.883
H	7.360	2.201	3.275
H	11.526	0.850	3.270
H	10.894	2.009	2.068
H	11.162	2.529	3.735
H	10.403	-1.332	3.947
H	9.563	-2.139	2.603
H	10.772	-0.864	2.265
H	7.486	0.826	1.556
H	3.512	-2.511	7.486
H	9.995	-6.888	5.424
H	8.662	-2.053	6.031
H	8.913	2.132	5.490
H	7.267	-4.353	1.820
H	9.443	-1.265	0.484
H	3.175	-4.263	0.777
H	3.349	-4.065	5.414
H	2.479	-1.224	3.308
H	0.466	2.094	2.062
H	5.626	0.800	3.967
H	4.301	-0.367	4.276
H	4.977	0.897	1.528
H	1.370	0.772	3.740
O	0.827	1.226	1.735
H	3.382	2.035	3.643
H	3.099	2.319	1.895

Table A.4.18. Optimized coordinates of the QM region for the 3'-dAdoCbl/WT EAL ternary complex model.

Atom	X (Å)	Y (Å)	Z (Å)	Atom	X (Å)	Y (Å)	Z (Å)
Co	6.362	-1.111	3.220	H	9.016	-2.457	-1.501
N	7.790	-0.109	3.940	C	9.091	0.029	0.310
N	5.627	-1.304	5.022	C	9.864	1.287	-0.152
N	5.153	-2.381	2.358	H	10.527	1.089	-0.988
N	7.249	-0.845	1.582	C	8.286	0.249	1.612
C	8.973	0.186	3.013	H	8.677	-6.152	2.675
C	9.999	-0.975	3.043	N	8.493	-5.205	3.148
C	9.564	1.541	3.638	C	8.942	-4.824	4.440
C	11.090	1.696	3.452	C	7.753	-4.121	2.662
C	8.831	2.766	3.012	N	7.678	-3.097	3.535
H	9.244	3.736	3.273	C	8.456	-3.497	4.652
C	9.150	1.419	5.172	C	8.774	-2.795	5.839
C	10.235	0.869	6.168	C	9.567	-3.422	6.819
H	10.696	1.648	6.806	C	9.932	-2.687	8.100
C	7.909	0.525	5.115	C	10.028	-4.768	6.608
C	7.014	0.346	6.245	C	10.893	-5.442	7.646
C	7.280	1.182	7.498	C	9.713	-5.473	5.427
C	5.979	-0.595	6.199	C	5.418	0.732	2.717
C	5.079	-1.044	7.403	C	4.115	1.505	3.057
C	5.885	-1.296	8.704	O	3.015	1.159	2.115
C	3.987	0.046	7.694	C	2.298	0.114	2.851
H	3.368	-0.165	8.567	C	3.508	1.375	4.490
C	4.364	-2.327	6.809	C	2.131	0.645	4.279
C	4.676	-3.756	7.371	H	1.435	-0.219	2.330
H	5.665	-4.185	7.120	H	11.828	-4.879	7.821
C	4.653	-2.218	5.324	H	10.383	-5.537	8.625
C	4.014	-3.068	4.420	H	11.153	-6.449	7.299
C	4.298	-3.190	3.061	H	11.022	-2.503	8.176
C	3.754	-4.371	2.244	H	9.423	-1.709	8.163
C	2.212	-4.505	2.354	H	9.647	-3.266	8.999
C	4.398	-5.645	2.876	H	9.187	2.125	-0.377
C	4.258	-4.013	0.785	H	10.509	1.635	0.676
C	5.003	-5.146	0.009	H	7.807	-1.690	-2.570
H	4.454	-5.787	-0.706	H	9.351	-0.923	-2.342
C	5.194	-2.790	1.014	H	6.275	0.221	-1.842
C	5.958	-2.198	-0.003	H	6.910	1.342	-0.613
C	5.581	-2.480	-1.463	H	7.819	1.049	-2.120
C	7.025	-1.264	0.328	H	6.237	-3.184	-2.003
C	7.991	-0.577	-0.679	H	4.562	-2.889	-1.527
C	7.192	0.577	-1.353	H	5.589	-1.540	-2.038
C	8.575	-1.490	-1.805	H	5.818	-4.672	-0.563

Atom	X (Å)	Y (Å)	Z (Å)	Atom	X (Å)	Y (Å)	Z (Å)
H	5.501	-5.798	0.745	H	11.457	2.516	4.090
H	5.499	-5.576	2.922	H	10.359	-1.175	4.066
H	4.049	-5.746	3.920	H	9.541	-1.894	2.652
H	4.118	-6.568	2.344	H	10.873	-0.728	2.415
H	1.896	-4.403	3.408	H	7.737	1.206	1.539
H	1.692	-3.741	1.755	H	3.273	-2.222	6.918
H	1.878	-5.503	2.032	H	10.108	-6.482	5.297
H	4.549	-3.761	8.470	H	8.400	-1.781	5.996
H	3.897	-4.431	6.969	H	8.822	2.421	5.508
H	4.487	1.020	7.842	H	7.243	-4.084	1.707
H	3.320	0.159	6.826	H	9.839	-0.745	0.545
H	6.888	-1.710	8.519	H	3.381	-3.665	0.204
H	6.010	-0.358	9.267	H	3.284	-3.759	4.848
H	5.335	-1.984	9.365	H	2.971	-0.771	2.927
H	7.931	0.667	8.228	H	1.104	2.203	5.041
H	7.770	2.134	7.239	H	3.390	2.363	4.977
H	6.348	1.433	8.027	H	5.434	0.610	1.621
H	9.797	0.106	6.833	H	6.258	1.375	3.042
H	11.032	0.365	5.595	H	4.345	2.563	2.820
H	8.909	2.705	1.915	H	1.998	-0.183	4.999
H	7.752	2.739	3.257	O	0.965	1.547	4.307
H	11.670	0.802	3.713	H	4.186	0.780	5.112
H	11.322	1.960	2.405				

Table A.4.19. Optimized coordinates of the QM region for the free 2',3'-ddAdoCbl model.

Atom	X (Å)	Y (Å)	Z (Å)	Atom	X (Å)	Y (Å)	Z (Å)
Co	1.377	0.395	-0.096	C	3.812	0.657	1.676
N	2.888	-0.442	-0.870	C	4.207	1.483	2.944
N	2.404	0.657	1.552	C	5.447	1.050	3.770
N	-0.297	1.185	0.547	C	4.451	2.959	2.375
N	0.603	0.145	-1.787	H	3.802	3.763	2.711
C	2.702	-1.080	-2.246	C	2.883	1.346	3.799
C	2.250	-2.551	-2.067	C	2.794	0.184	4.852
C	4.172	-0.904	-2.869	H	2.722	-0.852	4.468
C	4.561	-1.862	-4.019	C	1.854	1.212	2.686
C	4.308	0.584	-3.351	C	0.535	1.640	2.823
H	5.307	0.947	-3.571	C	-0.445	1.668	1.818
C	5.062	-1.112	-1.574	C	-1.845	2.229	2.108
C	5.441	-2.595	-1.188	C	-1.747	3.712	2.577
H	6.521	-2.798	-1.047	C	-2.455	1.370	3.258
C	4.180	-0.441	-0.510	C	-2.559	2.088	0.691
C	4.687	0.152	0.709	C	-3.997	1.455	0.724
C	6.197	0.340	0.852	H	-4.876	2.128	0.616

Atom	X (Å)	Y (Å)	Z (Å)
C	-1.501	1.346	-0.178
C	-1.688	0.979	-1.513
C	-2.995	1.352	-2.210
C	-0.616	0.373	-2.289
C	-0.684	-0.008	-3.805
C	-0.630	1.310	-4.651
C	-1.928	-0.859	-4.235
H	-2.222	-1.710	-3.580
C	0.668	-0.822	-3.989
C	1.320	-0.780	-5.403
H	1.303	-1.759	-5.870
C	1.564	-0.234	-2.879
H	-2.080	-3.188	1.849
N	-1.101	-2.860	1.566
C	0.122	-3.485	1.931
C	-0.757	-1.724	0.832
N	0.569	-1.574	0.684
C	1.154	-2.683	1.350
C	2.509	-3.029	1.543
C	2.832	-4.151	2.335
C	4.293	-4.497	2.584
C	1.785	-4.945	2.933
C	2.140	-6.115	3.837
C	0.427	-4.615	2.721
C	2.090	2.220	-0.572
C	1.660	3.064	-1.775
O	0.248	3.528	-1.695
C	0.252	4.688	-0.780
C	2.469	4.402	-1.831
C	1.634	5.400	-0.962
H	-0.614	5.286	-0.962
H	2.811	-6.835	3.334
H	2.668	-5.762	4.746
H	1.238	-6.657	4.165
H	4.593	-5.426	2.061
H	4.953	-3.687	2.229
H	4.501	-4.652	3.658
H	0.849	-0.040	-6.067
H	2.379	-0.475	-5.329
H	-2.803	-0.196	-4.351
H	-1.717	-1.265	-5.244
H	-1.344	2.068	-4.300
H	0.374	1.770	-4.601

Atom	X (Å)	Y (Å)	Z (Å)
H	-0.851	1.094	-5.712
H	-3.768	0.563	-2.149
H	-3.412	2.271	-1.778
H	-2.832	1.555	-3.276
H	-4.085	0.684	-0.058
H	-4.120	0.915	1.677
H	-2.470	0.295	3.000
H	-1.836	1.478	4.166
H	-3.477	1.689	3.521
H	-1.389	4.367	1.764
H	-2.722	4.089	2.927
H	-1.038	3.812	3.419
H	3.660	0.258	5.534
H	1.892	0.373	5.467
H	5.496	3.250	2.584
H	4.369	2.936	1.272
H	5.465	-0.028	4.000
H	6.391	1.306	3.265
H	5.435	1.608	4.725
H	6.655	-0.368	1.564
H	6.703	0.222	-0.118
H	6.429	1.362	1.195
H	4.918	-2.879	-0.256
H	5.076	-3.281	-1.971
H	3.730	0.704	-4.286
H	3.843	1.261	-2.615
H	4.231	-2.901	-3.863
H	4.132	-1.519	-4.977
H	5.658	-1.869	-4.149
H	2.933	-3.109	-1.412
H	1.249	-2.573	-1.608
H	2.206	-3.072	-3.037
H	1.998	0.709	-3.253
H	2.696	2.257	4.393
H	-0.348	-5.220	3.203
H	3.296	-2.396	1.125
H	5.996	-0.545	-1.701
H	-1.444	-0.983	0.447
H	0.476	-1.870	-3.711
H	-2.613	3.106	0.256
H	0.270	2.073	3.791
H	0.175	4.316	0.265
H	3.182	2.045	-0.620

Atom	X (Å)	Y (Å)	Z (Å)
H	1.863	2.774	0.354
H	1.727	2.519	-2.731
H	2.112	5.587	0.014
H	1.547	6.373	-1.475

Atom	X (Å)	Y (Å)	Z (Å)
H	3.502	4.284	-1.460
H	2.518	4.751	-2.878

Table A.4.20. Optimized coordinates of QM region for the 2',3'-ddAdoCbl /WT EAL holoenzyme model.

Atom	X (Å)	Y (Å)	Z (Å)
Co	6.397	-1.597	3.484
N	7.822	-0.477	4.010
N	5.884	-1.780	5.371
N	5.126	-2.870	2.774
N	7.007	-1.242	1.734
C	8.865	-0.131	2.955
C	9.988	-1.196	2.925
C	9.380	1.296	3.475
C	10.816	1.683	3.072
C	8.387	2.379	2.967
H	8.633	3.391	3.258
C	9.230	1.137	5.047
C	10.470	0.604	5.863
H	10.955	1.368	6.501
C	8.033	0.194	5.148
C	7.255	0.039	6.355
C	7.516	1.029	7.493
C	6.267	-0.948	6.446
C	5.336	-1.187	7.675
C	6.053	-1.317	9.045
C	4.385	0.090	7.718
H	3.317	-0.042	7.602
C	4.611	-2.537	7.267
C	5.009	-3.921	7.905
H	5.985	-4.383	7.651
C	4.840	-2.579	5.767
C	4.136	-3.458	4.945
C	4.328	-3.640	3.572
C	3.709	-4.836	2.837
C	2.178	-4.928	3.084
C	4.384	-6.098	3.446
C	4.097	-4.527	1.330
C	4.866	-5.639	0.545
H	4.332	-6.286	-0.174

Atom	X (Å)	Y (Å)	Z (Å)
C	4.996	-3.269	1.433
C	5.615	-2.674	0.325
C	5.124	-3.023	-1.083
C	6.665	-1.686	0.514
C	7.531	-0.999	-0.598
C	6.725	0.208	-1.174
C	7.968	-1.882	-1.819
H	8.452	-2.865	-1.643
C	8.742	-0.460	0.281
C	9.552	0.748	-0.242
H	10.142	0.530	-1.126
C	8.046	-0.161	1.631
H	8.659	-6.470	2.767
N	8.510	-5.522	3.246
C	8.985	-5.160	4.535
C	7.800	-4.413	2.770
N	7.791	-3.387	3.638
C	8.578	-3.806	4.737
C	8.988	-3.098	5.890
C	9.757	-3.759	6.867
C	10.218	-3.008	8.109
C	10.092	-5.148	6.692
C	10.873	-5.880	7.759
C	9.715	-5.849	5.525
C	5.079	-0.047	3.534
C	4.332	0.519	2.322
O	3.542	-0.513	1.596
C	2.289	-0.631	2.358
C	3.244	1.569	2.790
C	1.862	0.823	2.683
H	1.604	-1.242	1.816
H	11.857	-5.409	7.939
H	10.336	-5.893	8.728
H	11.033	-6.921	7.452

Atom	X (Å)	Y (Å)	Z (Å)	Atom	X (Å)	Y (Å)	Z (Å)
H	11.321	-2.931	8.160	H	6.599	1.250	8.058
H	9.811	-1.981	8.129	H	10.162	-0.233	6.516
H	9.895	-3.510	9.040	H	11.228	0.202	5.171
H	8.897	1.619	-0.408	H	8.417	2.371	1.863
H	10.269	1.054	0.538	H	7.348	2.150	3.267
H	7.097	-2.045	-2.473	H	11.532	0.862	3.208
H	8.649	-1.274	-2.435	H	10.869	2.022	2.022
H	5.851	-0.128	-1.745	H	11.153	2.536	3.688
H	6.383	0.894	-0.380	H	10.430	-1.351	3.921
H	7.372	0.779	-1.855	H	9.587	-2.159	2.580
H	5.753	-3.746	-1.626	H	10.791	-0.880	2.237
H	4.123	-3.472	-1.059	H	7.490	0.790	1.545
H	5.064	-2.116	-1.706	H	3.532	-2.500	7.476
H	5.668	-5.142	-0.024	H	10.013	-6.895	5.418
H	5.375	-6.272	1.288	H	8.690	-2.058	6.033
H	5.487	-6.031	3.413	H	8.941	2.117	5.463
H	4.106	-6.174	4.511	H	7.266	-4.356	1.829
H	4.064	-7.029	2.952	H	9.440	-1.299	0.456
H	1.655	-4.020	2.754	H	3.165	-4.284	0.795
H	1.741	-5.797	2.571	H	3.392	-4.090	5.436
H	1.972	-5.058	4.163	H	2.498	-1.165	3.313
H	4.906	-3.866	9.002	H	5.675	0.762	4.001
H	4.215	-4.615	7.567	H	4.341	-0.400	4.278
H	4.556	0.626	8.669	H	5.021	0.936	1.568
H	4.696	0.795	6.925	H	1.289	0.887	3.624
H	6.894	-2.026	9.015	H	1.248	1.255	1.874
H	6.449	-0.351	9.391	H	3.428	1.879	3.828
H	5.331	-1.658	9.809	H	3.270	2.469	2.153
H	8.276	0.674	8.214				
H	7.865	1.997	7.093				

Table A.4.21. Optimized coordinates of QM region for the 2',3'-ddAdoCbl/WT EAL ternary complex model.

Atom	X (Å)	Y (Å)	Z (Å)	Atom	X (Å)	Y (Å)	Z (Å)
Co	6.412	-1.160	3.216	C	11.097	1.718	3.408
N	7.821	-0.125	3.925	C	8.834	2.760	2.979
N	5.688	-1.358	5.020	H	9.203	3.734	3.285
N	5.218	-2.445	2.360	C	9.174	1.412	5.147
N	7.277	-0.872	1.572	C	10.270	0.858	6.133
C	8.994	0.183	2.991	H	10.716	1.630	6.789
C	10.038	-0.962	3.019	C	7.938	0.507	5.098
C	9.577	1.542	3.610	C	7.053	0.315	6.235

Atom	X (Å)	Y (Å)	Z (Å)
C	7.319	1.148	7.490
C	6.023	-0.632	6.195
C	5.109	-1.069	7.395
C	5.896	-1.293	8.713
C	4.011	0.022	7.662
H	3.360	-0.189	8.511
C	4.417	-2.367	6.809
C	4.741	-3.782	7.399
H	5.746	-4.192	7.179
C	4.728	-2.284	5.327
C	4.115	-3.164	4.430
C	4.389	-3.279	3.069
C	3.887	-4.481	2.251
C	2.370	-4.746	2.410
C	4.637	-5.716	2.842
C	4.313	-4.066	0.784
C	5.032	-5.165	-0.057
H	4.454	-5.798	-0.755
C	5.233	-2.832	1.011
C	5.959	-2.203	-0.011
C	5.535	-2.440	-1.465
C	7.030	-1.274	0.318
C	7.984	-0.578	-0.696
C	7.181	0.583	-1.352
C	8.557	-1.489	-1.830
H	8.983	-2.465	-1.532
C	9.096	0.019	0.286
C	9.859	1.286	-0.170
H	10.522	1.091	-1.007
C	8.302	0.231	1.593
H	8.736	-6.163	2.651
N	8.558	-5.212	3.121
C	9.008	-4.828	4.413
C	7.825	-4.122	2.630
N	7.755	-3.100	3.500
C	8.524	-3.499	4.619
C	8.836	-2.798	5.807
C	9.617	-3.426	6.794
C	9.970	-2.691	8.079
C	10.079	-4.772	6.588
C	10.936	-5.446	7.632
C	9.771	-5.478	5.404
C	5.419	0.641	2.678

Atom	X (Å)	Y (Å)	Z (Å)
C	4.197	1.481	3.148
O	3.020	1.213	2.274
C	2.451	0.023	2.923
C	3.665	1.310	4.594
C	2.450	0.318	4.449
H	1.545	-0.271	2.447
H	11.875	-4.887	7.805
H	10.424	-5.531	8.610
H	11.191	-6.458	7.293
H	11.058	-2.502	8.164
H	9.455	-1.715	8.139
H	9.680	-3.271	8.975
H	9.175	2.118	-0.395
H	10.500	1.636	0.659
H	7.786	-1.672	-2.595
H	9.343	-0.928	-2.359
H	6.254	0.240	-1.830
H	6.915	1.345	-0.603
H	7.800	1.056	-2.125
H	6.186	-3.108	-2.053
H	4.521	-2.863	-1.509
H	5.501	-1.479	-2.004
H	5.816	-4.673	-0.657
H	5.571	-5.824	0.640
H	5.729	-5.563	2.873
H	4.313	-5.861	3.889
H	4.415	-6.646	2.294
H	2.084	-4.650	3.473
H	1.763	-4.051	1.809
H	2.121	-5.780	2.128
H	4.582	-3.780	8.494
H	3.987	-4.478	6.984
H	4.513	0.992	7.831
H	3.372	0.148	6.779
H	6.906	-1.702	8.553
H	6.005	-0.344	9.260
H	5.336	-1.971	9.377
H	7.992	0.640	8.207
H	7.783	2.114	7.234
H	6.391	1.374	8.035
H	9.848	0.068	6.777
H	11.078	0.389	5.548
H	8.968	2.730	1.885

Atom	X (Å)	Y (Å)	Z (Å)
H	7.747	2.699	3.172
H	11.689	0.820	3.627
H	11.316	2.021	2.368
H	11.469	2.521	4.066
H	10.399	-1.165	4.040
H	9.599	-1.886	2.620
H	10.910	-0.694	2.397
H	7.747	1.183	1.513
H	3.320	-2.274	6.887
H	10.165	-6.488	5.277
H	8.459	-1.786	5.964
H	8.848	2.410	5.495
H	7.318	-4.086	1.674

Atom	X (Å)	Y (Å)	Z (Å)
H	9.845	-0.759	0.503
H	3.400	-3.716	0.262
H	3.405	-3.872	4.865
H	3.168	-0.811	2.759
H	1.525	0.772	4.840
H	3.356	2.283	5.013
H	5.272	0.432	1.605
H	6.305	1.281	2.825
H	4.459	2.536	2.940
H	2.633	-0.625	4.991
H	4.463	0.915	5.234

Table A.5.1. Metal-ligand bond distances of the QM/MM-optimized Zn^{II} - and Fe^{II} -bound SCD models.

Parameter	Zn^{II} -bound SCD		Fe^{II} -bound SCD	
	B3LYP	M-06L	B3LYP	M-06L
$r(\text{M}_\text{B}-\text{N}_{\text{H116}})$	2.05	2.05	2.09	2.09
$r(\text{M}_\text{B}-\text{N}_{\text{H121}})$	2.13	2.09	2.14	2.09
$r(\text{M}_\text{B}-\text{N}_{\text{H153}})$	2.13	2.10	2.18	2.15
$r(\text{M}_\text{B}-\text{N}_{\text{H157}})$	2.22	2.16	2.16	2.15
$r(\text{M}_\text{B}-\text{N}_{\text{H297}})$	2.11	2.10	2.16	2.14
$r(\text{M}_\text{W}-\text{N}_{\text{H156}})$	2.07	2.07	2.12	2.12
$r(\text{M}_\text{W}-\text{N}_{\text{H265}})$	2.04	2.03	2.08	2.07
$r(\text{M}_\text{W}-\text{N}_{\text{H294}})$	2.06	2.06	2.16	2.11
$r(\text{M}_\text{W}-\text{N}_{\text{H298}})$	2.11	2.10	2.13	2.12
$r(\text{M}_\text{W}-\text{O}_{\text{W75}})$	2.42	2.32	2.29	2.20

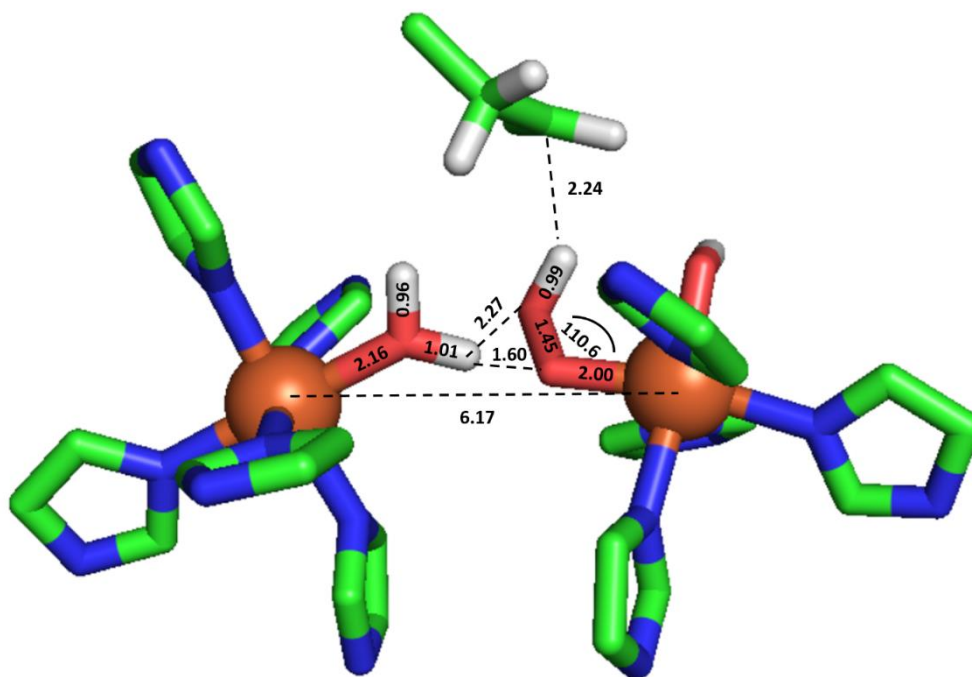


Figure A.5.1. QM/MM-optimized geometry of intermediate C, including important bond lengths (in Å) and bond angles (in degrees).

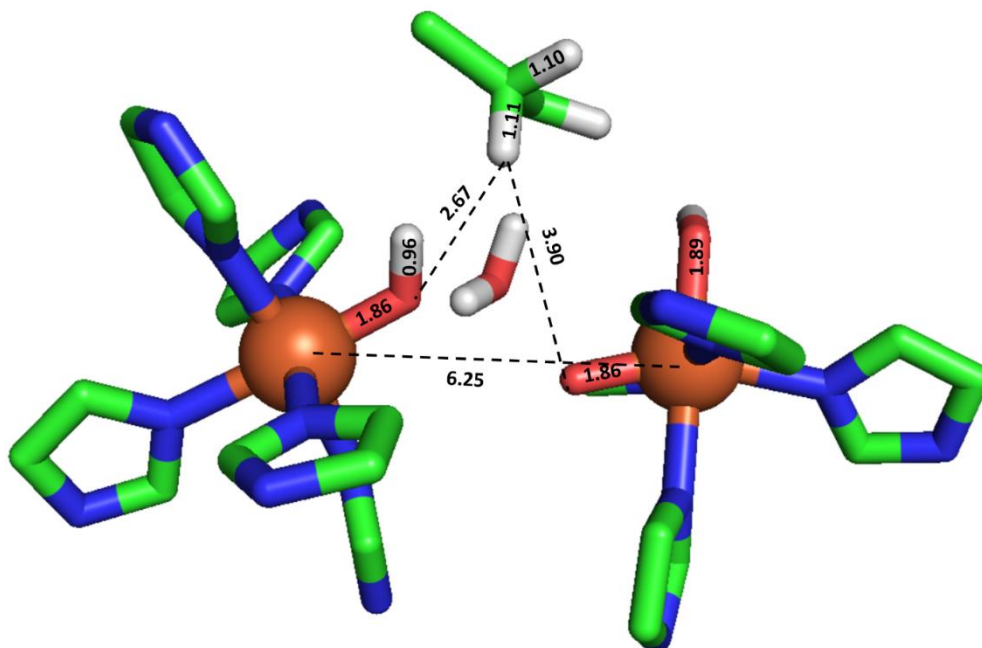


Figure A.5.2. QM/MM-optimized geometry of intermediate **D**, including important bond lengths (in Å). The nascent H₂O molecule was included in the optimization of this structure.

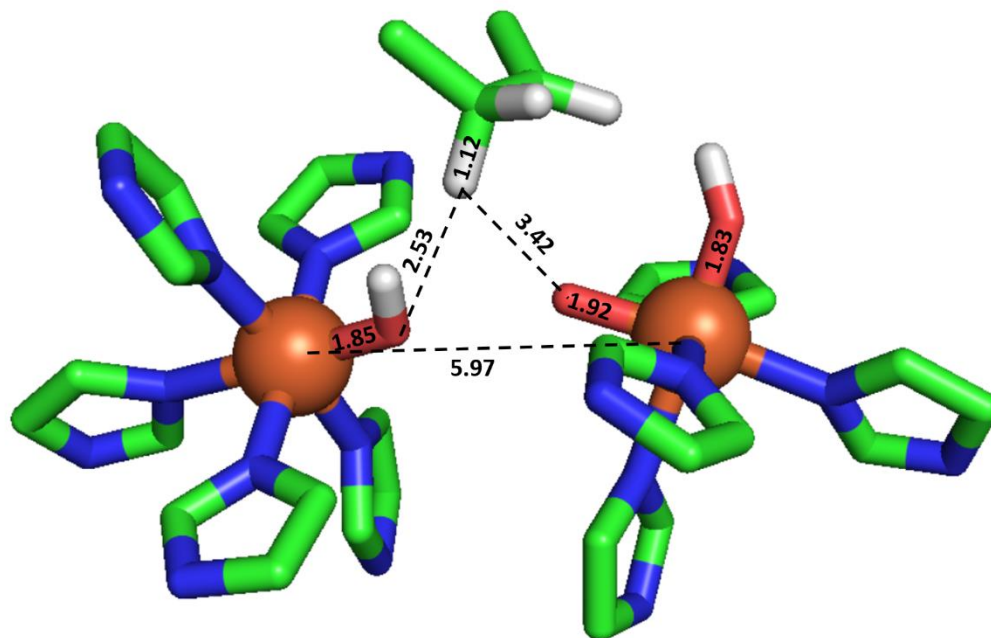


Figure A.5.3. QM/MM-optimized geometry of intermediate **D**, including important bond lengths (in Å). The nascent H₂O molecule was not included in the optimization of this structure.

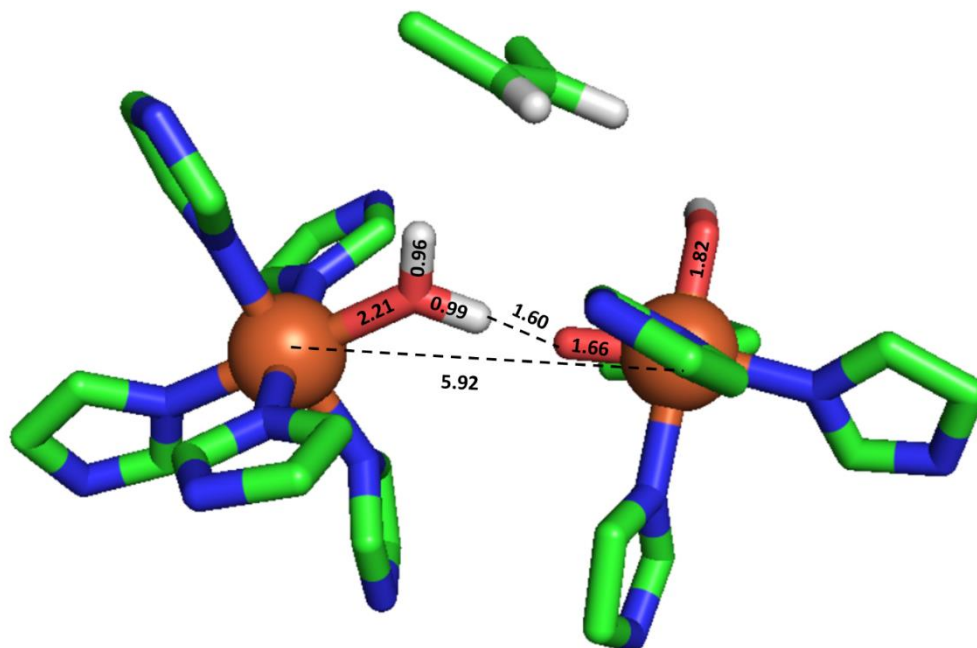


Figure A.5.4. QM/MM-optimized geometry of intermediate **E**, including important bond lengths (in Å).

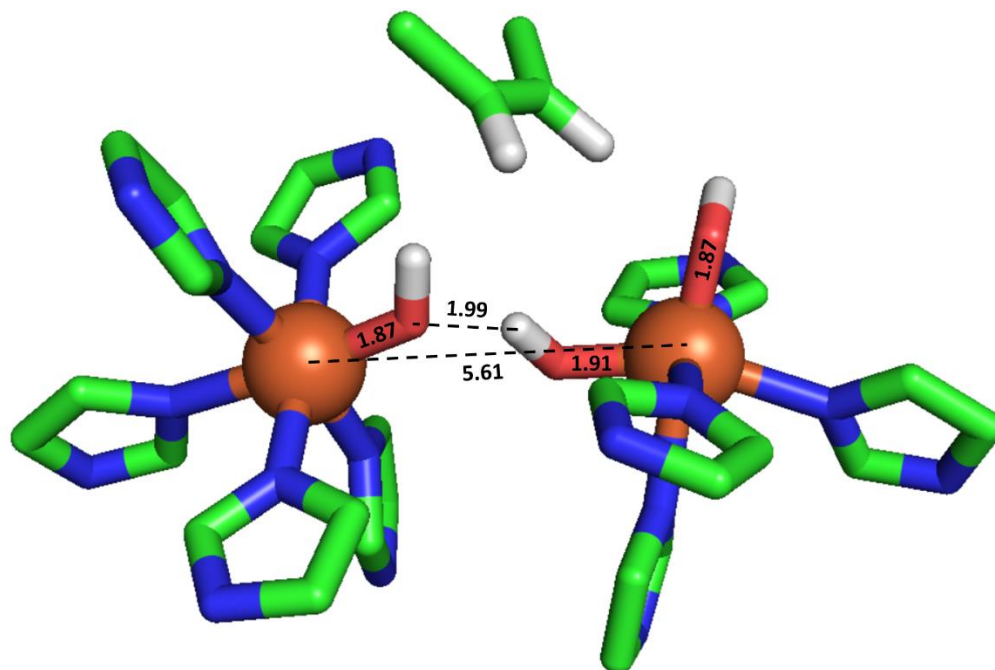


Figure A.5.5. QM/MM-optimized geometry of intermediate **F**, including important bond lengths (in Å).

Table A.5.1. Optimized coordinates of the QM region for the Zn₂-bound SCD model using the B3LYP functional.

Atom	X (Å)	Y (Å)	Z (Å)	Atom	X (Å)	Y (Å)	Z (Å)
H	22.263	-3.273	-5.950	C	24.534	-8.076	3.390
C	21.606	-2.945	-5.147	H	26.946	-8.147	5.449
C	21.001	-4.106	-4.459	H	24.697	-7.910	6.613
H	20.842	-2.271	-5.546	C	24.838	-7.990	5.539
H	22.195	-2.338	-4.438	N	26.042	-8.120	4.956
C	21.462	-5.393	-4.329	N	23.887	-7.963	4.613
H	19.221	-3.267	-3.550	H	23.985	-8.075	2.453
H	18.777	-5.541	-2.575	H	24.964	-12.052	0.555
C	19.617	-5.311	-3.218	C	24.613	-11.946	-0.471
N	19.814	-4.090	-3.761	C	23.440	-11.046	-0.621
N	20.596	-6.137	-3.568	C	23.322	-9.714	-0.936
H	22.377	-5.820	-4.724	N	22.137	-11.490	-0.491
H	22.600	-10.029	-8.293	N	21.987	-9.368	-1.047
C	21.733	-10.132	-7.648	C	21.302	-10.456	-0.748
C	21.972	-9.829	-6.222	H	24.119	-8.997	-1.119
H	21.349	-11.157	-7.770	H	21.859	-12.445	-0.248
H	20.952	-9.458	-8.019	H	24.342	-12.947	-0.848
C	21.331	-8.951	-5.383	H	25.451	-11.599	-1.093
H	23.685	-11.082	-5.708	H	20.218	-10.535	-0.734
H	23.543	-10.183	-3.386	H	20.036	-7.487	10.746
C	22.883	-9.891	-4.198	C	21.107	-7.655	10.611
N	22.953	-10.405	-5.441	C	21.460	-8.060	9.216
N	21.904	-9.000	-4.133	C	21.254	-7.451	7.994
H	20.513	-8.273	-5.609	N	22.056	-9.265	8.892
H	27.353	-6.473	-1.535	N	21.703	-8.269	6.977
C	26.743	-5.914	-2.250	C	22.203	-9.354	7.557
C	25.280	-6.108	-2.046	H	22.668	-10.205	7.064
H	27.022	-6.219	-3.266	H	22.485	-9.970	9.503
H	26.986	-4.844	-2.149	H	21.416	-8.452	11.299
C	24.340	-6.896	-2.669	H	21.646	-6.743	10.917
H	22.541	-5.517	-0.373	H	20.823	-6.476	7.786
C	23.296	-5.889	-1.062	H	15.770	-7.264	4.179
N	24.585	-5.481	-1.033	C	16.366	-6.636	4.850
N	23.113	-6.754	-2.050	C	17.822	-6.593	4.557
H	24.480	-7.553	-3.521	H	16.235	-7.002	5.874
H	24.992	-4.818	-0.355	H	15.959	-5.610	4.822
H	27.502	-9.367	2.681	C	18.872	-7.192	5.211
C	27.052	-8.366	2.660	H	18.018	-5.240	2.844
C	25.893	-8.183	3.587	H	20.460	-5.609	2.894
H	26.718	-8.149	1.639	C	19.760	-6.088	3.577
H	27.846	-7.638	2.897	N	18.422	-5.896	3.521

Atom	X (Å)	Y (Å)	Z (Å)
N	20.058	-6.895	4.587
H	18.852	-7.773	6.123
H	15.874	-9.705	-0.116
C	16.228	-8.678	-0.025
C	17.343	-8.434	-0.984
H	16.580	-8.512	1.002
H	15.375	-8.002	-0.197
C	18.684	-8.175	-0.805
H	16.365	-8.918	-2.853
H	18.580	-8.614	-3.996
C	18.417	-8.506	-2.928
N	17.209	-8.629	-2.346
N	19.337	-8.234	-2.022
H	19.216	-7.959	0.120
H	18.589	-12.294	1.969
C	18.940	-12.224	2.996
C	20.062	-11.287	3.274
C	20.106	-9.929	3.487
N	21.337	-11.727	3.584
N	21.347	-9.570	3.968
C	22.078	-10.676	3.996
H	23.117	-10.757	4.313
H	21.689	-12.687	3.543
H	19.274	-13.226	3.300
H	18.080	-11.974	3.633
H	19.299	-9.210	3.392
ZN	21.348	-7.845	-2.533
ZN	21.857	-7.807	5.001
C	18.410	5.036	0.240
C	19.320	4.049	-0.480
C	19.126	2.616	0.012
C	20.089	1.595	-0.589
C	19.707	0.166	-0.215
C	20.446	-0.938	-0.973
C	19.985	-2.346	-0.541
C	21.015	-3.152	0.248
C	21.297	-2.559	1.624
C	22.490	-3.135	2.376
C	23.884	-2.900	1.803
C	24.309	-1.434	1.777
C	25.724	-1.240	1.235

Atom	X (Å)	Y (Å)	Z (Å)
C	26.137	0.211	0.986
C	26.516	1.002	2.250
C	27.973	0.761	2.652
H	28.710	1.340	2.083
H	22.342	-4.217	2.553
H	22.485	-2.661	3.369
H	23.973	-3.327	0.787
H	24.603	-3.464	2.428
H	24.216	-1.048	2.806
H	23.601	-0.863	1.156
H	25.793	-1.798	0.280
H	26.443	-1.737	1.911
H	25.319	0.701	0.438
H	27.001	0.194	0.303
H	25.856	0.691	3.079
H	26.319	2.071	2.086
H	28.205	-0.304	2.472
H	28.133	0.959	3.720
H	17.348	4.811	0.061
H	18.563	4.990	1.331
H	18.590	6.074	-0.067
H	20.375	4.334	-0.331
H	19.141	4.077	-1.567
H	18.096	2.286	-0.209
H	19.225	2.590	1.113
H	21.120	1.813	-0.263
H	20.097	1.689	-1.685
H	18.628	0.022	-0.402
H	19.835	0.013	0.873
H	21.538	-0.835	-0.844
H	20.252	-0.816	-2.051
H	19.666	-2.939	-1.410
H	19.077	-2.237	0.073
H	21.945	-3.235	-0.337
H	20.628	-4.181	0.401
H	21.408	-1.469	1.564
H	20.405	-2.738	2.245
O	22.395	-5.451	4.939
H	21.729	-4.726	4.861
H	23.196	-4.897	4.768

Table A.5.2. Optimized coordinates of the QM region for the Zn₂-bound SCD model using the M-06L functional.

Atom	X (Å)	Y (Å)	Z (Å)	Atom	X (Å)	Y (Å)	Z (Å)
H	22.276	-3.241	-5.809	C	24.533	-8.083	3.444
C	21.690	-2.854	-4.978	H	26.969	-7.990	5.464
C	21.184	-3.917	-4.104	H	24.719	-7.764	6.646
H	20.875	-2.237	-5.360	C	24.855	-7.895	5.577
H	22.327	-2.160	-4.406	N	26.057	-8.008	4.987
C	21.654	-5.180	-3.848	N	23.897	-7.947	4.663
H	19.461	-2.974	-3.181	H	23.969	-8.139	2.515
H	19.131	-5.075	-1.870	H	24.868	-12.013	0.664
C	19.902	-4.945	-2.621	C	24.482	-11.901	-0.347
N	20.068	-3.800	-3.313	C	23.347	-10.969	-0.451
N	20.841	-5.816	-2.949	C	23.268	-9.613	-0.643
H	22.532	-5.672	-4.259	N	22.035	-11.386	-0.381
H	22.258	-9.411	-8.118	N	21.948	-9.223	-0.725
C	21.478	-9.265	-7.382	C	21.229	-10.315	-0.549
C	21.878	-9.159	-5.973	H	24.084	-8.903	-0.757
H	20.764	-10.093	-7.488	H	21.740	-12.353	-0.223
H	20.931	-8.355	-7.650	H	24.171	-12.894	-0.704
C	21.382	-8.317	-5.010	H	25.311	-11.589	-0.995
H	23.361	-10.736	-5.635	H	20.143	-10.368	-0.564
H	23.369	-10.123	-3.236	H	20.021	-7.642	10.724
C	22.755	-9.631	-3.989	C	21.086	-7.844	10.592
N	22.756	-9.976	-5.293	C	21.431	-8.203	9.194
N	21.926	-8.622	-3.788	C	21.271	-7.543	7.994
H	20.670	-7.504	-5.129	N	21.960	-9.424	8.830
H	27.459	-6.457	-1.438	N	21.675	-8.346	6.951
C	26.837	-5.882	-2.124	C	22.112	-9.473	7.495
C	25.402	-6.051	-1.831	H	22.529	-10.329	6.968
H	27.066	-6.187	-3.149	H	22.305	-10.185	9.432
H	27.110	-4.823	-2.027	H	21.357	-8.675	11.253
C	24.402	-6.826	-2.364	H	21.649	-6.968	10.940
H	22.847	-5.459	0.107	H	20.893	-6.540	7.814
C	23.529	-5.828	-0.658	H	15.750	-7.243	4.140
N	24.814	-5.431	-0.754	C	16.368	-6.626	4.799
N	23.248	-6.680	-1.629	C	17.816	-6.622	4.518
H	24.445	-7.480	-3.230	H	16.219	-6.968	5.826
H	25.292	-4.782	-0.112	H	15.987	-5.595	4.753
H	27.470	-9.341	2.724	C	18.858	-7.186	5.215
C	27.033	-8.336	2.700	H	18.033	-5.343	2.760
C	25.895	-8.135	3.627	H	20.484	-5.698	2.870
H	26.691	-8.127	1.684	C	19.770	-6.146	3.561
H	27.840	-7.621	2.913	N	18.433	-5.972	3.466

Atom	X (Å)	Y (Å)	Z (Å)
N	20.051	-6.902	4.612
H	18.824	-7.733	6.149
H	15.841	-9.623	-0.098
C	16.192	-8.601	0.030
C	17.344	-8.320	-0.850
H	16.494	-8.464	1.074
H	15.344	-7.926	-0.155
C	18.657	-8.014	-0.575
H	16.517	-8.810	-2.784
H	18.795	-8.399	-3.765
C	18.550	-8.312	-2.710
N	17.310	-8.492	-2.217
N	19.391	-8.023	-1.739
H	19.119	-7.797	0.388
H	18.559	-12.212	1.951
C	18.937	-12.122	2.967
C	20.052	-11.183	3.206
C	20.112	-9.827	3.418
N	21.336	-11.623	3.453
N	21.373	-9.469	3.833
C	22.099	-10.577	3.829
H	23.149	-10.663	4.109
H	21.668	-12.590	3.417
H	19.277	-13.117	3.277
H	18.090	-11.876	3.618
H	19.304	-9.101	3.354
ZN	21.425	-7.623	-2.072
ZN	21.865	-7.795	5.006
C	18.436	4.936	0.191
C	19.307	3.939	-0.535
C	19.073	2.520	-0.059
C	20.031	1.486	-0.613
C	19.612	0.089	-0.217
C	20.481	-1.055	-0.695
C	19.930	-2.396	-0.212
C	20.981	-3.335	0.346
C	21.400	-2.862	1.724
C	22.643	-3.468	2.329
C	23.981	-3.077	1.739
C	24.314	-1.599	1.810
C	25.717	-1.329	1.293

Atom	X (Å)	Y (Å)	Z (Å)
C	26.079	0.116	1.009
C	26.435	0.947	2.236
C	27.872	0.722	2.668
H	28.642	1.273	2.111
H	22.558	-4.570	2.389
H	22.663	-3.120	3.370
H	24.064	-3.402	0.687
H	24.761	-3.637	2.292
H	24.185	-1.267	2.855
H	23.580	-1.032	1.215
H	25.834	-1.911	0.358
H	26.447	-1.777	1.990
H	25.256	0.565	0.437
H	26.945	0.103	0.331
H	25.764	0.666	3.066
H	26.233	2.007	2.037
H	28.100	-0.350	2.532
H	28.002	0.942	3.732
H	17.367	4.745	0.025
H	18.594	4.879	1.278
H	18.633	5.972	-0.102
H	20.371	4.187	-0.386
H	19.141	3.985	-1.621
H	18.044	2.205	-0.303
H	19.132	2.490	1.044
H	21.054	1.692	-0.258
H	20.090	1.557	-1.709
H	18.586	-0.105	-0.579
H	19.536	0.021	0.884
H	21.519	-0.922	-0.343
H	20.540	-1.055	-1.797
H	19.329	-2.890	-0.987
H	19.199	-2.205	0.590
H	21.844	-3.402	-0.341
H	20.564	-4.360	0.441
H	21.503	-1.767	1.737
H	20.560	-3.064	2.409
O	22.384	-5.535	4.947
H	21.749	-4.788	4.844
H	23.211	-5.018	4.802

Table A.5.3. Optimized coordinates of the QM region for the Fe^{II}-bound SCD model using the B3LYP functional.

Atom	X (Å)	Y (Å)	Z (Å)	Atom	X (Å)	Y (Å)	Z (Å)
H	22.204	-3.347	-5.719	C	24.610	-8.173	3.435
C	21.627	-2.928	-4.889	H	27.140	-8.107	5.346
C	21.119	-3.977	-3.972	H	24.951	-7.824	6.628
H	20.811	-2.311	-5.275	C	25.031	-7.976	5.554
H	22.287	-2.237	-4.335	N	26.205	-8.133	4.912
C	21.749	-5.087	-3.473	N	24.029	-8.005	4.685
H	19.170	-3.253	-3.388	H	24.012	-8.219	2.528
H	18.853	-5.409	-2.122	H	24.986	-12.253	0.454
C	19.737	-5.154	-2.695	C	24.642	-12.172	-0.577
N	19.836	-4.045	-3.465	C	23.491	-11.246	-0.722
N	20.878	-5.830	-2.706	C	23.427	-9.893	-0.940
H	22.791	-5.363	-3.561	N	22.170	-11.643	-0.573
H	22.222	-9.503	-8.317	N	22.108	-9.481	-0.965
C	21.417	-9.365	-7.602	C	21.376	-10.557	-0.727
C	21.817	-9.256	-6.182	H	24.249	-9.203	-1.106
H	20.727	-10.220	-7.707	H	21.863	-12.602	-0.381
H	20.859	-8.462	-7.882	H	24.351	-13.176	-0.928
C	21.465	-8.331	-5.226	H	25.488	-11.851	-1.202
H	23.060	-11.027	-5.844	H	20.290	-10.562	-0.686
H	23.170	-10.413	-3.448	H	20.047	-7.574	10.797
C	22.623	-9.845	-4.197	C	21.112	-7.788	10.681
N	22.569	-10.191	-5.500	C	21.459	-8.202	9.286
N	21.963	-8.716	-4.000	C	21.348	-7.556	8.073
H	20.886	-7.420	-5.347	N	21.947	-9.453	8.954
H	27.630	-6.590	-1.585	N	21.769	-8.388	7.050
C	26.991	-6.053	-2.290	C	22.135	-9.530	7.623
C	25.555	-6.277	-1.983	H	22.552	-10.402	7.125
H	27.218	-6.390	-3.308	H	22.274	-10.209	9.574
H	27.223	-4.977	-2.227	H	21.378	-8.603	11.371
C	24.531	-6.935	-2.624	H	21.686	-6.901	10.991
H	23.126	-6.155	0.177	H	20.999	-6.549	7.870
C	23.723	-6.294	-0.723	H	15.711	-7.283	4.224
N	25.010	-5.885	-0.778	C	16.330	-6.690	4.905
N	23.395	-6.925	-1.839	C	17.782	-6.653	4.593
H	24.540	-7.404	-3.601	H	16.216	-7.094	5.916
H	25.467	-5.263	-0.093	H	15.935	-5.659	4.923
H	27.497	-9.497	2.569	C	18.844	-7.188	5.284
C	27.070	-8.485	2.562	H	17.958	-5.403	2.803
C	25.979	-8.259	3.558	H	20.394	-5.786	2.834
H	26.665	-8.278	1.563	C	19.706	-6.230	3.553
H	27.894	-7.769	2.729	N	18.363	-6.051	3.489

Atom	X (Å)	Y (Å)	Z (Å)
N	20.025	-6.938	4.630
H	18.829	-7.708	6.234
H	15.748	-9.679	-0.190
C	16.134	-8.661	-0.116
C	17.283	-8.450	-1.047
H	16.464	-8.480	0.918
H	15.299	-7.969	-0.315
C	18.618	-8.202	-0.808
H	16.399	-8.965	-2.955
H	18.680	-8.718	-3.989
C	18.460	-8.579	-2.933
N	17.219	-8.676	-2.410
N	19.338	-8.296	-1.988
H	19.100	-7.970	0.141
H	18.498	-12.228	1.930
C	18.866	-12.167	2.954
C	20.009	-11.248	3.219
C	20.061	-9.914	3.546
N	21.308	-11.698	3.409
N	21.325	-9.580	3.993
C	22.063	-10.680	3.881
H	23.115	-10.782	4.145
H	21.651	-12.660	3.322
H	19.195	-13.171	3.256
H	18.019	-11.908	3.605
H	19.245	-9.201	3.555
FE	21.441	-7.824	-2.180
FE	21.943	-7.841	5.055
C	18.201	5.506	0.380
C	19.158	4.597	-0.380
C	18.858	3.129	-0.110
C	19.840	2.114	-0.683
C	19.474	0.718	-0.196
C	20.364	-0.434	-0.661
C	20.218	-1.604	0.299
C	21.121	-2.814	0.068
C	21.236	-3.660	1.353
C	22.642	-3.956	1.926
C	23.897	-3.197	1.475
C	23.999	-1.695	1.777
C	25.486	-1.264	1.829

Atom	X (Å)	Y (Å)	Z (Å)
C	25.884	0.093	1.205
C	26.423	1.122	2.211
C	27.860	0.793	2.659
H	28.663	1.303	2.111
H	22.868	-5.023	1.782
H	22.652	-3.806	3.017
H	24.131	-3.370	0.410
H	24.714	-3.680	2.046
H	23.498	-1.501	2.745
H	23.448	-1.117	1.020
H	26.067	-2.051	1.325
H	25.809	-1.309	2.881
H	25.033	0.506	0.646
H	26.663	-0.106	0.451
H	25.755	1.127	3.088
H	26.355	2.127	1.772
H	28.027	-0.289	2.510
H	27.998	0.995	3.729
H	17.155	5.334	0.084
H	18.252	5.298	1.463
H	18.425	6.571	0.239
H	20.194	4.813	-0.072
H	19.112	4.783	-1.461
H	17.844	2.881	-0.466
H	18.842	2.976	0.985
H	20.860	2.355	-0.337
H	19.880	2.150	-1.781
H	18.424	0.483	-0.449
H	19.508	0.736	0.907
H	21.423	-0.121	-0.677
H	20.108	-0.747	-1.691
H	19.167	-1.956	0.302
H	20.410	-1.229	1.317
H	22.114	-2.488	-0.272
H	20.692	-3.424	-0.742
H	20.645	-3.166	2.141
H	20.712	-4.619	1.192
O	22.386	-5.614	4.774
H	21.659	-4.950	4.782
H	23.148	-4.997	4.649

Table A.5.4. Optimized coordinates of the QM region for the Fe^{II}-bound SCD model using the M-06L functional.

Atom	X (Å)	Y (Å)	Z (Å)	Atom	X (Å)	Y (Å)	Z (Å)
H	22.226	-3.250	-5.685	C	24.552	-8.171	3.404
C	21.624	-2.854	-4.868	H	27.030	-7.915	5.354
C	21.174	-3.874	-3.912	H	24.808	-7.667	6.573
H	20.775	-2.294	-5.269	C	24.917	-7.853	5.509
H	22.232	-2.103	-4.337	N	26.109	-7.967	4.899
C	21.668	-5.112	-3.589	N	23.937	-7.983	4.627
H	19.518	-2.860	-2.944	H	23.970	-8.295	2.496
H	19.299	-4.837	-1.435	H	24.868	-12.046	0.626
C	19.993	-4.781	-2.268	C	24.466	-11.923	-0.377
N	20.108	-3.701	-3.061	C	23.327	-10.990	-0.447
N	20.919	-5.673	-2.584	C	23.249	-9.627	-0.575
H	22.536	-5.635	-3.984	N	22.014	-11.411	-0.397
H	22.205	-9.305	-8.017	N	21.927	-9.234	-0.637
C	21.441	-9.150	-7.265	C	21.207	-10.336	-0.517
C	21.876	-9.067	-5.863	H	24.065	-8.912	-0.653
H	20.707	-9.961	-7.361	H	21.718	-12.382	-0.263
H	20.907	-8.225	-7.516	H	24.148	-12.911	-0.739
C	21.411	-8.231	-4.877	H	25.284	-11.602	-1.035
H	23.332	-10.678	-5.576	H	20.119	-10.385	-0.542
H	23.410	-10.089	-3.170	H	20.028	-7.671	10.692
C	22.788	-9.576	-3.904	C	21.089	-7.879	10.540
N	22.759	-9.902	-5.215	C	21.408	-8.252	9.140
N	21.976	-8.560	-3.670	C	21.202	-7.615	7.937
H	20.708	-7.404	-4.971	N	21.965	-9.462	8.782
H	27.557	-6.498	-1.521	N	21.613	-8.417	6.895
C	26.937	-5.930	-2.215	C	22.093	-9.525	7.446
C	25.512	-6.099	-1.884	H	22.525	-10.373	6.924
H	27.147	-6.261	-3.235	H	22.335	-10.208	9.387
H	27.215	-4.871	-2.139	H	21.370	-8.705	11.203
C	24.485	-6.828	-2.428	H	21.663	-7.003	10.871
H	23.148	-5.860	0.339	H	20.788	-6.631	7.755
C	23.724	-6.020	-0.572	H	15.678	-7.265	4.143
N	24.994	-5.593	-0.716	C	16.289	-6.645	4.803
N	23.384	-6.779	-1.605	C	17.733	-6.606	4.512
H	24.477	-7.397	-3.355	H	16.156	-7.002	5.826
H	25.501	-4.985	-0.057	H	15.887	-5.622	4.773
H	27.484	-9.388	2.644	C	18.787	-7.180	5.181
C	27.041	-8.387	2.609	H	17.919	-5.260	2.803
C	25.920	-8.173	3.553	H	20.374	-5.565	2.900
H	26.677	-8.199	1.595	C	19.675	-6.050	3.582
H	27.847	-7.662	2.792	N	18.332	-5.893	3.494

Atom	X (Å)	Y (Å)	Z (Å)
N	19.976	-6.847	4.599
H	18.761	-7.765	6.089
H	15.763	-9.624	-0.157
C	16.113	-8.601	-0.043
C	17.269	-8.326	-0.919
H	16.410	-8.451	1.001
H	15.265	-7.929	-0.239
C	18.576	-8.003	-0.638
H	16.460	-8.842	-2.851
H	18.746	-8.429	-3.826
C	18.491	-8.324	-2.773
N	17.249	-8.510	-2.285
N	19.321	-8.012	-1.798
H	19.031	-7.770	0.328
H	18.497	-12.207	1.936
C	18.885	-12.120	2.948
C	19.994	-11.172	3.183
C	20.053	-9.817	3.396
N	21.278	-11.611	3.438
N	21.310	-9.457	3.822
C	22.037	-10.565	3.816
H	23.086	-10.650	4.093
H	21.618	-12.575	3.385
H	19.244	-13.111	3.246
H	18.043	-11.891	3.611
H	19.249	-9.091	3.332
FE	21.412	-7.585	-1.910
FE	21.853	-7.747	4.957
C	18.156	5.223	0.258
C	19.109	4.320	-0.486
C	18.867	2.858	-0.180
C	19.883	1.902	-0.759
C	19.562	0.478	-0.376
C	20.598	-0.563	-0.748
C	20.409	-1.794	0.103
C	21.535	-2.803	0.109
C	21.473	-3.666	1.363
C	22.790	-3.943	2.100
C	24.079	-3.291	1.628
C	24.293	-1.805	1.888
C	25.680	-1.423	1.372

Atom	X (Å)	Y (Å)	Z (Å)
C	25.988	0.028	1.047
C	26.403	0.904	2.222
C	27.857	0.682	2.603
H	28.617	1.239	2.030
H	22.942	-5.030	2.170
H	22.695	-3.618	3.143
H	24.246	-3.477	0.555
H	24.898	-3.817	2.156
H	24.171	-1.612	2.968
H	23.515	-1.204	1.391
H	25.828	-2.001	0.439
H	26.438	-1.832	2.062
H	25.127	0.449	0.510
H	26.813	0.017	0.320
H	25.755	0.676	3.086
H	26.207	1.956	1.975
H	28.084	-0.389	2.453
H	28.016	0.886	3.667
H	17.109	5.029	-0.015
H	18.223	5.055	1.345
H	18.352	6.286	0.088
H	20.150	4.565	-0.215
H	19.039	4.471	-1.572
H	17.861	2.555	-0.519
H	18.860	2.714	0.916
H	20.886	2.156	-0.377
H	19.955	2.004	-1.852
H	18.580	0.163	-0.774
H	19.430	0.440	0.719
H	21.615	-0.167	-0.584
H	20.546	-0.819	-1.823
H	19.442	-2.286	-0.138
H	20.285	-1.452	1.143
H	22.490	-2.264	0.067
H	21.517	-3.429	-0.793
H	20.788	-3.172	2.071
H	20.955	-4.615	1.131
O	22.389	-5.621	4.812
H	21.743	-4.893	4.669
H	23.209	-5.078	4.759

Table A.5.5. Optimized coordinates of the QM region for the O₂-bound model **1** shown in Figure 5.6.

Atom	X (Å)	Y (Å)	Z (Å)	Atom	X (Å)	Y (Å)	Z (Å)
H	22.208	-3.200	-5.791	C	24.720	-8.074	3.176
C	21.631	-2.810	-4.951	H	26.998	-7.985	5.380
C	21.130	-3.884	-4.062	H	24.664	-7.719	6.383
H	20.813	-2.182	-5.315	C	24.882	-7.861	5.329
H	22.291	-2.134	-4.380	N	26.126	-7.995	4.833
C	21.706	-5.079	-3.714	N	23.994	-7.911	4.342
H	19.310	-3.053	-3.226	H	24.242	-8.141	2.204
H	18.997	-5.210	-1.996	H	25.029	-12.049	0.516
C	19.817	-5.008	-2.672	C	24.688	-11.988	-0.519
N	19.920	-3.872	-3.397	C	23.499	-11.121	-0.710
N	20.877	-5.778	-2.865	C	23.381	-9.790	-1.016
H	22.663	-5.473	-4.034	N	22.197	-11.572	-0.587
H	22.293	-9.675	-8.390	N	22.045	-9.445	-1.113
C	21.472	-9.578	-7.687	C	21.359	-10.538	-0.833
C	21.852	-9.378	-6.271	H	24.175	-9.072	-1.189
H	20.844	-10.481	-7.774	H	21.914	-12.524	-0.341
H	20.860	-8.723	-8.003	H	24.446	-13.005	-0.867
C	21.389	-8.460	-5.357	H	25.524	-11.637	-1.141
H	23.315	-10.959	-5.859	H	20.276	-10.615	-0.803
H	23.357	-10.213	-3.505	H	19.891	-7.681	10.470
C	22.742	-9.754	-4.272	C	20.959	-7.846	10.299
N	22.715	-10.180	-5.552	C	21.337	-8.141	8.881
N	21.942	-8.710	-4.121	C	21.243	-7.436	7.698
H	20.699	-7.637	-5.518	N	21.898	-9.349	8.503
H	27.591	-6.537	-1.569	N	21.722	-8.198	6.643
C	26.980	-5.975	-2.279	C	22.126	-9.345	7.178
C	25.532	-6.184	-2.025	H	22.572	-10.185	6.656
H	27.232	-6.295	-3.295	H	22.226	-10.125	9.095
H	27.224	-4.905	-2.187	H	21.280	-8.694	10.923
C	24.543	-6.879	-2.678	H	21.501	-6.962	10.671
H	23.012	-5.982	0.020	H	20.857	-6.434	7.538
C	23.649	-6.161	-0.844	H	15.698	-7.407	4.317
N	24.933	-5.739	-0.865	C	16.287	-6.810	5.017
N	23.379	-6.861	-1.937	C	17.708	-6.655	4.628
H	24.602	-7.402	-3.625	H	16.264	-7.307	5.994
H	25.369	-5.113	-0.171	H	15.816	-5.821	5.142
H	27.650	-9.377	2.611	C	18.835	-7.231	5.162
C	27.257	-8.354	2.593	H	17.678	-5.219	2.982
C	26.064	-8.139	3.464	H	20.140	-5.522	2.760
H	26.977	-8.093	1.566	C	19.515	-6.034	3.491
H	28.076	-7.674	2.878	N	18.173	-5.893	3.569

Atom	X (Å)	Y (Å)	Z (Å)
N	19.942	-6.865	4.436
H	18.917	-7.875	6.029
H	15.868	-9.761	-0.118
C	16.226	-8.735	-0.028
C	17.327	-8.468	-1.001
H	16.588	-8.571	0.998
H	15.367	-8.061	-0.181
C	18.664	-8.182	-0.830
H	16.348	-8.946	-2.870
H	18.554	-8.600	-4.024
C	18.393	-8.495	-2.955
N	17.190	-8.649	-2.365
N	19.314	-8.212	-2.054
H	19.197	-7.972	0.095
H	18.544	-12.400	1.979
C	18.880	-12.330	3.013
C	19.984	-11.378	3.312
C	20.016	-10.017	3.519
N	21.269	-11.800	3.594
N	21.263	-9.648	3.971
C	22.010	-10.741	3.982
H	23.065	-10.800	4.245
H	21.639	-12.754	3.542
H	19.233	-13.328	3.308
H	18.004	-12.111	3.641
H	19.211	-9.296	3.413
FE	21.409	-7.760	-2.313
FE	21.904	-7.673	4.574
C	18.227	5.675	0.415
C	19.187	4.758	-0.329
C	18.814	3.293	-0.130
C	19.783	2.263	-0.697
C	19.379	0.862	-0.250
C	20.303	-0.279	-0.678
C	20.206	-1.423	0.319
C	21.140	-2.611	0.103
C	21.241	-3.450	1.393
C	22.629	-3.835	1.940
C	23.912	-3.117	1.519
C	24.074	-1.630	1.848
C	25.570	-1.246	1.752
C	25.937	0.132	1.165

Atom	X (Å)	Y (Å)	Z (Å)
C	26.446	1.153	2.192
C	27.870	0.828	2.668
H	28.692	1.330	2.139
H	22.793	-4.908	1.758
H	22.595	-3.734	3.033
H	24.128	-3.282	0.450
H	24.713	-3.644	2.074
H	23.675	-1.460	2.866
H	23.466	-1.018	1.166
H	26.057	-2.018	1.135
H	26.013	-1.373	2.752
H	25.068	0.528	0.619
H	26.717	-0.033	0.406
H	25.759	1.145	3.056
H	26.376	2.164	1.767
H	28.034	-0.258	2.545
H	27.977	1.039	3.742
H	17.195	5.570	0.043
H	18.192	5.407	1.486
H	18.508	6.733	0.345
H	20.213	4.916	0.043
H	19.208	4.992	-1.401
H	17.805	3.099	-0.534
H	18.745	3.105	0.958
H	20.799	2.468	-0.314
H	19.856	2.328	-1.793
H	18.341	0.632	-0.555
H	19.356	0.875	0.854
H	21.351	0.068	-0.705
H	20.059	-0.643	-1.694
H	19.168	-1.806	0.353
H	20.408	-1.011	1.320
H	22.133	-2.266	-0.218
H	20.737	-3.231	-0.714
H	20.706	-2.905	2.185
H	20.661	-4.377	1.261
O	22.323	-5.496	4.830
H	21.669	-4.763	4.735
H	23.144	-4.991	4.623
O	21.857	-7.457	2.349
O	21.521	-8.309	1.528

Table A.5.6. Optimized coordinates of the QM region for the O₂-bound model **2** shown in Figure 5.6.

Atom	X (Å)	Y (Å)	Z (Å)	Atom	X (Å)	Y (Å)	Z (Å)
H	22.277	-2.982	-5.538	C	24.811	-8.018	3.468
C	21.611	-2.574	-4.773	H	26.994	-7.731	5.760
C	21.034	-3.657	-3.940	H	24.667	-7.674	6.680
H	20.825	-1.981	-5.242	C	24.905	-7.783	5.624
H	22.185	-1.871	-4.146	N	26.166	-7.834	5.159
C	21.651	-4.776	-3.442	N	24.043	-7.895	4.618
H	18.934	-3.135	-3.702	H	24.352	-8.093	2.490
H	18.626	-5.249	-2.420	H	25.174	-11.887	0.731
C	19.581	-4.932	-2.840	C	24.824	-11.751	-0.293
N	19.720	-3.785	-3.545	C	23.642	-10.852	-0.419
N	20.748	-5.561	-2.771	C	23.517	-9.495	-0.599
H	22.694	-5.057	-3.504	N	22.340	-11.320	-0.406
H	22.614	-9.141	-8.029	N	22.184	-9.152	-0.726
C	21.776	-8.998	-7.347	C	21.501	-10.275	-0.595
C	22.080	-8.892	-5.900	H	24.306	-8.753	-0.679
H	21.063	-9.829	-7.485	H	22.061	-12.298	-0.294
H	21.255	-8.077	-7.644	H	24.559	-12.739	-0.704
C	21.622	-7.965	-4.993	H	25.654	-11.366	-0.901
H	23.260	-10.684	-5.359	H	20.422	-10.366	-0.674
H	23.217	-9.988	-3.056	H	19.671	-7.764	10.536
C	22.743	-9.413	-3.846	C	20.756	-7.789	10.368
N	22.795	-9.795	-5.135	C	21.202	-8.104	8.971
N	22.040	-8.301	-3.721	C	21.096	-7.455	7.756
H	21.024	-7.078	-5.171	N	21.929	-9.242	8.669
H	27.623	-6.472	-1.353	N	21.748	-8.181	6.770
C	27.051	-5.873	-2.065	C	22.251	-9.253	7.367
C	25.600	-5.981	-1.781	H	22.893	-10.020	6.929
H	27.288	-6.180	-3.089	H	22.288	-9.971	9.298
H	27.343	-4.818	-1.948	H	21.189	-8.549	11.036
C	24.543	-6.631	-2.372	H	21.178	-6.821	10.686
H	23.166	-5.544	0.320	H	20.638	-6.495	7.525
C	23.776	-5.777	-0.539	H	15.695	-7.851	4.094
N	25.079	-5.443	-0.623	C	16.213	-7.244	4.844
N	23.414	-6.501	-1.582	C	17.652	-6.992	4.587
H	24.527	-7.192	-3.297	H	16.148	-7.743	5.816
H	25.600	-4.886	0.066	H	15.688	-6.278	4.937
H	27.732	-9.230	2.930	C	18.779	-7.477	5.210
C	27.367	-8.193	2.939	H	17.593	-5.581	2.947
C	26.148	-7.994	3.787	H	20.099	-5.503	3.028
H	27.119	-7.903	1.907	C	19.482	-6.133	3.666
H	28.182	-7.531	3.268	N	18.135	-6.133	3.616

Atom	X (Å)	Y (Å)	Z (Å)
N	19.908	-6.959	4.611
H	18.852	-8.128	6.071
H	15.991	-10.202	-0.406
C	16.188	-9.132	-0.385
C	17.377	-8.772	-1.209
H	16.361	-8.816	0.653
H	15.282	-8.611	-0.727
C	18.594	-8.250	-0.842
H	16.833	-9.423	-3.213
H	19.103	-8.805	-3.971
C	18.760	-8.690	-2.947
N	17.515	-9.032	-2.558
N	19.450	-8.216	-1.929
H	18.891	-7.866	0.128
H	18.744	-12.542	2.037
C	19.070	-12.438	3.074
C	20.140	-11.440	3.388
C	20.123	-10.082	3.617
N	21.423	-11.826	3.742
N	21.338	-9.679	4.136
C	22.107	-10.750	4.183
H	23.128	-10.788	4.563
H	21.813	-12.769	3.725
H	19.468	-13.414	3.390
H	18.187	-12.243	3.699
H	19.305	-9.381	3.489
FE	21.450	-7.396	-1.917
FE	21.927	-7.720	4.760
C	17.906	5.889	0.079
C	19.033	4.953	-0.346
C	18.728	3.489	-0.038
C	19.807	2.496	-0.468
C	19.455	1.075	-0.033
C	20.448	-0.029	-0.433
C	20.363	-1.194	0.549
C	21.343	-2.364	0.383
C	21.397	-3.196	1.688
C	22.763	-3.632	2.267
C	24.049	-2.960	1.791
C	24.271	-1.474	2.041
C	25.745	-1.127	1.774
C	26.031	0.305	1.304
C	26.366	1.259	2.455

Atom	X (Å)	Y (Å)	Z (Å)
C	27.722	0.921	3.081
H	28.564	1.417	2.586
H	22.916	-4.702	2.068
H	22.704	-3.562	3.368
H	24.165	-3.147	0.707
H	24.875	-3.503	2.287
H	23.981	-1.231	3.078
H	23.614	-0.870	1.396
H	26.147	-1.840	1.031
H	26.315	-1.324	2.698
H	25.168	0.675	0.728
H	26.879	0.288	0.601
H	25.576	1.206	3.224
H	26.354	2.297	2.090
H	27.916	-0.163	3.022
H	27.730	1.171	4.150
H	16.958	5.657	-0.436
H	17.702	5.814	1.160
H	18.133	6.945	-0.129
H	19.974	5.244	0.153
H	19.212	5.050	-1.425
H	17.783	3.208	-0.536
H	18.540	3.379	1.046
H	20.781	2.777	-0.031
H	19.953	2.549	-1.559
H	18.444	0.820	-0.401
H	19.362	1.082	1.068
H	21.478	0.368	-0.419
H	20.265	-0.367	-1.470
H	19.329	-1.587	0.563
H	20.525	-0.768	1.553
H	22.342	-1.972	0.143
H	21.060	-2.986	-0.486
H	20.892	-2.601	2.458
H	20.770	-4.108	1.589
O	22.364	-5.599	5.073
H	21.636	-4.940	5.067
H	23.182	-5.072	4.947
O	21.796	-7.524	2.754
O	22.563	-6.809	2.047
O	20.865	-6.438	-0.061
H	21.168	-6.851	0.755
H	20.551	-5.541	0.102

Table A.5.7. Optimized coordinates of the QM region for the O₂-bound model **3** shown in Figure 5.6.

Atom	X (Å)	Y (Å)	Z (Å)	Atom	X (Å)	Y (Å)	Z (Å)
H	21.792	-3.454	-5.663	C	24.254	-8.533	3.196
C	21.192	-3.095	-4.825	H	26.889	-8.573	4.962
C	20.847	-4.160	-3.855	H	24.788	-8.212	6.366
H	20.287	-2.603	-5.198	C	24.803	-8.354	5.288
H	21.768	-2.307	-4.309	N	25.933	-8.536	4.579
C	21.562	-5.247	-3.420	N	23.751	-8.353	4.477
H	18.952	-3.470	-3.073	H	23.598	-8.555	2.329
H	18.921	-5.503	-1.595	H	25.499	-11.902	0.763
C	19.697	-5.276	-2.315	C	25.121	-11.884	-0.258
N	19.668	-4.213	-3.141	C	23.872	-11.104	-0.416
N	20.831	-5.945	-2.481	C	23.658	-9.774	-0.667
H	22.548	-5.570	-3.731	N	22.606	-11.654	-0.320
H	22.390	-9.456	-7.892	N	22.302	-9.533	-0.764
C	21.591	-9.311	-7.170	C	21.692	-10.679	-0.533
C	22.004	-9.147	-5.755	H	24.397	-8.993	-0.806
H	20.911	-10.175	-7.237	H	22.400	-12.633	-0.102
H	21.012	-8.429	-7.476	H	24.936	-12.922	-0.581
C	21.522	-8.287	-4.795	H	25.910	-11.485	-0.911
H	23.500	-10.721	-5.411	H	20.617	-10.830	-0.524
H	23.543	-10.087	-3.043	H	20.220	-7.988	10.845
C	22.911	-9.600	-3.779	C	21.260	-8.276	10.666
N	22.892	-9.962	-5.076	C	21.503	-8.622	9.230
N	22.091	-8.579	-3.571	C	21.342	-7.898	8.068
H	20.815	-7.474	-4.918	N	21.878	-9.880	8.792
H	27.595	-6.121	-1.458	N	21.616	-8.696	6.971
C	26.918	-5.614	-2.150	C	21.953	-9.889	7.450
C	25.511	-5.930	-1.799	H	22.249	-10.763	6.874
H	27.143	-5.935	-3.173	H	22.179	-10.698	9.340
H	27.086	-4.528	-2.087	H	21.490	-9.152	11.290
C	24.555	-6.758	-2.330	H	21.917	-7.459	11.004
H	23.131	-5.868	0.429	H	21.054	-6.857	7.950
C	23.742	-6.021	-0.453	H	15.572	-6.964	4.439
N	24.959	-5.478	-0.617	C	16.234	-6.430	5.129
N	23.462	-6.811	-1.481	C	17.678	-6.466	4.784
H	24.595	-7.329	-3.250	H	16.120	-6.868	6.127
H	25.397	-4.800	0.025	H	15.899	-5.380	5.201
H	27.029	-9.919	2.132	C	18.703	-7.157	5.385
C	26.657	-8.888	2.184	H	17.917	-5.052	3.129
C	25.625	-8.654	3.241	H	20.327	-5.591	3.084
H	26.220	-8.620	1.214	C	19.622	-6.038	3.783
H	27.524	-8.224	2.339	N	18.296	-5.761	3.763

Atom	X (Å)	Y (Å)	Z (Å)
N	19.892	-6.904	4.749
H	18.664	-7.776	6.272
H	16.122	-10.420	-0.075
C	16.330	-9.351	-0.032
C	17.487	-8.994	-0.900
H	16.564	-9.078	1.005
H	15.407	-8.815	-0.306
C	18.735	-8.535	-0.566
H	16.841	-9.663	-2.858
H	19.136	-9.111	-3.714
C	18.812	-8.980	-2.686
N	17.564	-9.255	-2.257
N	19.557	-8.543	-1.682
H	19.096	-8.224	0.406
H	17.782	-11.965	1.837
C	18.185	-11.979	2.851
C	19.414	-11.185	3.143
C	19.612	-9.866	3.480
N	20.647	-11.781	3.355
N	20.900	-9.682	3.944
C	21.510	-10.856	3.830
H	22.547	-11.074	4.083
H	20.895	-12.763	3.206
H	18.425	-13.025	3.093
H	17.379	-11.684	3.539
H	18.886	-9.057	3.475
FE	21.556	-7.715	-1.639
FE	21.700	-8.004	5.017
C	18.296	5.604	0.520
C	19.223	4.666	-0.241
C	18.881	3.205	0.017
C	19.843	2.175	-0.563
C	19.447	0.777	-0.106
C	20.366	-0.370	-0.536
C	20.306	-1.481	0.501
C	21.262	-2.659	0.337
C	21.340	-3.444	1.658
C	22.730	-3.837	2.215
C	23.994	-3.126	1.729
C	24.176	-1.631	2.008
C	25.647	-1.248	1.720
C	25.955	0.144	1.130

Atom	X (Å)	Y (Å)	Z (Å)
C	26.511	1.169	2.127
C	27.969	0.864	2.513
H	28.751	1.371	1.926
H	22.910	-4.917	2.109
H	22.677	-3.677	3.301
H	24.148	-3.297	0.650
H	24.829	-3.641	2.245
H	23.897	-1.444	3.062
H	23.484	-1.038	1.391
H	26.030	-1.997	1.009
H	26.227	-1.416	2.641
H	25.051	0.527	0.634
H	26.696	-0.003	0.328
H	25.876	1.156	3.030
H	26.406	2.179	1.705
H	28.139	-0.221	2.386
H	28.145	1.084	3.575
H	17.247	5.484	0.211
H	18.327	5.384	1.601
H	18.570	6.658	0.392
H	20.264	4.848	0.072
H	19.186	4.863	-1.321
H	17.863	2.984	-0.347
H	18.857	3.040	1.110
H	20.865	2.390	-0.206
H	19.887	2.231	-1.661
H	18.410	0.546	-0.411
H	19.420	0.789	0.997
H	21.409	-0.018	-0.619
H	20.079	-0.762	-1.530
H	19.272	-1.873	0.562
H	20.505	-1.026	1.485
H	22.256	-2.298	0.036
H	20.906	-3.315	-0.471
H	20.844	-2.843	2.433
H	20.707	-4.345	1.570
O	22.412	-5.614	5.109
H	21.800	-4.843	5.028
H	23.247	-5.160	4.851
O	21.158	-7.191	0.225
O	21.392	-7.809	1.309

Table A.5.8. Optimized coordinates of the QM region for the O₂-bound model **4** shown in Figure 5.6.

Atom	X (Å)	Y (Å)	Z (Å)	Atom	X (Å)	Y (Å)	Z (Å)
H	22.245	-3.253	-5.826	C	24.686	-8.206	3.525
C	21.667	-2.823	-5.007	H	27.185	-8.162	5.466
C	21.149	-3.868	-4.098	H	24.984	-7.897	6.718
H	20.858	-2.202	-5.399	C	25.078	-8.037	5.645
H	22.329	-2.138	-4.448	N	26.260	-8.183	5.018
C	21.773	-4.983	-3.608	N	24.088	-8.048	4.764
H	19.201	-3.142	-3.518	H	24.101	-8.232	2.615
H	18.880	-5.273	-2.230	H	25.007	-12.117	0.468
C	19.761	-5.032	-2.812	C	24.655	-12.030	-0.560
N	19.866	-3.932	-3.590	C	23.506	-11.105	-0.718
N	20.906	-5.702	-2.813	C	23.443	-9.758	-0.958
H	22.813	-5.265	-3.721	N	22.188	-11.499	-0.567
H	22.171	-9.385	-8.286	N	22.122	-9.345	-0.984
C	21.380	-9.242	-7.556	C	21.390	-10.423	-0.737
C	21.798	-9.119	-6.143	H	24.264	-9.069	-1.126
H	20.684	-10.094	-7.642	H	21.876	-12.452	-0.356
H	20.821	-8.338	-7.834	H	24.356	-13.031	-0.908
C	21.443	-8.186	-5.199	H	25.498	-11.713	-1.189
H	23.070	-10.874	-5.778	H	20.304	-10.449	-0.688
H	23.189	-10.231	-3.406	H	19.981	-7.565	10.882
C	22.632	-9.679	-4.157	C	21.051	-7.758	10.764
N	22.567	-10.038	-5.449	C	21.417	-8.147	9.367
N	21.958	-8.550	-3.970	C	21.322	-7.491	8.155
H	20.853	-7.283	-5.327	N	21.912	-9.394	9.035
H	27.629	-6.503	-1.624	N	21.752	-8.322	7.135
C	27.013	-5.950	-2.339	C	22.108	-9.464	7.708
C	25.576	-6.150	-2.034	H	22.526	-10.336	7.213
H	27.238	-6.296	-3.354	H	22.232	-10.155	9.648
H	27.263	-4.880	-2.278	H	21.325	-8.580	11.441
C	24.543	-6.799	-2.665	H	21.610	-6.868	11.096
H	23.182	-6.004	0.161	H	20.977	-6.482	7.953
C	23.761	-6.137	-0.748	H	15.694	-7.278	4.446
N	25.044	-5.744	-0.828	C	16.244	-6.710	5.206
N	23.418	-6.777	-1.860	C	17.690	-6.609	4.904
H	24.541	-7.277	-3.638	H	16.129	-7.195	6.181
H	25.518	-5.134	-0.145	H	15.802	-5.702	5.288
H	27.565	-9.490	2.654	C	18.792	-7.147	5.533
C	27.149	-8.478	2.669	H	17.763	-5.271	3.178
C	26.050	-8.285	3.662	H	20.190	-5.631	3.069
H	26.754	-8.247	1.673	C	19.548	-6.091	3.819
H	27.973	-7.770	2.859	N	18.212	-5.926	3.822

Atom	X (Å)	Y (Å)	Z (Å)
N	19.942	-6.854	4.838
H	18.822	-7.725	6.449
H	15.825	-9.768	-0.220
C	16.154	-8.730	-0.197
C	17.283	-8.483	-1.143
H	16.490	-8.500	0.824
H	15.283	-8.088	-0.401
C	18.589	-8.166	-0.878
H	16.468	-9.043	-3.075
H	18.745	-8.683	-4.057
C	18.500	-8.551	-3.007
N	17.258	-8.713	-2.508
N	19.347	-8.221	-2.041
H	19.019	-7.916	0.082
H	18.524	-12.241	2.010
C	18.784	-12.215	3.070
C	19.950	-11.363	3.431
C	20.047	-10.026	3.733
N	21.204	-11.870	3.725
N	21.307	-9.726	4.203
C	21.985	-10.864	4.187
H	23.022	-11.000	4.490
H	21.509	-12.845	3.675
H	19.016	-13.241	3.390
H	17.897	-11.902	3.638
H	19.274	-9.265	3.653
FE	21.464	-7.666	-2.174
FE	21.980	-7.823	5.127
C	18.342	5.659	0.381
C	19.229	4.688	-0.387
C	18.875	3.244	-0.060
C	19.792	2.177	-0.644
C	19.410	0.808	-0.095
C	20.257	-0.376	-0.558
C	20.156	-1.503	0.458
C	21.036	-2.730	0.222
C	21.208	-3.551	1.519
C	22.647	-3.865	2.012
C	23.890	-3.112	1.514
C	24.025	-1.616	1.827
C	25.517	-1.198	1.817
C	25.886	0.172	1.200
C	26.436	1.196	2.208

Atom	X (Å)	Y (Å)	Z (Å)
C	27.882	0.897	2.640
H	28.676	1.436	2.103
H	22.907	-4.921	1.832
H	22.663	-3.754	3.109
H	24.070	-3.280	0.438
H	24.725	-3.613	2.042
H	23.574	-1.434	2.821
H	23.443	-1.023	1.106
H	26.072	-1.980	1.275
H	25.883	-1.266	2.854
H	25.010	0.580	0.675
H	26.639	-0.010	0.417
H	25.780	1.176	3.096
H	26.341	2.207	1.785
H	28.074	-0.181	2.485
H	28.015	1.092	3.714
H	17.280	5.524	0.125
H	18.422	5.477	1.467
H	18.605	6.709	0.201
H	20.287	4.862	-0.124
H	19.148	4.846	-1.470
H	17.836	3.028	-0.366
H	18.897	3.126	1.040
H	20.835	2.391	-0.350
H	19.781	2.181	-1.744
H	18.343	0.591	-0.289
H	19.495	0.869	1.004
H	21.317	-0.078	-0.645
H	19.938	-0.733	-1.559
H	19.106	-1.841	0.535
H	20.407	-1.089	1.448
H	22.012	-2.430	-0.185
H	20.552	-3.360	-0.543
H	20.673	-3.040	2.333
H	20.627	-4.483	1.402
O	22.374	-5.594	4.890
H	21.684	-4.891	4.896
H	23.153	-5.000	4.741
O	21.007	-6.793	-0.441
O	21.259	-7.155	0.717
O	21.866	-7.479	3.028
H	21.959	-6.609	2.682
H	21.668	-8.051	2.288

Table A.5.9. Optimized coordinates of the QM region for species **A** described in Scheme 5.3.

Atom	X (Å)	Y (Å)	Z (Å)	Atom	X (Å)	Y (Å)	Z (Å)
H	22.457	-3.182	-5.504	H	27.365	-7.345	5.703
C	21.785	-2.735	-4.761	H	24.986	-7.221	6.564
C	21.259	-3.746	-3.810	C	25.259	-7.356	5.520
H	20.971	-2.221	-5.273	N	26.541	-7.436	5.096
H	22.334	-1.953	-4.209	N	24.428	-7.480	4.503
C	21.937	-4.768	-3.198	H	24.769	-7.745	2.396
H	19.107	-3.358	-3.611	H	25.605	-11.654	0.825
H	18.946	-5.295	-2.106	C	25.259	-11.565	-0.205
C	19.884	-4.969	-2.558	C	24.048	-10.713	-0.338
N	19.956	-3.896	-3.380	C	23.891	-9.365	-0.522
N	21.079	-5.529	-2.437	N	22.759	-11.213	-0.293
H	22.991	-5.007	-3.252	N	22.547	-9.055	-0.623
H	22.939	-9.335	-7.915	C	21.891	-10.193	-0.471
C	22.114	-9.123	-7.234	H	24.663	-8.607	-0.616
C	22.439	-8.976	-5.794	H	22.503	-12.193	-0.158
H	21.363	-9.924	-7.334	H	25.033	-12.572	-0.594
H	21.629	-8.195	-7.569	H	26.074	-11.162	-0.822
C	21.989	-8.031	-4.899	H	20.813	-10.305	-0.524
H	23.632	-10.754	-5.225	H	19.797	-7.325	10.270
H	23.594	-10.024	-2.936	C	20.880	-7.261	10.105
C	23.114	-9.458	-3.733	C	21.371	-7.634	8.743
N	23.162	-9.862	-5.018	C	21.324	-7.002	7.519
N	22.411	-8.345	-3.622	N	22.063	-8.805	8.486
H	21.388	-7.147	-5.092	N	21.984	-7.752	6.565
H	27.887	-6.206	-1.214	C	22.436	-8.825	7.187
C	27.284	-5.609	-1.899	H	23.061	-9.624	6.779
C	25.842	-5.797	-1.612	H	22.378	-9.541	9.129
H	27.522	-5.884	-2.933	H	21.382	-7.917	10.835
H	27.539	-4.546	-1.765	H	21.205	-6.238	10.350
C	24.842	-6.504	-2.230	H	20.907	-6.032	7.266
H	23.292	-5.444	0.393	H	15.868	-7.626	3.951
C	23.982	-5.707	-0.406	C	16.422	-6.929	4.585
N	25.269	-5.305	-0.457	C	17.858	-6.794	4.243
N	23.694	-6.442	-1.462	H	16.346	-7.254	5.627
H	24.882	-7.060	-3.159	H	15.942	-5.936	4.515
H	25.746	-4.712	0.235	C	18.999	-7.125	4.934
H	28.131	-8.937	2.993	H	17.756	-5.790	2.332
C	27.781	-7.898	2.937	H	20.293	-5.716	2.353
C	26.546	-7.634	3.730	C	19.676	-6.239	3.085
H	27.576	-7.654	1.886	N	18.317	-6.241	3.060
H	28.600	-7.236	3.259	N	20.109	-6.788	4.199
C	25.213	-7.646	3.383	H	19.086	-7.523	5.936

Atom	X (Å)	Y (Å)	Z (Å)
H	16.283	-9.999	-0.330
C	16.461	-8.929	-0.354
C	17.678	-8.581	-1.137
H	16.583	-8.560	0.672
H	15.555	-8.460	-0.765
C	18.897	-8.089	-0.724
H	17.178	-9.232	-3.149
H	19.495	-8.658	-3.836
C	19.119	-8.542	-2.824
N	17.855	-8.856	-2.477
N	19.784	-8.078	-1.782
H	19.153	-7.687	0.255
H	19.171	-12.216	2.034
C	19.579	-12.023	3.033
C	20.659	-10.985	3.173
C	20.667	-9.607	3.147
N	21.929	-11.315	3.627
N	21.882	-9.117	3.592
C	22.619	-10.175	3.872
H	23.614	-10.169	4.321
H	22.283	-12.246	3.848
H	20.010	-12.966	3.402
H	18.741	-11.782	3.704
H	19.860	-8.933	2.881
FE	21.823	-7.412	-1.828
FE	22.249	-7.073	4.546
C	17.477	5.954	0.716
C	18.694	5.274	0.086
C	18.522	3.755	0.038
C	19.684	2.923	-0.510
C	19.464	1.440	-0.196
C	20.562	0.451	-0.619
C	20.558	-0.766	0.305
C	21.554	-1.901	0.026
C	21.550	-2.911	1.203
C	22.876	-3.300	1.909
C	24.192	-2.627	1.516
C	24.420	-1.156	1.870
C	25.904	-0.792	1.681
C	26.193	0.693	1.423

Atom	X (Å)	Y (Å)	Z (Å)
C	26.473	1.544	2.669
C	27.857	1.258	3.262
H	28.676	1.771	2.737
H	23.023	-4.386	1.790
H	22.757	-3.213	2.999
H	24.377	-2.755	0.433
H	24.984	-3.193	2.041
H	24.089	-0.972	2.907
H	23.797	-0.503	1.237
H	26.291	-1.379	0.828
H	26.476	-1.143	2.559
H	25.352	1.113	0.851
H	27.071	0.767	0.761
H	25.694	1.367	3.432
H	26.388	2.610	2.401
H	28.073	0.176	3.212
H	27.898	1.523	4.330
H	16.549	5.777	0.146
H	17.280	5.574	1.732
H	17.601	7.045	0.804
H	19.591	5.513	0.685
H	18.880	5.678	-0.923
H	17.612	3.510	-0.542
H	18.324	3.420	1.075
H	20.628	3.243	-0.039
H	19.817	3.103	-1.591
H	18.491	1.115	-0.605
H	19.346	1.365	0.900
H	21.549	0.940	-0.571
H	20.428	0.139	-1.670
H	19.537	-1.193	0.330
H	20.741	-0.407	1.333
H	22.555	-1.478	-0.139
H	21.295	-2.405	-0.922
H	20.896	-2.486	1.972
H	21.055	-3.850	0.888
O	22.386	-5.205	4.443
H	23.199	-4.668	4.402

Table A.5.10. Optimized coordinates of the QM region for species **B** described in Scheme 5.3.

Atom	X (Å)	Y (Å)	Z (Å)	Atom	X (Å)	Y (Å)	Z (Å)
H	22.395	-3.158	-5.616	H	27.209	-7.480	5.976
C	21.723	-2.725	-4.868	H	24.820	-7.394	6.794
C	21.141	-3.782	-4.006	C	25.115	-7.542	5.759
H	20.948	-2.140	-5.366	N	26.399	-7.584	5.352
H	22.293	-2.003	-4.258	N	24.300	-7.708	4.727
C	21.776	-4.871	-3.466	H	24.676	-7.951	2.630
H	19.002	-3.325	-3.783	H	25.531	-11.645	1.010
H	18.771	-5.345	-2.399	C	25.210	-11.525	-0.026
C	19.719	-5.030	-2.840	C	23.997	-10.680	-0.202
N	19.832	-3.906	-3.591	C	23.815	-9.333	-0.404
N	20.890	-5.634	-2.752	N	22.719	-11.208	-0.218
H	22.820	-5.153	-3.527	N	22.471	-9.057	-0.571
H	22.800	-9.338	-7.858	C	21.838	-10.205	-0.442
C	21.973	-9.120	-7.183	H	24.571	-8.556	-0.463
C	22.310	-8.939	-5.746	H	22.470	-12.187	-0.067
H	21.240	-9.942	-7.263	H	24.992	-12.524	-0.433
H	21.470	-8.208	-7.535	H	26.047	-11.128	-0.619
C	21.768	-8.060	-4.835	H	20.766	-10.347	-0.532
H	23.748	-10.531	-5.242	H	19.689	-7.220	10.496
H	23.645	-9.830	-2.913	C	20.778	-7.173	10.351
C	23.076	-9.339	-3.700	C	21.277	-7.527	8.984
N	23.155	-9.730	-4.991	C	21.305	-6.865	7.773
N	22.243	-8.325	-3.569	N	21.915	-8.728	8.721
H	21.057	-7.256	-5.010	N	21.941	-7.645	6.822
H	27.879	-6.407	-1.258	C	22.305	-8.759	7.434
C	27.286	-5.885	-2.014	H	22.881	-9.590	7.028
C	25.829	-5.957	-1.736	H	22.176	-9.492	9.356
H	27.519	-6.289	-3.007	H	21.253	-7.863	11.067
H	27.572	-4.822	-2.012	H	21.128	-6.166	10.622
C	24.779	-6.658	-2.274	H	20.955	-5.868	7.519
H	23.301	-5.114	0.138	H	15.904	-7.612	4.235
C	23.954	-5.517	-0.626	C	16.416	-6.986	4.973
N	25.270	-5.238	-0.698	C	17.849	-6.717	4.699
N	23.620	-6.380	-1.568	H	16.338	-7.456	5.959
H	24.785	-7.352	-3.107	H	15.888	-6.019	5.028
H	25.789	-4.637	-0.049	C	19.009	-7.212	5.240
H	28.073	-8.997	3.236	H	17.668	-5.214	3.166
C	27.680	-7.976	3.186	H	20.211	-5.092	3.142
C	26.430	-7.783	3.984	C	19.622	-5.780	3.738
H	27.460	-7.737	2.135	N	18.270	-5.802	3.747
H	28.463	-7.275	3.512	N	20.096	-6.635	4.621
C	25.108	-7.856	3.617	H	19.148	-7.892	6.069

Atom	X (Å)	Y (Å)	Z (Å)
H	16.106	-10.036	-0.248
C	16.320	-8.975	-0.317
C	17.551	-8.678	-1.100
H	16.440	-8.575	0.698
H	15.428	-8.501	-0.753
C	18.764	-8.171	-0.697
H	17.063	-9.380	-3.098
H	19.414	-8.896	-3.767
C	19.018	-8.725	-2.769
N	17.745	-9.014	-2.427
N	19.667	-8.212	-1.740
H	19.023	-7.730	0.263
H	18.983	-12.299	2.146
C	19.338	-12.176	3.176
C	20.367	-11.126	3.494
C	20.363	-9.749	3.590
N	21.597	-11.491	4.027
N	21.528	-9.306	4.186
C	22.258	-10.379	4.414
H	23.243	-10.404	4.883
H	22.007	-12.429	4.066
H	19.801	-13.132	3.462
H	18.459	-12.049	3.826
H	19.594	-9.044	3.289
FE	21.664	-7.339	-1.715
FE	22.190	-7.146	4.730
C	18.377	6.244	-0.076
C	19.346	5.155	-0.516
C	18.831	3.742	-0.238
C	19.779	2.631	-0.695
C	19.399	1.244	-0.169
C	20.425	0.145	-0.493
C	20.439	-0.971	0.552
C	21.608	-1.962	0.475
C	21.685	-2.819	1.757
C	23.054	-3.307	2.304
C	24.352	-2.675	1.797
C	24.648	-1.195	2.030
C	26.036	-0.840	1.479
C	26.274	0.652	1.234
C	26.510	1.492	2.495
C	27.894	1.245	3.099

Atom	X (Å)	Y (Å)	Z (Å)
H	28.711	1.760	2.575
H	23.158	-4.385	2.116
H	23.020	-3.230	3.401
H	24.443	-2.861	0.710
H	25.165	-3.241	2.284
H	24.570	-0.953	3.103
H	23.897	-0.575	1.518
H	26.167	-1.364	0.514
H	26.817	-1.254	2.141
H	25.414	1.038	0.666
H	27.144	0.760	0.566
H	25.736	1.260	3.247
H	26.379	2.560	2.256
H	28.125	0.167	3.083
H	27.918	1.542	4.159
H	17.392	6.144	-0.563
H	18.195	6.199	1.010
H	18.756	7.250	-0.306
H	20.312	5.302	-0.005
H	19.567	5.257	-1.588
H	17.846	3.613	-0.722
H	18.648	3.639	0.849
H	20.799	2.861	-0.342
H	19.850	2.624	-1.795
H	18.395	0.954	-0.528
H	19.303	1.320	0.929
H	21.432	0.596	-0.514
H	20.259	-0.264	-1.507
H	19.480	-1.519	0.538
H	20.482	-0.489	1.545
H	22.538	-1.392	0.345
H	21.521	-2.593	-0.429
H	21.199	-2.243	2.556
H	21.044	-3.714	1.617
O	22.623	-5.367	4.833
H	23.504	-5.019	5.074
O	22.045	-7.225	2.635
O	23.013	-6.628	1.971
O	21.007	-6.298	0.122
H	21.514	-6.574	0.907
H	20.685	-5.402	0.267

Table A.5.11. Optimized coordinates of the QM region for species **C** described in Scheme 5.3.

Atom	X (Å)	Y (Å)	Z (Å)	Atom	X (Å)	Y (Å)	Z (Å)
H	22.387	-3.237	-5.470	H	26.932	-7.162	6.001
C	21.687	-2.816	-4.741	H	24.530	-6.938	6.726
C	21.074	-3.878	-3.904	C	24.850	-7.144	5.707
H	20.931	-2.228	-5.261	N	26.143	-7.256	5.349
H	22.234	-2.098	-4.106	N	24.070	-7.336	4.652
C	21.689	-4.976	-3.360	H	24.502	-7.744	2.595
H	18.932	-3.417	-3.728	H	25.476	-11.575	1.003
H	18.665	-5.432	-2.348	C	25.207	-11.498	-0.051
C	19.623	-5.123	-2.770	C	23.947	-10.740	-0.259
N	19.758	-3.994	-3.509	C	23.674	-9.397	-0.325
N	20.786	-5.741	-2.663	N	22.718	-11.356	-0.399
H	22.731	-5.265	-3.410	N	22.327	-9.202	-0.542
H	23.054	-9.478	-7.791	C	21.775	-10.399	-0.570
C	22.181	-9.311	-7.154	H	24.368	-8.566	-0.258
C	22.407	-9.109	-5.700	H	22.558	-12.366	-0.408
H	21.506	-10.178	-7.266	H	25.079	-12.513	-0.458
H	21.641	-8.433	-7.538	H	26.037	-11.046	-0.611
C	21.821	-8.215	-4.830	H	20.723	-10.601	-0.744
H	23.734	-10.755	-5.114	H	19.542	-7.225	10.385
H	23.493	-10.042	-2.776	C	20.623	-7.227	10.183
C	22.993	-9.544	-3.602	C	21.067	-7.521	8.778
N	23.154	-9.936	-4.884	C	20.981	-6.848	7.574
N	22.186	-8.502	-3.532	N	21.824	-8.639	8.474
H	21.149	-7.391	-5.054	N	21.670	-7.537	6.586
H	27.755	-6.278	-1.201	C	22.176	-8.610	7.176
C	27.186	-5.786	-1.996	H	22.851	-9.355	6.752
C	25.723	-5.939	-1.790	H	22.174	-9.368	9.105
H	27.486	-6.190	-2.970	H	21.089	-7.983	10.836
H	27.430	-4.712	-1.988	H	21.029	-6.256	10.510
C	24.749	-6.771	-2.289	H	20.520	-5.889	7.357
H	23.117	-5.230	0.022	H	15.644	-7.585	4.094
C	23.803	-5.609	-0.725	C	16.170	-6.910	4.775
N	25.084	-5.210	-0.810	C	17.585	-6.653	4.418
N	23.562	-6.560	-1.607	H	16.138	-7.320	5.790
H	24.831	-7.517	-3.071	H	15.632	-5.947	4.792
H	25.545	-4.544	-0.181	C	18.768	-7.031	4.999
H	27.869	-8.833	3.345	H	17.332	-5.407	2.685
C	27.501	-7.802	3.270	H	19.839	-5.224	2.555
C	26.221	-7.545	3.999	C	19.307	-5.847	3.267
H	27.345	-7.567	2.208	N	17.960	-5.900	3.325
H	28.289	-7.124	3.630	N	19.827	-6.526	4.273
C	24.910	-7.585	3.584	H	18.930	-7.582	5.916

Atom	X (Å)	Y (Å)	Z (Å)
H	15.949	-10.064	-0.188
C	16.186	-9.008	-0.272
C	17.429	-8.763	-1.055
H	16.320	-8.595	0.737
H	15.310	-8.512	-0.714
C	18.661	-8.308	-0.652
H	16.915	-9.473	-3.038
H	19.274	-9.029	-3.728
C	18.890	-8.853	-2.727
N	17.606	-9.101	-2.382
N	19.559	-8.371	-1.697
H	18.943	-7.885	0.307
H	18.856	-12.241	2.159
C	19.236	-12.055	3.171
C	20.255	-10.968	3.387
C	20.225	-9.588	3.404
N	21.514	-11.274	3.877
N	21.410	-9.085	3.907
C	22.170	-10.131	4.171
H	23.173	-10.117	4.601
H	21.916	-12.206	4.009
H	19.723	-12.984	3.503
H	18.376	-11.904	3.839
H	19.417	-8.923	3.118
FE	21.569	-7.488	-1.670
FE	21.939	-6.926	4.460
C	17.720	6.582	0.324
C	18.872	5.693	-0.140
C	18.507	4.209	-0.062
C	19.582	3.230	-0.550
C	19.294	1.792	-0.107
C	20.362	0.748	-0.468
C	20.292	-0.478	0.446
C	21.300	-1.607	0.177
C	21.282	-2.660	1.323
C	22.476	-2.739	2.231
C	23.889	-2.488	1.811
C	24.379	-1.032	1.981
C	25.848	-0.850	1.594
C	26.246	0.608	1.336
C	26.494	1.455	2.593
C	27.868	1.189	3.215

Atom	X (Å)	Y (Å)	Z (Å)
H	28.697	1.695	2.697
H	22.748	-4.935	2.571
H	22.292	-2.985	3.285
H	24.021	-2.757	0.743
H	24.565	-3.137	2.400
H	24.191	-0.709	3.017
H	23.760	-0.382	1.343
H	26.037	-1.422	0.666
H	26.503	-1.298	2.364
H	25.459	1.061	0.714
H	27.161	0.612	0.720
H	25.710	1.250	3.343
H	26.395	2.525	2.343
H	28.084	0.107	3.212
H	27.874	1.495	4.271
H	16.808	6.401	-0.268
H	17.436	6.383	1.371
H	17.943	7.659	0.255
H	19.762	5.880	0.487
H	19.159	5.959	-1.172
H	17.575	4.039	-0.631
H	18.261	3.976	0.992
H	20.564	3.533	-0.149
H	19.678	3.293	-1.649
H	18.312	1.470	-0.501
H	19.177	1.802	0.993
H	21.363	1.204	-0.377
H	20.267	0.444	-1.525
H	19.269	-0.897	0.419
H	20.444	-0.135	1.485
H	22.304	-1.169	0.080
H	21.093	-2.085	-0.797
H	20.404	-2.461	1.953
H	21.072	-3.675	0.899
O	22.153	-5.081	4.738
H	23.041	-4.718	4.942
O	22.163	-6.768	2.480
O	23.134	-5.738	2.154
O	20.972	-6.511	0.181
H	21.354	-6.662	1.102
H	20.655	-5.603	0.123

Table A.5.12. Optimized coordinates of the QM region for species **D** described in Scheme 5.3, including the nascent water molecule.

Atom	X (Å)	Y (Å)	Z (Å)	Atom	X (Å)	Y (Å)	Z (Å)
H	22.201	-3.113	-5.623	C	25.154	-7.894	3.513
C	21.467	-2.741	-4.902	H	27.241	-7.551	5.886
C	20.969	-3.820	-4.016	H	24.867	-7.521	6.706
H	20.643	-2.256	-5.426	C	25.153	-7.643	5.664
H	21.940	-1.949	-4.295	N	26.437	-7.651	5.253
C	21.676	-4.841	-3.439	N	24.345	-7.794	4.626
H	18.852	-3.416	-3.781	H	24.711	-7.915	2.527
H	18.731	-5.405	-2.239	H	25.529	-11.639	0.877
C	19.639	-5.066	-2.739	C	25.150	-11.545	-0.143
N	19.679	-3.990	-3.561	C	23.946	-10.677	-0.268
N	20.848	-5.603	-2.649	C	23.789	-9.324	-0.451
H	22.726	-5.079	-3.534	N	22.653	-11.180	-0.243
H	22.646	-9.140	-7.746	N	22.448	-9.023	-0.576
C	21.805	-8.976	-7.069	C	21.785	-10.158	-0.429
C	22.102	-8.864	-5.620	H	24.555	-8.554	-0.515
H	21.090	-9.807	-7.202	H	22.388	-12.159	-0.095
H	21.285	-8.059	-7.381	H	24.892	-12.553	-0.516
C	21.703	-7.904	-4.716	H	25.958	-11.166	-0.785
H	23.168	-10.720	-5.063	H	20.706	-10.273	-0.492
H	23.128	-10.040	-2.772	H	19.742	-7.293	10.305
C	22.685	-9.429	-3.553	C	20.824	-7.256	10.099
N	22.732	-9.817	-4.843	C	21.294	-7.635	8.720
N	22.066	-8.267	-3.433	C	21.249	-7.023	7.481
H	21.156	-6.987	-4.911	N	22.034	-8.785	8.490
H	27.727	-6.235	-1.516	N	21.942	-7.771	6.546
C	27.188	-5.756	-2.341	C	22.414	-8.823	7.197
C	25.721	-5.828	-2.132	H	23.084	-9.600	6.825
H	27.476	-6.216	-3.293	H	22.372	-9.491	9.155
H	27.468	-4.695	-2.385	H	21.330	-7.933	10.807
C	24.740	-6.753	-2.384	H	21.180	-6.244	10.348
H	23.155	-4.625	-0.537	H	20.817	-6.067	7.205
C	23.837	-5.205	-1.144	H	15.799	-7.630	4.098
N	25.104	-4.851	-1.379	C	16.372	-6.915	4.695
N	23.570	-6.353	-1.750	C	17.805	-6.831	4.330
H	24.791	-7.678	-2.947	H	16.299	-7.191	5.751
H	25.614	-4.102	-0.896	H	15.910	-5.919	4.583
H	28.127	-8.982	3.062	C	18.942	-7.150	5.032
C	27.728	-7.959	3.077	H	17.769	-5.951	2.325
C	26.476	-7.816	3.882	H	20.242	-6.230	2.237
H	27.507	-7.653	2.044	C	19.624	-6.494	3.092
H	28.516	-7.283	3.449	N	18.270	-6.410	3.092

Atom	X (Å)	Y (Å)	Z (Å)
N	20.055	-6.947	4.248
H	19.027	-7.473	6.063
H	16.175	-9.951	-0.118
C	16.384	-8.882	-0.114
C	17.595	-8.559	-0.917
H	16.562	-8.553	0.917
H	15.489	-8.350	-0.477
C	18.816	-8.060	-0.526
H	17.077	-9.250	-2.917
H	19.401	-8.732	-3.628
C	19.027	-8.581	-2.620
N	17.762	-8.870	-2.256
N	19.695	-8.088	-1.590
H	19.115	-7.643	0.432
H	19.010	-12.362	2.151
C	19.370	-12.267	3.179
C	20.446	-11.265	3.466
C	20.423	-9.899	3.632
N	21.719	-11.636	3.876
N	21.614	-9.469	4.166
C	22.384	-10.528	4.288
H	23.398	-10.543	4.689
H	22.115	-12.575	3.913
H	19.780	-13.245	3.476
H	18.503	-12.077	3.829
H	19.610	-9.209	3.436
FE	21.666	-7.228	-1.481
FE	22.205	-7.380	4.401
C	17.455	5.670	-0.068
C	18.645	4.758	-0.356
C	18.343	3.281	-0.110
C	19.469	2.324	-0.505
C	19.205	0.894	-0.036
C	20.299	-0.126	-0.395
C	20.418	-1.237	0.651
C	21.656	-2.133	0.536
C	21.846	-2.999	1.800
C	23.207	-3.111	2.420
C	24.480	-2.598	1.844
C	24.754	-1.085	1.943
C	26.092	-0.715	1.309
C	26.315	0.789	1.141
C	26.567	1.568	2.438

Atom	X (Å)	Y (Å)	Z (Å)
C	27.945	1.258	3.025
H	28.777	1.762	2.516
H	23.885	-5.136	2.069
H	23.214	-3.557	3.418
H	24.509	-2.845	0.764
H	25.327	-3.129	2.312
H	24.706	-0.764	2.995
H	23.951	-0.540	1.422
H	26.145	-1.177	0.305
H	26.917	-1.168	1.887
H	25.446	1.192	0.603
H	27.177	0.931	0.467
H	25.789	1.317	3.179
H	26.458	2.648	2.248
H	28.135	0.173	2.957
H	27.993	1.506	4.097
H	16.585	5.429	-0.701
H	17.119	5.587	0.979
H	17.703	6.729	-0.238
H	19.503	5.061	0.272
H	18.975	4.891	-1.399
H	17.422	2.996	-0.653
H	18.116	3.141	0.963
H	20.420	2.669	-0.065
H	19.630	2.358	-1.597
H	18.222	0.559	-0.415
H	19.096	0.920	1.062
H	21.270	0.394	-0.457
H	20.128	-0.551	-1.401
H	19.498	-1.853	0.663
H	20.457	-0.753	1.642
H	22.531	-1.483	0.388
H	21.597	-2.753	-0.380
H	21.184	-2.607	2.586
H	21.432	-4.021	1.641
O	22.432	-5.547	4.676
H	23.347	-5.309	4.939
O	22.309	-7.431	2.762
O	24.184	-5.842	1.465
O	21.404	-6.383	0.149
H	20.987	-5.519	0.234
H	23.337	-6.26	1.261

Table A.5.13. Optimized coordinates of the QM region for species **D** described in Scheme 5.3, excluding the nascent water molecule.

Atom	X (Å)	Y (Å)	Z (Å)	Atom	X (Å)	Y (Å)	Z (Å)
H	22.136	-3.177	-5.626	C	25.141	-7.952	3.399
C	21.479	-2.752	-4.862	H	27.291	-7.774	5.738
C	20.940	-3.805	-3.966	H	24.936	-7.609	6.596
H	20.677	-2.182	-5.334	C	25.198	-7.734	5.548
H	22.059	-2.022	-4.272	N	26.474	-7.845	5.118
C	21.622	-4.812	-3.326	N	24.363	-7.803	4.528
H	18.767	-3.508	-3.911	H	24.677	-7.970	2.419
H	18.596	-5.468	-2.426	H	25.301	-11.804	0.776
C	19.540	-5.112	-2.836	C	24.926	-11.674	-0.241
N	19.619	-4.020	-3.632	C	23.727	-10.798	-0.356
N	20.748	-5.617	-2.645	C	23.578	-9.445	-0.524
H	22.687	-4.996	-3.294	N	22.435	-11.292	-0.370
H	22.355	-9.176	-7.859	N	22.239	-9.133	-0.669
C	21.553	-8.964	-7.148	C	21.575	-10.269	-0.559
C	21.922	-8.825	-5.713	H	24.351	-8.688	-0.577
H	20.807	-9.771	-7.230	H	22.164	-12.272	-0.267
H	21.048	-8.040	-7.462	H	24.667	-12.665	-0.648
C	21.548	-7.865	-4.797	H	25.738	-11.281	-0.868
H	23.033	-10.666	-5.190	H	20.501	-10.381	-0.648
H	23.130	-9.928	-2.906	H	19.802	-7.203	10.263
C	22.637	-9.342	-3.675	C	20.884	-7.176	10.070
N	22.629	-9.748	-4.962	C	21.330	-7.572	8.693
N	21.988	-8.202	-3.531	C	21.326	-6.932	7.468
H	20.968	-6.966	-4.969	N	21.966	-8.773	8.434
H	27.613	-6.392	-1.263	N	21.942	-7.719	6.510
C	26.977	-5.775	-1.902	C	22.332	-8.816	7.136
C	25.541	-5.973	-1.568	H	22.925	-9.642	6.738
H	27.179	-6.007	-2.955	H	22.238	-9.523	9.081
H	27.237	-4.716	-1.736	H	21.379	-7.850	10.788
C	24.470	-6.524	-2.222	H	21.251	-6.164	10.301
H	23.153	-5.916	0.689	H	20.978	-5.932	7.223
C	23.755	-5.990	-0.224	H	15.866	-7.568	4.026
N	25.053	-5.649	-0.312	C	16.458	-6.909	4.669
N	23.371	-6.522	-1.379	C	17.898	-6.789	4.317
H	24.419	-6.930	-3.222	H	16.376	-7.251	5.706
H	25.601	-5.213	0.437	H	16.009	-5.901	4.622
H	28.036	-9.259	2.910	C	19.041	-7.086	5.017
C	27.679	-8.222	2.902	H	17.784	-5.893	2.352
C	26.470	-7.988	3.744	H	20.345	-5.698	2.435
H	27.424	-7.950	1.868	C	19.704	-6.174	3.168
H	28.504	-7.559	3.202	N	18.353	-6.206	3.143

Atom	X (Å)	Y (Å)	Z (Å)
N	20.147	-6.707	4.287
H	19.134	-7.476	6.022
H	15.955	-9.993	-0.344
C	16.134	-8.923	-0.415
C	17.356	-8.619	-1.203
H	16.267	-8.516	0.596
H	15.233	-8.454	-0.837
C	18.562	-8.132	-0.771
H	16.904	-9.332	-3.207
H	19.276	-8.877	-3.826
C	18.860	-8.705	-2.839
N	17.575	-8.970	-2.524
N	19.489	-8.197	-1.794
H	18.822	-7.691	0.186
H	18.891	-12.204	2.020
C	19.299	-12.040	3.026
C	20.387	-11.018	3.225
C	20.467	-9.640	3.171
N	21.601	-11.393	3.785
N	21.670	-9.202	3.692
C	22.334	-10.287	4.041
H	23.311	-10.323	4.525
H	21.930	-12.342	3.973
H	19.738	-12.997	3.348
H	18.463	-11.847	3.714
H	19.726	-8.928	2.824
FE	21.429	-7.310	-1.514
FE	22.286	-7.072	4.386
C	18.233	6.254	0.032
C	19.246	5.186	-0.360
C	18.728	3.760	-0.165
C	19.679	2.670	-0.665
C	19.265	1.269	-0.209
C	20.222	0.141	-0.623
C	20.152	-1.058	0.321
C	21.150	-2.188	0.038
C	21.255	-3.162	1.239
C	22.584	-3.321	1.901
C	23.901	-2.893	1.360
C	24.308	-1.427	1.649
C	25.779	-1.174	1.295

Atom	X (Å)	Y (Å)	Z (Å)
C	26.134	0.297	1.041
C	26.422	1.135	2.295
C	27.811	0.852	2.876
H	28.633	1.345	2.334
H	22.586	-3.624	2.953
H	23.958	-3.053	0.269
H	24.672	-3.528	1.828
H	24.098	-1.193	2.705
H	23.666	-0.757	1.054
H	26.012	-1.749	0.378
H	26.425	-1.597	2.084
H	25.315	0.745	0.456
H	27.022	0.330	0.390
H	25.653	0.939	3.062
H	26.329	2.206	2.048
H	28.014	-0.233	2.858
H	27.854	1.145	3.935
H	17.291	6.168	-0.537
H	17.955	6.181	1.096
H	18.622	7.269	-0.137
H	20.166	5.324	0.234
H	19.550	5.327	-1.408
H	17.749	3.652	-0.668
H	18.529	3.603	0.913
H	20.697	2.872	-0.289
H	19.758	2.715	-1.766
H	18.241	1.044	-0.560
H	19.200	1.284	0.894
H	21.258	0.522	-0.610
H	20.032	-0.173	-1.666
H	19.124	-1.464	0.352
H	20.352	-0.686	1.342
H	22.132	-1.734	-0.165
H	20.884	-2.720	-0.893
H	20.561	-2.819	2.021
H	20.834	-4.163	0.983
O	22.726	-5.353	4.842
H	23.284	-4.610	4.554
O	22.558	-6.683	2.523
O	20.818	-6.507	0.038
H	20.493	-5.602	-0.062

Table A.5.14. Optimized coordinates of the QM region for species **E** described in Scheme 5.3

Atom	X (Å)	Y (Å)	Z (Å)	Atom	X (Å)	Y (Å)	Z (Å)
H	22.218	-2.949	-5.249	H	27.231	-7.470	5.570
C	21.540	-2.587	-4.470	H	24.869	-7.476	6.478
C	21.041	-3.702	-3.627	C	25.128	-7.631	5.434
H	20.714	-2.041	-4.927	N	26.400	-7.596	4.975
H	22.079	-1.851	-3.849	N	24.294	-7.890	4.444
C	21.712	-4.814	-3.189	H	24.587	-8.196	2.346
H	18.923	-3.274	-3.259	H	25.602	-11.852	0.754
H	18.816	-5.320	-1.879	C	25.203	-11.713	-0.253
C	19.724	-4.986	-2.381	C	23.990	-10.854	-0.319
N	19.774	-3.832	-3.096	C	23.817	-9.497	-0.445
N	20.892	-5.600	-2.424	N	22.704	-11.361	-0.267
H	22.742	-5.093	-3.353	N	22.472	-9.190	-0.499
H	22.638	-9.079	-7.846	C	21.829	-10.333	-0.384
C	21.832	-8.899	-7.133	H	24.579	-8.733	-0.529
C	22.209	-8.786	-5.697	H	22.443	-12.343	-0.154
H	21.099	-9.716	-7.235	H	24.949	-12.703	-0.665
H	21.317	-7.972	-7.420	H	25.996	-11.302	-0.892
C	21.706	-7.945	-4.727	H	20.752	-10.452	-0.398
H	23.651	-10.414	-5.307	H	19.812	-7.748	10.224
H	23.633	-9.806	-2.949	C	20.895	-7.717	10.034
C	23.044	-9.278	-3.694	C	21.353	-7.991	8.627
N	23.074	-9.619	-5.002	C	21.248	-7.315	7.425
N	22.226	-8.265	-3.492	N	22.120	-9.104	8.310
H	21.008	-7.128	-4.848	N	21.922	-7.999	6.430
H	27.887	-6.427	-1.403	C	22.448	-9.067	7.002
C	27.242	-5.850	-2.069	H	23.108	-9.818	6.565
C	25.816	-5.979	-1.679	H	22.490	-9.856	8.910
H	27.408	-6.161	-3.108	H	21.379	-8.461	10.686
H	27.519	-4.788	-1.991	H	21.271	-6.736	10.369
C	24.738	-6.635	-2.215	H	20.776	-6.363	7.216
H	23.437	-5.445	0.485	H	15.704	-7.858	4.146
C	24.037	-5.755	-0.362	C	16.263	-7.192	4.806
N	25.337	-5.424	-0.507	C	17.696	-7.069	4.455
N	23.644	-6.487	-1.387	H	16.191	-7.542	5.837
H	24.683	-7.209	-3.129	H	15.801	-6.192	4.755
H	25.881	-4.885	0.175	C	18.852	-7.483	5.073
H	28.044	-9.059	2.868	H	17.554	-5.996	2.579
C	27.635	-8.044	2.803	H	20.045	-5.987	2.495
C	26.393	-7.852	3.616	C	19.469	-6.468	3.270
H	27.402	-7.829	1.751	N	18.125	-6.427	3.311
H	28.415	-7.330	3.111	N	19.940	-7.098	4.324
C	25.059	-8.014	3.305	H	18.969	-7.948	6.043

Atom	X (Å)	Y (Å)	Z (Å)
H	16.096	-10.030	-0.170
C	16.340	-8.971	-0.133
C	17.566	-8.645	-0.913
H	16.511	-8.676	0.909
H	15.461	-8.420	-0.492
C	18.802	-8.190	-0.509
H	17.019	-9.209	-2.942
H	19.349	-8.692	-3.640
C	18.987	-8.598	-2.623
N	17.717	-8.884	-2.267
N	19.669	-8.172	-1.579
H	19.133	-7.813	0.455
H	18.984	-12.439	1.916
C	19.422	-12.375	2.917
C	20.502	-11.369	3.192
C	20.497	-10.001	3.363
N	21.765	-11.753	3.618
N	21.688	-9.586	3.920
C	22.439	-10.660	4.044
H	23.445	-10.711	4.462
H	22.164	-12.696	3.624
H	19.863	-13.359	3.143
H	18.602	-12.227	3.637
H	19.699	-9.299	3.169
FE	21.695	-7.410	-1.551
FE	22.079	-7.465	4.359
C	17.333	5.275	0.134
C	18.528	4.433	-0.302
C	18.433	2.978	0.150
C	19.601	2.089	-0.280
C	19.433	0.659	0.231
C	20.482	-0.353	-0.242
C	20.527	-1.571	0.681
C	21.674	-2.569	0.442
C	21.938	-3.338	1.711
C	23.118	-3.443	2.340
C	24.452	-2.947	1.858
C	24.698	-1.453	2.105
C	26.171	-1.081	1.893
C	26.390	0.340	1.354
C	26.787	1.352	2.431

Atom	X (Å)	Y (Å)	Z (Å)
C	28.253	1.165	2.834
H	28.942	1.693	2.162
H	23.154	-3.878	3.340
H	24.590	-3.135	0.780
H	25.237	-3.513	2.392
H	24.352	-1.190	3.116
H	24.060	-0.875	1.419
H	26.623	-1.813	1.200
H	26.715	-1.204	2.844
H	25.481	0.668	0.825
H	27.190	0.314	0.601
H	26.124	1.243	3.306
H	26.620	2.376	2.060
H	28.525	0.097	2.812
H	28.428	1.513	3.860
H	16.381	4.892	-0.269
H	17.223	5.311	1.229
H	17.422	6.312	-0.213
H	19.461	4.878	0.088
H	18.613	4.453	-1.401
H	17.496	2.541	-0.247
H	18.338	2.940	1.251
H	20.553	2.505	0.094
H	19.701	2.095	-1.379
H	18.426	0.297	-0.040
H	19.442	0.691	1.334
H	21.480	0.117	-0.255
H	20.280	-0.657	-1.287
H	19.557	-2.101	0.662
H	20.635	-1.192	1.711
H	22.577	-2.011	0.157
H	21.451	-3.226	-0.423
H	21.062	-3.724	2.239
O	22.405	-5.713	4.724
H	23.341	-5.450	4.693
O	22.156	-7.328	2.704
O	21.253	-6.510	0.424
H	21.518	-6.865	1.310
H	20.897	-5.624	0.539

Table A.5.15. Optimized coordinates of the QM region for species **F** described in Scheme 5.3

Atom	X (Å)	Y (Å)	Z (Å)	Atom	X (Å)	Y (Å)	Z (Å)
H	22.404	-3.076	-5.675	H	27.438	-7.294	5.651
C	21.748	-2.642	-4.915	H	25.041	-7.106	6.440
C	21.205	-3.682	-4.011	C	25.340	-7.317	5.417
H	20.949	-2.077	-5.397	N	26.629	-7.399	5.025
H	22.327	-1.906	-4.332	N	24.539	-7.496	4.379
C	21.884	-4.700	-3.393	H	24.899	-7.813	2.305
H	19.041	-3.319	-3.846	H	25.556	-11.551	0.754
H	18.872	-5.281	-2.385	C	25.163	-11.434	-0.258
C	19.810	-4.949	-2.830	C	23.953	-10.573	-0.346
N	19.889	-3.868	-3.637	C	23.793	-9.219	-0.495
N	21.012	-5.478	-2.675	N	22.663	-11.078	-0.335
H	22.944	-4.917	-3.404	N	22.452	-8.917	-0.618
H	22.680	-9.098	-7.782	C	21.795	-10.057	-0.502
C	21.864	-8.889	-7.085	H	24.561	-8.457	-0.548
C	22.204	-8.723	-5.646	H	22.404	-12.060	-0.208
H	21.134	-9.714	-7.160	H	24.907	-12.431	-0.655
H	21.345	-7.981	-7.422	H	25.958	-11.038	-0.906
C	21.823	-7.746	-4.752	H	20.718	-10.176	-0.565
H	23.303	-10.557	-5.078	H	20.047	-7.373	10.105
H	23.342	-9.806	-2.802	C	21.126	-7.321	9.893
C	22.865	-9.226	-3.586	C	21.567	-7.648	8.496
N	22.874	-9.647	-4.865	C	21.567	-6.949	7.305
N	22.235	-8.070	-3.471	N	22.193	-8.841	8.173
H	21.256	-6.842	-4.949	N	22.171	-7.687	6.304
H	27.872	-6.185	-1.385	C	22.547	-8.819	6.871
C	27.264	-5.606	-2.084	H	23.103	-9.638	6.418
C	25.825	-5.740	-1.751	H	22.477	-9.615	8.787
H	27.476	-5.923	-3.112	H	21.641	-8.021	10.571
H	27.538	-4.544	-1.993	H	21.480	-6.317	10.173
C	24.766	-6.434	-2.281	H	21.212	-5.945	7.109
H	23.427	-5.190	0.389	H	16.003	-7.610	4.025
C	24.039	-5.511	-0.446	C	16.610	-6.911	4.607
N	25.325	-5.163	-0.599	C	18.022	-6.808	4.167
N	23.662	-6.282	-1.456	H	16.584	-7.208	5.660
H	24.726	-7.042	-3.176	H	16.145	-5.910	4.538
H	25.862	-4.603	0.074	C	19.213	-6.984	4.826
H	28.249	-8.954	2.899	H	17.766	-6.194	2.108
C	27.919	-7.907	2.886	H	20.273	-6.248	1.871
C	26.673	-7.646	3.666	C	19.736	-6.461	2.791
H	27.732	-7.619	1.841	N	18.386	-6.469	2.875
H	28.746	-7.274	3.243	N	20.262	-6.781	3.955
C	25.353	-7.690	3.283	H	19.384	-7.208	5.872

Atom	X (Å)	Y (Å)	Z (Å)
H	16.228	-9.965	-0.253
C	16.451	-8.902	-0.251
C	17.667	-8.560	-1.040
H	16.630	-8.596	0.787
H	15.560	-8.355	-0.597
C	18.847	-7.989	-0.631
H	17.230	-9.297	-3.038
H	19.545	-8.675	-3.705
C	19.139	-8.527	-2.709
N	17.885	-8.882	-2.368
N	19.753	-7.980	-1.673
H	19.087	-7.550	0.331
H	19.074	-12.306	2.044
C	19.462	-12.178	3.058
C	20.537	-11.159	3.271
C	20.526	-9.790	3.418
N	21.836	-11.521	3.582
N	21.757	-9.342	3.839
C	22.528	-10.402	3.917
H	23.568	-10.418	4.243
H	22.217	-12.465	3.634
H	19.895	-13.142	3.365
H	18.614	-11.988	3.730
H	19.691	-9.112	3.280
FE	21.696	-7.092	-1.476
FE	22.406	-7.095	4.093
C	18.134	6.409	0.028
C	19.183	5.357	-0.305
C	18.674	3.922	-0.151
C	19.653	2.871	-0.678
C	19.338	1.451	-0.211
C	20.362	0.404	-0.664
C	20.408	-0.808	0.261
C	21.421	-1.899	-0.129
C	21.540	-2.888	0.996
C	22.619	-3.177	1.747
C	24.038	-2.728	1.483
C	24.432	-1.276	1.801
C	25.910	-1.025	1.457
C	26.284	0.432	1.149
C	26.542	1.331	2.368

Atom	X (Å)	Y (Å)	Z (Å)
C	27.959	1.171	2.926
H	28.738	1.701	2.355
H	22.470	-3.829	2.617
H	24.262	-2.869	0.411
H	24.715	-3.400	2.042
H	24.204	-1.033	2.850
H	23.803	-0.612	1.187
H	26.147	-1.622	0.555
H	26.559	-1.428	2.256
H	25.490	0.856	0.513
H	27.191	0.421	0.522
H	25.811	1.098	3.161
H	26.361	2.385	2.097
H	28.236	0.101	2.942
H	28.002	1.509	3.972
H	17.208	6.269	-0.555
H	17.834	6.370	1.087
H	18.498	7.426	-0.179
H	20.064	5.497	0.346
H	19.550	5.511	-1.331
H	17.703	3.814	-0.668
H	18.465	3.729	0.918
H	20.674	3.123	-0.343
H	19.696	2.921	-1.779
H	18.321	1.156	-0.530
H	19.305	1.456	0.894
H	21.363	0.866	-0.674
H	20.167	0.089	-1.705
H	19.405	-1.263	0.340
H	20.651	-0.461	1.280
H	22.396	-1.439	-0.350
H	21.089	-2.389	-1.065
H	20.587	-3.326	1.315
O	22.587	-5.248	4.353
H	23.482	-4.891	4.533
O	22.657	-7.385	2.227
O	21.236	-6.142	0.064
H	21.161	-5.176	0.072
H	22.347	-6.708	1.614